

Power Systems

André Veltman, Duco W.J. Pulle and Rik W. De Doncker
Fundamentals of Electrical Drives

André Veltman, Duco W.J. Pulle
and Rik W. De Doncker

Fundamentals of Electrical Drives

With 288 Figures



Dr.ir. André Veltman

Technische Universiteit Eindhoven
Dept. of Electrical Engineering
P.O. Box 513
5600 MB Eindhoven
The Netherlands
a.veltman@piak.nl

ISBN-10 1-4020-5503-X (HB)
ISBN-13 978-1-4020-5503-4 (HB)
ISBN-10 1-4020-5504-8 (ebook)
ISBN-13 978-1-4020-5504-1 (ebook)

This work is subject to copyright. All rights are reserved, whether the whole or part of the material is concerned, specifically the rights of translation, reprinting, reuse of illustrations, recitation, broadcasting, reproduction on microfilm or in any other way, and storage in data banks. Duplication of this publication or parts thereof is permitted only under the provisions of the German Copyright Law of September 9, 1965, in its current version, and permission for use must always be obtained from Springer. Violations are liable for prosecution under the German Copyright Law.

Springer is a part of Springer Science+Business Media
springer.com
© 2007 Springer

The use of general descriptive names, registered names, trademarks, etc. in this publication does not imply, even in the absence of a specific statement, that such names are exempt from the relevant protective laws and regulations and therefore free for general use.

Typesetting: by the authors and techbooks using a Springer L^AT_EX macro package

Cover design: *design & production* GmbH, Heidelberg

Printed on acid-free paper SPIN: 11760481 62/techbooks 5 4 3 2 1 0

*This book is dedicated to our
families and friends*

Contents

Dedication	v
Foreword	xi
Preface	xiii
Acknowledgments	xvii
Symbol Conventions	xix
1. INTRODUCTION	1
1.1 Why use electro-mechanical energy conversion?	1
1.2 Key components of an electrical drive system	4
1.3 What characterizes high performance drives?	6
1.4 Notational conventions	8
1.5 Use of building blocks to represent equations	9
1.6 Magnetic principles	12
1.7 Machine sizing principles	22
1.8 Tutorials for Chapter 1	23
2. SIMPLE ELECTRO-MAGNETIC CIRCUITS	29
2.1 Introduction	29
2.2 Linear inductance	29
2.3 Coil resistance	32
2.4 Magnetic saturation	32
2.5 Use of phasors for analyzing linear circuits	33
2.6 Tutorials for Chapter 2	36

3. THE TRANSFORMER	45
3.1 Introduction	45
3.2 Ideal transformer (ITF) concept	45
3.3 Basic transformer	49
3.4 Transformer with magnetizing inductance	50
3.5 Steady-state analysis	53
3.6 Three inductance model	55
3.7 Two inductance models	57
3.8 Mutual and self inductance based model	60
3.9 Two inductance model with coil resistance	62
3.10 Tutorials for Chapter 3	64
4. THREE-PHASE CIRCUITS	75
4.1 Introduction	75
4.2 Star/Wye connected circuit	76
4.3 Delta connected circuit	80
4.4 Space vectors	84
4.5 Amplitude and power invariant space vectors	86
4.6 Application of space vectors for three-phase circuit analysis	89
4.7 Relationship between space vectors and phasors	99
4.8 Tutorials for Chapter 4	103
5. CONCEPT OF REAL AND REACTIVE POWER	121
5.1 Introduction	121
5.2 Power in single phase systems	121
5.3 Power in three-phase systems	129
5.4 Phasor representation of real and reactive power	136
5.5 Tutorials for Chapter 5	137
6. SPACE VECTOR BASED TRANSFORMER MODELS	149
6.1 Introduction	149
6.2 Development of a space vector based ITF model	149
6.3 Two-phase ITF based generalized transformer model	157
6.4 Tutorials for Chapter 6	160

7.	INTRODUCTION TO ELECTRICAL MACHINES	169
7.1	Introduction	169
7.2	Ideal Rotating Transformer (IRTF) concept	169
7.3	Conditions required to realize constant torque	178
7.4	General machine model	183
7.5	Tutorials for Chapter 7	186
8.	VOLTAGE SOURCE CONNECTED SYNCHRONOUS MACHINES	193
8.1	Introduction	193
8.2	Machine configuration	193
8.3	Operating principles	195
8.4	Symbolic model	196
8.5	Generalized symbolic model	197
8.6	Steady-state characteristics	201
8.7	Tutorials for Chapter 8	209
9.	VOLTAGE SOURCE CONNECTED ASYNCHRONOUS MACHINES	231
9.1	Introduction	231
9.2	Machine configuration	231
9.3	Operating principles	232
9.4	Symbolic model, simplified version	234
9.5	Generalized symbolic model	235
9.6	Steady-state analysis	237
9.7	Tutorials for Chapter 9	249
10.	DIRECT CURRENT MACHINES	265
10.1	Introduction	265
10.2	Machine configuration	266
10.3	Operating principles	267
10.4	Symbolic model, simplified form	268
10.5	General symbolic DC machine model	272
10.6	Steady-state characteristics	276
10.7	Tutorials for Chapter 10	279

11. ANALYSIS OF A SIMPLE DRIVE SYSTEM	295
11.1 Introduction	295
11.2 Basic single phase uni-polar drive circuit	295
11.3 Basic single phase bipolar drive circuit	305
11.4 Control algorithm	307
11.5 Tutorials for Chapter 11	310
Appendices	327
A Concept of sinusoidal distributed windings	327
B Generic module library	333
References	341
Index	343

Foreword

Within one academic lifetime the electric drive has progressed from the three machine, DC drive called a Ward-Leonard system to today's sophisticated AC drives utilizing PWM inverter power electronics and field orientation or direct torque control. Over roughly this same period machine theory progressed from the classical, one machine at a time approach, through the generalized or unified approach emphasizing similarities between machine types. This unified theory also utilized much more sophisticated mathematical tools to obtain models applicable to transients as well as steady-state. This enabled theoretical modeling of a host of important machine problems but almost always required computer solutions as opposed to more general analytic solutions and often left one with a feeling of detachment from the physical reality of inrush currents, the whine of spinning rotors and the smell of over-warm electrical insulation.

Part way through my academic lifetime I was introduced to the next phase of unified theory, the use of complex notation to model the effective spatial orientation of quantities within a machine. This concept, often called space vector theory, provides a much clearer mathematical picture of what is happening in a machine, but at the expense of another level of abstraction in the model. However, the insights provided to one initiated in the method are so significant that today essentially all work in drive control is presented in this format. And therein lies a problem. To the uninitiated these presentations appear quite unintelligible. And a route to becoming initiated is generally hard to find and often harder to follow once found.

This then is the purpose of this book. To introduce, at a beginning level, the theory and notation used in modern electric drive analysis and design. The authors, together, bring an exceptional breadth of experience to this task. But it is not just another book providing a mathematical foundation for advanced work; a strong effort is also made to present the physical basis for all of the major steps in the development and to give the space vector a physical as well as

mathematical meaning. Readers using the book for self study will find the set of simulation tutorials at the end of each chapter of special value in mastering the implications and fine points of the material in the chapter.

Electric machine theory with its interacting temporal and spatial variations and multi-winding topologies can appear to be a very complicated and difficult subject. The approach followed in this book is, I believe, one that will help eliminate this perception by providing a fundamental, coherent and user friendly introduction to electric machines for those beginning a serious study of electric drive systems.

Donald W. Novotny
Madison, Wisconsin U.S.A.

Preface

Our motivation and purpose for writing this book stems from our belief that there is a practical need for a learning platform which will allow the motivated reader to gain a basic understanding of the modern multidisciplinary principles which govern electrical drives. The book in question should appeal to those readers who have an elementary understanding of electrical circuits and magnetics and who have an interest or need to comprehend advanced textbooks in the field of electrical drives. Consideration has also been given to those interested in using this book as a basis for teaching this subject matter. In this context a CD is presented with this work which contains the simulation examples and tutorials discussed in this book. Furthermore, all the figures in this book are given on the CD, in order to assist lecturers with the preparation of electronic ‘PowerPoint’ type lectures.

Electrical drives consist of a number of components, the electrical machine, converter and controller, all of which are discussed at various levels. A brief résumé of magnetic and electrical circuit principles is given in chapter 1 together with a set of generic building modules which are used throughout this book to represent dynamic models. Chapter 2 is designed to familiarize the reader with the process of building a dynamic model of a coil with the aid of generic modules. This part of the text also contains an introduction on phasors as required for steady-state analysis. The approach taken in this and the following chapters is to present a physical model, which is then represented by a symbolic model with the relevant equation set. A generic model is then presented which forms the basis for a set of ‘build and play’ simulations set out in various steps in the tutorial at the end of the chapter.

Chapter 3 introduces a single phase ‘ideal transformer’ (ITF) which forms the basis of a generic transformer model with leakage and magnetizing inductance. A phasor analysis is given to familiarize the reader with the steady-state model. The ‘build and play’ tutorials at the end of the chapter give the reader the opportunity to build and analyze the transformer model under varying con-

ditions. It is emphasized that the use of these ‘build and play’ tutorials is an essential component of the learning process throughout this book.

Chapter 4 deals with star and delta connected three phase systems and introduces the generic modules required to model such systems. The space vector type representation is also introduced in this part of the text. A set of ‘build and play’ tutorials are given which reinforce the concepts introduced in this chapter.

Chapter 5 deals with the concepts of real and reactive power in single as well as three phase systems. Additional generic modules are introduced in this part of the text and tutorial examples are given to familiarize the reader with this material.

Chapter 6 extends the ITF concept introduced earlier to a space vector type model which is represented in a symbolic and generic form. In addition a phasor based model is also given in this part of the text. The ‘build and play’ tutorials are self-contained step by step simulation exercises which are designed to show the reader the operating principles of the transformer under steady-state and dynamic conditions. At this stage of the text the reader should be familiar with building and using simulation tools for space vector type generic models which form the basis for a transition to rotating electrical machines.

Chapter 7 introduces a unique concept namely the ‘ideal rotating transformer’ (IRTF), which is the fundamental building block that forms the basis of the dynamic electrical machine models discussed in this book. A generic space vector based IRTF model is given in this part of the text which is instrumental in the process of familiarizing the reader with the torque production mechanism in electrical machines. This chapter also explores the conditions under which the IRTF module is able to produce a constant torque output. It is emphasized that the versatility of the IRTF module extends well beyond the electrical machine models discussed in this book. These advanced IRTF based machine concepts are discussed in a second book ‘Advanced Electrical Drives’ currently under development by the authors of this text. The ‘build and play’ tutorials at the end of this chapter serve to reinforce the IRTF concept and allow the reader to ‘play’ with the conditions needed to produce a constant torque output from this module.

Chapters 8-10 deal with the implementation of the IRTF module for synchronous, asynchronous and DC machines. In all cases a simplified IRTF based symbolic and generic model is given of the machine in question to demonstrate the operating principles. This model is then extended to a ‘full’ dynamic model as required for modelling standard electrical machines. A steady-state analysis of the machines is also given in each chapter. In the sequel of each chapter a series of ‘build and play’ tutorials are introduced which take the reader through a set of simulation examples which step up from a very basic model designed to show the operating principles, to a full dynamic model which can be used to represent the majority of modern electrical machines in use today.

Chapter 11 deals with the converter, modulation and control aspects of the electrical drive at a basic level. The half bridge converter concept is discussed together with the pulse width modulation (PWM) strategies that are in use in modern drives. A predictive dead-beat current control algorithm is presented in combination with a DC machine. The ‘build and play’ tutorials in the sequel of this chapter clearly show the operating principles of PWM based current controlled electrical drives.

The purpose, content and approach of our book has been presented above. On the basis of this material the following set of unique points are presented below in response to the question as to why prospective readers should purchase our book:

- The introduction of an ‘ideal rotating transformer’ (IRTF) module concept is a basic didactic tool for introducing the uninitiated reader to the elementary principles of torque production in electrical machines. The apparent simplicity of this module provides the reader with a powerful tool which can be used for the understanding and modelling of a very wide range of electrical machines well beyond those considered in this book.
- The application of the IRTF module to a synchronous, asynchronous and DC machine provides a unique insight into their operation principles. The book shows the transitional steps needed to move from a very basic IRTF model to a full IRTF based dynamic model usable for representing the dynamic and steady-state behavior of most machines in use today. Furthermore, the IRTF based module can be readily extended to include more specific machine effects such as ‘skin effect’ in asynchronous machines. In addition the IRTF module can be extended to machine models outside the scope of this book. Examples which will appear in the book ‘Advanced Electrical Drives’ by the authors of this text are the brushless DC machine and single phase IRTF based machine.
- This text is designed to bridge the gap between advanced textbooks covering electrical drives and textbooks at either a fundamental electrical circuit level or more generalized mechatronic books. Our text with its CD with tutorials is self-contained. As such the book should fit well into the undergraduate curriculum for students who have completed first or second year and who have an interest in seeking a career in the area of electrical drives. The book should also appeal to engineers with a non drive background who have a need to acquire a better understanding of modern electrical drive principles.
- The use of ‘build and play’ type tutorials is of fundamental importance to understanding the theory presented in the text. The didactic role of modern simulation tools in engineering cannot be overestimated and it is for this reason that extensive use is made of generic modules which are in turn used

to build complete models of the drive. Such an approach allows the reader to visualize the complex equation set which is at the basis of these models. Two simulation tools are used in these tutorials namely ‘Simulink®’ and ‘Caspoc’. The tutorials are linked directly to the generic modules discussed in the corresponding chapter and are included in the CD given in the book. The Simulink tutorials can be run by readers who have licensed access to Simulink. The Caspoc tutorials contain a set of modules which are precisely tailored to the generic module set used in this book. Furthermore, the Caspoc based tutorial set can be run in a ‘stand alone’ mode, hence there is direct access (without additional software tools) to a set of ‘build and play’ tutorials which will encourage the reader in his or her quest for understanding the field of electrical drives.

D.W.J. PULLE, A. VELTMAN AND R.W. DE DONCKER

Acknowledgments

The process of writing this book has not been without its difficulties. That this work has come to fruition stems from a deep belief that the material presented in this book will be of profound value to the engineering community as a whole and the educational institutions in particular.

The content of this book reflects upon the collective academic and industrial experience of the authors concerned. In this context the input of students in general and other colleagues cannot be overestimated. In particular the authors wish to thank the staff and students of the following educational institutions: Australian Defence Force Academy, University College, The University of New South Wales, Canberra, Australia. The University of Lund, IEA, Lund, Sweden. Technische Universiteit Eindhoven, Eindhoven, the Netherlands. RWTH-Aachen University, Germany and the University of Newcastle, Newcastle, Australia.

In addition the authors would like to thank the various industrial institutions (in alphabetical order) who have been involved with this work namely: GTI elec-troproject, Zaandam, the Netherlands; Piak Electronic Design, Culemborg, the Netherlands; Simulation Research, Alphen aan den Rijn, the Netherlands and Zener Electric, Sydney, Australia.

A number of individuals have played a particular role in terms of bringing this book to fruition. We would like to particularly thank the following persons (in alphabetical order) for their contributions: M. Alaküla, R.E. Betz, P.P.J. van den Bosch, A.J.C.M. van Coenen, P.J. van Duijsen, P. van der Hulst, R. Jackson, H.C. Pulle and J.A. Schot.

Symbol Conventions

Variables

Variables which are a function of time	u, i, ψ, p
Space vectors	$\vec{u}, \vec{i}, \vec{\psi}$
Phasors	$\underline{u}, \underline{i}, \underline{\psi}$
RMS-values	$\overline{U}, \overline{I}, \overline{P}, Q$
Peak-values	\hat{u}, \hat{i}
Pull-out slip	\hat{s}
Real part of complex variable x	$\Re\{x\}$
Imaginary part of complex variable x	$\Im\{x\}$
Absolute value of complex variable x	$ x $
Quasi stationary variable x	\overline{x}

Symbols

Abbreviation	Variable	Unit
A	-area	m^2
AC	-alternate current	
B	-flux density	T
C	-constant	
CAD	-computer aided design	
A/D	-analog to digital converter	
DSP	-digital signal processor	
DC	-direct current	
e	-induced voltage	V
EMF	-electro motive force	V
f	-frequency	Hz
F	-force	N
H	-magnetic field	At/m

i, I	-current	A
IRTF	-ideal rotating transformer	
ITF	-ideal transformer	
j	-imaginary operator, $\sqrt{-1}$	
j	-current density	A/m ²
J	-inertia	kgm ²
k	-transformation ratio	
l	-length	m
L	-inductance	H
MMF	-magneto motive force (m.m.f.)	At
N, n	-number of turns	
P, p	-real power	W
p	-instantaneous power	VA
p	-number of pole pairs	
PI	-proportional-integral	
PWM	-pulse width modulation	
Q	-reactive power	VA
R	-resistance	Ω
R	-reluctance	At/Wb
rpm	-revolutions per second	
SV	-stator volume	m ³
s	-slip	
T	-torque	Nm
T_s	-sampling interval period	s
TRV	-torque rotor volume ratio	N/m ²
t	-time	s
u, U	-voltage	V
W	-energy	J
Z	-impedance	Ω
μ P	-micro processor	

Greek Symbols

Abbreviation	Variable	Unit
Δ	-incremental	
γ	-angle displacement $2\pi/3$	rad
κ	-coupling factor	
μ	-permeability	H/m
ρ, θ	-angle variable	rad
σ	-leakage factor	
ϕ	-flux	Wb
Ψ	-incremental flux	Vs
ψ	-flux-linkage	Wb t
ω	-rotational speed (angular frequency)	rad/s

Subscripts

$i_{r,R}$	-rotor current
i_1	-primary current
i_2	-secondary current
$i_{m,M}$	-magnetizing current
i_s	-stator current
i_F	-field current
L_σ	-leakage inductance
t_k	-discrete time point
T_e	-electro mechanical torque
T_l	-mechanical load torque
u_{DC}	-DC supply
z_α	-real part of variable
z_β	-imaginary part of variable
z_x	-real part of variable in 'xy' rotor coordinates
z_y	-imaginary part of variable in 'xy' rotor coordinates
ω_m	-mechanical shaft speed

Superscripts

i'	-referred current
t^f	-falling edge
t^r	-rising edge
\vec{x}^*	-complex conjugate of vector
\underline{x}^*	-complex conjugate of phasor
x^*	-reference (set point) value
$\vec{z}^{\alpha,\beta}, \vec{x}$	-vector in stationary coordinates
\vec{z}^{xy}	-vector in rotating coordinates

Chapter 1

INTRODUCTION

1.1 Why use electro-mechanical energy conversion?

Electric motors are around us everywhere. Generators in power plants are connected to a three-phase power grid of alternating current (AC), pumps in your heating system, refrigerator and vacuum cleaner are connected to a single phase AC grid and switched on or off by means of a simple contactor. In cars a direct current (DC) battery is used to provide power to the starter motor, windshield wiper motors and other utilities. These motors run on direct current and in most cases they are activated by a relay switch without any control.

Many applications driven by electric motors require more or less advanced control. Lowering the speed of a fan or pump can be considered relatively simple. Perhaps one of the most difficult ones is the dynamic positioning of a tug in a wafer-stepper with nanometer accuracy while accelerating at several g's. Another challenging controlled drive is an electric crane in a harbor that needs to be able to move an empty hook at high speed, navigate heavy loads up and down at moderate velocities and make a soft touchdown as close as possible to its intended final position. Other applications such as assembly robots, electric elevators, electric motor control in hybrid vehicles, trains, streetcars, or CD-players can, with regard to complexity, be situated somewhere in between.

Design and analysis of all electric drive systems require not only knowledge of dynamic properties of different motor types, but also a good understanding of the way these motors interact with power-electronic converters. These power converters are used to control motor currents or voltages in various manners.

Compared to other drive systems such as steam engines (still used for aircraft launch assist), hydraulic engines (famous for their extreme power per volume), pneumatic drives (famous for their simplicity, softness and hissing sound), combustion engines in vehicles or turbo-jet drives in helicopters or aircraft, electric

drive systems have a very wide field of applications thanks to some strong points:

- Large power range available: actuators and drives are used in a very wide range of applications from wrist-watch level to machines at the multi-megawatt level, i.e. as used in coal mines and the steel industry.
- Electrical drives are capable of full torque at standstill, hence no clutches are required.
- Electrical drives can provide a very large speed range, usually gearboxes can be omitted.
- Clean operation, no oil-spills to be expected.
- Safe operation possible in environments with explosive fumes (pumps in oil-refineries).
- Immediate use: electric drives can be switched on immediately.
- Low service requirement: electrical drives do not require regular service as there are very few components subject to wear, except the bearings. This means that electrical drives have a long life expectancy, typically in excess of twenty years.
- Low no-load losses: when a drive is running idle, little power is dissipated since no oil needs to be pumped around to keep it lubricated. Typical efficiency levels for a drive is in the order of 85% in some cases this may be as high as 98%. The higher the efficiency the more costly the drive technology, in terms of initial costs.
- Electric drives produce very little acoustic noise compared to combustion engines.
- Excellent control ability: electrical drives can be made to conform to precise user requirements. This may, for example, be in relation to realizing a certain shaft speed or torque level.
- ‘Four-quadrant operation’: Motor- and braking-mode are both possible in forward or reverse direction, yielding four different quadrants: forward motoring, forward braking, reverse motoring and reverse braking. Positive speed is called forward, reverse indicates negative speed. A machine is in motor mode when energy is transferred from the power source to the shaft i.e. when both torque and speed have the same sign.

1.1.1 Modes of operation

When a machine is in motoring mode, most of the energy is transferred from the electrical power source to the mechanical load. Motoring mode takes place in quadrants 1 and 3 (see figure 1.1(b)). If the shaft torque and shaft speed are in opposition then the flow of energy is reversed, in which case the drive is in the so-called ‘braking’ mode.

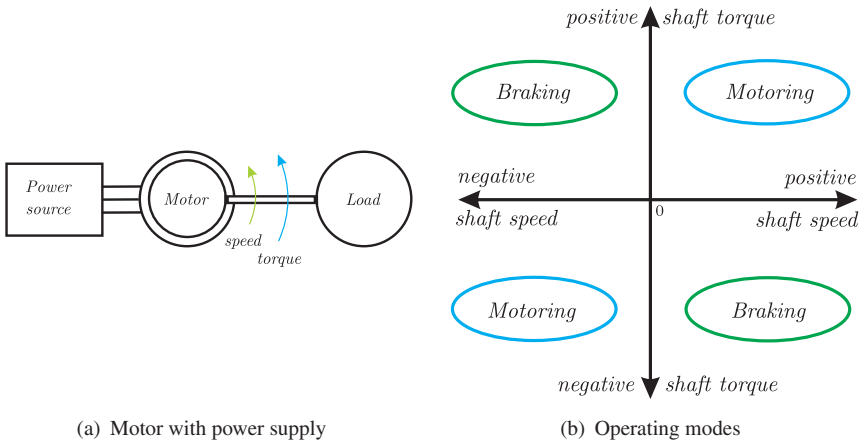


Figure 1.1. Motoring and braking operation

Braking comes in three ‘flavours’. The first is referred to as ‘regenerative’ braking operation, where most of the mechanical energy from the load is returned to the power source. Most drives which contain a converter (see section 1.2) between motor and supply use a diode rectifier as a front end, hence power can only flow from the AC power-grid to the DC-link in the drive and not the other way around. In such converters regenerative operation is only possible when the internal DC-link of the drive is shared with other drives that are able to use the regenerated power immediately. Sharing a common rectifier with many drives is economic and becoming standard practise. Furthermore, attention is drawn to the fact that some power sources are not able to accept any (or only a limited amount (batteries)) regenerated energy.

The second option is referred to as ‘dissipative’ braking operation where most of the mechanical load energy is burned up in an external brake-chopper-resistor. A brake-chopper can burn away a substantial part of the rated power for several seconds, designed to be sufficient to stop the mechanical system in a fast and safe fashion. One can regard such a brake-chopper as a big zener-diode that prevents the DC-link voltage in the converter from rising too high. Brake choppers come in all sizes, in off-shore cranes and locomotives, power levels of several megawatts are common practise.

The third braking mode is one where mechanical power is completely returned to the motor at the same time some or none electrical power is delivered, i.e. both mechanical and electrical input power are dissipated in the motor. Think of a permanent magnet motor being shorted, or an induction motor that carries a DC current in its stator, acting as an eddy-current-brake.

Of course there are also disadvantages when using electrical drive technology, a few of these are briefly outlined below.

- Low torque/force density compared to combustion engines or hydraulic systems. This is why aircraft control systems are still mostly hydraulic. However, there is an emerging trend in this industry to use electrical drives instead of hydraulic systems.
- High complexity: A modern electrical drive encompasses a range of technologies as will become apparent in this book. This means that it requires highly skilled personnel to repair or modify such systems.

1.2 Key components of an electrical drive system

The ‘drive’ shown in figure 1.1(a) is in fact only an electrical machine connected directly to a power supply. This configuration is widely in use but one cannot exert very much control in terms of controlling torque and/or speed. Such drives are either on or off with rather wild starting dynamics. The drive concept of primary interest in this book is capable of what is referred to as ‘adjustable speed’ operation [Miller, 1989] which means that the machine can be made to operate over a wide speed range. A simplified structure of a drive is shown in figure 1.2. A brief description of the components is given below:

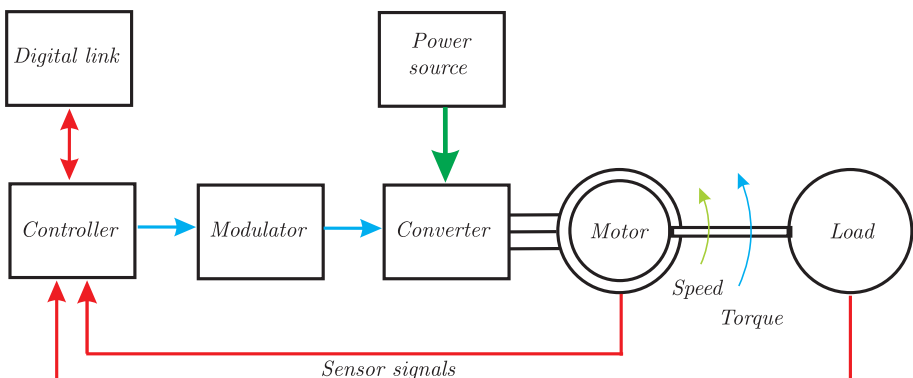


Figure 1.2. Typical drive set-up

- Load: This component is central to the drive in that the purpose of the drive is to meet specific mechanical load requirements. It is emphasized

that it is important to fully understand the nature of the load and the user requirements which must be satisfied by the drive. The load component may or may not have sensors to measure either speed, torque or shaft angle. The sensors which can be used are largely determined by the application. The nature of the load may be translational or rotational and the drive designer must make a prudent choice whether to use a direct-drive with a large motor or geared drive with a smaller but faster one. Furthermore, the nature of the load in terms of the need for continuous or intermittent operation must be determined.

- Motor: A limited range of motor types is presently in use. Among these are the so-called ‘classical’ machines, which have their origins at the turn of the 19th century. This classical machine set has displaced a large assortment of ‘specialized’ machines used prior to the introduction of power electronic converters for speed control. This classical machine set contains the DC (Direct Current) machine, asynchronous (induction) machine, synchronous machine and ‘variable reluctance’ machine. Of these the ‘variable reluctance’ machine will not be discussed in this book. A detailed discussion of this machine appears in the second book ‘Advanced Electrical Drives’ written by the authors of this book. An illustration of the improvements in terms of the power to weight ratio which has been achieved over the past century is given in figure 1.3.

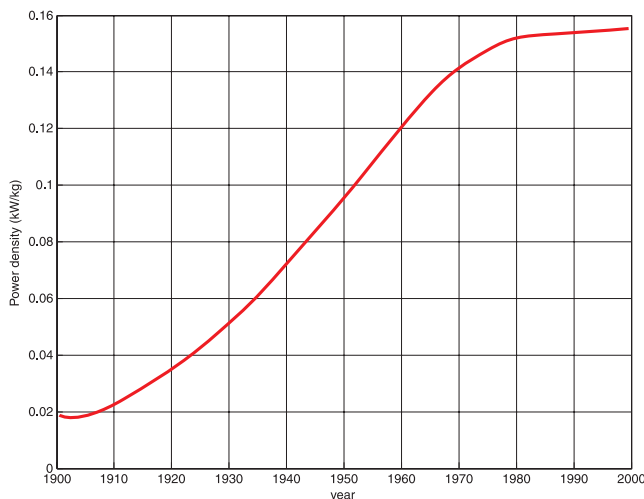


Figure 1.3. Power density of electrical machines over the past century

The term ‘motor’ refers to a machine which operates as a motor, i.e. energy flows from the motor to the load. When the energy flows in the opposite direction a machine is said to operate as a generator.

- **Converter:** This unit contains a set of power electronic switches which are used to manipulate the energy transfer between power supply and motor. The use of switches is important given that no power is dissipated (in the ideal case) when the switches are either open or closed. Hence, theoretically the efficiency of such a converter is 100%, which is important particularly for large converters given the impossibility of absorbing large losses which usually appear in the form of heat. A large range of power electronic switches is available to the designer to meet a wide range of applications.
- **Modulator:** The switches within the converter are controlled by the modulator which determines which switches should be on, and for what time interval, normally on a micro-second timescale. An example is the Pulse Width Modulator that realizes a required pulse width at a given carrier-frequency of a few kHz.
- **Controller:** The controller, typically a digital signal processor (DSP), or micro-controller contains a number of software based control loops which control, for example, the currents in the converter and machine. In addition torque, speed and shaft angle control loops may be present within this module. Shown in the diagram are the various sensor signals which form the key inputs to the controller together with a number of user set-points (not shown in the diagram). The output of the controller is a set of control parameters which are used by the modulator.
- **Digital Link:** This unit serves as the interface between the controller and an external computer. With the aid of this link drive set-points and diagnostical information can be exchanged with a remote user.
- **Power supply:** In most cases the converter requires a DC voltage source. The power can be obtained from a DC power source, in case one is available. However, in most cases the DC power requirements are met via a rectification process, which makes use of the single or three-phase AC (referred to as the ‘grid’) power supply as provided by the utility grid.

1.3 What characterizes high performance drives?

Prior to moving to a detailed discussion of the various drive components it is important to understand the reasons behind the ongoing development of drives. Firstly, an observation of the drive structure (see figure 1.2) learns that the drive has components which cover a very wide field of knowledge. For example, moving from load to controller one needs to appreciate the nature of the load, have a thorough understanding of the motor, comprehend the functioning of the converter and modulator. Finally, one needs to understand the control principles involved and how to implement (in software) the control algorithms into a micro-processor or DSP. Hence there is a need to have a detailed understanding of a

very wide range of topics which is perhaps one of the most challenging aspects of working in this field.

The development of electrical machines occurred, as was mentioned earlier, more than a century ago. However, the step to a high performance drive took considerably longer and is in fact still ongoing. The main reasons as to why drive technology has improved over the last decades are briefly outlined below:

- Availability of fast and reliable power semiconductor switches for the converter: A range of switches is available to the user today to design and build a wide range of converter topologies. The most commonly used switching devices for motor drives are MOSFET's for low voltage applications, IGBT's for medium (kW) and higher (MW) powers. In addition GCT's are available for medium and high voltage applications.
- Availability of fast computers for (real time) embedded control: the controller needs to provide the control input to the modulator at a sampling rate which is typically in the order of $100\mu\text{s}$. Within that time frame the computer needs to acquire the input data from sensors and user set-points and apply the control algorithm in order to calculate the control outputs for the next cycle. The presence of low cost fast micro-processors or DSP's has been of key importance for drive development.
- Better sensors: A range of reliable and low cost sensors is available to the user which provides accurate inputs for the controller such as LEM's, incremental encoders and Hall-effect sensors.
- Better simulation packages: Sophisticated so-called ‘finite-element’ computer aided design (CAD) packages for motor design have been instrumental in gaining a better understanding of machines. Furthermore, they have been and continue to be used for designing machines and for optimization purposes. In terms of simulating the entire drive structure there are simulators with graphical user interfaces, such as among others MATLAB/Simulink® and Caspoc, which allow the user to analyze a detailed dynamic model of the entire system. This means that one can analyze the behaviour of such a system under a range of conditions and explore new control techniques without the need of actually building the entire system. This does not mean that implementing real life systems is no longer required. The proof of the pudding is in the eating, and only experimental validation can prove that the supposed models are indeed valid for a real drive system.

Simulation and experiment are never exactly the same. When the models are not able to describe the drive system under certain conditions, it might be useful to enhance the simulation model to incorporate some of the found differences. As engineers we should be aware of the fact that drive systems are often closed-loop systems that are able to tolerate deviations in parameters

and unknown load torques without any problem. To paraphrase Einstein, ‘A simulation model should be as simple as possible, but no simpler’ is the key to a successful simulation. This means that essential dynamics or non-linearities found in the real world system, need to be implemented in the (physics based) simulation model in order to study extreme situations with acceptable accuracy.

The simulation model used depends on what needs to be studied. Simulating pulse-width modulated outputs requires a very short simulation time-step, in the order of sub- μs or so, while the overall mechanical system and the motor’s response can be calculated at a hundred times larger time-step with negligible loss of accuracy, as long as the power converter is regarded as a non-switching controlled voltage source. Another extreme example is the study of thermal effects on the motor, in that case only the average power dissipation in terms of seconds or even minutes is of interest.

- Better materials: The availability of improved magnetic, electrical and insulation materials has provided the basis for efficient machines capable of withstanding higher temperatures, thereby offering long application life and low life cycle costs.

1.4 Notational conventions

1.4.1 Voltage and current conventions

The conventions used in this book for the voltage and current variables are shown with the aid of figure 1.4. The diagram shows the variables voltage u and

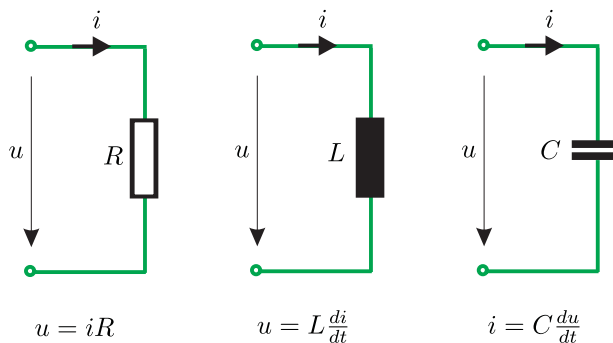


Figure 1.4. Notation conventions used for electrical quantities

current i , which are specifically given in ‘lower case’ notation, because they represent instantaneous values, i.e. a function of time. The ‘voltage arrows’ shown in figure 1.4 point to the negative terminal of the respective circuit.

1.4.2 Mechanical conventions

The mechanical conventions used in this book are shown with the aid of figure 1.5. The electro magnetic torque T_e produced by the machine corresponds with a power output $p_e = T_e \omega_m$, where ω_m represents the rotational speed, otherwise known as the angular frequency. The load torque T_l is linked to the power delivered to the load $p_L = T_l \omega_m$. The torque difference $T_e - T_l$ results in an acceleration $J d\omega_m / dt$ of the rotating mass with inertia J . This rotating structure is represented as a lumped mass formed by the rotor of the motor, motor shaft and load. The corresponding mechanical equation which governs this system is of the form

$$J \frac{d\omega_m}{dt} = T_e - T_l \quad (1.1)$$

The angular frequency may also be written as $\omega_m = d\theta / dt$ where θ represents the rotor angle.

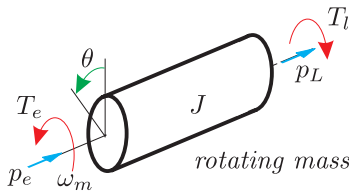


Figure 1.5. Notation conventions used for mechanical quantities

Figure 1.5 shows the machine operating as a motor, i.e. $T_e > 0$, $\omega_m > 0$. These motor conventions are used throughout this book.

1.5 Use of building blocks to represent equations

Throughout this book so-called ‘generic models’ of drive components will be applied to build a useful simulation model of an electrical drive system [Leonhard, 1990]. Models of this type are directly derived from the so-called ‘symbolic’ representation of a given drive component. The generic models are dynamic models which can be directly implemented in a practical simulation environment such as MATLAB/Simulink® [Mathworks, 2000] or Caspoc [van Duijzen, 2005]. Models in this form can then be analyzed by the reader in terms of the expected transient or steady-state response. Furthermore, changes can be made to a model to observe their effect. This interactive type of learning process is particularly useful to become familiar with the material.

An example of moving from symbolic to generic and Simulink representation is given in figure 1.6. Note that the Caspoc simulation environment allows dynamic models to be directly represented in terms of the generic building blocks given in this book. This means that the transition from a generic diagram to actual simulation is greatly simplified. The symbolic model shown in figure 1.6

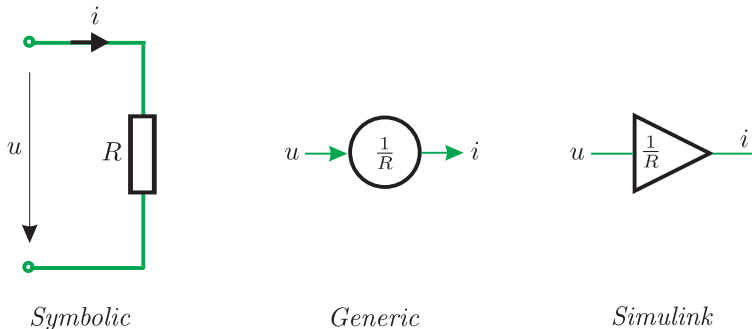


Figure 1.6. Symbolic, generic and Simulink representations

represents a resistance. The resistance represents a relation between voltage and current by Ohm's law: you can calculate current from voltage, voltage from current or resistance from both voltage and current. The generic diagram assumes in this case that the voltage u is an input and the current i represents the output variable for this building block known as a gain module. The gain for this module must in this case be set to $\frac{1}{R}$. In Simulink a gain module is represented in a different form as may be observed from figure 1.6. Throughout this book additional building blocks will be introduced as they are required. At this point, a basic set will be given which will form the basis for the first set of generic models to be discussed in this book. The complete generic set of models used in this book are given in the appendix B on page 333.

1.5.1 Basic generic building block set

The first set of building blocks as given in figure 1.7 are linked to 'example' transfer functions. For example, the *GAIN* module has as input the current i_s and as output u_s , the gain is set to R_s . The *INTEGRATOR* example module has as input the variable ΔT and output ω_m . The gain of the integrator is $\frac{1}{J}$. *Note that the module shows the gain as J and not $\frac{1}{J}$* [Leonhard, 1990]. When multiplying two variables in the time domain a *MULTIPLIER* module is used. This module differs from the given *GAIN* module in that the latter is used to multiply a variable with a constant. Finally, an example of a *SUMMATION* module is given. In this case the output is a variable ΔT and subtracts the input variable T_l from input variable T_e . *Note that in the case of adding two variables no 'plus' symbol is placed. A 'minus' sign is used when subtracting two variables.*

An example of combining some of these modules is readily given by considering the following equation

$$u = iR + L \frac{di}{dt} \quad (1.2)$$

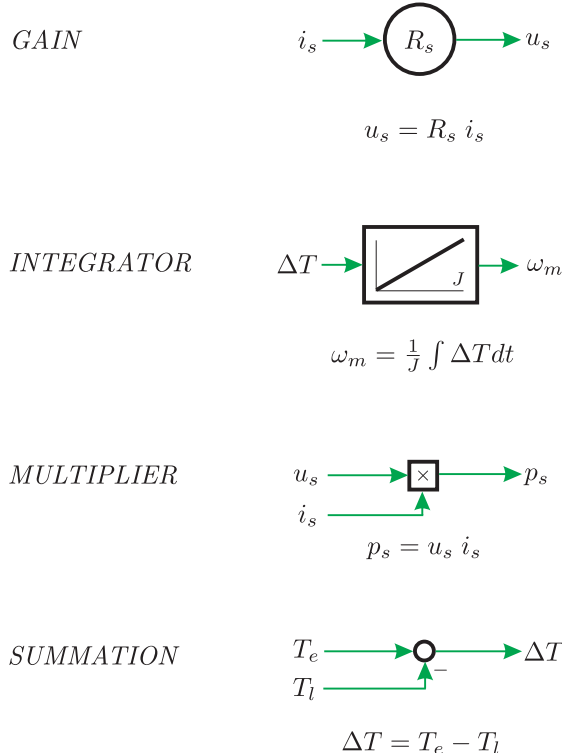


Figure 1.7. Basic building block set

which represents the voltage across a series network in the form of an inductance L and resistance R . To build a generic representation with the voltage as input variable and current as output variable, it is helpful to rewrite the expression in its differential equation form

$$\frac{di}{dt} = \frac{1}{L} (u - iR) \quad (1.3)$$

In this case the output of the integrator is the variable i and the input of the integrator is given as $(u - iR)$, hence

$$i = \frac{1}{L} \int (u - iR) dt \quad (1.4)$$

The initial current is assumed to be zero, i.e. $i(0) = 0$. An observation of equation (1.4) learns that the integrator input is formed by the input variable u from which the term iR must be subtracted where use is made of a summation unit. The gain $\frac{1}{L}$ present in equation (1.4) appears in the generic integrator module as L as discussed previously. The resultant generic and symbolic diagrams for this example are given in figure 1.8.

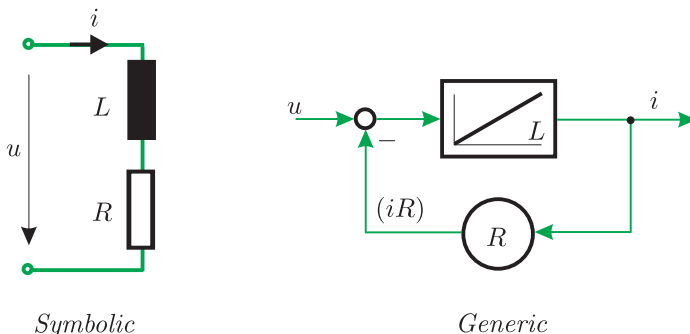


Figure 1.8. Example of using basic building blocks

1.6 Magnetic principles

Prior to looking at the various components of a drive it is important to revive the basic magnetic principles. On the basis of these principles we will examine the so-called ‘ideal transformer’ (ITF) and ‘ideal rotating transformer’ (IRTF). The book by Hughes [Hughes, 1994] is highly recommended as it provides an excellent primer in the area of magnetic principles and drives. We will follow a similar line of thinking for the magnetic principles section in this book.

1.6.1 Force production

The production of electro magnetic torque T_e in rotating electrical machines, such as those considered in this book, is directly linked to the question how forces are produced. It is noted that other types of machines exist where torque production is based on either reluctance, electro-static, piezo-electric or magneto-restrictive principles. Machines which abide with those principles are not considered in this book. The basic relationship between force, current in a conductor and magnetic field has been discovered by Lorentz. The directions of the three variables are at right angles with respect to each other and under

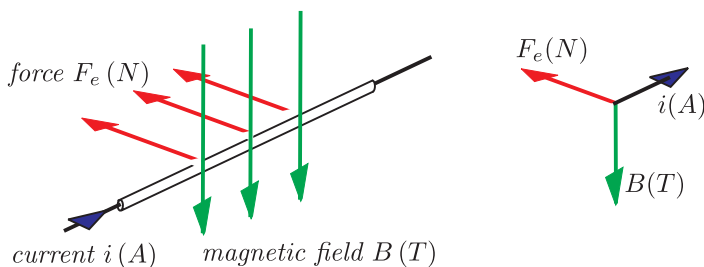


Figure 1.9. Relationship between current, magnetic field and force

in these circumstances the force magnitude acting on a conductor (exposed over a length l to a flux density B and carrying a current i) is given as

$$F_e = B i l \quad (1.5)$$

where l is the length (in meters) of the conductor section which is exposed to the field. Force is expressed in newtons (N).

1.6.2 Magnetic flux and flux density

Prior to discussing the concept of flux density it is helpful to understand the meaning of flux lines. Consider a permanent bar magnet, a cross-section of

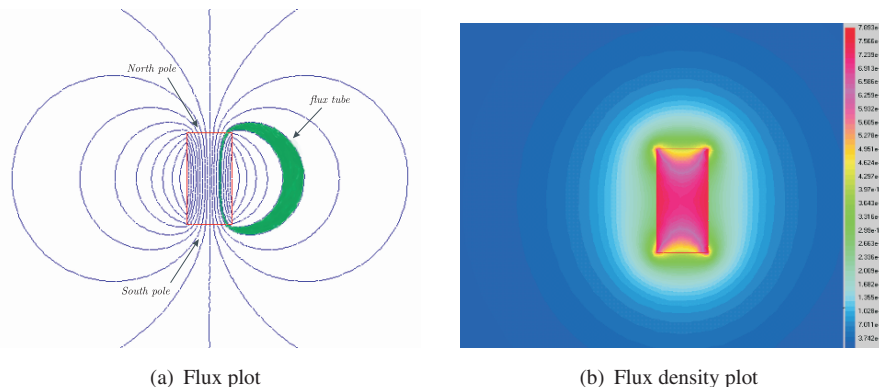


Figure 1.10. Bar magnet flux and flux density plot

which is shown in figure 1.10(a), together with a set of so-called magnetic field lines. Between each pair of adjacent lines there is a fixed quantity of magnetic flux. This amount is represented as a ‘flux tube’ and an example is given in figure 1.10(a). The meaning of flux density B within such a tube is defined as the flux in the tube divided by the tube cross-section. For simplicity we will assume a unity length tube in the dimension perpendicular to the plane shown in figure 1.10(a), hence the cross-section (of the tube) is directly proportional to the width of the tube shown in figure 1.10(a). This means that the flux density in the tube increases as the tube becomes narrower. Within the magnet the flux density is considerably higher than outside. A flux density plot of the same magnet is shown in figure 1.10(b). This type of plot is extremely valuable to designers as it enables one to look at ‘hot spots’, i.e. places where the flux density is very high. The colour scale shown on the right of the flux density plot shows the highest flux density in red. Clearly the bar magnet in its present form cannot be considered as a source with a uniform flux density.

1.6.3 Magnetic circuits

It is interesting to see what can be achieved when magnetic steel is used to ‘shape’ the field pattern. Furthermore, the permanent magnet will be replaced with a n turns circular coil, which carries a current i . The use of a coil has advantages in terms of being able to better control the flux. However, machines generally become more compact when permanent magnets are used. Furthermore, magnets provide flux without the use of an external power supply. An example of the field distribution produced by a coil *without* any steel is shown in figure 1.11(a). The coil is shown in cross-sectional form where the right section has the current ‘into’ the diagram and the left side has the current coming out. The flux direction which corresponds to the current going ‘into’ the winding half is clockwise. Hence the ‘north’ pole is on the top of the diagram which corresponds to the pole alignment shown for the bar magnet. Note that the field distribution is almost identical to that produced by the magnet. As with the bar magnet the flux density is highest in the coil, as may be observed from the flux density plot of the coil shown in figure 1.11(b). The observant reader will note

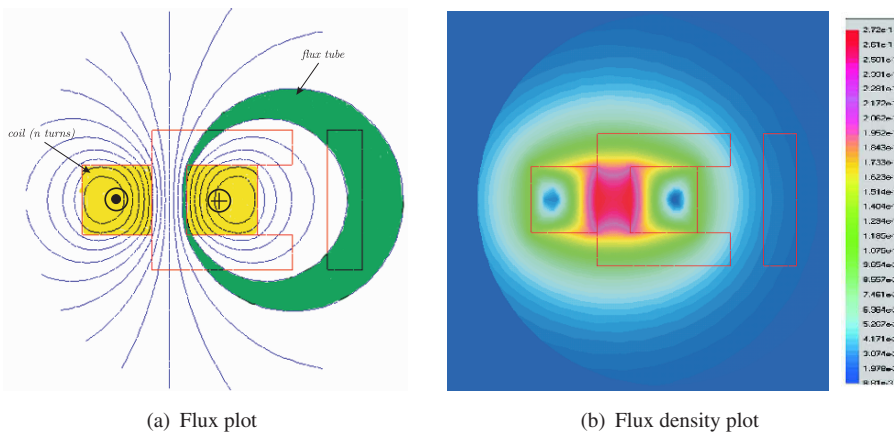


Figure 1.11. Coil flux and flux density plot

that there is also a ‘C’ and ‘I’ outline shown in red in both figures. These are in fact the outlines of a steel structure which in this case has been constructed of ‘air’, i.e. the coil does not see this structure at this point of our discussion.

If we now introduce a steel ‘C’ core and ‘I’ section (known as the armature) with our coil, then we see a remarkable change to the field distribution, as may be observed from figure 1.12(a). The flux lines are now mostly confined to the steel. However, when the flux lines cross from the ‘C’ core to the armature they tend to spread out, an effect referred to as ‘fringing’. If one looks to the ‘green’ flux tube we see that it is very narrow in the coil and steel regions. The flux tube in question widens out when it crosses the airgaps located between

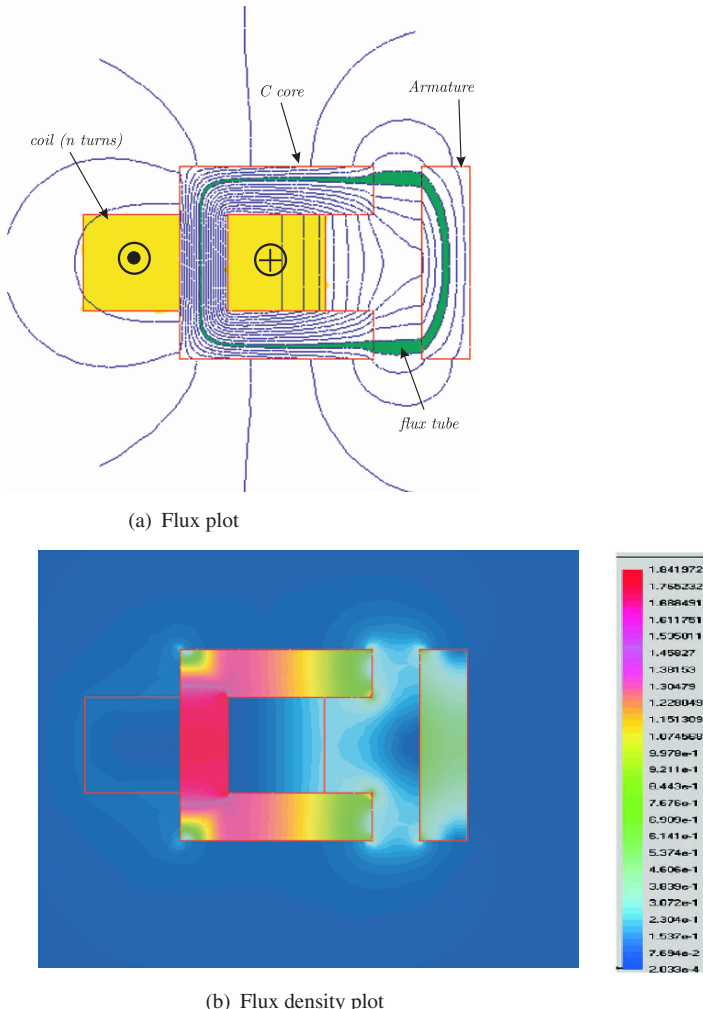


Figure 1.12. Coil, with ‘C’ core and ‘I’ shaped armature: flux and flux density plot

the ‘C’ core and armature. The airgap is large, to demonstrate clearly how the flux lines are affected when moving through air. However, in real induction machines the airgap is in the order of 0.3mm to 0.7mm which means that most of the flux tube area, when it passes through air, is not much wider than in the steel. In permanent magnet synchronous motors however, airgaps can be as high as several cm’s. The flux density in the structure of figure 1.12(a) is still relatively uneven, which means that the flux density is high within the steel that has the coil wrapped around it. The flux density plot shown in figure 1.12(b)

clearly shows this. The colour scale shows that red represents the highest flux density.

1.6.4 Electrical circuit analogy and reluctance

The flux and flux density plots given in the previous section were derived with a two-dimensional ‘finite element’ package, which enables the user to quickly observe flux patterns for a particular application. However, there is a need to make some ‘sanity checks’ in every type of simulation. Hence, some way must be found to make a simple analytical calculation which will give us confidence in the results produced by a particular simulation. We can do this check by making use of Hopkinson’s law, which for a magnetic circuit allows us to create, for example, an electric circuit of the structure given in figure 1.12. Hopkinson’s law is in fact equivalent to Ohm’s law for electrical circuits. Electrically Ohm’s law tells us that the electric voltage u across a resistance is equal to the product of the current i and resistance R , i.e. $u = iR$. Hopkinson’s law defines a ‘magnetic potential u_M ’, which is the product of the flux ϕ in the magnetic circuit times the so-called magnetic reluctance R_m , i.e. $u_M = \phi R_m$. The method presented here is confined to so-called linear magnetic circuits, which implies that the reluctance is neither a function of ϕ nor of u_M . In the equivalent circuit, the flux ϕ is in electrical terms equivalent to the current i . An approximate magnetic equivalent circuit of the structure given in figure 1.12 is of the form shown in figure 1.13. The approximation used

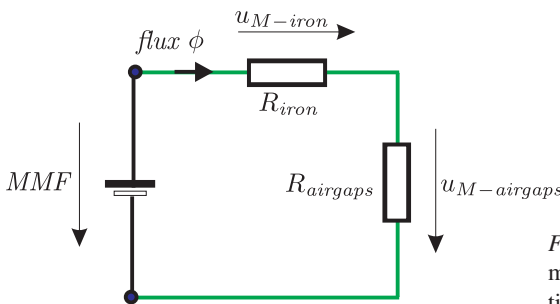


Figure 1.13. Equivalent magnetic circuit representation

is that all the flux lines cross the airgaps between the ‘C’ core and the armature ‘T’. Clearly, this is not the case here (see figure 1.12(a)) because the airgap is unrealistically large. The reluctance R_m is generally proportional to the length of the path and inversely proportional to the product of the cross-sectional area and the so-called permeability μ of the medium in which the flux travels. In the example given above two reluctances are given namely R_{iron} and $R_{airgaps}$. The ‘iron’ reluctance represents the total reluctance of the steel sections (‘C’ core and armature). The term ‘iron’ is commonly used to describe the magnetic steel sections. The ‘airgap’ reluctance represents the total reluctance of both

airgaps. Mathematically the reluctance may be written as

$$R_{iron} = \frac{l_{iron}}{A_{iron} \mu_{iron}} \quad (1.6a)$$

$$R_{airgaps} = \frac{l_{airgaps}}{A_{airgaps} \mu_{airgaps}} \quad (1.6b)$$

where l_{iron} and $l_{airgaps}$ respectively represent the total length the flux travels through steel and airgaps between ‘C’ core and armature. Furthermore, A_{iron} and $A_{airgaps}$ respectively represent the cross-sectional areas of the steel sections and airgaps. The latter is not easily defined due to fringing effects. Hence we will assume for this example that the airgap cross-section is equal to that in the steel sections. This means that we assume that the flux density in air and steel (iron) are equal, which they clearly are not in this case. The permeability of the steel μ_{iron} and air μ_{airgap} differ considerably. Typically the permeability in steel(iron) is a factor 1000 higher than that of air. Consequently, the reluctance of the steel sections is considerably lower than that in air.

The magnetic potential across each reluctance is shown as u_{M-iron} and $u_{M-airgaps}$ respectively. Together they form the total magnetic potential of the circuit, which is equal to the magneto-motive force MMF. The MMF is equal to the product of the number of coil turns n and current i as shown below

$$MMF = n i \quad (1.7)$$

The MMF can, as was mentioned above, also be expressed in terms of the circuit magnetic potentials namely

$$MMF = u_{M-iron} + u_{M-airgaps} \quad (1.8)$$

The magnetic field H (A/m) is directly linked to the MMF in the circuit by the expression:

$$MMF = \underbrace{H_{iron} l_{iron}}_{u_{M-iron}} + \underbrace{H_{airgaps} l_{airgaps}}_{u_{M-airgaps}} \quad (1.9)$$

where $H = B/\mu$, with μ as the permeability. Consequently a material with a high permeability will, for a given flux density (and geometry), yield a low magnetic field value and corresponding low magnetic potential.

The circuit flux ϕ in the circuit is of the form

$$\phi = \frac{MMF}{R_{iron} + R_{airgaps}} \quad (1.10)$$

An interesting observation of equations (1.8), (1.10) is that in most cases the reluctance in steel can be ignored given that $R_{iron} \ll R_{airgaps}$, which implies

that under these circumstances $MMF \approx u_{M-airgaps}$. Note that the airgap reluctance will become zero when the armature is placed against the ‘C’ core. In that case the $u_{M-airgaps}$ also goes to zero, and this also applies to the MMF. This in turn means that the current becomes zero. Flux *remains*, as its value is controlled by the applied electrical voltage as will become apparent shortly. An alternative view of this problem is to consider the case where a current is forced into the coil, under these conditions a finite MMF would be present with zero reluctance, in which case the flux would theoretically become infinite.

Note that the flux ϕ is the same in each part of the circuit (see figure 1.13) consequently, the product of flux density times cross-sectional area remains the same. Hence in a narrow part of the circuit the flux density will be higher than in a wider part. In the airgaps the effective cross-sectional area is increased due to fringing, hence the flux density in the airgap will be lower than in the adjacent iron circuit.

The magnetic example to be compared with the magnetic structure shown in figure 1.12 has a set of parameters as given in table 1.1.

Table 1.1. Parameters for magnetic ‘C’ core example

Parameters	Value
Total path length in iron	l_c 150 mm
Total path length in air	l_a 20 mm
Core cross-section	A_c 100 mm ²
Airgap cross-section	A_a 100 mm ²
Copper cross-section	A_{cu} 1600 mm ²
Permeability in iron	μ_c 0.008 H/m
Permeability in air	μ_o $4\pi 10^{-7}$ H/m
Number of turns coil	n 1000 turns
Coil current	I 5 A

The m-file written to calculate the magnetic potentials, flux density and flux is as follows:

m-file to flux calculation for C core

```
%M file to flux calculation for C core
clear all % clears all variables in work area
close all % closes figures which were open
%%%%%define variables
A_c=10e-3*10e-3; % cross-section of core and armature 10mm x10 mm
A_a=10e-3*10e-3; % assumed cross-section of airgap
g=10e-3; % distance (airgap) between armature and C core
mu_c=0.64/79.58; % permeability of iron (steel ) sections
mu_o=4*pi*1e-7; % permeability in air
l_c=150e-3; % total length (m) the flux travels in Core and armature
l_a=2*g; % total length flux travels in air
n=1000; % number of turns coil
I=5; % current in coil (Amps)
```

```

MMF=n*I; % MMF coil
R_c=l_c/(A_c*mu_c); % reluctance of steel sections
R_a=l_a/(A_c*mu_0); % reluctance of airgaps
psi=MMF/(R_c+R_a); % flux in circuit
B_c=psi/A_c; % flux density in core and armature
L=n^2/(R_c+R_a); % inductance coil (H)
u_a=R_a*psi; % magnetic potential airgaps
u_c=R_c*psi; % magnetic potential armature and core

```

When this m-file is executed the following data is provided:

Table 1.2. Data from m-file

Parameters		Value
Iron reluctance	R_c	1.8652e+005 At/Wb
Airgap reluctance	R_a	1.5915e+008 At/Wb
Circuit flux	ϕ	3.1379e-005 Wb
Flux density in core, armature and air	B_c	0.3138 T
Magnetic potential across iron	u_c	5.8527 At
Magnetic potential across airgaps	u_a	4.9941e+003 At
Inductance coil	L	6.3 mH

Some interesting observations can be made from the data in table 1.2 namely:

- The magnetic potential across the airgaps is an order of magnitude higher than in the steel. This confirms earlier comments with regard to this topic. Note that the sum of the magnetic potential in air and steel is equal to the MMF ($n * I = 5000$ At (ampère-turns)).
- The flux density value $B_c = 0.31$ T is considerably lower than the values found in figure 1.12(b). The flux density values, as indicated by the colour, in the core and airgap were found to be 1.8T and 0.3T respectively. The main reason for this is that the equivalent circuit model is a linear model which does not exhibit so-called saturation effects. This topic will be discussed shortly. Secondly, the airgap reluctance is not modelled well, i.e. the assumption that all the flux crosses from the ‘C’ core to the armature is not valid.
- The so-called inductance value is also given and this concept will shortly be discussed.

1.6.5 Flux-linkage and self inductance

The term flux-linkage is often required when dealing with the electrical equations which link to the magnetic circuit. The flux-linkage refers to the amount of flux linked with the coil. Each winding turn of the coil ‘sees’ the circuit flux ϕ as can be observed from figure 1.12(a) and this means that the

coil as a whole ‘sees’ the product of the circuit flux and number of turns. This quantity is referred to as the flux-linkage $\psi = n\phi$. Note that this is in fact a simplification and only holds for relatively simple examples as treated in this chapter. For example, if one observes figure 1.11(a), it is hopefully clear that not all the turns are linked with the same circuit flux. Some flux lines stray in between the windings, forming the so-called stray or leakage flux. Leakage inductance and the effects of leakage flux will be considered in later chapters. However, the calculation of the flux-linkage and leakage inductance based on the geometry of magnetic circuits is beyond the scope of this book.

The relationship between flux-linkage and current is readily found by using Hopkinson’s law, which states that the circuit flux is equal to the coil MMF divided by the total reluctance of the magnetic circuit. For the linear example treated above the flux-linkage can be written as

$$\psi = n \frac{MMF}{R_{iron} + R_{airgaps}} \quad (1.11)$$

which can be further simplified using $MMF = n i$ to

$$\psi = \left(\frac{n^2}{R_{iron} + R_{airgaps}} \right) i \quad (1.12)$$

where the term $\left(\frac{n^2}{R_{iron} + R_{airgaps}} \right)$ is known as the coil inductance L (H). Hence the relationship between flux-linkage and current for a *linear* magnetic circuit is given by equation (1.13).

$$\psi = L i \quad (1.13)$$

Expression (1.13) is also represented in graphical form, see figure 1.14. Note that the inductance is determined by the geometry, material properties of the magnetic circuit and the coil number of turns. Figure 1.14 shows a linear relationship between flux-linkage and current. Furthermore, the gradient of the slope is equal to the inductance. This means that the gradient of the function will increase in case the inductance increases, which in turn will take place when the total magnetic reluctance R_m of a magnetic circuit reduces. Zero magnetic reluctance (i.e. infinite inductance) corresponds to a flux-linkage current curve which is aligned with the vertical axis of this figure. This tells us that for a given flux there is *no* current required.

1.6.6 Magnetic saturation

The magnetic reluctance of steel (iron) is not constant as the flux density increases. When the flux density rises to levels typically approaching 2T (tesla or Vs/m²) a marked increase in the magnetic reluctance of the steel occurs. This

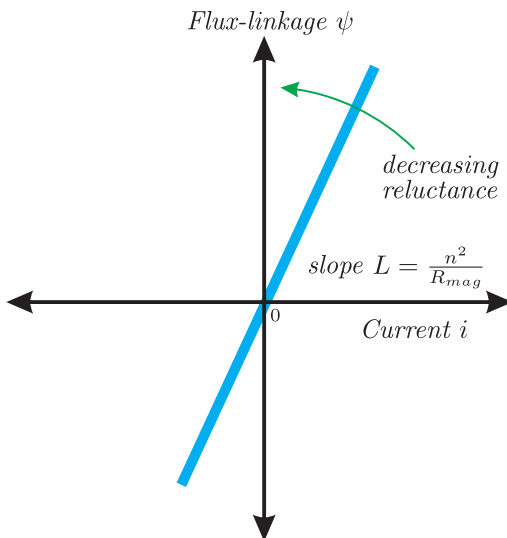


Figure 1.14. Flux-linkage versus current: linear circuit

change in reluctance refers to a phenomenon called saturation which in effect constrains the flux density in magnetic circuits using, for example, Si-steel to values below 2T as may be observed from figure 1.15. The exact saturation

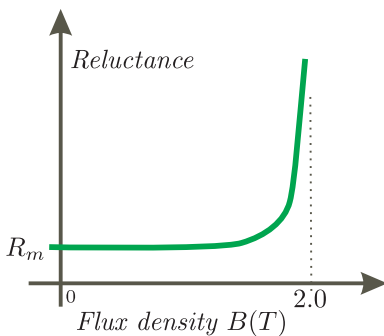


Figure 1.15. Reluctance change due to saturation

level depends very much on the magnetic steel used. Cheaper steel or ferrites tend to have a lower saturation level. Note that the reluctance in air does *not* exhibit saturation.

The change in reluctance directly influences the flux-linkage current curve as an increasing R_m will reduce the slope of the $\psi(i)$ curve as the flux density increases. Note that the latter is proportional to the circuit flux ϕ and flux-linkage ψ value. An example of a flux-linkage current curve for the linear and general case is given in figure 1.16.

Note that the notion of inductance is for the general case not really applicable as the gradient of the function is no longer constant. Hence the term inductance is relevant when considering magnetically linear circuits. So-called non-linear

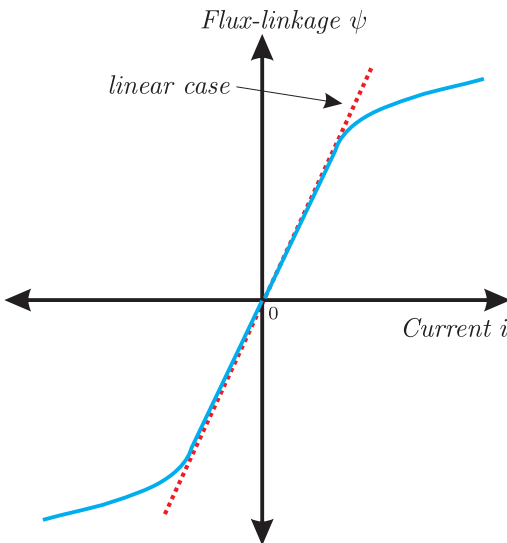


Figure 1.16. Flux-linkage versus current: with saturation effects

circuit analysis will require the use of the general flux-linkage current curve, which must be given or measured for the circuit to be analyzed. At a later stage an example of the use of this curve will be given.

1.7 Machine sizing principles

It is instructive at the end of this chapter to give the reader some insight into the concept of electrical machine sizing. This issue becomes important when faced with, for example, the task of choosing a certain machine size to accommodate a given load application.

In figure 1.9 we have introduced a single wire which was able to produce a force F_e when it was placed in a magnetic field and attached to a current source. This concept can be extended to electrical machines if we consider the latter in the form of a rotor and stator. The rotor, being the rotating component, is assumed to hold on its circumference a set of n wires of thickness d . For convenience of this calculation we will assume that the cross-section of these wires is square rather than round. A magnetic field with flux density B is assumed to be present in the airgap between the rotor and stator. Consequently a resultant force F will be created on the surface of the rotor in case the rotor windings are made to carry a current i . If the rotor radius is set to r and its length to l then the torque T_e produced by the machine will be equal to

$$T_e = rF \quad (1.14)$$

where $F = nBil$. It is instructive to introduce the concept of current density $j = i/A$ where $A = d^2$ represents the cross-sectional area of a wire. If we consider the entire circumference of the rotor packed with n wires placed next

to each other then we can approximate the total coil area $A_w = nA \approx d2\pi r$. Use of this approximation together with the expression for F_e , allows us to approximate expression (1.14) as

$$T_e \approx kBj\underbrace{\pi r^2 l}_{V_r} \quad (1.15)$$

where k is a machine constant ($k = 2d$ in this case). V_r represents the rotor volume. Equation (1.15) is significant in that it tells us that the torque is proportional to the product of flux density B , current density j and rotor volume V_r .

In this chapter we have already shown that magnetic saturation places a constraint on the flux density value we can practically use. Furthermore, current density values are typically constrained to values less than 10A/mm^2 given thermal considerations. Hence it follows that the rotor size and consequently the total size of a machine will need to be chosen to meet a certain torque requirement. The ratio between torque and rotor volume, known as *TRV* [Miller, 1989], is therefore an important figure for machine sizing. For industrial machines this value is typically in the order of $15\text{-}30\text{kNm/m}^3$. In linear-motors as well as rotating machines the same number can be interpreted as the maximum shear-stress of $15\text{-}30\text{kN/m}^2$ (thrust per unit area).

The overall size of the machine is determined by the stator volume which is determined amongst other factors by the rotor volume V_r . A rough estimate of the stator volume SV as given by [Miller, 1989] is of the form

$$SV \approx \frac{V_r}{srs^2} \quad (1.16)$$

where srs is a constant in the order of 0.6.

It is instructive to give a numerical example of such a sizing calculation. Consider a machine which must produce a torque of 70Nm . If we assume that the rotor diameter is equal to its length then the rotor diameter (and length) would be equal to 164mm in case we assume a TRV of 20kNm/m^3 . The corresponding stator diameter would according to equation (1.16) be 259mm which is a realistic expectation for a machine. In reality, the machine length would be longer than the estimated value of 164mm given the need to accommodate the stator winding at both ends of the machine as well as the rotor bearings and cooling fan-blades.

1.8 Tutorials for Chapter 1

1.8.1 Tutorial 1

The model given in figure 1.17 (cross-section shown) is rotational symmetric. A single $n = 1000$ turn coil is shown which carries a current of $i_{coil} = 5\text{A}$. The steel used has a permeability of $10^6\mu_0$, where μ_0 represents the permeability in vacuum (air). The key dimensions (in millimeters) are shown in figure 1.17.

The model in question was analyzed with a finite element package and gave the results as given in table 1.3.

Table 1.3. Output finite element program

Output variable		Value
Flux density in airgap	B_a	0.62 T
Flux linked with coil	ψ	10.9 Wb
Self inductance	L	2.19 H

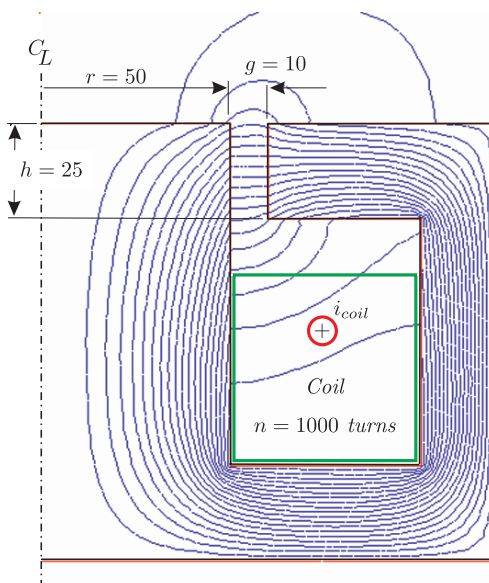


Figure 1.17. Magnetic model

Perform a ‘sanity check’ on the results obtained from your magnetic (finite element) analysis by using an alternative method. An example solution to this type of problem is given below: Firstly, we know that the steel used has a high permeability which is very much larger than that of air. Consequently we can assume that the magnetic potential across the steel will be very much lower than that across the airgap. Hence the first assumption to make is that the magnetic potential u_a across the airgap is approximately equal to the applied MMF, hence $u_a \approx ni_{coil}$. The second critical issue here is to make a sensible judgement with respect to the cross-sectional area which the flux ‘sees’ when crossing the airgap g . If there was no ‘fringing’ then the airgap cross-section would be equal to $A_c = 2 * \pi * (r + g/2) h$, where we have chosen a ring of width ‘ h ’ placed on the middle of the airgap at radius $r + g/2$. An observation of figure 1.17 learns that the flux crossing the airgap has a larger cross-sectional

area. The difficulty lies in finding a good estimate for this airgap area, which takes fringing into account. The so-called ‘Carter’ factor is often used to allow for fringing effect. In our calculation we will assume that this factor is equal to $C = 2$, this is based on the fact that we observe a significant number of flux lines at twice the ‘ h ’ value.

The magnetic reluctance is then found using equation (1.6b) with $l_{airgap} = g$, $A_{airgap} = A_c C$. This in turn leads to the circuit flux $\phi = MMF_a/R_{airgap}$, flux-linkage $\psi = n\phi$ and self inductance $L = \psi/i_{coil}$.

The m-file as given below, shows the calculations carried out to arrive at the required variables.

m-file Tutorial 1, chapter 1

```
% Tutorial 1, chapter 1
% parameters
r=50e-3; % radius
g=10e-3; % gap
h=25e-3; % core height
n=1000; % number of turns coil
i_coil=5; % coil current (A)
uo=4*pi*1e-7; % permeability vacuum
%%%%
C=2; % multiplication factor to account for fringing
% (Carter factor)
A_g=2*pi*(r+g/2)*h*C; % airgap area
R_g=g/(uo*A_g); % reluctance airgap
%%%%
MMF=n*i_coil; % MMF coil
u_a=MMF; %
phi_a=u_a/R_g; % calculation flux-density in airgap
B_g=phi_a/A_g % calculation flux linked with coil
psi=n*phi_a % self inductance
L=psi/i_coil %
```

After running this m-file the results as given in table 1.4 were found. The results from the m-file agree very well with those obtained from the finite element program. The reason for this is that we have chosen a good estimate for the airgap cross-sectional area. In reality estimating the effect of flux fringing is difficult.

Table 1.4. Output m-file

Output variable	Value
Flux density in airgap	B_a
Flux linked with coil	ψ
Self inductance	L

1.8.2 Tutorial 2

This tutorial considers an ‘E’ core type structure as shown in figure 1.18. The distance between the ‘I’ segment, which is also part of the total magnetic circuit and ‘E’ core is 10mm. A 500 turn coil is wound around the center leg of the ‘E’ core and carries a current of 20A. The depth of both magnetic components is taken to be 20mm. Furthermore, the magnetic material is taken to be magnetically ideal. Key dimensions (in mm) are shown in figure 1.18 which relate to the airgaps between the two magnetic components. The permeability of air is given in the previous tutorial.

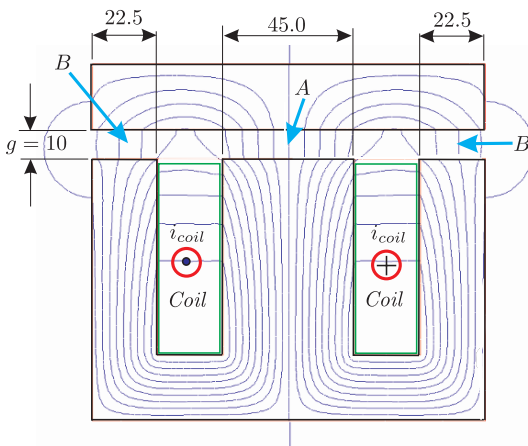


Figure 1.18. Magnetic ‘E’ core example

The aim of the tutorial is to demonstrate the importance of finite element modelling and to emphasize that the results obtained with linear models should be used with care.

Perform a linear analysis of this problem and estimate with the aid of an equivalent magnetic circuit the flux density in the airgaps at locations A and B respectively. In addition, estimate the total flux ψ_A linked with the coil. A possible solution to this problem is as follows.

The equivalent magnetic circuit with the conditions specified, i.e. ideal magnetic material, is shown in figure 1.19.

The ‘MMF’ which is equal to $MMF = n_{coil} i_{coil}$ must be equal to the sum of the magnetic potentials u_A and u_B . The reluctances R_A and R_B of the center and side legs of the ‘E’ core require an estimation of the area of the flux which crosses between the two magnetic circuit components. A relatively large airgap is used in this example which leads to considerable magnetic fringing. If we ignore fringing for the linear calculation, we are able to determine the reluctances with the aid of the dimensions given in figure 1.19. The m-file shown at the end of this tutorial shows the calculations which lead to the required variables namely: $B_A = 0.628\text{T}$, $B_B = 0.628\text{T}$ and $\psi_A = 0.28\text{Wb}$. It is noted

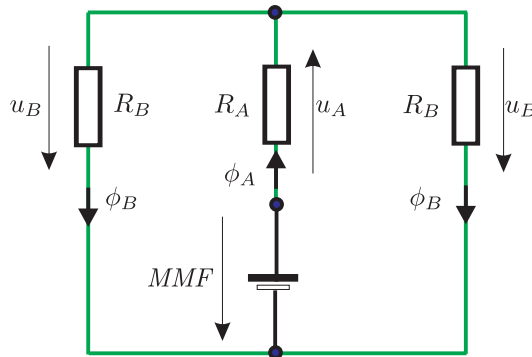


Figure 1.19. Magnetic ‘E’ core equivalent circuit

that the flux density polarities at locations A, B will according to figure 1.19 be in opposition (flux goes out of the center ‘E’ core leg and back into the side legs). The amplitudes are equal because the circuit flux in the side legs is half that of the center legs. Furthermore, the airgap areas of the side legs are half that of the center leg if flux fringing is ignored.

An example of the absolute flux density plot as function of the position along an imaginary line (the length of which corresponds to the width of the ‘E’ core) which passes through points A and B in the airgap is shown in figure 1.20. The flux density plot according to figure 1.20 was obtained with the aid of a

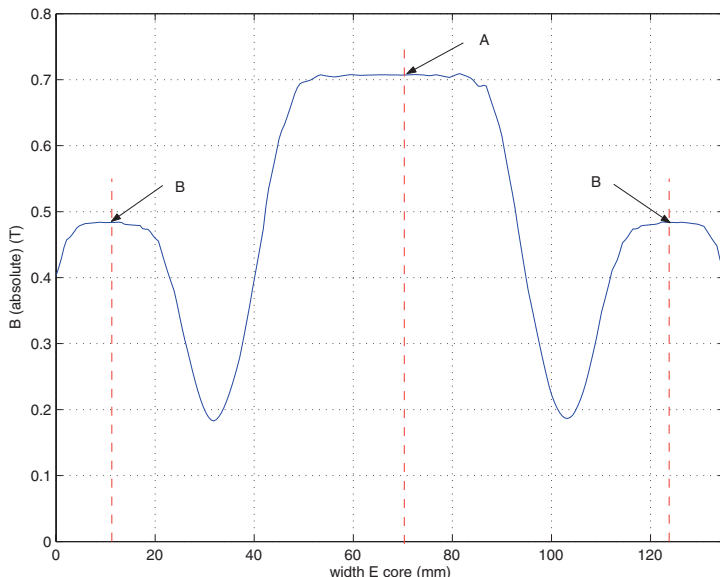


Figure 1.20. Flux density plot along airgap in the ‘E’ core

two-dimensional finite element package which was also used to calculate the flux distribution shown in figure 1.18. Observation of figure 1.20 learns that the flux density values at points A , B are markedly different when compared to the linear case. Furthermore, the coil flux-linkage was calculated with the same finite element program and the value was found to be 0.63Wb, which is considerably higher than the value obtained via the linear analysis (as given above). The reasons for the differences between the two computation methods can to a large extend be attributed to the effects of fringing, i.e. the difficulty of determining an accurate estimate of the flux area required to calculate the reluctances R_A and R_B . Furthermore, the assumption of an ideal magnetic material may also severely affect the result, in particular if saturation effects come into play. Finally, it is noted that even a two-dimensional finite element may not always be suitable, in which case a three-dimensional analysis may need to be undertaken.

m-file Tutorial 2, chapter 1

```
% Tutorial 2, chapter 1
% parameters
depth=20e-3;           % thickness E and I core
g=10e-3;                % gap
w_A=45e-3;              % E core center leg width
w_B=22.5e-3;            % E core side leg width
n=500;                  % number of turns coil
i_coil=20;               % coil current (A)
uo=4*pi*1e-7;           % permeability vacuum
%%%%%%%%%%%%%%%%%%%%%%%%%%%%%%%%%%%%%
A_gA=w_A*depth;         % airgap area center leg
A_gB=w_B*depth;         % airgap area side leg
R_A=g/(uo*A_gA);        % reluctance center leg
R_B=g/(uo*A_gB);        % reluctance side leg
R_tot=R_A+R_B/2;         % total reluctance seen by MMF
%%%%%%%%%%%%%%%%%%%%%%%%%%%%%%%%%%%%%
MMF_c=n*i_coil;         % MMF coil
phi_A=MMF_c/R_tot % calculation fluxdensity in center leg airgap
B_A=phi_A/A_gA % calculation fluxdensity in side leg airgap
phi_B=phi_A/2;          % flux to both side legs equal
B_B=phi_B/A_gB % calculation flux linked with coil
psi=n*phi_A
```

Chapter 2

SIMPLE ELECTRO-MAGNETIC CIRCUITS

2.1 Introduction

The simplest component utilising electro-magnetic interaction is the coil. The coil is a buffer component which stores energy in magnetic form. Air-cored coils are frequently used (for example in loudspeaker filters), but coils with a core of (possibly gapped-) magnetic material are more common because of their increased inductance (or reduced size), which comes at the cost of reduced maximum field strength and increased non-linearity.

In this chapter we will develop a generic model of a coil with linear and non-linear self inductance. Furthermore, the effect of coil resistance is considered. The use of phasors is introduced in this chapter as a means to verify simulation of such circuits when connected to a sinusoidal source.

2.2 Linear inductance

The physical representation of the coil considered here is given in figure 2.1. The figure shows a coil with n turns which is wrapped around a toroidally shaped non-gapped magnetic core with cross-sectional area A_m . The permeability of the material is given as μ and the average flux path length is equal to l_m . Analog to equations (1.6), the magnetic reluctance of the circuit is: $R_m = \frac{l_m}{A_m \mu}$ and the inductance is $L = n^2 \mu A_m / l_m = n^2 / R_m$.

The relation between the magnetic flux and the current in the coil is described by the expression

$$\psi = L i \quad (2.1)$$

With Faraday's law

$$u = \frac{d\psi}{dt} \quad (2.2)$$

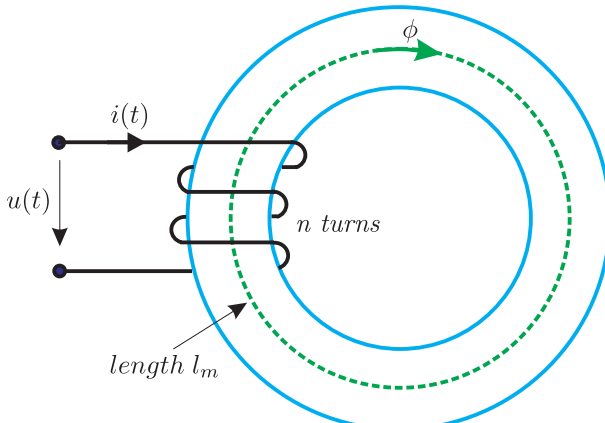


Figure 2.1. Toroidal inductance

equation (2.1) can be rewritten to the more familiar differential form of the coil's voltage terminal equation

$$u = L \frac{di}{dt} \quad (2.3)$$

Equation (2.3) can be integrated on both sides and rewritten as the general equation

$$i(t) = \frac{1}{L} \int_{-\infty}^t u(t) dt \quad (2.4)$$

The whole integrated history of the inductor voltage is reflected by the inductor current, so equation (2.4) can be expressed in a more practical form starting at $t = 0$ with initial condition $i(0)$ according

$$i(t) = \frac{1}{L} \int_0^t u(t) dt + i(0) \quad (2.5)$$

This integral form can be developed further

$$\Delta i = \frac{\Delta \psi}{L} \quad (2.6)$$

$$\underbrace{\psi(t) - \psi(0)}_{\Delta \psi} = \int_0^{t_0} u(t) dt \quad (2.7)$$

introducing the concept of ‘incremental flux-linkage’ $\Delta\psi = \psi(t) - \psi(0)$ which is fundamental to the control of electrical drives. The equation basically states that a flux-linkage variation corresponds with a voltage-time integral. At a later stage we will introduce the variable ‘incremental flux’ $\Delta\Psi$, which is equal to $\Delta\psi$ in case the coil resistance is zero.

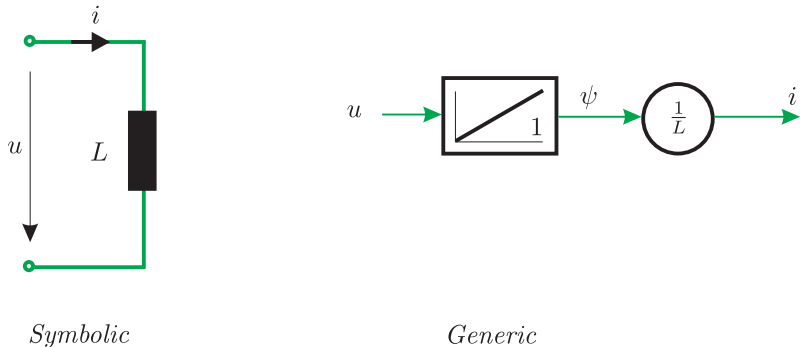


Figure 2.2. Symbolic and generic model of linear inductance

A symbolic and generic model of the ideal coil is given in figure 2.2. With the model of figure 2.2 we will now simulate the time-response of a coil in reaction to a voltage pulse of magnitude \hat{u} and duration T , starting at $t = t_0$, as displayed in figure 2.3. Integrating the supply voltage u over time, we get the flux Ψ in the coil, which linearly increases from 0 at $t = t_0$ to $\hat{u}T$ at $t = T$. The current is then obtained by dividing the flux Ψ by L .

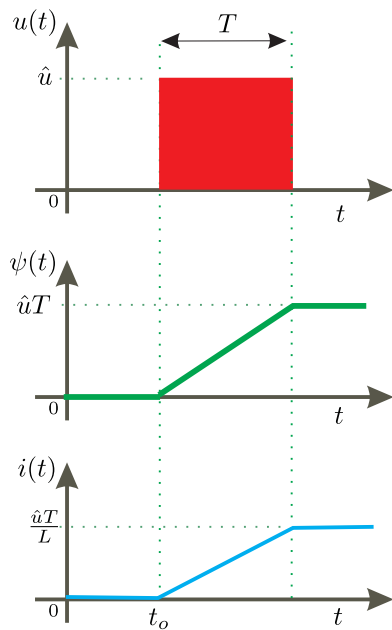


Figure 2.3. Transient response of inductance

2.3 Coil resistance

In practical situations the resistance of the coil wire can usually not be neglected. Wire resistance can simply be modelled as a resistor in series with the ideal coil. The modified symbolic model is shown in figure 2.4.

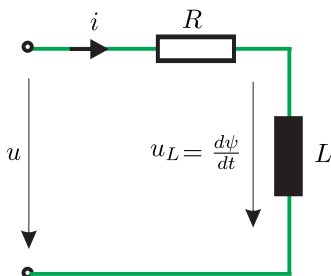


Figure 2.4. Symbolic model of linear inductance with coil resistance

Figure 2.4 shows that the coil flux is no longer equal to the integrated supply voltage u . Instead the variable u_L is introduced, which refers to the voltage across the ‘ideal’ (zero resistance) inductance $u_L = \frac{d\psi}{dt}$. The terminal equation for this circuit is now

$$u = iR + \frac{d\psi}{dt} \quad (2.8)$$

where R represents the coil resistance. The corresponding generic model of the ‘L, R’ circuit is shown in figure 2.5. The generic model clearly shows how the inductor voltage u_L is decreased by the resistor voltage caused by the current through the coil.

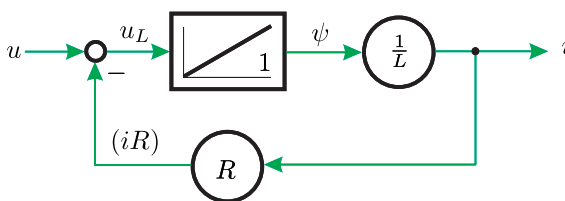


Figure 2.5. Generic model of linear inductance with coil resistance, dynamic simulation shown in figure 2.12

2.4 Magnetic saturation

As discussed in chapter 1, the maximum magnetic flux density in magnetic materials is limited. Above the saturation flux density, the magnetic permeability μ drops and the material will increasingly behave like air, i.e. $\mu \rightarrow \mu_0$ as flux is increased further. Since motors usually work at high flux density levels, with noticeable saturation, it is essential to incorporate saturation in our coil model.

The relationship between flux-linkage and current is in the magnetically linear case determined by the inductance as was shown by figure 1.14. In reality

the $\psi(i)$ relationship is only relatively linear over a limited region (in case the magnetic circuit contains ‘iron’ (steel) elements) as was shown in figure 1.16. The generic model according to figure 2.5 needs to be revised in order to cope with the general case.

The generic building block for non-linear functions [Leonhard, 1990] is shown in figure 2.6. The double edged box indicates a non-linear module with

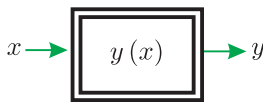


Figure 2.6. Non-linear generic building block

input variable x and output variable y . The relationship between output and input is shown as $y(x)$ (y as a function of the input x). In some cases a symbolic graph of the function to be implemented may also be shown on this building block.

The non-linear module has the coil flux ψ as input and the current i as output. Hence the non-linear function of the module is described as $i(\psi)$, which expresses the current of the coil as a function of the coil flux. The terminal equation (2.8) remains unaffected by the introduction of saturation, only the gain module $\frac{1}{L}$ shown in figure 2.5 must be replaced by the non-linear module described above. The revised generic model of the coil is shown in figure 2.7.

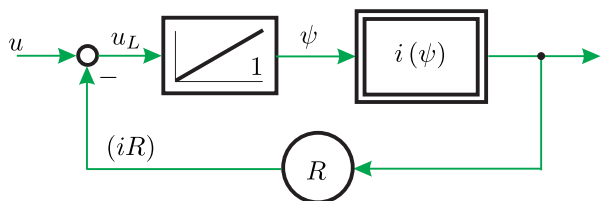


Figure 2.7. Generic model of general inductance model with coil resistance, dynamic simulation shown in figures 2.17 and 2.18

2.5 Use of phasors for analyzing linear circuits

The implementation of generic circuits (such as those discussed in this chapter) in Simulink allows us to study models for a range of conditions. The use of a sinusoidal excitation waveform is of most interest given their use in electrical machines/actuators. However, there must be a way to perform ‘sanity checks’ on the results given by simulations. Analysis by way of phasors provides us with a tool to look at the steady-state results of linear circuits.

The underlying principle of this approach lies with the fact that a sinusoidal excitation function, for example the applied voltage, will cause a sinusoidal output function of the same frequency, be it that the amplitude and phase (with respect to the excitation function) will be different. For example: in the symbolic circuit shown in figure 2.4, the excitation function will be defined as

$u(t) = \hat{u} \sin(\omega t)$, where \hat{u} and ω represent the peak amplitude and angular frequency (rad/s) respectively. Note that the latter is equal to $\omega = 2\pi f$, where f represents the frequency in Hz. The output variables are the flux-linkage $\psi(t)$ and current $i(t)$ waveforms. Both of these will also be sinusoidal, be it that their amplitude and phase differ from the input signal $u(t)$.

In general, a sinusoidal function can be described by

$$x(t) = \hat{x} \sin(\omega t + \rho) \quad (2.9)$$

This function can also be written in complex notation as

$$x(t) = \Im \left\{ \hat{x} e^{j(\omega t + \rho)} \right\} \quad (2.10)$$

Equation (2.10) makes use of ‘Euler’s rule’ $e^{jy} = \cos y + j \sin y$. The imaginary part of this expression is defined as $\Im \{e^{jy}\} = \sin y$. $\Im \{\cdot\}$ is the imaginary operator, which takes the imaginary part from a complex number. Note that the analysis would be identical with $x(t)$ in the form of a cosine function. In the latter case it would be more convenient to use the real component of $\hat{x} e^{j(\omega t + \rho)}$ using the real operator $\Re \{\cdot\}$. Equation (2.10) can be rewritten to separate the time dependent component $e^{(j\omega t)}$ namely:

$$x(t) = \Im \left\{ \underbrace{\hat{x} e^{j\rho}}_{\underline{x}} e^{j(\omega t)} \right\} \quad (2.11)$$

The non time dependent component in equation (2.11) is known as a ‘phasor’ and is generally identified by the notation \underline{x} . Note that the phasor will in general have a real and imaginary component and can therefore be represented in a complex plane.

In many cases it is also convenient to use the time differential of $x(t)$ namely $\frac{dx}{dt}$. The time differential of the function $x(t) = \Im \left\{ \underline{x} e^{j(\omega t)} \right\}$ is

$$\frac{dx}{dt} = \Im \left\{ j\omega \underline{x} e^{j(\omega t)} \right\} \quad (2.12)$$

which implies that the differential of the phasor \underline{x} is calculated by multiplying \underline{x} with $j\omega$.

2.5.1 Application of phasors to a linear inductance with resistance network

As a first example of the use of phasors, we will analyze a coil with linear inductance and non-zero wire resistance, as shown in figure 2.4. We need to calculate the steady-state flux-linkage and current waveforms of the circuit. The

differential equation set for this system is

$$u = iR + \frac{d\psi}{dt} \quad (2.13a)$$

$$\psi = Li \quad (2.13b)$$

The flux-linkage differential equation is found by substitution of (2.13b) into (2.13a) which gives

$$u = \frac{R}{L}\psi + \frac{d\psi}{dt} \quad (2.14)$$

The applied voltage will be $u = \hat{u} \sin \omega t$, hence the phasor representation of the input signal according to (2.11) is: $\underline{u} = \hat{u}$.

The flux-linkage will also be a sinusoidal function, albeit with different amplitude and phase: $\psi = \hat{\psi} \sin(\omega t + \rho_\psi)$ in which the parameters $\hat{\psi}$, ρ_ψ are the unknowns at this stage. In phasor representation, the flux time function can be written as $\psi = \Im \{ \underline{\psi} e^{j\omega t} \}$ where $\underline{\psi} = \hat{\psi} e^{j\rho_\psi}$.

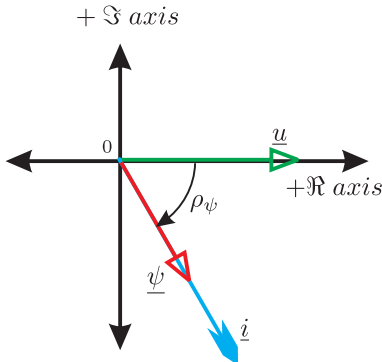


Figure 2.8. Complex plane with phasors: \underline{u} , $\underline{\psi}$, \underline{i}

Rewriting equation (2.14) using these phasors, we get

$$\underline{u} = \frac{R}{L} \underline{\psi} + j\omega \underline{\psi} \quad (2.15)$$

from which we can calculate the flux phasor by reordering, namely

$$\underline{\psi} = \frac{\underline{u}}{\left(\frac{R}{L} + j\omega \right)} \quad (2.16)$$

The amplitude and phase angle of the flux phasor are now

$$\hat{\psi} = \frac{\hat{u}}{\sqrt{\left(\frac{R}{L} \right)^2 + \omega^2}} \quad (2.17a)$$

$$\rho_\psi = -\arctan \left(\frac{\omega L}{R} \right) \quad (2.17b)$$

and the corresponding current phasor is according to equation (2.13b): $i = \frac{\psi}{L}$.

The transformation of phasors back to corresponding time variable functions is carried out with the aid of equation (2.11). A graphical representation of the input and output phasors is given in the complex plane shown in figure 2.8.

2.6 Tutorials for Chapter 2

2.6.1 Tutorial 1

In this chapter we analyzed a linear inductance and defined the symbolic and generic models as shown in figure 2.2. The aim is to build a Simulink model from this generic diagram. An example as to how this can be done is given in figure 2.9. Shown in figure 2.9 is the inductance model in the form of an integrator and gain module. Also given are two ‘step’ modules, which together with a ‘summation’ unit generate a voltage pulse of magnitude 1V. This pulse should start at $t = 0$ and end at $t = 0.5\text{s}$.

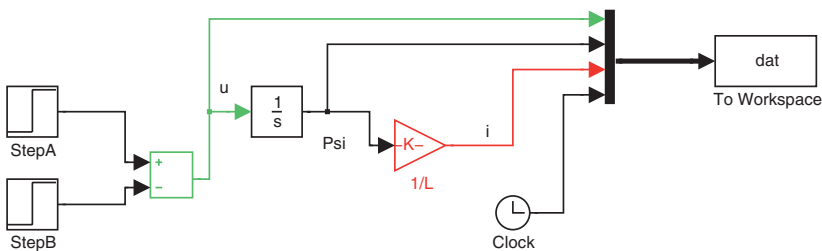


Figure 2.9. Simulink model of linear inductance with excitation function

Build this circuit and also add a ‘To Workspace’ module (select the option ‘array’) together with a ‘multiplexer’ which allows you to collect your data for use in MATLAB. In this exercise we look at the input voltage waveform, the flux-linkage and current versus time functions. Once you have built the circuit you need to run this simulation and for this purpose you need to set the ‘stop time’ (under Simulations/simulation parameters dialog window) to 1s. The inductance value used in this case is $L = 0.87\text{H}$. Plot your results by writing an m-file to process the data gathered by the ‘To Workspace’ module. An example of an m-file which will generate the required results is given at the end of this tutorial.

The results which should appear from your simulation after running this m-file are given in figure 2.10. The dynamic model as discussed above is to be extended to the generic model shown in figure 2.5. Add a coil resistance of $R = 2\Omega$ to the Simulink model given in figure 2.9. The new model should be of the form given in figure 2.11.

Rerun the simulation and m-file. The results should be of the form given by figure 2.12.

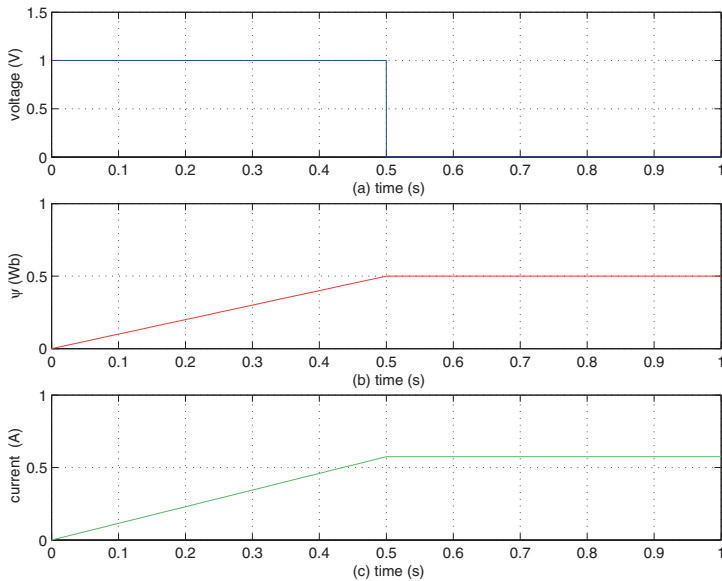


Figure 2.10. Simulink results: Ideal inductance simulation

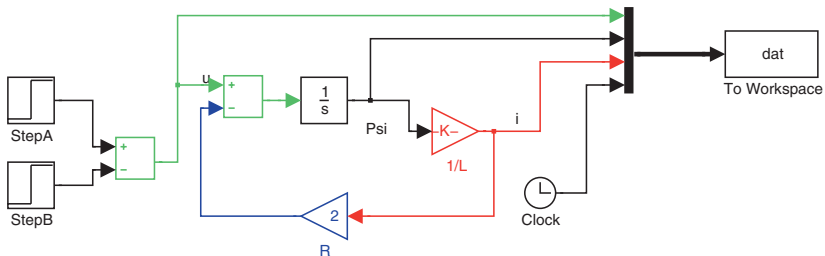


Figure 2.11. Simulink model of linear inductance with resistance and excitation function

m-file Tutorial 1 chapter 2

```
%Tutorial 1, chapter 2
close all
L=0.87; %inductance value (H)
subplot(3,1,1)
plot(dat(:,4),dat(:,1)); % voltage input
xlabel(' (a) time (s)')
ylabel('voltage (V)')
grid
axis([0 1 0 1.5]); %set axis values
subplot(3,1,2)
plot(dat(:,4),dat(:,2),'r'); % flux-linkage
xlabel(' (b) time (s)')
ylabel('\psi (Wb)')
grid
axis([0 1 0 1]); %set axis values
```

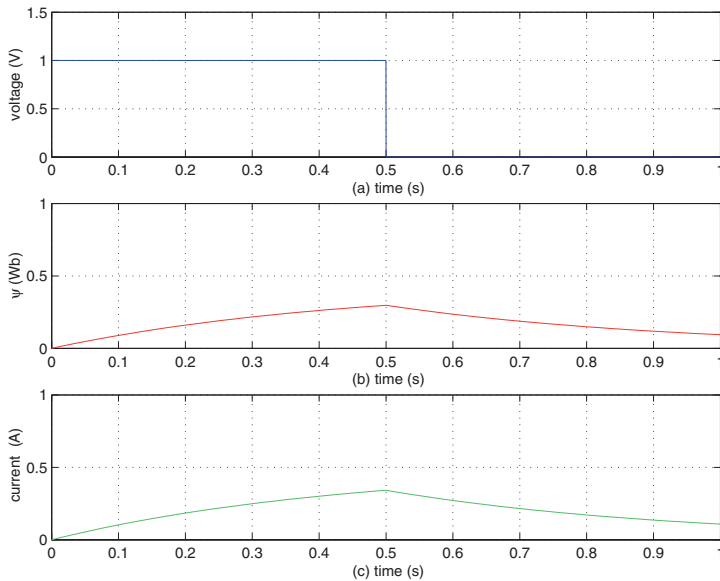


Figure 2.12. Simulink results: inductance simulation, with coil resistance

```

subplot(3,1,3)
plot(dat(:,4),dat(:,3),'g');    % current
xlabel(' (c) time (s)')
ylabel(' current (A)')
grid
axis([0 1 0 1]);             %set axis values

```

2.6.2 Tutorial 2

In this tutorial we will consider an alternative implementation of tutorial 1, based on the use of Caspoc [van Duijsen, 2005] instead of Simulink [Mathworks, 2000]. Build a Caspoc model of the generic model shown in figure 2.5 with the excitation and circuit parameters as discussed in tutorial 1.

An example of a Caspoc implementation is given in figure 2.13 on page 39. The values which are shown with the variables are those at the time instant when the simulation was stopped. The ‘scope’ modules given in figure 2.13 display the results of the simulation. Note that these display modules may be enlarged by ‘left clicking’ on the modules, in which case detailed simulation results are presented. The simulation results obtained with this simulation should match those given in figure 2.12.

2.6.3 Tutorial 3

In section 2.4 we have discussed the implications of saturation effects on the flux-linkage/current characteristic. In this tutorial we aim to modify the

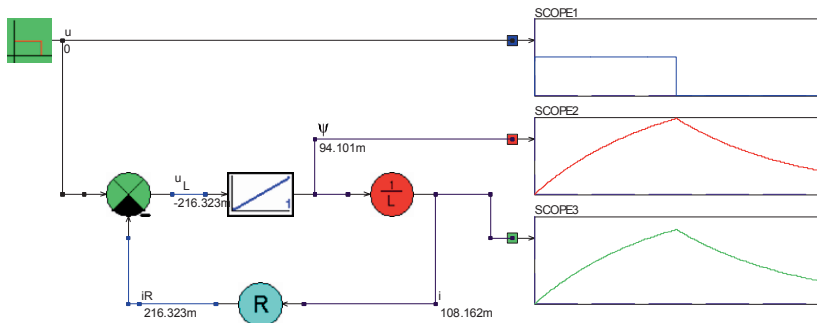


Figure 2.13. Caspoc simulation: linear inductance with coil resistance

simulation model discussed in the previous tutorial (see figure 2.11) by replacing the linear inductance component with a non-linear function module as shown in the generic model (see figure 2.7). In this case the flux-linkage/current $\psi(i)$ relationship is taken to be of the form $\psi = \tanh(i)$ as shown in figure 2.14. Note that in this example the gradient of the flux-linkage/current curve becomes zero for currents in excess of $\pm 3\text{ A}$. In reality the gradient will be non-zero when saturation occurs.

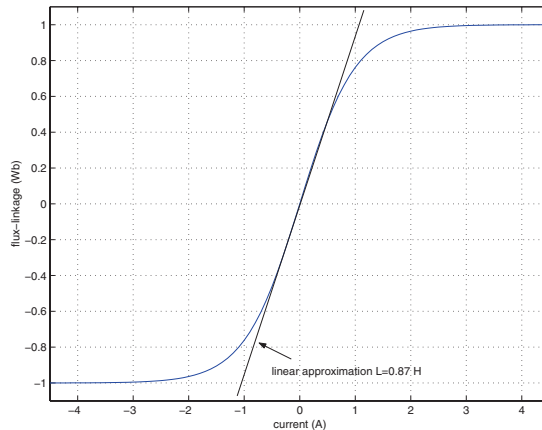


Figure 2.14. Flux-linkage/current $\psi(i)$ relationship

The coil resistance of the coil is increased to $R = 100\text{ }\Omega$. An example of a Simulink implementation as given in figure 2.15 clearly shows the presence of the non-linear module used to implement the function $i(\psi)$. The non-linear module has the form of a ‘look-up’ table which requires two vectors to be entered. When you open the dialog box for this module provide the following entries under: ‘vector of input values:’ set to $\tanh([-5:0.1:5])$, and ‘vector

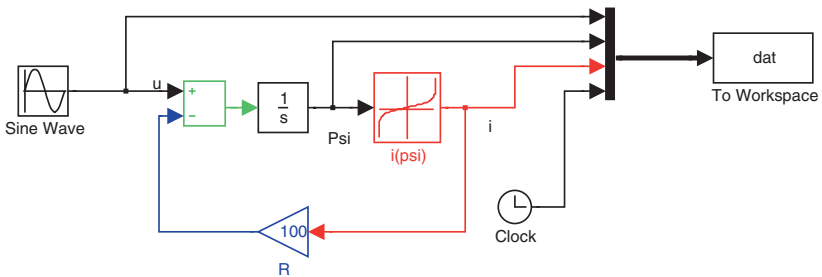


Figure 2.15. Simulink model of non-linear inductance with sinusoidal excitation function

of output values': set to $[-5:0.1:5]$. Also given in figure 2.15 is a 'sine wave' module, which in this case must generate the function $u = \hat{u} \cos \omega t$, where $\omega = 100 \pi (\text{rad/s})$ and \hat{u} is initially set to $\hat{u} = 140 \sqrt{2} \text{V}$. Note that a cosine function is used, which means that in the 'sinus module' dialog box (under 'phase') a phase angle entry is required, which must be set to $\pi/2$ (Simulink knows the meaning of π hence you can write this as 'pi' in Simulink/MATLAB).

Once the new Simulink model has been completed run this simulation for a time interval of 40ms. For this purpose set the 'stop time' (under Simulations/simulation parameters dialog window) to 40ms. Rerun your m-file to obtain the output in the form of the excitation voltage, current and flux-linkage versus time functions. An example of the results obtained with this simulation under the present conditions is given in figure 2.16. The results as given in figure 2.16, also include two 'm-file' functions which represent the results obtained via a phasor analysis to be discussed below.

To obtain some idea as to whether or not the simulation results discussed in this tutorial are correct, we calculate the steady-state flux-linkage and current versus time functions by way of a phasor analysis. An observation of the current amplitude shows that according to figure 2.14 operation is within the linear part of the current/flux-linkage curve. Assume a linear approximation of this function as shown in figure 2.14. This approximation corresponds to an inductance value of $L = 0.87 \text{H}$.

The input function $u = \hat{u} \cos \omega t$ may also be written as

$$u(t) = \Re \left\{ \underbrace{\hat{u}}_u e^{j(\omega t)} \right\} \quad (2.18)$$

where in this case the phasor $\underline{u} = \hat{u} = 140\sqrt{2}$.

The actual phasor analysis must be done in MATLAB which also allows you to use complex numbers directly. For example, you can specify a phasor in MATLAB form by $xp=3+j*5$ and a reactance $X=100*pi*L$, where $L = 0.87 \text{H}$.

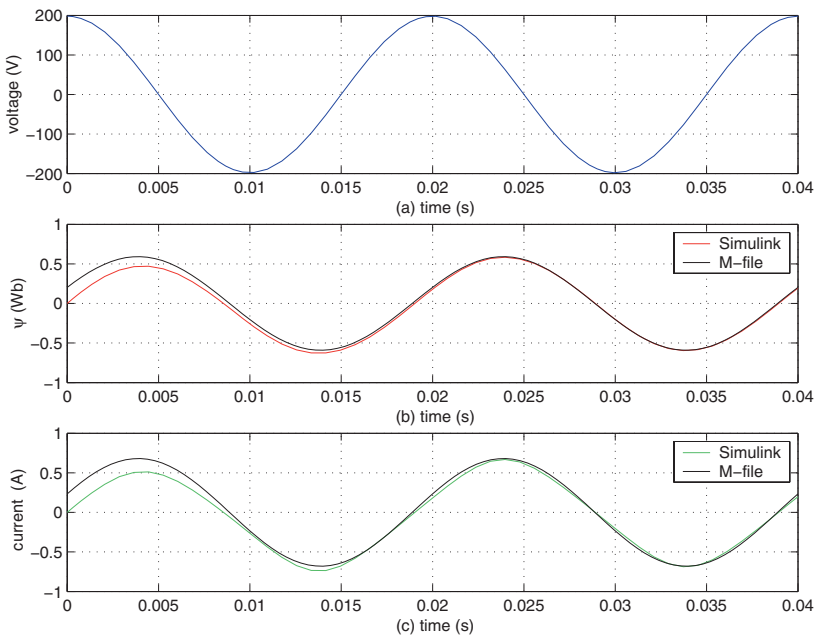


Figure 2.16. Simulink/m-file results: Inductance simulation, with coil resistance and non-linear $i(\psi)$ function

Write an m-file which will calculate the current and flux phasors. In addition calculate and plot the instantaneous current and flux versus time waveforms and add these to the results from the Simulink simulation. An example of such an m-file is given at the end of this tutorial, which also shows the code required to plot the results from the Simulink model.

The results obtained after running this m-file are shown in figure 2.16 (in ‘black’), together with the earlier Simulink results. A comparison between the results obtained via the Simulink model and phasor analysis (see figure 2.16), shows that the results merge towards the end of the simulation time. In the first part of the simulation the transient effects dominate, hence the discrepancy between the simulation results and those calculated via a phasor analysis.

m-file Tutorial 3 chapter 2

```
%Tutorial 3, chapter 2
close all
L=0.87;                                %inductance value (H)
R=100;                                   %resistance
subplot(3,1,1)
plot(dat(:,4),dat(:,1));                 % voltage input
xlabel(' (a) time (s)')
ylabel('voltage (V)')
grid
```

```

%%%%%
% subplot(3,1,2)
plot(dat(:,4),dat(:,2),'r'); % flux-linkage
xlabel(' (b) time (s)')
ylabel('\psi (Wb)')
grid
%%%%%
% subplot(3,1,3)
plot(dat(:,4),dat(:,3),'g'); % current
xlabel(' (c) time (s)')
ylabel(' current (A)')
grid
%%%%%
% complex analysis
u_ph=140*sqrt(2); %voltage phasor
w=2*pi*50; %excitation frequency (rad/)
X=w*L;%reactance
i_ph=u_ph/(R+j*X); %current phasor
i_pk=abs(i_ph); %peak current value
i_rho=angle(i_ph); % angle current phasor
psi_ph=i_pk*L;%flux phasor
psi_pk=abs(psi_ph); %peak value flux
psi_rho=angle(psi_ph); %angle current phasor
%%%%%plot results
time=[0:40e-3/100:40e-3];
i_t=i_pk*cos(w*time+i_rho); %current/time function
psi_t=psi_pk*cos(w*time+psi_rho); %flux/time function
subplot(3,1,3)
hold on
plot(time,i_t,'k'); %add result to plot 3
legend('Simulink','m-file')
subplot(3,1,2)
hold on
plot(time,psi_t,'k'); %add result to plot 2
legend('Simulink','m-file')

```

2.6.4 Tutorial 4

It is instructive to repeat the analysis given in tutorial 3 by changing the peak supply voltage to $\hat{u} = 240\sqrt{2}$ in the Simulink model and m-file. An example of the results which should appear after running your files is given in figure 2.17.

A comparison between the results obtained via the phasor analysis and Simulink simulation shows that the two are now decidedly different. The reason for the discrepancy is that the increased supply voltage level has increased the flux levels as to cause operation of the inductance into the non-linear regions of the flux-linkage/current curve. Note that the phasor analysis uses the same $L = 0.87\text{H}$ inductance value. To prevent invalid conclusions, we must be aware that this analysis tool is only usable for linear models.

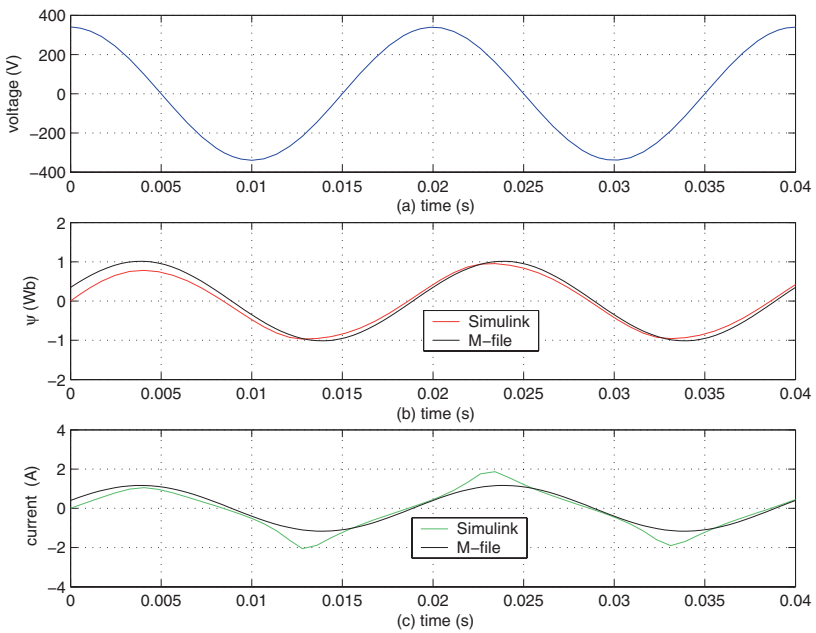


Figure 2.17. Simulink/m-file results: Induction simulation, with coil resistance, non-linear $i(\psi)$ and higher peak voltage

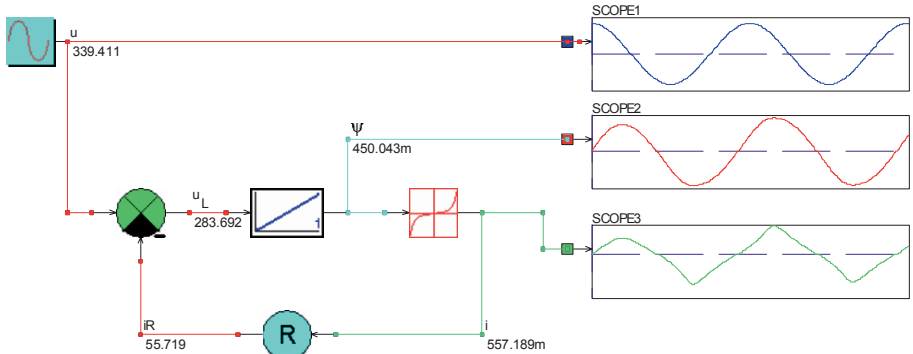


Figure 2.18. Caspoc simulation: general inductance model with coil resistance

2.6.5 Tutorial 5

A Caspoc based implementation of tutorial 4 is considered here. Build a Caspoc model of the generic diagram shown in figure 2.7. Use the parameters and excitation as defined in tutorial 4. A Caspoc implementation example as given in figure 2.18 shows the simulation results. These results should correspond with those given in figure 2.17.

Chapter 3

THE TRANSFORMER

3.1 Introduction

The aim of this chapter is to introduce the ‘ideal transformer’ (ITF) concept. Initially, a single phase version is discussed which forms the basis for a transformer model. This model will then be extended to accommodate the so-called ‘magnetizing’ inductance and ‘leakage’ inductance. Furthermore, coil resistances will be added to complete the model. Finally, a reduced parameter model will be shown which is fundamental to machine models. As in the previous chapters, symbolic and generic models will be used to support the learning process and to assist the readers with the development of Simulink/Caspoc models in the tutorial session at the end of this chapter.

Phasor analysis remains important as to be able to check the steady-state solution of the models when connected to a sinusoidal source.

3.2 Ideal transformer (ITF) concept

The physical model of the transformer shown in figure 3.1 replaces the toroidal shaped magnetic circuit used earlier. The transformer consists of an inner rod and outer tube made up of ideal magnetic material, i.e. infinite permeability. The inner bar and outer tube are each provided with a n_2 and n_1 turn winding respectively. The outer n_1 winding referred to as the ‘primary’ carries a primary current i_1 . The inner n_2 winding is known as the secondary winding and it carries a current i_2 . The cross-sectional view shows the layout of the windings in the unity length inner rod and outer tube together with the assumed current polarity. Furthermore, a flux ϕ_m is shown in figure 3.1 which is linked with both coils. It is assumed at this stage that the total flux in the transformer is fully linked with both windings. In addition, the airgap between

the inner rod and outer tube of the transformer is taken to be infinitely small at this stage.

The magnetic material of the transformer is, as was mentioned above, assumed to have infinite permeability at this stage, which means that the reluctance R_m of the magnetic circuit is in fact zero. Consequently, the magnetic potential $u_{iron\ core}$ across the iron circuit must be zero given that $u_{iron\ core} = \phi_m R_m$, where ϕ_m represents the circuit flux in the core, which is assumed to take on a finite value. The fact that the total magnetic potential in the core must be zero

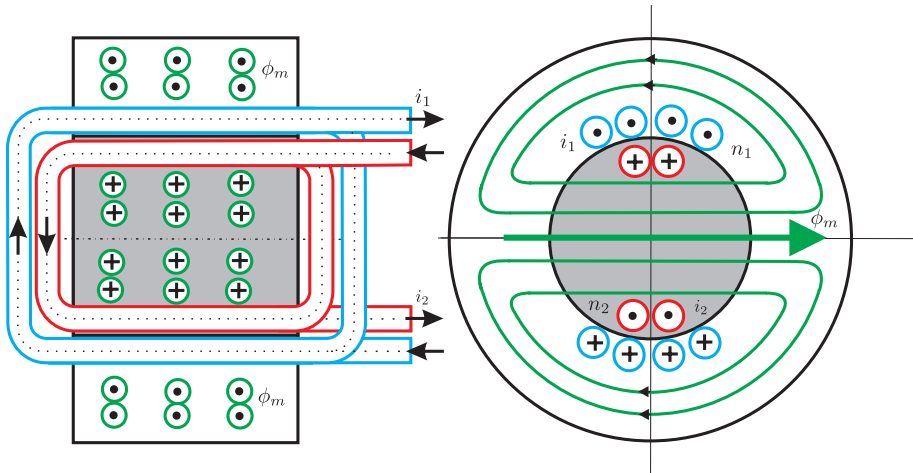


Figure 3.1. Example real ITF model

shows us the basic mechanism of the transformer in terms of the interaction between primary and secondary current.

Let us assume a primary and secondary current as indicated in figure 3.1. Note carefully the direction of current flow in each coil. Positive current direction is ‘out of the page’, negative ‘into the page’. The MMF of the two coils may be written as

$$MMF_{coil\ 1} = +n_1 i_1 \quad (3.1a)$$

$$MMF_{coil\ 2} = -n_2 i_2 \quad (3.1b)$$

The MMF’s of the two coils are purposely chosen to be in opposition given that it is the ‘natural’ current direction as will become apparent shortly. The resultant coil MMF ‘seen’ by the magnetic circuit must be zero given that the magnetic potential $u_{iron} = 0$ at present. This means that the following MMF condition holds:

$$n_1 i_1 - n_2 i_2 = 0 \quad (3.2)$$

Equation (3.2) is known as the basic ITF current relationship. This expression basically tells us that a secondary current i_2 must correspond with a primary current $i_1 = \frac{n_2}{n_1} i_2$ (see equation (3.2)).

The second basic equation which exists for the ITF relates to the primary and secondary flux-linkage values. If we assume, for example, that a voltage source is connected to the primary then a primary flux-linkage ψ_1 value will be present. This in turn means that the circuit flux ϕ_m will be equal to $\phi_m = \frac{\psi_1}{n_1}$. The corresponding flux linked with the secondary is then of the form $\psi_2 = n_2 \phi_m$. The relationship between primary and secondary flux-linkage values can therefore be written as

$$\psi_2 = \frac{n_2}{n_1} \psi_1 \quad (3.3)$$

The corresponding terminal voltage equations for the primary and secondary are of the form

$$u_1 = \frac{d\psi_1}{dt} \quad (3.4a)$$

$$u_2 = \frac{d\psi_2}{dt} \quad (3.4b)$$

These equations are similar to equation (2.2) which was developed for a single coil with zero resistance. A symbolic representation of the ITF is shown in figure 3.2.

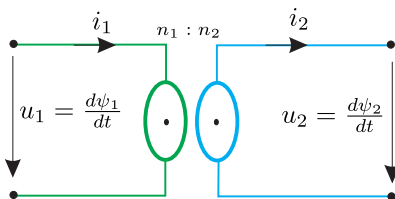


Figure 3.2. Symbolic model of ITF

The complete equation set of the ITF is given by equation (3.5).

$$u_1 = \frac{d\psi_1}{dt} \quad (3.5a)$$

$$u_2 = \frac{d\psi_2}{dt} \quad (3.5b)$$

$$\psi_2 = \frac{n_2}{n_1} \psi_1 \quad (3.5c)$$

$$i_1 = \frac{n_2}{n_1} i_2 \quad (3.5d)$$

where $\frac{n_2}{n_1}$ represents the so-called winding ratio of the ITF. Note that the current directions shown in figure 3.2 for primary and secondary are the same, i.e.

pointing to the right. In some applications it is more convenient to reverse both current directions, i.e. both pointing to the left. The ITF model (figure 3.1) is directly linked to the symbolic model of figure 3.2 in terms of current polarities. If we choose the primary current ‘into’ the ITF model then the secondary direction follows ‘naturally’ (because of the reality that the total MMF must be zero) i.e. must come ‘out’ of the secondary side of the model.

The generic diagram of the basic ITF module is linked to the flux-linkage and current relations given by equations (3.5c) and (3.5d) respectively. The generic diagram that corresponds with figure 3.2 is given by figure 3.3(a).

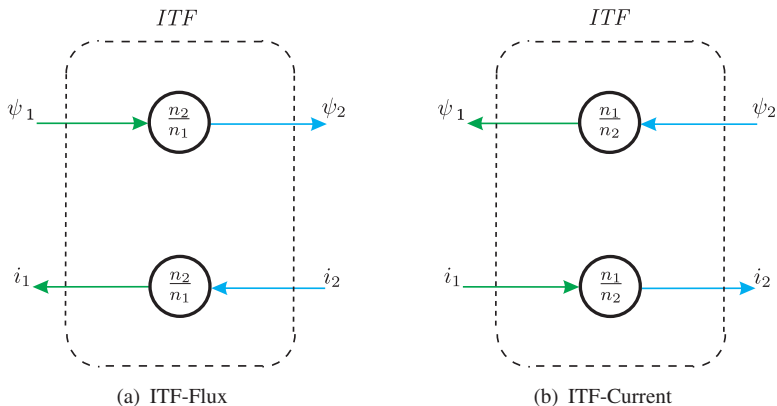


Figure 3.3. Generic models of ITF

It is, as was mentioned earlier, sometimes beneficial to reverse the current direction in the ITF, which means that i_2 becomes an output and i_1 an input. Under these circumstances we must also reverse the flux directions, i.e. ψ_1 output, ψ_2 input. This version of the ITF module, named ‘ITF-Current’ is given in figure 3.3(b).

The instantaneous power is given as the product of voltage and current, i.e. $u_1 i_1$ and $u_2 i_2$. For the ITF model, power *into* the primary side corresponds to positive power ($p_{in} = u_1 i_1$). Positive output power for the ITF is defined as ($p_{out} = u_2 i_2$) *out* of the secondary as shown in figure 3.4.

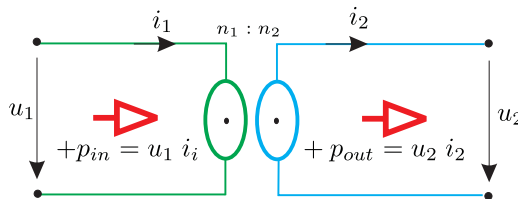


Figure 3.4. Power convention ITF

3.3 Basic transformer

The ITF module forms the cornerstone for transformer modelling in this book and is also the stepping stone to the so-called IRTF module used for machine analysis. An example of the transformer connected to a resistive load is shown in figure 3.5.

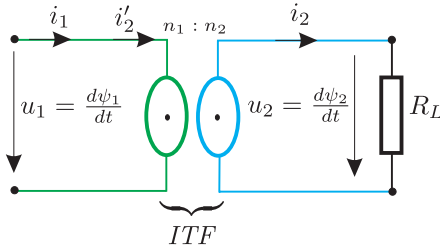


Figure 3.5. Symbolic model of transformer with resistive load

In this example an excitation voltage u_1 is assumed, which in turn corresponds to a secondary voltage u_2 across the load resistance. The ITF equation set is given by equation (3.6).

$$u_1 = \frac{d\psi_1}{dt} \quad (3.6a)$$

$$u_2 = \frac{d\psi_2}{dt} \quad (3.6b)$$

$$\psi_2 = \frac{n_2}{n_1} \psi_1 \quad (3.6c)$$

$$i'_2 = \frac{n_2}{n_1} i_2 \quad (3.6d)$$

The ITF current on the primary side is renamed i'_2 and is known as the primary referred secondary current. It is the current which is ‘seen’ on the primary side, due to a current i_2 on the secondary side. In this case $i_1 = i'_2$ as may be observed from figure 3.5. The equation set of this transformer must be extended with the equation $u_2 = i_2 R_L$. A generic representation of the symbolic diagram according to figure 3.5 is given in figure 3.6.

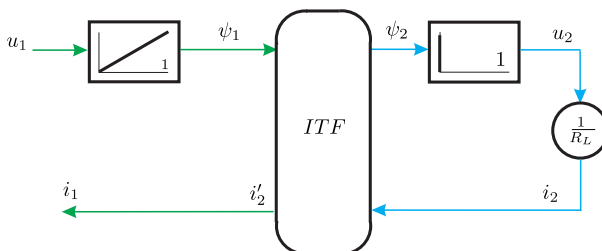


Figure 3.6. Generic model of transformer with load

The ITF module is shown as a ‘sub-module’, which in fact represents the generic model according to figure 3.3(a) with the change that the current i_1 is renamed i'_2 .

It is important to realize how the transformer functions. Basically the integrated applied primary voltage gives a primary flux-linkage value, which in turn leads to a circuit flux ϕ_m . The circuit flux in turn results in ψ_2 , which is the flux linked with the secondary winding. The secondary flux-linkage time differential represents the secondary voltage which will cause a current i_2 in the load. The secondary current leads to a MMF equal to $i_2 n_2$ on the secondary side which must be countered by an MMF of $n_1 i_1$ on the primary side given that the magnetic reluctance of the transformer is taken to be zero at present. Note that an open-circuited secondary winding ($R_L = \infty$) corresponds to a zero secondary and a zero primary current value. The fluxes are not affected as these are determined by the primary voltage, time and winding ratio in this case (we have assumed that the primary coil is connected to a voltage source and the secondary to a load impedance).

Note that a differentiator module is used in the generic model given in figure 3.6. Differentiators *should be avoided where possible* in actual simulations, given that simulations tend to operate poorly with such modules. In most cases the use of a differentiator module in actual simulations is not required, given that we can either implement the differentiator by alternative means or build models that avoid the use of such modules.

3.4 Transformer with magnetizing inductance

In electrical machines airgaps are introduced in the magnetic circuit which, as was made apparent in chapter 2, will significantly increase the total magnetic circuit reluctance R_m . Furthermore, the magnetic material used will in reality have a finite permeability which will further increase the overall magnetic circuit reluctance. The transformer according to figure 3.7 has an airgap between the primary and secondary windings.

The circuit flux ϕ_m now needs to cross this airgap twice. Consequently, a given circuit flux will according to Hopkinson’s law correspond to a non-zero magnetic circuit potential u_M in case $R_m > 0$. The required magnetic potential must be provided by the coil MMF which is connected to the voltage source. In our case we have chosen the primary side for excitation with a voltage source while the secondary side is connected to, for example, a resistive load. The implication of the above is that an MMF equal to $n_1 i_m$ must be provided via the primary winding. The current i_m is known as the ‘magnetizing current’, which is directly linked with the primary flux-linkage value ψ_1 and the so-called magnetizing inductance L_m . The relationship between these variables is of the

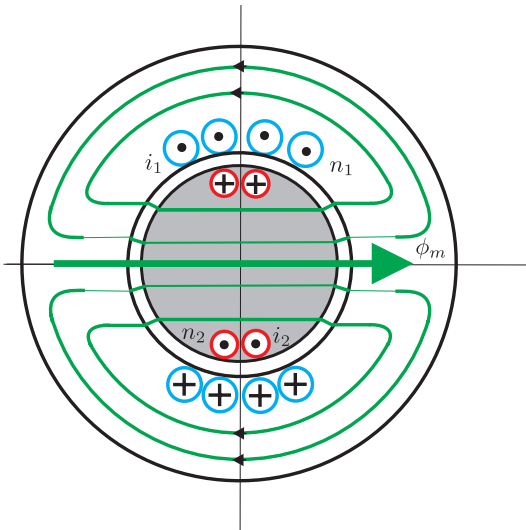


Figure 3.7. Transformer model with finite airgap

form

$$i_m = \frac{\psi_1}{L_m} \quad (3.7)$$

Note that the magnetizing inductance is directly linked with the magnetic reluctance R_m namely $L_m = \frac{n_1^2}{R_m}$, as was discussed in chapter 2. Zero magnetic reluctance corresponds to an infinite magnetizing inductance and according to equation (3.7) zero magnetizing current i_m .

The presence of a core MMF requires us to modify equation (3.2) given that the sum of the coil MMF's is no longer zero. The revised MMF equation is now of the form

$$n_1 i_1 - n_2 i_2 = n_1 i_m \quad (3.8)$$

which may also be rewritten as:

$$i_1 = i_m + \underbrace{\frac{n_2}{n_1} i_2'}_{i'_2} \quad (3.9)$$

In expression (3.9) the variable i'_2 is shown, which is the primary referred secondary current, as introduced in the previous section. Note that in the magnetically ideal case (where $i_m = 0$) the primary current is given as $i_1 = i'_2$. The ITF equation set according to equation (3.6) remains directly applicable to the revised transformer model.

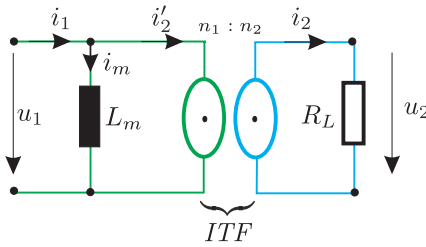


Figure 3.8. Symbolic model of transformer with load and finite L_m

The symbolic transformer diagram according to figure 3.5 must be revised to accommodate the presence of the magnetizing inductance on the primary side of the ITF. The revised symbolic diagram is given in figure 3.8.

The complete equation set which is tied to the symbolic transformer model according to figure 3.8 is given as

$$u_1 = \frac{d\psi_1}{dt} \quad (3.10a)$$

$$u_2 = \frac{d\psi_2}{dt} \quad (3.10b)$$

$$i_1 = i_m + i'_2 \quad (3.10c)$$

$$i_m = \frac{\psi_1}{L_m} \quad (3.10d)$$

$$u_2 = i_2 R_L \quad (3.10e)$$

For modelling a system of this type it is important to be able to build a generic model which is directly based on figure 3.8 and the corresponding equation set (3.10). The generic module of the transformer as given in figure 3.9 is directly based on the earlier model given in figure 3.6. Shown in figure 3.9

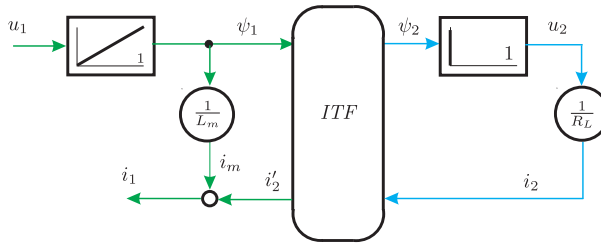


Figure 3.9. Generic model of transformer with load and finite L_m

is an ITF sub-module which is in fact of the form given in figure 3.3(a), with the provision that the current output i_1 (of the ITF module) is now renamed i'_2 , which is known as the primary referred secondary current.

3.5 Steady-state analysis

The model representations discussed to date are dynamic, which means that they can be used to analyze a range of excitation conditions, which includes transient as well as steady-state. Of particular interest is to determine how such systems behave when connected to a sinusoidal voltage source. Systems, such as a transformer with resistive loads will (after being connected to the excitation source) initially display some transient behaviour but will then quickly settle down to their steady-state.

As was discussed earlier the steady-state analysis of linear systems connected to sinusoidal excitation sources is of great importance. Firstly, it allows us to gain a better understanding of such systems by making use of phasor analysis tools. Secondly, we can use the outcome of the phasor analysis as a way to check the functioning of our dynamic models once they have reached their steady-state.

3.5.1 Steady-state analysis under load with magnetizing inductance

In steady-state the primary excitation voltage is of the form $u_1 = \hat{u}_1 \cos \omega t$, which corresponds to a voltage phasor $\underline{u}_1 = \hat{u}_1$. The supply frequency is equal to $\omega = 2\pi f$ where f represents the frequency in Hz.

The aim is to use complex number theory together with the equations (3.10) and (3.6) to analytically calculate the phasors: $\underline{\psi}_1$, $\underline{\psi}_2$, \underline{i}_2 , \underline{i}'_2 , \underline{i}_1 and \underline{u}_2 . The flux-linkage phasor is directly found using equation (3.10a) which in phasor form is given as $\underline{u}_1 = j\omega \underline{\psi}_1$. The corresponding flux-linkage phasor on the secondary side of the ITF module is found using (3.6d) which gives $\underline{\psi}_2 = \frac{n_2}{n_1} \underline{\psi}_1$. The secondary voltage equation (3.10b) gives us the secondary voltage (in phasor form) $\underline{u}_2 = j\omega \underline{\psi}_2$, which in turn allows us to calculate the current phasor according to $\underline{i}_2 = \frac{1}{R_L} \underline{u}_2$. This phasor may also be written in terms of the primary voltage phasor $\underline{u}_1 = \hat{u}_1$ as

$$\underline{i}_2 = \left(\frac{n_2}{n_1} \right) \frac{\underline{u}_1}{R_L} \quad (3.11)$$

The corresponding primary referred secondary current phasor is found using equations (3.6d), (3.11) which gives $\underline{i}'_2 = \left(\frac{n_2}{n_1} \right)^2 \frac{\underline{u}_1}{R_L}$. The primary current phasor is found using (3.10c), where the magnetizing current phasor \underline{i}_m is found using (3.10d) namely $\underline{i}_m = \frac{1}{L_m} \underline{\psi}_1$. The resultant primary current phasor may also be written as

$$\underline{i}_1 = \frac{\underline{u}_1}{j\omega L_m} + \left(\frac{n_2}{n_1} \right)^2 \frac{\underline{u}_1}{R_L} \quad (3.12)$$

It is instructive to consider equation (3.12) in terms of an equivalent circuit model as shown in figure 3.10.

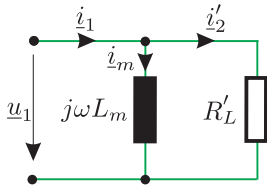


Figure 3.10. Primary referred phasor model of transformer with load and finite L_m

The diagram shows the load resistance in its so-called ‘referred’ form with $R'_L = \left(\frac{n_1}{n_2}\right)^2 R_L$ on the primary side of the transformer. Hence, we are able to determine the currents (in phasor form) directly from this diagram. A phasor diagram of the transformer with a resistive load R_L and magnetizing inductance L_m which corresponds with the given phasor analysis and equivalent circuit (figure 3.10), is shown in figure 3.11.

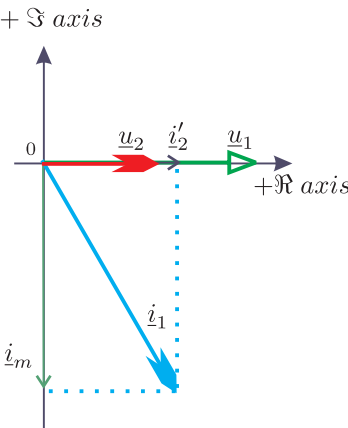


Figure 3.11. Phasor diagram of transformer with load and finite L_m

Some interesting observations can be made from this diagram. Firstly, the primary and secondary voltages are in phase. Secondly, the magnetizing current phasor lags the primary voltage phasor by $\pi/2$. The primary referred secondary current phasor i'_2 is in phase with u_2 given that we have a resistive load. Furthermore, the primary current is found by adding (in vector form) the phasors i'_2 and i_m . Note that the primary current will be equal to the magnetizing current when the load resistance is removed, i.e. $R_L = \infty$.

The corresponding steady-state time function of, for example, the current i_1 can be found by using

$$i_1(t) = \Re \left\{ i_1 e^{j\omega t} \right\} \quad (3.13)$$

where i_1 is found using (3.12).

3.6 Three inductance model

The model according to figure 3.7 assumes that all the flux is linked with both coils. In reality this is not the case as may be observed from figure 3.12. This diagram shows two flux contributions $\phi_{\sigma 1}$ and $\phi_{\sigma 2}$, which are known as the primary and secondary leakage flux components respectively. The leakage fluxes physically arise from the fact that not all the flux in one coil is ‘seen’ by the other.

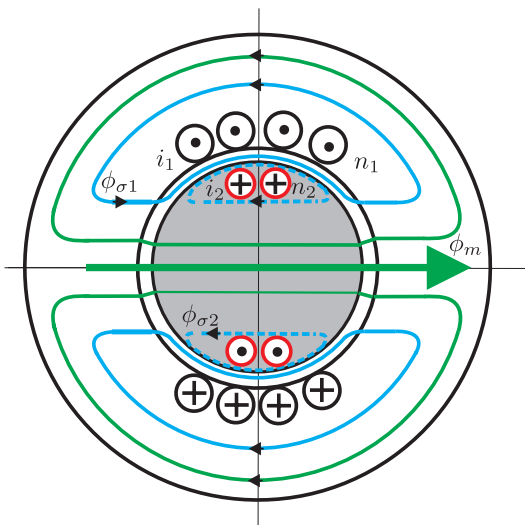


Figure 3.12. Transformer model with finite airgap and leakage

Consequently these components are *not* linked with both coils and they are represented by primary and secondary leakage inductances

$$L_{\sigma 1} = \frac{\psi_{\sigma 1}}{i_1} \quad (3.14a)$$

$$L_{\sigma 2} = \frac{\psi_{\sigma 2}}{i_2} \quad (3.14b)$$

where the primary and secondary leakage flux-linkage values are given by $\psi_{\sigma 1} = n_1 \phi_{\sigma 1}$ and $\psi_{\sigma 2} = n_2 \phi_{\sigma 2}$ respectively. The total flux-linkage seen by the primary and secondary is thus equal to

$$\psi_1 = \psi_m + \psi_{\sigma 1} \quad (3.15a)$$

$$\psi_2 = \psi'_m - \psi_{\sigma 2} \quad (3.15b)$$

The flux ϕ_m which is linked with the primary coil is now renamed $\psi_m = n_1 \phi_m$. Similarly the circuit flux ϕ_m which is linked with the secondary coil gives us the flux-linkage $\psi'_m = n_2 \phi_m$. The terminal equations for the transformer in its

current form are given as

$$u_1 = \frac{d\psi_m}{dt} + L_{\sigma 1} \frac{di_1}{dt} \quad (3.16a)$$

$$u_2 = \frac{d\psi'_m}{dt} - L_{\sigma 2} \frac{di_2}{dt} \quad (3.16b)$$

where

$$u_1 = \frac{d\psi_1}{dt} \quad (3.17a)$$

$$u_2 = \frac{d\psi_2}{dt} \quad (3.17b)$$

The symbolic representation of the transformer according to figure 3.8 must be extended to include the leakage inductance. The revised symbolic model as given in figure 3.13 shows the leakage inductances. The generic model that corresponds to figure 3.13 is given in figure 3.14.

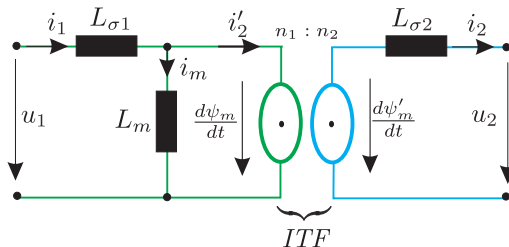


Figure 3.13. Symbolic representation, transformer with magnetizing and leakage inductance

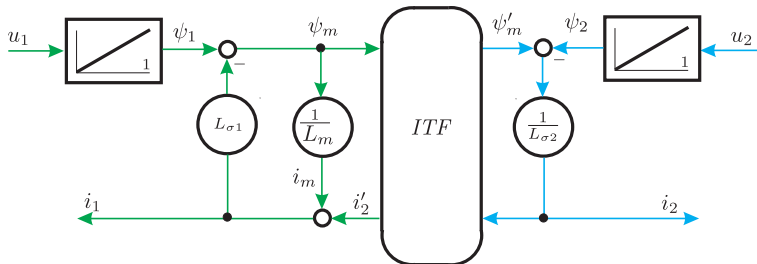


Figure 3.14. Generic representation, transformer with magnetizing and leakage inductance, including algebraic loops

It is further noted that the model is not suited to simulate the no-load situation (with a passive load), i.e. open circuited secondary winding, since current i_2 is an output and thus cannot be forced zero by any load.

The model in figure 3.14 contains two algebraic loops which may cause numerical problems during the execution of the simulation. The term ‘algebraic loop’ refers to the problem where the output of a simulation model is algebraically linked to itself. For example in the equation

$$y = (x - y) G \quad (3.18)$$

output variable y is not only a function of the input x but also of itself.

In the generic diagram of figure 3.14, the following two loops appear (identified by the modules in the loop, where Σ is used to indicate a *summation unit*):

First algebraic loop: Starting at $L_{\sigma 1}$ to upper Σ then down through $\frac{1}{L_m}$, closing the loop via lower Σ back to $L_{\sigma 1}$.

Second algebraic loop: Starting at $L_{\sigma 1}$ to upper left Σ , then through flux input of ITF to the upper right Σ . From here down through $\frac{1}{L_{\sigma 2}}$, back through current input of ITF , closing the loop via lower Σ back to $L_{\sigma 1}$.

Execution of this simulation would cause an ‘algebraic loop error’ message in the simulation. The simulation results obtained with the presence of an algebraic loop may be erroneous. Hence, such loops should be avoided if possible. In the example, rewriting equation (3.18) into

$$y = x \frac{G}{G + 1} \quad (3.19)$$

solves the algebraic loop.

3.7 Two inductance models

The problem with the three inductance model as discussed in section 3.6 lies with the fact that it is extremely difficult to determine individual values for the two leakage inductances in case access to the secondary side of the model is not possible. For transformers this is not an issue (when the winding ratio is known) but for squirrel cage asynchronous machines, to be discussed at a later stage, this is certainly the case. A triple inductance model of the transformer is in fact not needed given that its behaviour can be perfectly modelled by a two inductance based model when all inductances are linear.

In this section two such models will be examined together with a third model which makes use of mutual and self inductance parameters.

Prior to discussing these new models it is instructive to introduce the so-called coupling factor κ which is defined as

$$\kappa = \sqrt{1 - \frac{L_{\text{short-circuit}}}{L_{\text{open-circuit}}}} \quad (3.20)$$

Equation 3.20 contains the parameters $L_{open-circuit}$ (the inductance of the first winding while the second winding is open-circuit) and $L_{short-circuit}$ (the inductance of the first winding while the second winding is shorted). Note that the open and short-circuit inductance will be different when the transformer is viewed from the primary or secondary side, however the coupling factor κ will be the same.

For example when considering the transformer according to figure 3.13 from the primary side the open and short-circuit inductances are defined as

$$L_{open-circuit}^p = L_1 \quad (3.21a)$$

$$L_{short-circuit}^p = L_{\sigma 1} + \frac{L_m L'_{\sigma 2}}{L_m + L'_{\sigma 2}} \quad (3.21b)$$

with $L_1 = L_{\sigma 1} + L_m$ and $L'_{\sigma 2} = \left(\frac{n_1}{n_2}\right)^2 L_{\sigma 2}$.

Alternatively the open and short-circuit inductance can also be determined from the secondary side of the model shown in figure 3.13 which gives

$$L_{open-circuit}^s = L_2 \quad (3.22a)$$

$$L_{short-circuit}^s = L_{\sigma 2} + \frac{L'_m L'_{\sigma 1}}{L'_m + L'_{\sigma 1}} \quad (3.22b)$$

with $L_2 = L_{\sigma 2} + L'_m$, $L'_{\sigma 1} = \left(\frac{n_2}{n_1}\right)^2 L_{\sigma 1}$ and $L'_m = \left(\frac{n_2}{n_1}\right)^2 L_m$. It may be shown that the calculation of the coupling factor according to equation 3.20 is identical when using equation 3.21 or 3.22.

3.7.1 Primary based model

The symbolic model given in figure 3.15 is referred to as a primary based model because the two inductances are located on the primary side of the transformer. The new configuration is defined by a new magnetizing inductance L_M , new leakage inductance L_σ and ITF transformer ratio k . These parameters must be chosen in such a manner as to insure that the new model is identical

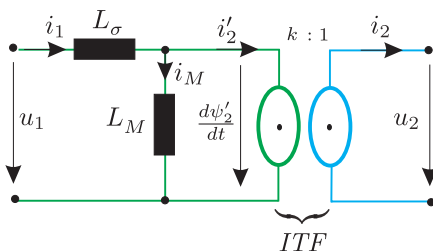


Figure 3.15. Two inductance symbolic transformer model

to the original (figure 3.13) when viewed from either the primary or secondary side of the transformer. It can be shown that the following choice of parameters satisfies these criteria.

$$k = \kappa \sqrt{\frac{L_1}{L_2}} \quad (3.23a)$$

$$L_M = \kappa^2 L_1 \quad (3.23b)$$

$$L_\sigma = L_1 (1 - \kappa^2) \quad (3.23c)$$

where κ , L_1 and L_2 are defined by equations 3.20, 3.21 and 3.22 respectively.

The equation set which corresponds to the two inductance symbolic model of figure 3.15 is given by equation (3.24).

$$u_1 = \frac{d\psi_1}{dt} \quad (3.24a)$$

$$u_2 = \frac{d\psi_2}{dt} \quad (3.24b)$$

$$\psi_1 = i_1 L_\sigma + \psi'_2 \quad (3.24c)$$

$$\psi'_2 = i_M L_M \quad (3.24d)$$

$$i_M = i_1 - i'_2 \quad (3.24e)$$

$$\psi'_2 = k\psi_2 \quad (3.24f)$$

$$i_2 = k i'_2 \quad (3.24g)$$

Equations (3.24f), (3.24g) represent those implemented by the ITF module.

3.7.2 Alternative model

The two inductance model described above is particularly useful when the excitation is provided from the primary side of the ITF. In some cases it is however convenient to consider an alternative two inductance model, which is useful in case the excitation is provided by the secondary side. An example where this occurs is with the DC machine.

The two inductance model representation is now of the form given by figure 3.16. The new configuration is again defined by a magnetizing inductance

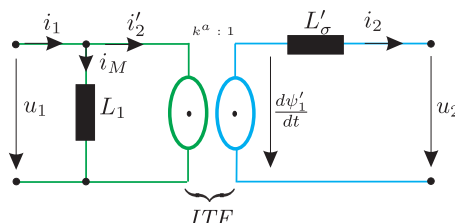


Figure 3.16. Two inductance alternative symbolic transformer model

which is equal to L_1 (as defined by equation (3.21)), leakage inductance L'_σ and ITF winding ratio k^a . These parameters must be chosen in such a manner as to insure that this new model is identical (when viewed from the outside) to the original (figure 3.13). It can be shown that the new parameter set which satisfies this condition is given by equation (3.25).

$$k^a = \frac{1}{\kappa} \sqrt{\frac{L_1}{L_2}} \quad (3.25a)$$

$$L'_\sigma = L_2 (1 - \kappa^2) \quad (3.25b)$$

It is emphasized that this ‘alternative’ three parameter model is only used in this book for modelling the DC machine. Henceforth, whenever we discuss a two inductance model, we will assume by default the configuration given by figure 3.15.

3.8 Mutual and self inductance based model

A model often used in the field of communications is of the form given in figure 3.17. The positive current directions for this type of model are inwards as is customary for this configuration. The aim of this section is to establish the link, in terms of the parameters which exist between this model and the model in figure 3.15.

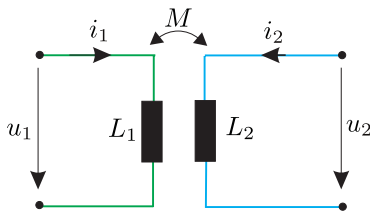


Figure 3.17. Mutual coupling type model of transformer

Mutual and self inductance based transformer models are defined in terms of the parameters L_1 and L_2 respectively. In addition, the magnetic coupling between the primary and secondary coils is defined in terms of a so-called mutual inductance parameter M as, indicated in figure 3.17. The mutual inductance can be defined from either the primary or secondary side.

From the primary side it is defined as the ratio of the flux linked with the secondary winding and current in the primary side, i.e. $M = \psi_2/i_1$ with the condition $i_2 = 0$. Vice versa the mutual coupling can also be defined as the ratio between the primary flux linkage and secondary current, i.e. $M = \psi_1/i_2$ with the condition $i_1 = 0$. The actual mutual inductance value remains unchanged whether viewed from the primary or secondary side as will become apparent shortly. As such the mutual inductance is also (like L_1 , L_2) an ‘independent’ parameter.

The basic equation set which applies to figure 3.17 can be written as

$$u_1 = L_1 \frac{di_1}{dt} + M \frac{di_2}{dt} \quad (3.26a)$$

$$u_2 = M \frac{di_1}{dt} + L_2 \frac{di_2}{dt} \quad (3.26b)$$

The revised model states that the flux-linkage time differential on for example the primary side consists of a term due to primary self inductance to which we must now add a mutual inductance term.

By determining the equivalent (to equation (3.26)) ITF based transformer model (see figure 3.15) equation set, we will be able to show how the parameters of the mutual coupling based model are linked to the ITF based model. A suitable starting point for this analysis is expression (3.24a), which remains unaffected by the model in use. From equation (3.24c) we can deduce that the term $\frac{d\psi_1}{dt}$ may also be written as

$$\frac{d\psi_1}{dt} = L_\sigma \frac{di_1}{dt} + \frac{d\psi'_2}{dt} \quad (3.27)$$

The primary referred flux-linkage ψ'_2 can according to equation (3.24d) also be written as $\psi'_2 = L_M i_M$, in which the magnetizing current can also be expressed as $i_M = i_1 - i'_2$. Given the above, we can with the aid of equations (3.24f), (3.24g), rewrite equation (3.27) in the following form

$$\frac{d\psi_1}{dt} = \underbrace{(L_\sigma + L_M)}_{L_1} \frac{di_1}{dt} - \underbrace{\left(\frac{L_M}{k}\right)}_{M} \frac{di_2}{dt} \quad (3.28)$$

A comparison between equations (3.28) and (3.26a) (right hand side), learns that they differ only in terms of the minus sign between the two terms. The reason for this is that the secondary current sign convention between the two models is in opposition. If we consider the parameters present in both equations (in front of the current differential terms) then it is hopefully apparent that the primary self inductance and mutual inductance terms may be expressed, using k from equation (3.23) as

$$L_1 = L_\sigma + L_M \quad (3.29a)$$

$$M = \frac{L_M}{k} \quad (3.29b)$$

Note that the mutual inductance may also be expressed in terms of the coupling factor which gives

$$M = \kappa \sqrt{L_1 L_2} \quad (3.30)$$

where κ , L_1 and L_2 are defined by equations 3.20, 3.21 and 3.22 respectively.

A similar type of analysis, as shown above, may also be carried out with respect to expressing the flux differential term $\frac{d\psi_2}{dt}$ in terms of ITF parameters and current differential terms. An analysis of this type, an exercise left to the reader, shows that this flux differential can be written as

$$\frac{d\psi_2}{dt} = \underbrace{\left(\frac{L_M}{k} \right)}_{M} \frac{di_1}{dt} - \underbrace{\left(\frac{L_M}{k^2} \right)}_{L_2} \frac{di_2}{dt} \quad (3.31)$$

A comparison between equations (3.31) and (3.26b) (right hand side) and taking into account the secondary current direction in both models learns that the secondary self inductance may be expressed as

$$L_2 = \frac{L_M}{k^2} \quad (3.32)$$

Note from equation (3.31) that a mutual inductance term is also present and indeed of the form given by expression (3.29b).

3.9 Two inductance model with coil resistance

The remaining extension which has to be made with respect to the model shown in section 3.7.1 is concerned with the introduction of the primary and secondary coil resistances R_1 and R_2 respectively. Use of these parameters requires a change to equations (3.24a) and (3.24b) which are now of the form

$$u_1 - R_1 i_1 = \frac{d\psi_1}{dt} \quad (3.33a)$$

$$u_2 + R_2 i_2 = \frac{d\psi_2}{dt} \quad (3.33b)$$

The symbolic representation of the transformer with resistances is given in figure 3.18. A generic form of the four parameter single phase transformer, as given in figure 3.19, can be directly converted to a Simulink type model *without*

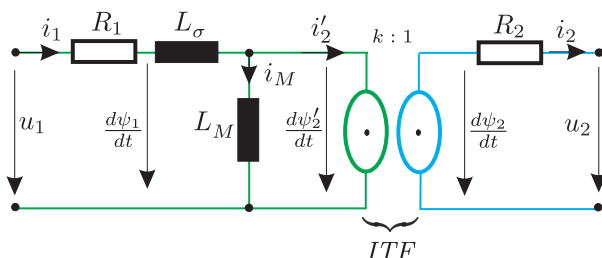


Figure 3.18. Symbolic representation of a four parameter transformer model

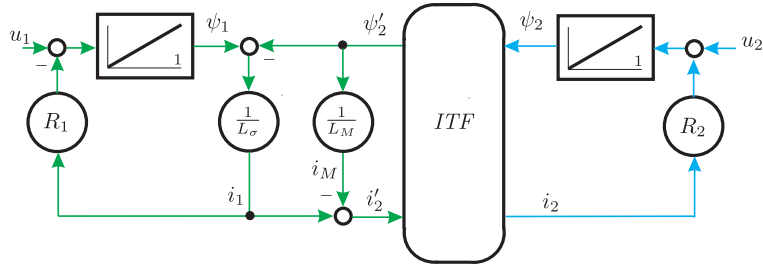


Figure 3.19. Generic representation of a four parameter transformer model

the need for a differentiator module. Note that the ITF module according to figure 3.3(b) is now used in figure 3.19. The flux and current relations for the ITF are now of the form given by equations (3.24f), (3.24g), where the modified winding ratio k is defined by equation (3.23a). Hence the ITF outputs are the primary referred secondary flux-linkage value ψ'_2 and the secondary current i_2 . It is by virtue of the fact that we have reversed the signal flow in the ITF (by using the ITF ‘current’ model, see figure 3.3(b)) that we are able to avoid the use of a differentiator on the secondary side.

3.9.1 Phasor analysis of revised model, with resistive load

The steady-state analysis of the extended model according to section 3.9 is carried out along the lines of the previous model given in section 3.5.1. As with the previous case a primary supply voltage $u_1 = \hat{u}_1 \cos \omega t$ is assumed which corresponds with a phasor $\underline{u}_1 = \hat{u}_1$. Prior to undertaking this analysis it is helpful to summarize in phasor form the complete equation set (including the ITF) for this system.

$$\underline{u}_1 = i_1 R_1 + j\omega \underline{\psi}_1 \quad (3.34a)$$

$$i_1 = \frac{1}{L_\sigma} (\underline{\psi}_1 - \underline{\psi}'_2) \quad (3.34b)$$

$$\underline{u}_2 = j\omega \underline{\psi}_2 - i_2 R_2 \quad (3.34c)$$

$$\underline{u}_2 = i_2 R_L \quad (3.34d)$$

$$\underline{i}'_2 = i_1 - i_M \quad (3.34e)$$

$$i_M = \frac{\underline{\psi}'_2}{L_M} \quad (3.34f)$$

$$\underline{\psi}'_2 = k \underline{\psi}_2 \quad (3.34g)$$

$$i_2 = k \underline{i}'_2 \quad (3.34h)$$

The analysis of this type of circuit is aimed at finding the primary current phasor \underline{i}_1 as a function of the circuit parameters and the input (known) voltage phasor

\underline{u}_1 . The required expression can be obtained by use of equation (3.34). An alternative approach is possible in this case, by realizing that the ITF module in fact acts as an impedance converter. For example, if we consider the impedance $Z_2 = \frac{\underline{e}_2}{\underline{i}_2}$ (where we have ignored the sign convention) then the equivalent impedance on the primary side, known as the primary referred secondary impedance, will be equal to $Z'_2 = \frac{\underline{e}'_2}{\underline{i}'_2}$ where $\underline{e}'_2 = j\omega\underline{\psi}'_2$.

The relationship between the two impedances is found by using equations (3.34g) and (3.34h) which gives $Z'_2 = k^2 Z_2$. In this case we can simply move the secondary elements (coil resistance and load resistance) to the primary side, provided we multiply the value by a factor k^2 . This process is known as building a primary referred model of the transformer which greatly simplifies the steady-state analysis. The result of moving the secondary circuit elements to the primary side of the ITF is shown in figure 3.20. Note that the inductances are represented in a phasor circuit as $j\omega L$.

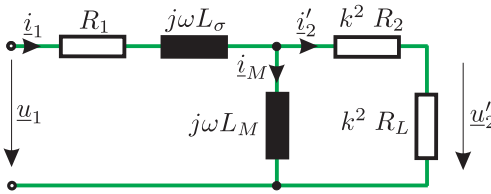


Figure 3.20. Equivalent primary referred model of transformer

The primary current phasor is then found by determining the equivalent impedance at the primary terminals, which according to figure 3.20 is of the form

$$Z_{prim} = R_1 + j\omega L_\sigma + \frac{j\omega L_M k^2 (R_2 + R_L)}{j\omega L_M + k^2 (R_2 + R_L)} \quad (3.35)$$

The current phasor is then calculated using $i_1 = \frac{\hat{u}_1}{Z_{prim}}$. Once this phasor is defined we can determine, with the aid of equation (3.34), the remaining phasors of this circuit. For example, the secondary current phasor is directly found using equation (3.34h). The corresponding voltage phasor \underline{u}_2 can with the aid of equation (3.34g) be written as $\underline{u}_2 = \underline{u}'_2/k$. Note in this context that the product $\underline{u}_2 \underline{i}_2$ is equal to $\underline{u}'_2 \underline{i}'_2$, i.e. the transformation is power invariant.

3.10 Tutorials for Chapter 3

3.10.1 Tutorial 1

The single phase transformer shown in figure 3.21 is to be used for current measurement. The secondary winding is connected to a resistance R_L , hence the voltage across u_2 will be a function of the primary current i_1 to be measured. The primary and secondary coil resistance as well as the leakage inductance

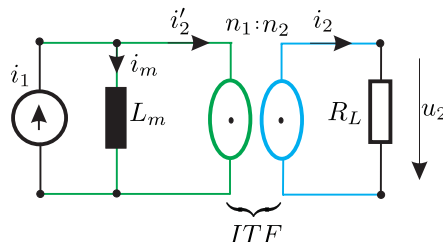


Figure 3.21. Current transformer with resistance R_L

of the transformer are ignored. The transformer has a magnetizing inductance L_m and a winding ratio of $n_1/n_2 = 1$.

Build a Simulink model diagram of the ITF based transformer circuit with the primary current i_1 as input variable. Differentiator modules may *not* be used in this example. Use a ‘To Workspace’ module to show the variables i_1, u_2 as function of time. The current function is of the form $i_1 = 10 \sin(\omega t)$, with $\omega = 100\pi \text{rad/s}$. The magnetizing inductance L_m and load resistance R_L are equal to 100mH and 5Ω respectively. Set your simulation ‘run time’ to 60ms .

An example of a Simulink implementation of this problem is given in figure 3.22. The results of the simulation in the form of the input current and

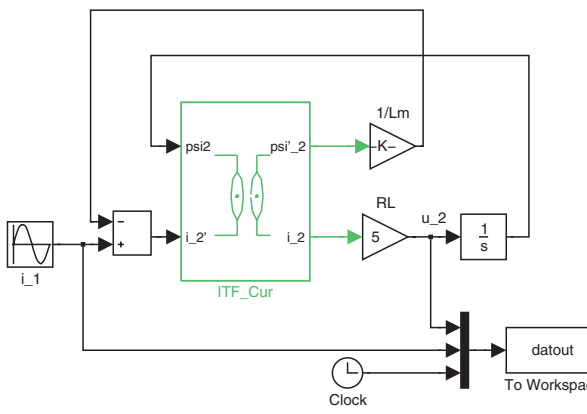


Figure 3.22. Simulation of current transformer

output voltage are shown in figure 3.23. Note that the voltage u_2 is scaled by a factor $1/5$ to improve readability. The m-file given below is used to process the results obtained from the simulation.

It is instructive to check the results from the simulation by a steady-state ‘phasor analysis’. The same m-file also shows the phasor analysis for this problem and the corresponding output voltage waveform is also added to the results shown in figure 3.23.

m-file Tutorial 1, chapter 3

```
%Tutorial 1, chapter 3
plot(datout(:,3),datout(:,1)/5); %u2/5
hold on
grid
plot(datout(:,3),datout(:,2),'r') %%%%
%%%calculation phasors
i1_ph=10; %current phasor i1
RL=5; Lm=100e-3; w=100*pi;
%%%%%%%%%%%
XL=j*w*Lm;
u2_ph=i1_ph*RL/(1+RL/XL);
u2_hat=abs(u2_ph);
u2_rho=angle(u2_ph);
%%%%%%%%plot time wave form u2(t)
t=[0:0.1e-3:60e-3];
u2_t=u2_hat*sin(w*t+u2_rho);
plot(t,u2_t/5,'g'); %plot u2(t)/5
legend('u2/5','i_1','u2/5 phasor')
xlabel('time (s)')
ylabel('u2/5, i1')
```

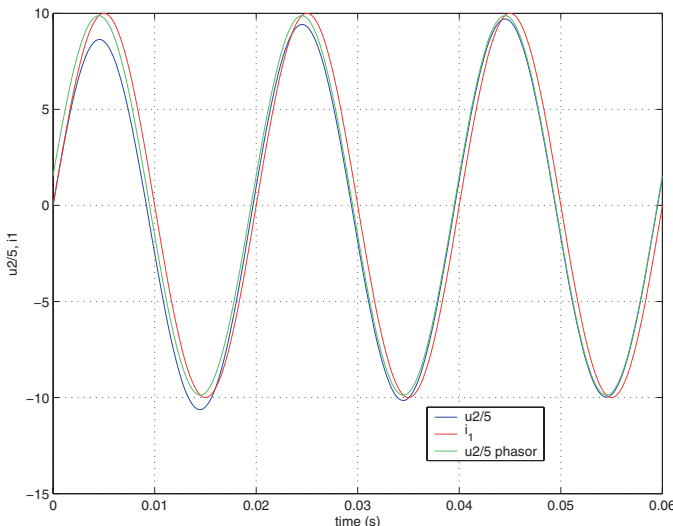


Figure 3.23. Simulink Results: Current transformer tutorial

An observation of figure 3.23 learns that the output voltage waveform from the simulation is aligned with the output obtained from the phasor analysis after a time interval of approximately 30ms. There is therefore a ‘transient’ effect present which cannot be ‘seen’ with the phasor analysis. A further observation of figure 3.23 learns that under steady-state conditions a phase angle error exists between input and output waveforms which is caused by the presence of the magnetizing inductance L_m . It can be shown that the output phasor \underline{u}_2 may be

expressed in terms of the input current phasor i_1 and parameters R_L and L_m .

$$u_2 = \frac{R_L i_1}{\left(1 + \frac{R_L}{j\omega L_m}\right)} \quad (3.36)$$

The denominator of equation (3.36) shows that the angle error is equal to: $\arctan\left(\frac{R_L}{\omega L_m}\right)$. Hence during the design/manufacture of transformers for this purpose it is prudent to maximize the L_m value and limit the size of R_L .

3.10.2 Tutorial 2

A Caspoc simulation approach to the previous tutorial is considered here. Build a Caspoc model with the circuit parameters and excitation as defined in tutorial 1. A Caspoc implementation example for this tutorial is given in figure 3.24. The results from this model as displayed with the aid of the ‘scope’

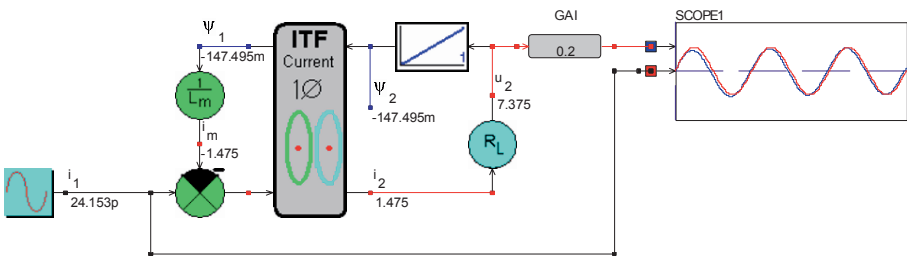


Figure 3.24. Caspoc simulation: current transformer model

module (which may be enlarged to show more details), should match those given in figure 3.23.

3.10.3 Tutorial 3

A 50Hz, 660V/240V supply transformer is considered in this tutorial. The object is to determine the parameters of the transformer in question using data obtained from a no-load and short-circuit test. In the second part of this tutorial a Simulink based dynamic model is to be built. This model will then be used to examine the behaviour of the transformer under load conditions. A phasor analysis is also required so that the steady-state results obtained with the Simulink model can be verified. The symbolic model of the transformer, as given in figure 3.25, is based on the symbolic model discussed in this chapter (see figure 3.18). The model used in this tutorial is extended by the addition of a resistance R_M placed across the terminals of the primary. The power dissipated in this resistance represents the so-called ‘iron losses’(due to eddy currents and hysteresis) in the transformer. In a three inductance model, shown in figure 3.13, this resistance is usually connected in parallel with the inductance

L_m . Positioning this resistance across the primary terminals (or the terminals which correspond to the supply side) simplifies the generic model at the price of a marginal reduction in accuracy. Under steady-state conditions the power (in Watts) dissipated in a resistance is given as $P_R = I^2R = U^2/R$, where U , I represent the RMS voltage and current seen by the resistance. The transformer

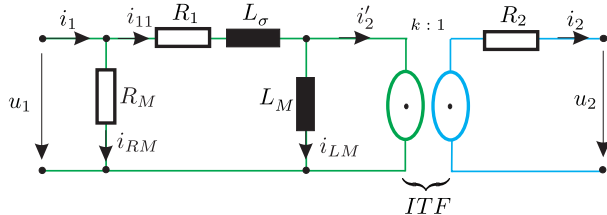


Figure 3.25. Transformer model with iron losses

was identified at the start of this tutorial by the voltage ratio 660/240, which represents the rated primary and secondary RMS voltage values of this unit. To determine the parameters of this transformer a ‘no-load’ test was carried out where the primary (terminal 1 side) was connected to a 660V, 50Hz sinusoidal supply source and the secondary side open circuited. The measured current and power under these conditions were found to be 0.2A(RMS) and 20W respectively. Furthermore, the voltage across the secondary winding was found to be 240V(RMS). A second ‘short-circuit’ test was also carried out, where the secondary winding was connected to a 8V(RMS), 50Hz voltage source, which gives a rated secondary current of 20A(RMS) with the primary winding short-circuited. Note that in this example the short-circuit test is carried out from the secondary side (voltage source connected to the secondary winding), which is often done in case the primary voltage is relatively high, as is the case here. The secondary power was also measured under these circumstances and found to be 20W. On the basis of these experimental tests the parameters of the model according to figure 3.25 can be identified with reasonable accuracy.

The solution to this problem requires a phasor analysis, given that the experimental data was obtained under ‘steady-state conditions’. Under ‘no-load’ conditions we can simplify the model according to figure 3.25 by assuming that the voltage drop across the primary resistance and leakage inductance is small in relation to the applied primary voltage. The primary current in phasor representation (under no-load only) is of the form $i_1 = i_{RM} + i_{LM}$, where (i_{RM} , i_{LM}) represent the current through components R_M and L_M respectively. The RMS current through the resistance R_M is found using $I_{RM} = P_1/U_1 = 20/660$, where P_1 and U_1 represent the measured no-load power and RMS voltage respectively. The winding ratio k is found using $k \approx U_1/U_2$. The current through L_M is found using $I_{LM} = \sqrt{(I_1)^2 - (I_{RM})^2}$, where I_1 represents the

measured (RMS) no-load primary current. Note that I_{RM} has already been calculated. On the basis of these calculations and no-load data the following parameters are obtained

$$k \simeq \frac{U_1}{U_2} \quad (3.37a)$$

$$R_M \simeq \frac{(U_1)^2}{P_1} \quad (3.37b)$$

$$L_M \simeq \frac{U_1}{\omega \sqrt{(I_1)^2 - \left(\frac{P_1}{U_1}\right)^2}} \quad (3.37c)$$

where U_1 , U_2 , I_1 and P_1 , shown in equation (3.37), represent the no-load experimental data.

Under short-circuit test conditions the model according to figure 3.25 can be simplified by ignoring the magnetizing current and iron losses. The reason for this is that the secondary voltage is very low compared to normal operation. Hence the current which flows in R_M and L_M is small in comparison to the rated primary current. Consequently, the currents which flow in these components can be ignored when the transformer is exposed to a short-circuit test. For the calculation linked to this test we will refer to the applied secondary voltage and measured secondary current to the primary side. Which means that we can consider (for calculation purposes) the short-circuit problem from the primary side. The total resistance R_p as seen from the primary side consists of the primary resistance R_1 to which we must add the primary referred secondary resistance $R'_2 = k^2 R_2$. The leakage reactance ωL_σ completes this series network, which is excited by a primary referred secondary voltage $U'_2 = kU_2$. The primary referred secondary current is equal to $I'_2 = I_2/k$. The short-circuit impedance Z_p as seen from the primary side is equal to $Z_p = U'_2/I'_2 = \sqrt{R_p^2 + (\omega L_\sigma)^2}$. The impedance Z_p can therefore be found on the basis of the applied secondary voltage U_2 , calculated winding ratio k and measured current I_2 . In addition, the short-circuit power P_2 was measured which may be written as $P_2 = (I'_2)^2 R_p$. From this equation the total resistance as 'seen' from the primary side can be obtained. The individual resistance values cannot be found (unless they are measured directly with the aid of an Ohm meter) from these measurements and the assumption made in this case is that $R'_2 = R_1$. The parameters, which are obtained from the short-circuit measurements are calculated as follows

$$R_p \simeq k^2 \frac{P_2}{I_2^2} \quad (3.38a)$$

$$R_1 \simeq \frac{R_p}{2} \quad (3.38b)$$

$$R_2 \approx \frac{R_p}{2 k^2} \quad (3.38c)$$

$$L_\sigma \approx \frac{1}{\omega} \sqrt{\left(k^2 \frac{U_2}{I_2} \right)^2 - R_p^2} \quad (3.38d)$$

where U_2 , I_2 and P_2 shown in equation (3.38) represent the short-circuit experimental data. The winding factor k was calculated using equation (3.37a). The first part of the m-file shown below calculates the parameters for this transformer based on the no-load and short-circuit test data.

m-file Tutorial 3, part 1, chapter 3

```
%Tutorial 3, part 1, chapter 3
%no-load data
U1_n=660; % RMS primary voltage
I1_n=0.2; % RMS primary current
U2_n=240; % RMS secondary voltage
P1_n=20; % noload measured power
%%%%%
w=2*pi*50;%frequency rad/s
%%%parameters from noload data
k=U1_n/U2_n; %winding ratio
RM=U1_n^2/P1_n; % resistance
LM=1/w*U1_n/sqrt(I1_n^2-(P1_n/U1_n)^2); %inductance LM
%%%%%
%%%short circuit data
U2_s=8; % secondary RMS
I2_s=20; % short circuit voltage
P2_s=20; % secondary RMS rated current
P2_s=20; % secondary power
%%%parameters from this data
Rp=k^2*P2_s/I2_s^2; %total primary resistance
R1=Rp/2; % primary resistance
R2=Rp/(2*k^2); %secondary resistance
Lsigma=1/w*sqrt((k^2*U2_s/I2_s)^2-Rp^2); %leakage inductance
```

The following parameters were obtained after running this m-file.

Table 3.1. Parameters for single phase transformer

Parameters	Value
Winding ratio	k
Loss resistance	R_M
Magnetizing inductance	L_M
Primary resistance	R_1
Secondary resistance	R_2
Leakage inductance	L_σ

The second part of this tutorial is concerned with the development of a dynamic model of the transformer in question. A load resistance R_L is connected to the secondary winding and its value will be set to: $R_L = 2000\Omega$, 0Ω and 10Ω

respectively. In the first case (a), a high load resistance is chosen which closely represents the (secondary) open-circuit case. The second case (b), $R_L = 0$ corresponds to the case where the secondary winding is short-circuited. The primary RMS voltage for this example is set to $8 k = 22$, which represents the voltage which would need to be applied to the primary side in case the short-circuit test was carried out from that winding rather than from the secondary side. By considering these two cases we are able to check the simulation model in steady-state conditions against the experimental data from the no-load and short-circuit test. The third load resistance value $R_L = 10\Omega$ has been chosen arbitrarily to demonstrate the operation of the transformer under load conditions.

Implementation of the Simulink model, as shown in figure 3.26, is directly based on the generic model of figure 3.19. However a resistance $1/R_M$ is present on the primary side of the ITF module. On the secondary side a two resistance network is present which consists of the two series connected resistances R_2 and R_L . The total resistance on the secondary side is therefore equal to $R_{sec} = R_2 + R_L$ and this value must be used on the secondary ITF side (see figure 3.19). The input to the secondary integrator is the flux differential $d\psi_2/dt$, not the voltage u_2 , which is now found using $u_2 = \frac{d\psi_2}{dt} \frac{R_L}{R_L + R_2}$. Hence, the gain module ‘att’ in figure 3.26 is used to obtain the variable u_2 . The simulation run time is set to 100ms, solver type ‘ode4’ and step size $1\mu s$.

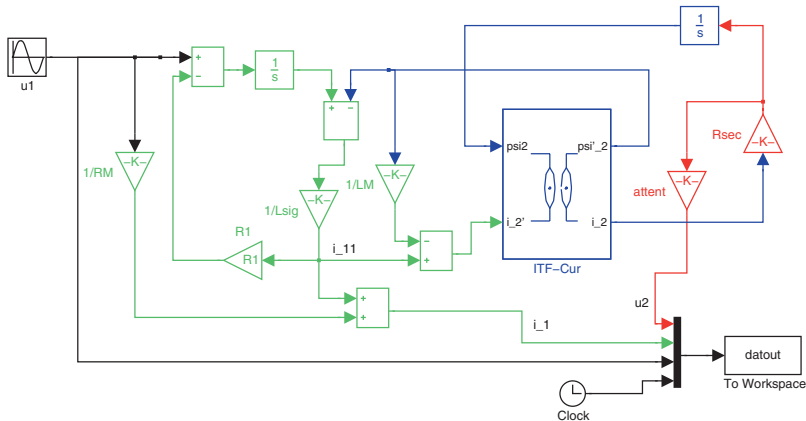


Figure 3.26. Simulink model: transformer with iron losses

The simulation model needs to be executed three times with different R_L and U_1 values as indicated in table 3.2. This implies that prior to each simulation run the appropriate R_L value must be set in the MATLAB Workspace area. Furthermore, the corresponding excitation voltage must be set in the simulation module U_1 . After running the simulation rename the output file in the MATLAB

Table 3.2. Simulation data

Simulation setup	U_1 (RMS)V	R_L (Ω)	file name
No-load	660	2000	D1
Short-circuit	22	0	D2
Load	660	10	D3

Workspace to the file name given in table 3.2. For example ‘D1=datout’ (for the no-load simulation). The results from the three simulations, as represented by the files $D1$, $D2$ and $D3$ need to be processed to show the results in the form of the input voltage $u_1 = U_1 \sqrt{2} \cos(\omega t)$, current i_1 and secondary voltage u_2 . An example of a m-file which can process this data is as follows

m-file Tutorial 3, part 2, chapter 3

```
%Tutorial 3, part 2, chapter 3
close all
subplot(3,1,1)
%%%% no-load case (a) RL=2000
plot(D1(:,4),D1(:,3)/50); % u1/50
grid; hold on
plot(D1(:,4),D1(:,2),'r'); % i1
plot(D1(:,4),D1(:,1)/10,'g'); % u_2/10
legend('u_1/50','i_1','u_2/10')
xlabel(' (a) time (s)')
ylabel('voltage/current')
subplot(3,1,2)
%%%% short-circuit secondary, U1=k*8 case (b)
plot(D2(:,4),D2(:,3)/50); % u1/50
grid; hold on
plot(D2(:,4),D2(:,2),'r'); % i1
plot(D2(:,4),D2(:,1)/10,'g'); % u_2/10
legend('u_1/50','i_1','u_2/10')
xlabel(' (b) time (s)')
ylabel('voltage/current')
%%%%%%% case (c)
subplot(3,1,3)
%RL=10, U1=660
plot(D3(:,4),D3(:,3)/50); % u1/50
grid; hold on
plot(D3(:,4),D3(:,2),'r'); % i1
plot(D3(:,4),D3(:,1)/10,'g'); % u_2/10
legend('u_1/50','i_1','u_2/10')
xlabel(' (c) time (s)')
ylabel('voltage/current')
```

The results obtained from these simulations are given in figure 3.27. It is left to the reader to run these Simulink/MATLAB files and analyze the results in detail. Some indication with respect to the correct functioning of the Simulink model can be made by observation of sub-plots ‘a’, ‘b’ of figure 3.27 and a comparison of the results according to table 3.3. The results show that there

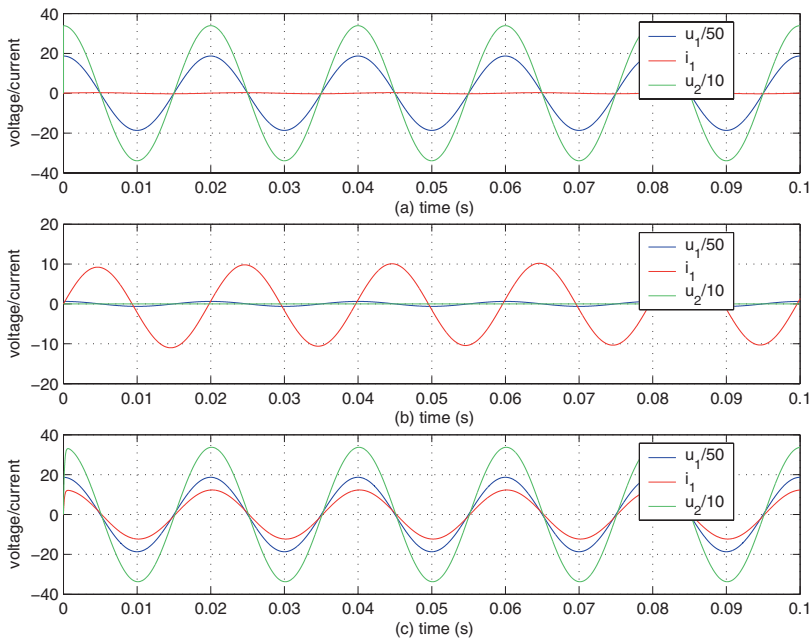


Figure 3.27. Simulink results: transformer with iron losses

Table 3.3. Comparison simulation and experimental results

-	$I_1(\text{RMS})\text{A}$	$U_2(\text{RMS})\text{V}$
Simulation (no-load, $U_1 = 660\text{V}$)	0.210	239.8
Experimental (no-load, $U_1 = 660\text{V}$)	0.2	240
Simulation (short-circuit, $U_1 = 22\text{V}$)	7.24	0
Experimental (short-circuit, $U_2 = 8\text{V}$)	7.27	0
Simulation ($R_L = 10\Omega$, $U_1 = 660\text{V}$)	8.70	238.4
Experimental ($R_L = 10\Omega$, $U_1 = 660\text{V}$)	-	-

is good agreement between the data for the no-load and short-circuit tests. No experimental data is available for case ‘c’. However, a phasor analysis could be carried out to verify the steady-state results. This exercise is left to the reader.

3.10.4 Tutorial 4

A Caspoc implementation of the previous tutorial is considered here. The load resistance is set to $R_L = 10\Omega$ for this tutorial. The transformer parameters are given in table 3.1. Furthermore, the RMS primary supply voltage is set to $U_1 = 660\text{V}$. A possible Caspoc implementation of this problem is shown in

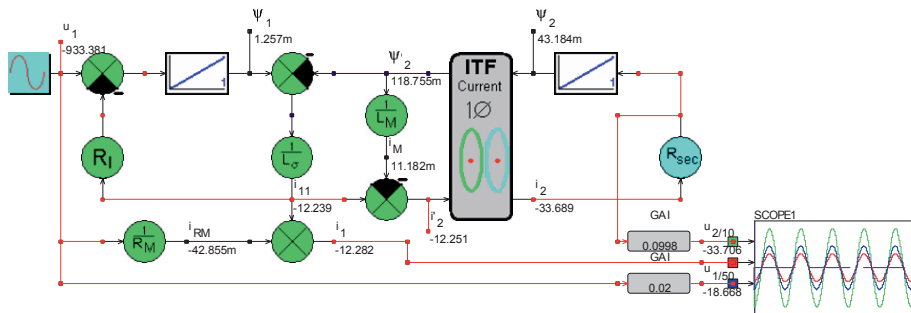


Figure 3.28. Caspoc model: transformer with iron losses

figure 3.28, where the standard gain parameters L_m , R_L represent (in this example) the parameters L_M and R_{sec} respectively.

The model representation and variables as shown in figure 3.28 correspond to those given in figure 3.19. The values of the variables shown in figure 3.28 are those which are present at that point in time when the simulation is stopped. The ‘Scope1’ unit shows the secondary voltage (with an attenuation factor of 10), primary current and primary voltage (with an attenuation factor of 50). The ‘gain’ unit with value 0.0998 represents the factor $\frac{R_L}{10(R_L+R_2)}$ required to find the variable $\frac{u_2}{10}$. Note that the gain factor $R_{sec} = R_2 + R_L$ must be set in accordance with the load resistance value assumed. The results obtained from this simulation should correspond to subplot ‘c’ given in figure 3.27.

Chapter 4

THREE-PHASE CIRCUITS

4.1 Introduction

The majority of electrical drive systems in use are powered by a so-called three-phase (three wire) supply. The main reason for this is that a more efficient energy transfer from supply to the load, such as a three-phase AC machine, is possible in comparison with a single (two wire) AC circuit. The load, being the machine acting as a motor, is formed by three phases. Each phase-winding of which has two terminals, yielding a total of six terminal-bolts, usually configured as sketched in figure 4.1. The phase impedances are assumed to be equal.

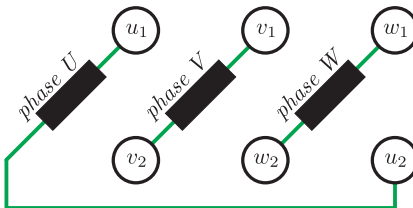


Figure 4.1. Connector on a three phase machine, with a total of six terminals

The terminal lay-out as shown in figure 4.1 has been purposely chosen to allow the user to readily connect the machine's phase windings in two distinct configurations. The star and delta configurations are depicted in figure 4.3 and figure 4.9 respectively. Voltages and currents in the different configurations are identified by the subscripts $S1$, $S2$, $S3$ when the machine is in star, wye or Y-configuration. Subscripts $D1$, $D2$, $D3$ apply to the delta or Δ configuration.

The voltages/currents, identified by the subscripts R , S , T are linked to the supply source, which is usually a power electronic converter or the three-phase grid. Figure 4.2 shows an example of a three-phase voltage supply which generates three voltages (of arbitrary shape) u_R , u_S , u_T that are defined with respect to the $0V$ (neutral) of this system. In this chapter we will look into modelling

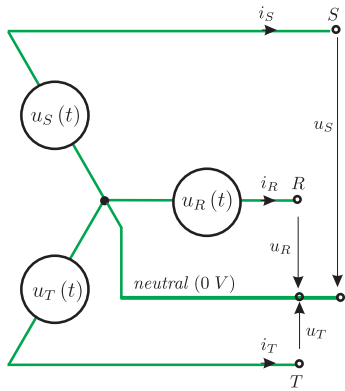


Figure 4.2. Supply convention (voltage sources shown)

three-phase circuits, and in this context introduce a new set of building blocks as required to move (in both directions) from machine phase variables to supply variables for either star or delta connected machines.

So-called space vectors are introduced as an important tool to simplify the dynamic analysis of three-phase circuits. In the sequel to this chapter the link between phasors and space vectors is made in order to examine three-phase circuits under steady-state conditions in case the supply is deemed to be sinusoidal in nature. Finally, a set of tutorials will be provided which serves to reinforce the concepts outlined in this chapter.

4.2 Star/Wye connected circuit

The term ‘star’ or ‘wye’ connected circuit refers to the configuration shown in figure 4.4, where the machine phases are connected in such a manner that a common ‘star’ or ‘neutral’ point is established. This star-point is usually *not* connected to the neutral or 0V reference point of the supply. For the ‘star’ connected configuration the lower three terminals v_2 , w_2 , u_2 are interconnected as shown by the red lines in figure 4.3. This figure also shows how the R , S and T supply is connected to the machine terminals.

The supply voltages u_R , u_S , u_T and u_{S0} are defined with respect to the 0V of the supply source (see figure 4.2). Note (again) that the supply voltages are instantaneous functions of time and need not be sinusoidal. Furthermore, the sum of the three voltages does not and indeed will not usually be zero when a power electronic converter is used as a supply source. On the basis of Kirchhoff’s voltage and current laws and observation of figure 4.4 we will determine the relationships that exist between supply and phase variables.

With respect to the phase variables the following expressions are valid

$$i_{S1} + i_{S2} + i_{S3} = 0 \quad (4.1a)$$

$$u_{S1} + u_{S2} + u_{S3} = 0 \quad (4.1b)$$

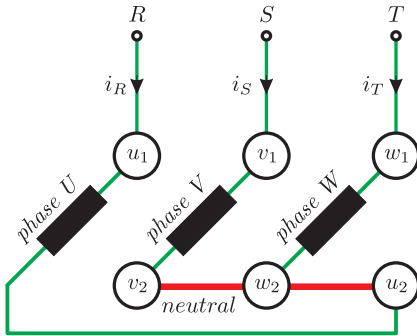


Figure 4.3. Three phase machine, star (Y) connected

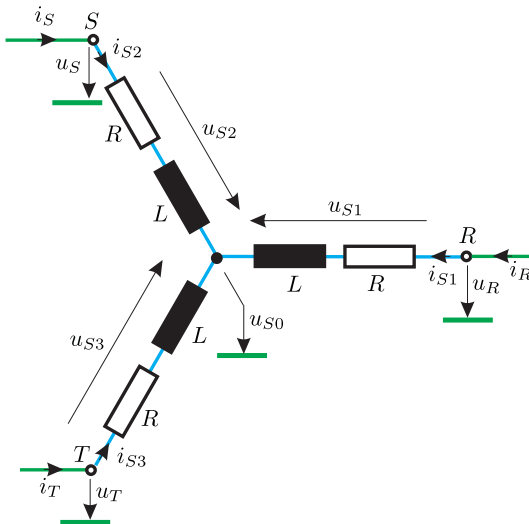


Figure 4.4. Star/Wye connected according figure 4.3

Note that equation (4.1b) shows that the sum of the phase voltages is zero. This is indeed the case here because the phase impedances are deemed to be equal. The supply currents i_R, i_S, i_T are in this case equal to the phase currents i_{S1}, i_{S2}, i_{S3} respectively. Hence, the building block as shown in figure 4.5(a) has a transfer function as given by equation (4.2).

$$\begin{bmatrix} i_{S1} \\ i_{S2} \\ i_{S3} \end{bmatrix} = \begin{bmatrix} 1 & 0 & 0 \\ 0 & 1 & 0 \\ 0 & 0 & 1 \end{bmatrix} \begin{bmatrix} i_R \\ i_S \\ i_T \end{bmatrix} \quad (4.2)$$

In the following analysis we will also directly discuss the inverse, i.e. the transfer function and building block(s) needed to return from phase to supply variables. This approach is instructive as cascading the two modules must give the original supply waveforms. In this case the inverse is the unity matrix as

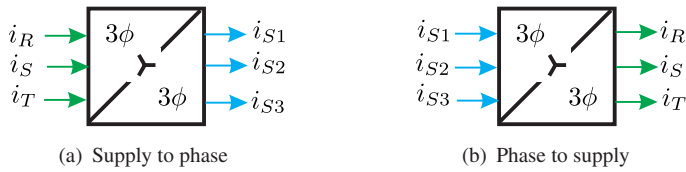


Figure 4.5. Current conversions: star connected

represented by equation (4.3) and building block as represented by figure 4.5(b).

$$\begin{bmatrix} i_R \\ i_S \\ i_T \end{bmatrix} = \begin{bmatrix} 1 & 0 & 0 \\ 0 & 1 & 0 \\ 0 & 0 & 1 \end{bmatrix} \begin{bmatrix} i_{S1} \\ i_{S2} \\ i_{S3} \end{bmatrix} \quad (4.3)$$

The conversion of supply to phase voltages is according to figure 4.4 of the form given by,

$$\begin{bmatrix} u_{S1} \\ u_{S2} \\ u_{S3} \end{bmatrix} = \begin{bmatrix} 1 & 0 & 0 \\ 0 & 1 & 0 \\ 0 & 0 & 1 \end{bmatrix} \begin{bmatrix} u_R \\ u_S \\ u_T \end{bmatrix} - \begin{bmatrix} 1 \\ 1 \\ 1 \end{bmatrix} u_{S0} \quad (4.4)$$

in which the voltage u_0 given in equation (4.4) is the potential of the star point with respect to the 0V reference of the supply. The voltage u_{S0} is the so-called zero sequence component and can be found with the aid of equations (4.1b), (4.4) which leads to

$$u_{S0} = \frac{u_R + u_S + u_T}{3} \quad (4.5)$$

The conversion module which represents equation (4.4) is given by figure 4.6(a). An important observation from figure 4.6(a) is that this module has a fourth output, the voltage u_{S0} , which is obtained from u_R , u_S , u_T and the superposition

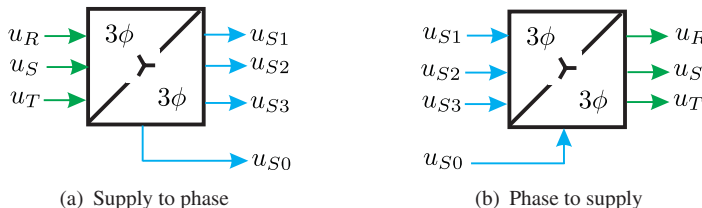


Figure 4.6. Voltage conversions: star connected

of symmetrical machine impedances. The inversion follows directly from figure 4.4 and is of the form

$$\begin{bmatrix} u_R \\ u_S \\ u_T \end{bmatrix} = \begin{bmatrix} 1 & 0 & 0 \\ 0 & 1 & 0 \\ 0 & 0 & 1 \end{bmatrix} \begin{bmatrix} u_{S1} \\ u_{S2} \\ u_{S3} \end{bmatrix} + \begin{bmatrix} 1 \\ 1 \\ 1 \end{bmatrix} u_{S0} \quad (4.6)$$

In equation (4.6) the value of u_{S0} can be chosen freely, hence the supply voltages u_R, u_S, u_T are not unique for a given set of phase voltages u_{S1}, u_{S2}, u_{S3} . The conversion module is given in figure 4.6(b).

4.2.1 Modelling star connected circuit

The single phase R, L circuit model has been discussed earlier and the generic implementation given in figure 2.5 on page 32 needs to be duplicated three times, as shown in figure 4.7. Note that the three-phase R-L model shown

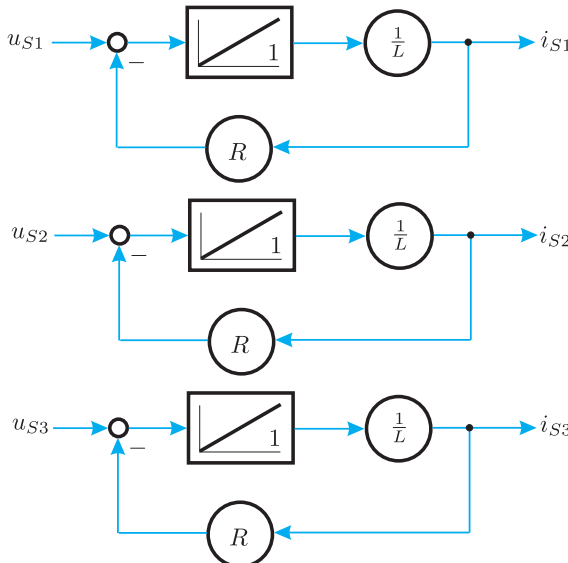


Figure 4.7. Generic three-phase R-L model

in figure 4.7 is a simplified representation of an AC machine. In reality, mutual coupling terms exist between the phases which severely complicates the three-phase circuit model. At a later stage in this chapter an alternative approach to modelling three-phase circuits will be given, which is able to handle more complex circuits than the R-L concept considered here. The combined conversion process with all the building blocks needed to arrive at the supply currents, on the basis of a given set of supply voltages, is given in figure 4.8.

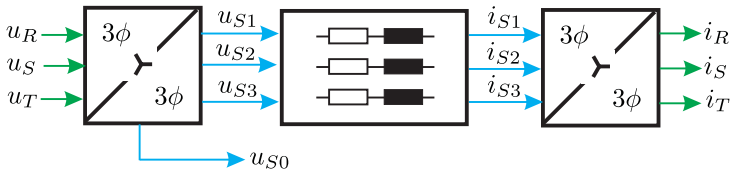


Figure 4.8. Star connected circuit model

4.3 Delta connected circuit

The term ‘delta’ connected circuit refers to the configuration shown in figure 4.10. In the terminal box on the machine, the terminal pairs (u_1, v_2) , (v_1, w_2) and (w_1, u_2) are interconnected, as shown by three red lines in figure 4.9. The delta connection is often used in applications with relatively low supply voltages. Furthermore, delta connected machines are commonly used in high power applications (typically from about 0.5 MW upwards).

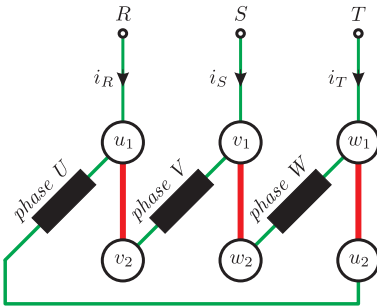
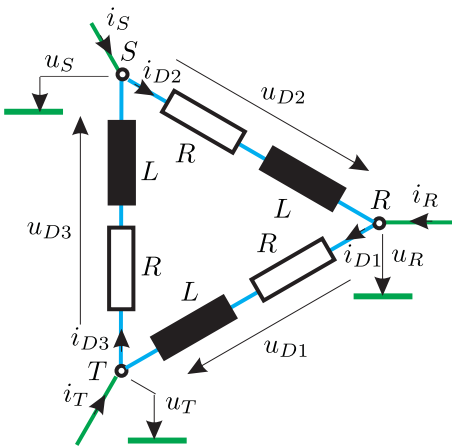
Figure 4.9. Three phase machine, delta (Δ) connected

Figure 4.10. Delta connected according to figure 4.9

The supply voltages u_R , u_S , u_T are defined with respect to the 0V of the supply source in the same manner as discussed in section 4.2. It is re-emphasized

that the supply voltages are instantaneous functions of time and need not be sinusoidal and the sum of the three do not need to be zero. On the basis of Kirchhoff's voltage and current laws and observation of figure 4.10 we can again determine the relationships that exist between supply and phase variables.

With respect to the phase variables the following expressions are valid

$$i_{D1} + i_{D2} + i_{D3} = 3i_{D0} \quad (4.7a)$$

$$u_{D1} + u_{D2} + u_{D3} = 0 \quad (4.7b)$$

where i_{D0} represents a so-called zero sequence current. In the circuit model as given in figure 4.10 no such current will exist. However, if for example a voltage source is introduced in each phase leg, which has a third harmonic component then a non-zero loop current i_{D0} will be generated, hence $i_{D1} = i_{D0}$, $i_{D2} = i_{D0}$ and $i_{D3} = i_{D0}$. Under these conditions the sum of these phase currents is equal to $3i_{D0}$ as shown by equation (4.7a). Measurements from a practical system with substantial loop-current are shown on page 98. Equation (4.7a) may also be written as

$$i_{D0} = \frac{i_{D1} + i_{D2} + i_{D3}}{3} \quad (4.8)$$

The relationship between supply currents i_R , i_S , i_T and phase currents i_{D1} , i_{D2} , i_{D3} is in this case found using Kirchhoff's current law and observation of figure 4.10. For example the current i_R may be expressed as $i_R = i_{D1} - i_{D2}$. If we extend this analysis to all three phases the transfer function according to equation (4.9) appears.

$$\begin{bmatrix} i_R \\ i_S \\ i_T \end{bmatrix} = \begin{bmatrix} 1 & -1 & 0 \\ 0 & 1 & -1 \\ -1 & 0 & 1 \end{bmatrix} \begin{bmatrix} i_{D1} \\ i_{D2} \\ i_{D3} \end{bmatrix} \quad (4.9)$$

The conversion module which represents equations (4.9), (4.5) is given by figure 4.11(a).

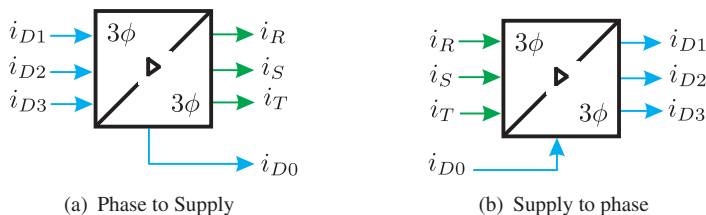


Figure 4.11. Current conversions: delta connected

An important observation from figure 4.11(a) is that this module has a fourth output the current i_{D0} , as defined by equation (4.8), which is required in order to

facilitate the conversion from phase currents to supply currents. This conversion follows from figure 4.10 and it is instructive to initially consider the process by which an expression for the branch current i_{D1} is formed. From figure 4.10 the following expressions can be found

$$i_{D1} = i_R + i_{D2} \quad (4.10a)$$

$$i_{D1} = -i_T + i_{D3} \quad (4.10b)$$

Adding equations (4.10a), (4.10b) gives

$$2i_{D1} = i_R - i_T + \underbrace{(i_{D2} + i_{D3})}_{-i_{D1}+3i_{D0}} \quad (4.11)$$

where the term $(i_{D2} + i_{D3})$ can according to equation (4.7a) also be written as $(-i_{D1} + 3i_{D0})$, which leads to $i_{D1} = \frac{1}{3}(i_R - i_T) + i_{D0}$. It is noted that this expression is in fact not an explicit function for i_{D1} given that i_{D0} is also a function of the currents i_{D1}, i_{D2}, i_{D3} . This means that the conversion from supply to phase current can only be made if the current i_{D0} is known, i.e. obtained from the ‘delta’ phase to supply current conversion module discussed earlier (see figure 4.11(a)). The exception to this rule is the case where the sum of the phase currents will be zero, as is the case when the latter are sinusoidal, of equal amplitude and displaced by an angle of $2\pi/3$ with respect to each other. If we extend this single phase analysis for i_{D1} to all three phases, the conversion matrix, as given by expression (4.12) and building module (figure 4.11(b)), appears.

$$\begin{bmatrix} i_{D1} \\ i_{D2} \\ i_{D3} \end{bmatrix} = \begin{bmatrix} \frac{1}{3} & 0 & -\frac{1}{3} \\ -\frac{1}{3} & \frac{1}{3} & 0 \\ 0 & -\frac{1}{3} & \frac{1}{3} \end{bmatrix} \begin{bmatrix} i_R \\ i_S \\ i_T \end{bmatrix} + \begin{bmatrix} 1 \\ 1 \\ 1 \end{bmatrix} i_{D0} \quad (4.12)$$

The conversion of supply voltages to phase voltage is according to figure 4.10 of the form given by equation (4.13).

$$\begin{bmatrix} u_{D1} \\ u_{D2} \\ u_{D3} \end{bmatrix} = \begin{bmatrix} 1 & 0 & -1 \\ -1 & 1 & 0 \\ 0 & -1 & 1 \end{bmatrix} \begin{bmatrix} u_R \\ u_S \\ u_T \end{bmatrix} \quad (4.13)$$

The conversion module which represents equation (4.13) is given by figure 4.12(a). Figure 4.12(a) has a fourth output, the voltage u_{S0} , as found using equation (4.5), which is again required to facilitate the conversion from phase voltage to supply voltages. The inversion follows directly from figure (4.10) and can be made more translucent by initially considering a single phase conversion

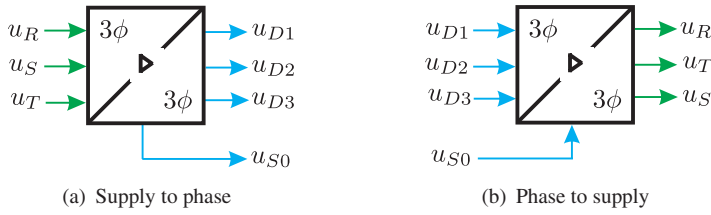


Figure 4.12. Voltage conversions: delta connected

first. An observation of figure 4.10 learns that the following two expressions may be found which contain the voltage u_R .

$$u_R = u_{D1} + u_T \quad (4.14a)$$

$$u_R = -u_{D2} + u_S \quad (4.14b)$$

Adding equations (4.14a), (4.14b) gives

$$2u_R = u_{D1} - u_{D2} + \underbrace{(u_T + u_S)}_{-u_R + 3u_{S0}} \quad (4.15)$$

where the term $(u_T + u_S)$ can according to equation (4.5) also be written as $(-u_R + 3u_{S0})$, which leads to $u_R = \frac{1}{3}(u_{D1} - u_{D2}) + u_{S0}$. It is noted (as was the case for the ‘current’ conversion) that this expression is in fact not an explicit expression for u_R given that u_{S0} is also a function of the voltages u_R , u_S , u_T . This means that the conversion from phase to supply voltages can only be made if the voltage u_{S0} is known. In the case where the sum of the supply voltages is zero, as is the case when the latter are sinusoidal, of equal magnitude and displaced by an angle of $2\pi/3$ with respect to each other the voltage u_{S0} will be zero. If we extend our single phase analysis shown above for u_R to the remaining two phases the conversion matrix as given by expression (4.16) and building module (figure 4.12(b)), appears.

$$\begin{bmatrix} u_R \\ u_S \\ u_T \end{bmatrix} = \begin{bmatrix} \frac{1}{3} & -\frac{1}{3} & 0 \\ 0 & \frac{1}{3} & -\frac{1}{3} \\ -\frac{1}{3} & 0 & \frac{1}{3} \end{bmatrix} \begin{bmatrix} u_{D1} \\ u_{D2} \\ u_{D3} \end{bmatrix} + \begin{bmatrix} 1 \\ 1 \\ 1 \end{bmatrix} u_{S0} \quad (4.16)$$

4.3.1 Modelling delta connected circuit

The three-phase R, L generic circuit model, as shown in figure 4.7, for the star connected phase configuration is directly applicable here with the important difference that the current/voltage phase variables u_{S1} , u_{S2} , u_{S3} , i_{S1} , i_{S2} , i_{S3} must be replaced by the variables u_{D1} , u_{D2} , u_{D3} , i_{D1} , i_{D2} , i_{D3} given that we are dealing with a delta connected load. The inputs to this module will be the

phase voltages from the delta connected circuit and the outputs are the three phase currents. The conversion process needed to arrive at the supply currents given a set of supply voltages is shown in figure 4.13.

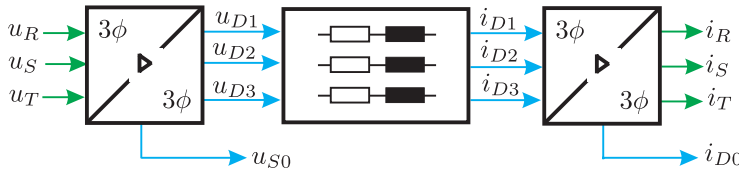


Figure 4.13. Delta connected circuit model

4.4 Space vectors

The question as to why we need ‘space vectors’ comes down to the difficulty of handling complex three phase systems as was mentioned earlier. It will be shown that the introduction of a space vector type representation for a three-phase system leads to considerable simplification.

The space vector formulation is in its general form given by equation (4.17).

$$\vec{x} = C \left\{ x_R + x_S e^{j\gamma} + x_T e^{j2\gamma} \right\} \quad (4.17)$$

with $\gamma = \frac{2\pi}{3}$. The variables x_R, x_S, x_T represent three instantaneous time dependent supply variables. These may for example, be the three supply voltages u_R, u_S, u_T , or in fact any other variable. Furthermore, these variables are real quantities and do *not* need to be sinusoidal. The constant C is a scalar and its value will be defined at a later stage.

The space vector \vec{x} itself is both complex and time dependent. The space vector is represented in a complex plane which at present is assumed to be stationary. The space vector can according to equation (4.18) also be written in terms of a real x_α and imaginary x_β component with $j = \sqrt{-1}$.

$$\vec{x} = x_\alpha + jx_\beta \quad (4.18)$$

Figure 4.14 shows the space vector in the complex plane. Note that x_α is equal to $x_\alpha = \Re \{\vec{x}\}$, while x_β may be written as $x_\beta = \Im \{\vec{x}\}$. An observation of equations (4.17) and (4.18) learns that the space vector deals with a transformation process, in which a linear combination of the three supply variables x_R, x_S, x_T , is converted to a two-phase x_α, x_β form.

It is important to realize that the space vector amplitude ($|\vec{x}|$) and argument ($\arctan \frac{x_\beta}{x_\alpha}$) can be a function of time. We may see non-continuous changes of both argument and amplitude in many cases such as three phase PWM.

It is instructive at this stage to give an example based on equation (4.17) with $C = 1$. In this case we will plot the space vector for three cases. Each

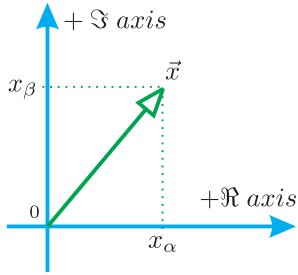


Figure 4.14. Space vector representation in a complex plane

case corresponds to one of the three supply variables of equation (4.17) being non-zero.

case 1: $x_R > 0, x_S = 0, x_T = 0$, the space vector is then of the form $\vec{x} = x_R$. This corresponds to $x_\alpha = x_R, x_\beta = 0$.

case 2: $x_S > 0, x_R = 0, x_T = 0$, the space vector is then of the form $\vec{x} = x_S e^{j\gamma}$. This corresponds to $x_\alpha = x_S \cos \gamma, x_\beta = x_S \sin \gamma$ which may also be written as $x_\alpha = -\frac{1}{2}x_S, x_\beta = \frac{\sqrt{3}}{2}x_S$

case 3: $x_T > 0, x_R = 0, x_S = 0$, the space vector is then of the form $\vec{x} = x_T e^{j2\gamma}$. This corresponds to $x_\alpha = x_T \cos 2\gamma, x_\beta = x_T \sin 2\gamma$, which may also be written as $x_\alpha = -\frac{1}{2}x_T, x_\beta = -\frac{\sqrt{3}}{2}x_T$

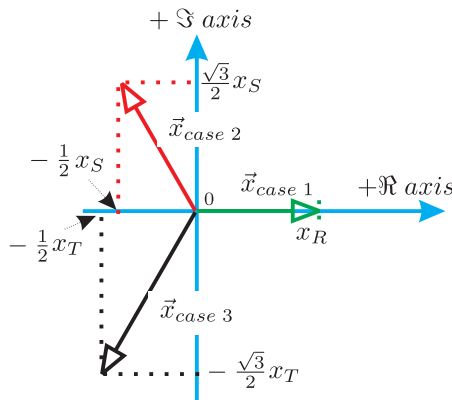


Figure 4.15. Space vector example, for three case studies

Figure 4.15 shows the three cases considered above where it is assumed that $x_T > x_S > x_R$. Note that it is interesting to observe one of the cases above in the event that one of the supply variables is for example a sinusoidal function of time.

4.5 Amplitude and power invariant space vectors

In this section we will consider the prudent choices we can make with respect to the value of the constant C (see equation 4.17). In support of this discussion we will use the three supply voltages which will be assumed sinusoidal and of the form given by equation (4.19). Note that this assumption does not undermine the generality of using space vectors for waveforms which are not sinusoidal nor for that matter does the sum of the three waveforms need to be zero as will become apparent shortly.

$$u_R = \hat{u} \cos(\omega t) \quad (4.19a)$$

$$u_S = \hat{u} \cos(\omega t - \gamma) \quad (4.19b)$$

$$u_T = \hat{u} \cos(\omega t - 2\gamma) \quad (4.19c)$$

The phase shift of the waveforms in equation (4.19) is represented by the variable $\gamma = \frac{2\pi}{3}$. The process of finding a space vector form for the three voltages u_R , u_S , u_T , as defined by equation (4.19), is readily realized by substituting said equation into (4.17) which gives

$$\frac{\vec{u}}{C\hat{u}} = \cos \omega t + \cos(\omega t - \gamma) e^{j\gamma} + \cos(\omega t - 2\gamma) e^{j2\gamma} \quad (4.20)$$

Expression (4.20) may be developed further by making use of the expression $\cos y = \frac{e^{jy} + e^{-jy}}{2}$ which, after some manipulation (which the reader should look at carefully), gives

$$\frac{\vec{u}}{C\hat{u}} = \frac{3}{2} e^{j\omega t} + \underbrace{\frac{1}{2} \left\{ e^{-j\omega t} + e^{-j(\omega t - 2\gamma)} + e^{-j(\omega t - 4\gamma)} \right\}}_{\text{vector sum is zero}} \quad (4.21)$$

The second term in the right hand side of equation (4.21) is zero, given that this term is formed by three vectors of the same amplitude which are phase shifted with respect to each other by an angle γ . This means that the vector sum of these three vectors is zero, hence the voltage space vector is reduced to the form given in equation (4.22)

$$\vec{u} = \frac{3}{2} C\hat{u} e^{j\omega t} \quad (4.22)$$

The space voltage vector is thus a function of time (argument ωt) and its amplitude is equal to $\frac{3}{2} C\hat{u}$. The voltage vector end point as presented in a complex plane will be circular as indicated in figure 4.16.

The analysis, as used to determine the voltage vector from the three phase voltages, can also be given for the currents. It is left to the reader to undertake this exercise in detail. Broadly speaking you must consider the three current

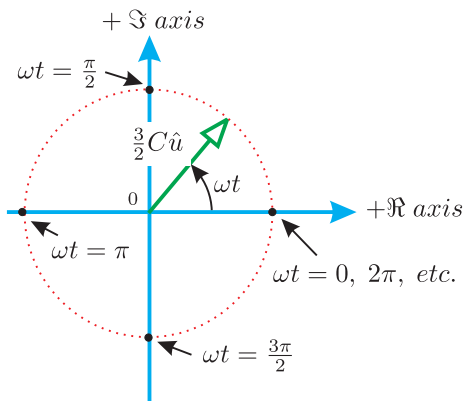


Figure 4.16. Voltage space vector as function of time

variables according to equation (4.23)

$$i_R = \hat{i} \cos(\omega t + \rho) \quad (4.23a)$$

$$i_S = \hat{i} \cos(\omega t + \rho - \gamma) \quad (4.23b)$$

$$i_T = \hat{i} \cos(\omega t + \rho - 2\gamma) \quad (4.23c)$$

and use equation (4.17), which then leads to equation (4.24).

$$\vec{i} = \frac{3}{2} C \hat{i} e^{j(\omega t + \rho)} \quad (4.24)$$

The issue of choosing a suitable value for the constant C , as defined by equation (4.17), is considered here. In the example linked to figure 4.15 this constant was conveniently set to unity but this is not a suitable value as will be come apparent shortly.

There are in fact two prudent values which may be assigned to the constant C . The first option we have is to set the constant to a value $C = 2/3$. Space vectors which abide with this C value are given in so-called ‘amplitude invariant’ form. The reason for this can be made clear by observing equations (4.22) and (4.24), with $C = 2/3$. With this value of C the equations are given as

$$\vec{u} = \hat{u} e^{j\omega t} \quad (4.25a)$$

$$\vec{i} = \hat{i} e^{j(\omega t + \rho)} \quad (4.25b)$$

An observation of equation (4.25) learns that the amplitude of the space vectors is now *equal* to the peak phase variable value, which is why this notation form is referred to as amplitude invariant.

The second notation form and the one used in this book refers to a so-called ‘power invariant’ notation form. For this notational form the constant is chosen to be $C = \sqrt{\frac{2}{3}}$. The voltage and current space vectors given by equations (4.22)

and (4.24) will then be of the form

$$\vec{u} = \sqrt{\frac{3}{2}} \hat{u} e^{j\omega t} \quad (4.26a)$$

$$\vec{i} = \sqrt{\frac{3}{2}} \hat{i} e^{j(\omega t + \rho)} \quad (4.26b)$$

This means that the space vector amplitude of for example the voltage is of the form $|\vec{u}| = \sqrt{\frac{3}{2}} \hat{u}$. Hence the space vector amplitude is a factor $\sqrt{\frac{3}{2}}$ greater than the amplitude of the corresponding phase variables. The power invariant notation form can be made more plausible by considering the total instantaneous power in the two-phase system represented by the variables u_α , u_β and i_α , i_β which is of the form

$$p_{2\phi} = u_\alpha i_\alpha + u_\beta i_\beta \quad (4.27)$$

Equation (4.27) may also be written in its space vector notation form namely

$$p_{2\phi} = \Re \left\{ \vec{u} \left(\vec{i} \right)^* \right\} \quad (4.28)$$

where \vec{u} , \vec{i} represent the voltage and current space vectors. It is shown in section 4.6 that the variables u_α , u_β and i_α , i_β given in equation (4.27) may also be expressed in terms of the three phase variables u_R , u_S , u_T and i_R , i_S , i_T which allows equation (4.27) to be written as

$$p_{2\phi} = \frac{3}{2} C^2 p_{3\phi} \quad (4.29)$$

where $p_{3\phi} = u_R i_R + u_S i_S + u_T i_T$ represents the total instantaneous power of a three-phase system. Note that it can be shown that equation (4.29) is valid if the sum of the supply currents i_R , i_S , i_T and/or the sum of the supply voltages u_R , u_S , u_T is equal to zero. In this book the sum of the supply currents is always taken to be zero, which implies that only three wires are present between the supply and the machine.

Equation (4.29) is significant as it conveys the meaning of the term ‘power invariant’ namely that the instantaneous power of a two-phase system is equal to that of a three-phase system in case the constant C is chosen to be equal to $C = \sqrt{\frac{2}{3}}$.

Note that the use of an amplitude invariant space vector notation would cause the instantaneous power of a three-phase system to be scaled by a factor $\frac{3}{2}$. When calculating for example the output power of a three-phase electrical machine using amplitude invariant space vectors, this factor must be added in order to ‘correct’ the power calculation. A more detailed discussion on the concept of ‘power’ in single and three-phase systems is given in chapter 5.

4.6 Application of space vectors for three-phase circuit analysis

In this section the aim is to introduce the space vector concept in the star and delta connected three-phase circuits, as discussed in sections 4.2 and 4.3.

Two common transfer modules, namely from three phase to space vector and vice versa need to be discussed. The first case concerns the conversion of phase x_{S1}, x_{S2}, x_{S3} (star connected), x_{D1}, x_{D2}, x_{D3} (delta connected) or supply x_R, x_S, x_T , variables, given in a general form as x_a, x_b, x_c , to a space vector form $\vec{x}_{abc} = x_\alpha + jx_\beta$. The sum of the three scalar variables is of the form $x_a + x_b + x_c = 3x_0$ where x_0 represents a zero sequence component which may have a non-zero value.

According to equation (4.17) the relationship between vector and scalar variables may be written as

$$\vec{x}_{abc} = C \left\{ x_a + x_b e^{j\gamma} + x_c e^{j2\gamma} \right\} \quad (4.30)$$

If we equate the real and imaginary components of equation (4.17) the conversion matrix according to equation (4.31) and figure 4.17(a) is found.

$$\begin{bmatrix} x_\alpha \\ x_\beta \end{bmatrix} = \begin{bmatrix} C & -\frac{C}{2} & -\frac{C}{2} \\ 0 & \frac{C\sqrt{3}}{2} & -\frac{C\sqrt{3}}{2} \end{bmatrix} \begin{bmatrix} x_a \\ x_b \\ x_c \end{bmatrix} \quad (4.31)$$

In this expression the value of $C = \sqrt{\frac{2}{3}}$ should be used for power invariant space vector representations. The building block according to figure 4.17(a)

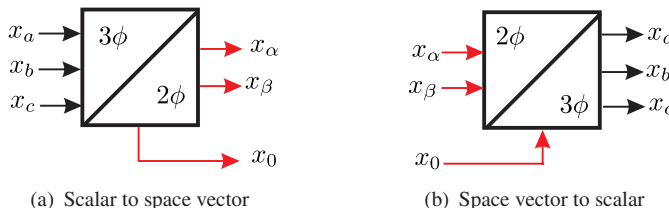


Figure 4.17. Conversion from and to space vector format: general case

has a fourth output which is the zero sequence variable x_0 introduced earlier as

$$x_0 = \frac{x_a + x_b + x_c}{3} \quad (4.32)$$

The process of finding the inverse conversion process which allows us to move from space vector variables to scalar variables is considered here. A suitable

starting point for this conversion is equation (4.31), which gives an expression for x_α namely

$$x_\alpha = Cx_a - \frac{C}{2} (x_b + x_c) \quad (4.33)$$

The sum of the three phase variables is according to equation (4.32) equal to $3x_0$ and this expression can also be written as $x_b + x_c = -x_a + 3x_0$. Substitution of this expression into (4.33) leads to

$$x_a = \frac{2}{3C} x_\alpha + x_0 \quad (4.34)$$

The variable x_b is also directly obtained from equation (4.31) in which we consider the second row namely

$$x_\beta = C \frac{\sqrt{3}}{2} (x_b - x_c) \quad (4.35)$$

Substitution of $x_c = -(x_b + x_a) + 3x_0$ and use of (4.34) gives after some manipulation

$$x_b = -\frac{1}{3C} x_\alpha + \frac{1}{C\sqrt{3}} x_\beta + x_0 \quad (4.36)$$

The remaining variable x_c is found by use of $x_c = -(x_a + x_b) + 3x_0$ together with equations (4.34) and (4.35). The resultant complete conversion in matrix form as given by equation (4.37), corresponds to the building block shown in figure 4.17(b).

$$\begin{bmatrix} x_a \\ x_b \\ x_c \end{bmatrix} = \begin{bmatrix} \frac{2}{3C} & 0 \\ -\frac{1}{3C} & \frac{1}{C\sqrt{3}} \\ -\frac{1}{3C} & -\frac{1}{C\sqrt{3}} \end{bmatrix} \begin{bmatrix} x_\alpha \\ x_\beta \end{bmatrix} + \begin{bmatrix} 1 \\ 1 \\ 1 \end{bmatrix} x_0 \quad (4.37)$$

4.6.1 Use of space vectors in star connected circuits

The conversion process from phase voltages and currents to a space vector form (in stationary coordinates) is identical for both, hence the phase variables x_{S1} , x_{S2} , x_{S3} are introduced which need to be converted to a form $\vec{x}_{S123} = x_{S\alpha} + jx_{S\beta}$. Note that the space vector variables are identified by subscripts $S\alpha$, $S\beta$ respectively. The conversion modules as shown in figure 4.18 are identical to those shown in figure 4.17. The zero sequence ‘out’ and ‘input’ lines are not shown in figure 4.18, given that the sum of the voltage and current phase variables is zero for this circuit configuration (see equation (4.1)).

In some cases a conversion is required where phase variables x_{S1} , x_{S2} , x_{S3} or space vector variables $x_{S\alpha}$, $x_{S\beta}$ need to be converted to supply (*RST*) based variables of the form $\vec{x}_{RST} = x_\alpha + jx_\beta$.

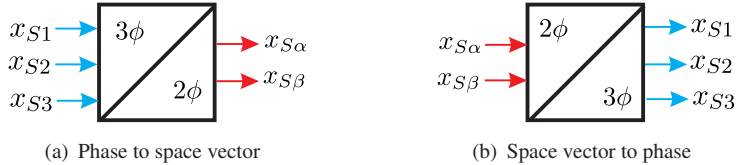


Figure 4.18. Voltage/current conversion to space vector ($\vec{x}_{RST} = \vec{x}_{S123}$) format: star connected

The starting point for this analysis is equation (4.17). The relationship between phase and supply variables for the star connected case can, according to equations (4.3), (4.6), be written as

$$x_R = x_{S1} + x_{S0} \quad (4.38a)$$

$$x_S = x_{S2} + x_{S0} \quad (4.38b)$$

$$x_T = x_{S3} + x_{S0} \quad (4.38c)$$

where x_{S0} will be zero in case the variable x represents the current i . Substitution of equation (4.38) into equation (4.17) leads to

$$\vec{x}_{RST} = C \underbrace{\left(x_{S1} + x_{S2}e^{j\gamma} + x_{S3}e^{j2\gamma} \right)}_{\vec{x}_{S123}} + Cx_{S0} \underbrace{\left(1 + e^{j\gamma} + e^{j2\gamma} \right)}_0 \quad (4.39)$$

An important observation of equation (4.39) is that the presence of a zero sequence component in the supply variables will *not* have any impact on the conversion process. The reason for this is that the constant Cx_{S0} is multiplied by zero (the vector sum of the three terms is zero). A direct consequence of this conversion is that the inverse transformation, i.e. from space vector to supply variables, is only possible in case the zero sequence component x_{S0} is zero. A non-zero value x_{S0} is ‘lost’ in the conversion $x_R, x_S, x_T \rightarrow \vec{x}_{RST}$. A further observation of equation (4.39) learns that the space vector representation in supply and phase format are the same, hence

$$\vec{x}_{RST} = \vec{x}_{S123}. \quad (4.40)$$

Note that according to equation (4.40) the real and imaginary components of these vectors will be equal for the star connect circuit, hence, $x_\alpha = x_{S\alpha}$, $x_\beta = x_{S\beta}$. This is *not* the case for a ‘delta’ connected circuit, as will become apparent shortly.

4.6.2 Circuit modelling using space vectors: star connected

In this section we will demonstrate how we can use the space vector approach to build a dynamic generic module of this system according to figure 4.7. It is at

this stage helpful to recall the differential equation set of the circuit in question which is of the form

$$u_{S1} = i_{S1}R + L \frac{di_{S1}}{dt} \quad (4.41a)$$

$$u_{S2} = i_{S2}R + L \frac{di_{S2}}{dt} \quad (4.41b)$$

$$u_{S3} = i_{S3}R + L \frac{di_{S3}}{dt} \quad (4.41c)$$

We can rewrite equations (4.41) in a space vector form by making use of, for example, equation (4.30). This equation tells us that we can build the space vector equation of this circuit by taking the following steps:

- multiply equation (4.41a) by a factor C .
- multiply equation (4.41b) by a factor $Ce^{j\gamma}$.
- multiply equation (4.41c) by a factor $Ce^{j2\gamma}$.
- Add the three previous terms together which in effect gives us the space vector form of the current and voltage space variables.

The resultant circuit equation in space vector form is then given as

$$\vec{u}_{S123} = \frac{d\vec{\psi}_{S123}}{dt} + \vec{i}_{S123}R \quad (4.42)$$

where $\vec{\psi}_{S123} = L\vec{i}_{S123}$. The development of the generic model proceeds along the lines discussed for the single phase R-L example. A possible generic implementation of the three-phase system is given in figure 4.19. The model

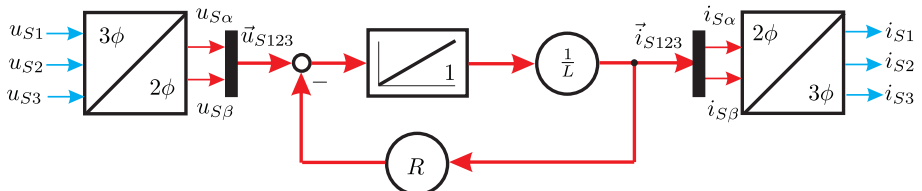


Figure 4.19. Generic, space vector based, model of three-phase R-L circuit (star connected)

according to figure 4.19 has as inputs the three phase voltage variables which are then used as inputs to a ‘three to two phase’ module, which produces the real and imaginary components of the voltage space vector $\vec{u}_{S123} = u_{S\alpha} + ju_{S\beta}$. A multiplexer function is used to convert to a so-called vector line format which simplifies the modelling process. The vector line format is represented as a

'wide' line which in this case represents the variables ($u_{S\alpha}$, $u_{S\beta}$) in array format. The integrator shown has as input the space vector flux-linkage differential which is formed by the terms \vec{u}_{S123} minus $R\vec{i}_{S123}$. The output of the integrator (with unity gain) is the flux-linkage space vector $\vec{\psi}_{S123}$, which is then multiplied by a gain $1/L$ in order to arrive at the current space vector \vec{i}_{S123} . A de-multiplexer is then used to convert from a vector line format in the form of the array variables ($i_{S\alpha}$, $i_{S\beta}$) to two scalar line variables ($i_{S\alpha}$, $i_{S\beta}$), which are the inputs to the 'two to three phase' conversion module. The outputs of this module represent the three phase currents i_{S1} , i_{S2} , i_{S3} of this system. In conclusion, the use of space vectors allows us to model three-phase circuits in the same way as single phase circuits thus simplifying the process. The space vector based circuit model as discussed here (see figure 4.19) replaces the earlier circuit model (see figure 4.7 on page 79). This new approach allows us to model more complex circuits such as electrical machines and three-phase transformers.

4.6.3 Use of space vectors in delta connected circuits

The conversion process from phase voltages and currents to a space vector form is identical for both, hence the phase variables x_{D1} , x_{D2} , x_{D3} are introduced, which need to be converted to a form $\vec{x}_{D123} = x_{D\alpha} + jx_{D\beta}$. Note that the space vector variables are identified by subscripts $D\alpha$, $D\beta$ ('D' for 'delta') respectively. The conversion modules as shown in figure 4.17 are directly applicable to the delta connected circuit as defined on page 80. The input and output variables are however tied to the 'delta' configuration as is apparent from figure 4.20. The zero sequence 'output' and 'input' lines are not shown

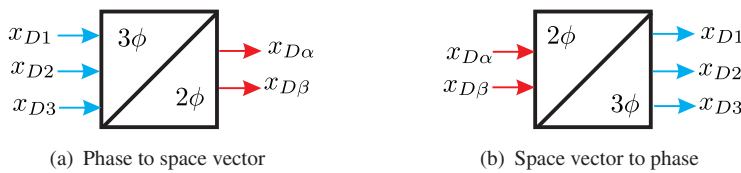


Figure 4.20. Voltage/current conversion to space vector format (\vec{x}_{D123}): delta connected

in figure 4.20. When considering this conversion for phase currents, the zero sequence connection between the two modules must be shown, given that the sum current can be non-zero.

In some cases a conversion is required where phase variables x_{D1} , x_{D2} , x_{D3} or space vector variables $x_{D\alpha}$, $x_{D\beta}$ must be converted to supply (RST) based variables of the form $\vec{x}_{RST} = x_\alpha + jx_\beta$. In this case the voltage and current phase conversions need to be examined separately.

A suitable starting point is again equation (4.17) which upon substitution of equation (4.16) may be written as

$$\vec{u}_{RST} = \frac{C}{3} \left((u_{D1} - u_{D2}) + (u_{D2} - u_{D3}) e^{j\gamma} + (u_{D3} - u_{D1}) e^{j2\gamma} \right)$$

$$+ C u_{S0} \underbrace{\left(1 + e^{j\gamma} + e^{j2\gamma} \right)}_0 \quad (4.43)$$

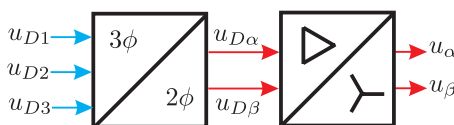
Equation (4.42) may be rearranged by grouping the phase variables as shown in equation (4.44)

$$\vec{u}_{RST} = \frac{C}{3} \left(u_{D1} \underbrace{\left(1 - e^{j2\gamma} \right)}_{\sqrt{3} e^{j\frac{\gamma}{4}}} + u_{D2} \underbrace{\left(-1 + e^{j\gamma} \right)}_{\sqrt{3} e^{j(\frac{\gamma}{4} + \gamma)}} + u_{D3} \underbrace{\left(-e^{j\gamma} + e^{j2\gamma} \right)}_{\sqrt{3} e^{j(\frac{\gamma}{4} + 2\gamma)}} \right) \quad (4.44)$$

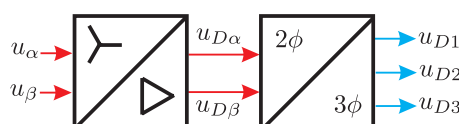
The braced terms contain a common term $\sqrt{3} e^{j\frac{\gamma}{4}}$, which allows equation (4.44) to be written as

$$\vec{u}_{RST} = \frac{1}{\sqrt{3}} e^{j\frac{\gamma}{4}} \underbrace{C \left(u_{D1} + u_{D2} e^{j\gamma} + u_{D3} e^{j2\gamma} \right)}_{\vec{u}_{D123}} \quad (4.45)$$

Equation (4.45) is significant in that it tells us that the voltage space vector $\vec{u}_{RST} = u_\alpha + j u_\beta$ can be found by converting the three phase voltages to the vector $\vec{u}_{D123} = u_{D\alpha} + j u_{D\beta}$, which needs to be rotated by an angle $\gamma/4$ (30°) and scaled by a factor $1/\sqrt{3}$. The three to two phase conversion required is carried out with the conversion matrix according to equation (4.31). In the generic representation as given by figure 4.21(a), the conversion as defined by equation (4.45) is clearly visible.



(a) Phase to space vector



(b) Space vector to phase

Figure 4.21. Phase voltage to space vector (\vec{u}_{RST}) conversions: delta connected

The second module shown with a ‘delta’ and ‘star’ symbol, symbolizes the conversion $\vec{u}_{D123} \rightarrow \vec{u}_{RST}$ which takes place when a delta connected circuit is used. The transfer matrix linked to this conversion is given by equation

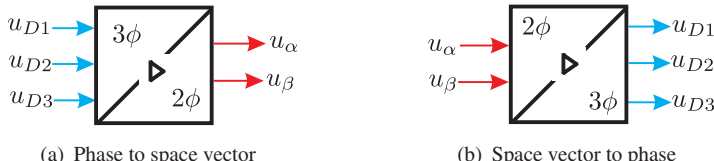
$$\begin{bmatrix} u_\alpha \\ u_\beta \end{bmatrix} = \frac{1}{\sqrt{3}} \begin{bmatrix} \cos \frac{\gamma}{4} & -\sin \frac{\gamma}{4} \\ \sin \frac{\gamma}{4} & \cos \frac{\gamma}{4} \end{bmatrix} \begin{bmatrix} u_{D\alpha} \\ u_{D\beta} \end{bmatrix} \quad (4.46)$$

The conversion module which converts the phase voltages to space vector format

$u_{D1,D2,D3} \rightarrow \vec{u}_{RST}$ is shown in figure 4.22(a). Its contents can either be according to the set of generic modules shown in figure 4.21(a) or the conversion matrix given by equation (4.47).

$$\begin{bmatrix} u_\alpha \\ u_\beta \end{bmatrix} = \begin{bmatrix} \frac{C}{2} & -\frac{C}{2} & 0 \\ \frac{C}{2\sqrt{3}} & \frac{C}{2\sqrt{3}} & -\frac{C}{\sqrt{3}} \end{bmatrix} \begin{bmatrix} u_{D1} \\ u_{D2} \\ u_{D3} \end{bmatrix} \quad (4.47)$$

This matrix is found by combining the matrices according to equations (4.31), (4.46). The inverse operation, namely the conversion process from supply



(a) Phase to space vector

(b) Space vector to phase

Figure 4.22. Alternative phase voltage to space vector (\vec{u}_{RST}) conversions: delta connected

space vector variables to phase voltage variables, follows directly from equation (4.45). This expression may also be written as

$$\vec{u}_{D123} = \sqrt{3} e^{-j\frac{\gamma}{4}} \vec{u}_{RST} \quad (4.48)$$

Equation (4.48) states that the space vector \vec{u}_{RST} must be rotated by an angle $-\gamma/4$ (-30°) and scaled by a factor $\sqrt{3}$ in order to arrive at the vector \vec{u}_{D123} which can be converted to phase voltage variables using equation (4.37). The generic modules required for this conversion are shown in figure 4.21(b). Included in this figure is a conversion module symbolized by the symbols ‘star’ and ‘delta’ and its transfer matrix is of the form given by equation (4.49).

$$\begin{bmatrix} u_{D\alpha} \\ u_{D\beta} \end{bmatrix} = \sqrt{3} \begin{bmatrix} \cos \frac{\gamma}{4} & \sin \frac{\gamma}{4} \\ -\sin \frac{\gamma}{4} & \cos \frac{\gamma}{4} \end{bmatrix} \begin{bmatrix} u_\alpha \\ u_\beta \end{bmatrix} \quad (4.49)$$

The conversion module which converts the supply space vector format to phase variables $\vec{u}_{RST} \rightarrow u_{D1,D2,D3}$ is shown in figure 4.22(b). Its contents can either be according to the set of generic modules shown in figure 4.21(b) or the conversion matrix given by equation (4.50).

$$\begin{bmatrix} u_{D1} \\ u_{D2} \\ u_{D3} \end{bmatrix} = \begin{bmatrix} \frac{1}{C} & \frac{1}{C\sqrt{3}} \\ -\frac{1}{C} & \frac{1}{C\sqrt{3}} \\ 0 & -\frac{2\sqrt{3}}{3C} \end{bmatrix} \begin{bmatrix} u_\alpha \\ u_\beta \end{bmatrix} \quad (4.50)$$

This matrix is found by combining the matrices according to equations (4.37) and (4.49), with $\cos \frac{\gamma}{4} = \frac{\sqrt{3}}{2}$ and $\sin \frac{\gamma}{4} = \frac{1}{2}$.

The starting point for determining the conversion modules for the phase currents is equation (4.17), which upon substitution of equation (4.9) may be written as

$$\vec{i}_{RST} = C \left((i_{D1} - i_{D2}) + (i_{D2} - i_{D3}) e^{j\gamma} + (i_{D3} - i_{D1}) e^{j2\gamma} \right) \quad (4.51)$$

Equation (4.51) can be rearranged by grouping the phase variables as shown in equation (4.52)

$$\vec{i}_{RST} = C \left(i_{D1} \underbrace{\left(1 - e^{j2\gamma} \right)}_{\sqrt{3} e^{j\frac{\gamma}{4}}} + i_{D2} \underbrace{\left(-1 + e^{j\gamma} \right)}_{\sqrt{3} e^{j(\frac{\gamma}{4} + \gamma)}} + i_{D3} \underbrace{\left(-e^{j\gamma} + e^{j2\gamma} \right)}_{\sqrt{3} e^{j(\frac{\gamma}{4} + 2\gamma)}} \right) \quad (4.52)$$

The braced terms contain a common term $\sqrt{3} e^{j\frac{\gamma}{4}}$, which allows equation (4.52) to be written as

$$\vec{i}_{RST} = \sqrt{3} e^{j\frac{\gamma}{4}} \underbrace{C \left(i_{D1} + i_{D2} e^{j\gamma} + i_{D3} e^{j2\gamma} \right)}_{\vec{i}_{D123}} \quad (4.53)$$

Equation (4.53) is significant because it tells us that the current space vector $\vec{i}_{RST} = i_\alpha + j i_\beta$ can be found by converting the three-phase currents to a phase vector $\vec{i}_{D123} = i_{D\alpha} + j i_{D\beta}$, which needs to be rotated by an angle $\gamma/4$ and scaled by a factor $\sqrt{3}$. The required three to two phase conversion is carried out with the conversion matrix according to equation (4.31). In the generic representation, as given by figure 4.23(a), the conversion steps as defined by equation (4.53) are clearly visible.

The second module, shown with a ‘delta’ and ‘star’ symbol, symbolizes the conversion $\vec{i}_{D123} \rightarrow \vec{i}_{RST}$ which takes place when a delta connected circuit (page 80) is used. The transfer matrix for this conversion is given by equation (4.54). Note that any zero sequence current component will not appear in

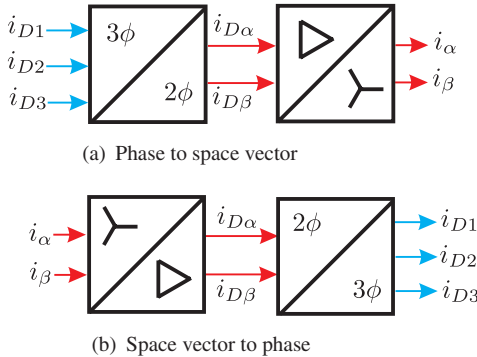


Figure 4.23. Phase to space vector \vec{i}_{RST} conversions: delta connected

these transformations.

$$\begin{bmatrix} i_\alpha \\ i_\beta \end{bmatrix} = \sqrt{3} \begin{bmatrix} \cos \frac{\gamma}{4} & -\sin \frac{\gamma}{4} \\ \sin \frac{\gamma}{4} & \cos \frac{\gamma}{4} \end{bmatrix} \begin{bmatrix} i_{D\alpha} \\ i_{D\beta} \end{bmatrix} \quad (4.54)$$

An alternative conversion from phasor to space vector format can be made by combining the transfer matrices of the modules shown in figure 4.23(a). The resultant transfer matrix found using equations (4.31) and (4.54) is given by equation (4.55).

$$\begin{bmatrix} i_\alpha \\ i_\beta \end{bmatrix} = \begin{bmatrix} \frac{3C}{2} & -\frac{3C}{2} & 0 \\ \frac{\sqrt{3}C}{2} & \frac{\sqrt{3}C}{2} & -\sqrt{3}C \end{bmatrix} \begin{bmatrix} i_{D1} \\ i_{D2} \\ i_{D3} \end{bmatrix} \quad (4.55)$$

The corresponding generic diagram for this module is shown in figure 4.24(a).

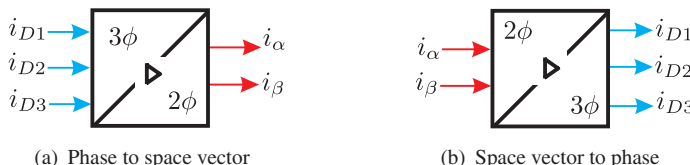


Figure 4.24. Alternative conversions phase current to space vector \vec{i}_{RST} : delta connected

An example of the practical use of conversion modules is given in figure 4.25. This figure shows three measured currents i_{D1} , i_{D2} , i_{D3} respectively. An amplitude invariant ($C = 2/3$) conversion to space vector format was made for the phase currents in this delta connected circuit, hence use was made of the model according to figure 4.24(a). A zero sequence current i_{D0} is also shown, calculated using equation (4.8), also with $C = 2/3$.

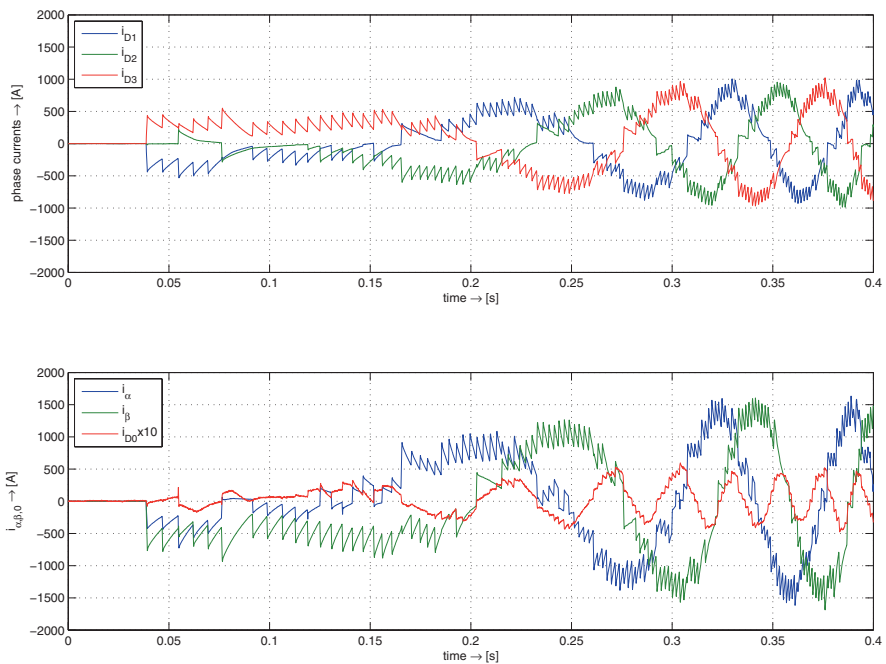


Figure 4.25. Measured data from a linear synchronous machine (LSM) rated 2.4MW in a roller-coaster launch application: Conversion from phase currents to space vector format $\vec{i}_{\alpha,\beta,0}$ showing substantial 3rd harmonic loop current (Courtesy of GTI electroproject, the Netherlands.)

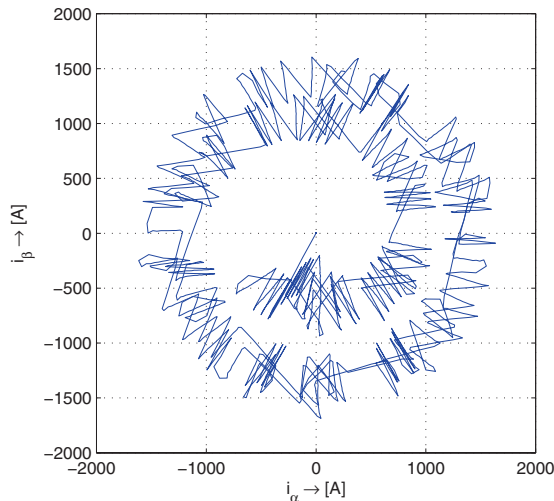


Figure 4.26. Measured data: Current vector locus diagram ($i_\alpha(t)$, $i_\beta(t)$), same data as in figure 4.25

The inverse operation, namely the conversion process from phase space vector variables to supply current variables follows directly from equation (4.53). This expression may also be written as

$$\vec{i}_{D123} = \frac{1}{\sqrt{3}} e^{-j\frac{\gamma}{4}} \vec{i}_{RST} \quad (4.56)$$

Equation (4.56) states that the space vector \vec{i}_{RST} must be rotated by an angle $-\gamma/4$ and scaled by a factor $1/\sqrt{3}$ in order to arrive at the phase vector \vec{i}_{D123} , which can be converted to phase current variables using equation (4.37). The generic modules required for this conversion are shown in figure 4.23(b). Included in this figure is a conversion module identified by the symbols ‘delta’ and ‘star’ which has a transfer matrix of the form given by equation (4.57).

$$\begin{bmatrix} i_{D\alpha} \\ i_{D\beta} \end{bmatrix} = \frac{1}{\sqrt{3}} \begin{bmatrix} \cos \frac{\gamma}{4} & \sin \frac{\gamma}{4} \\ -\sin \frac{\gamma}{4} & \cos \frac{\gamma}{4} \end{bmatrix} \begin{bmatrix} i_\alpha \\ i_\beta \end{bmatrix} \quad (4.57)$$

The two conversion modules shown in figure 4.23(b) can also be replaced by a single generic module as given in figure 4.24(b). The corresponding transfer matrix as given by equation (4.58) is found by combining the matrices represented by equations (4.37), (4.57). It is emphasized that this conversion will not contain any zero sequence component.

$$\begin{bmatrix} i_{D1} \\ i_{D2} \\ i_{D3} \end{bmatrix} = \begin{bmatrix} \frac{1}{3C} & \frac{1}{C3\sqrt{3}} \\ -\frac{1}{3C} & \frac{1}{C3\sqrt{3}} \\ 0 & -\frac{2\sqrt{3}}{9C} \end{bmatrix} \begin{bmatrix} i_\alpha \\ i_\beta \end{bmatrix} \quad (4.58)$$

4.6.4 Circuit modelling using space vectors: delta connection

The space vector based circuit model, as given in figure 4.19, for the star connected three-phase system is directly applicable for the delta connected circuit. The only change lies with the use of ‘delta’ input and output variables as shown in figure 4.27. The input variables of the three to two phase conversion unit are the phase voltages u_{D1}, u_{D2}, u_{D3} . The output of the two to three phase conversion unit are the phase currents i_{D1}, i_{D2}, i_{D3} . The model according to figure 4.27 replaces the component module shown in figure 4.13 which has as input the phase voltages u_{D1}, u_{D2}, u_{D3} and as output the phase currents i_{D1}, i_{D2}, i_{D3} .

4.7 Relationship between space vectors and phasors

The phasor in the form of a complex *non* time dependent variable has in an earlier chapter been introduced in the form \underline{x} . Basically the phasor type analysis

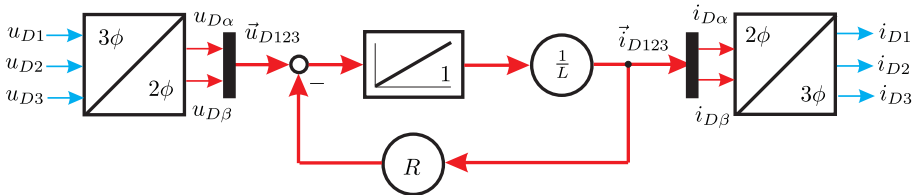


Figure 4.27. Generic, space vector based, model of three-phase R-L circuit (delta connected)

was and is used to study linear electrical circuits under steady-state conditions which carry sinusoidally time varying waveforms. To date we have considered phasors for single phase applications. In this section we will extend the use of phasors for three-phase systems.

In this context it is helpful to recall the three-phase example given in section 4.5 where a three-phase sinusoidal supply voltage was assumed (see equation (4.19)), together with a set of sinusoidal supply currents. The three-phase variables were then transformed to a space vector form as given by equation (4.26). This equation set forms an excellent platform for establishing the link to phasors. In this context, it is helpful to rewrite equation (4.26) in the following form

$$\vec{u}_{RST} = \underbrace{\sqrt{\frac{3}{2}} \hat{u}}_{\underline{u}_{RST}} e^{j\omega t} \quad (4.59a)$$

$$\vec{i}_{RST} = \underbrace{\sqrt{\frac{3}{2}} \hat{i}}_{\underline{i}_{RST}} e^{j\rho} e^{j\omega t} \quad (4.59b)$$

An observation of equation (4.59) learns that the time dependent component of the space vectors has been written separately from the remaining term, which is precisely the phasor component of the space vector. Hence for the example shown in equation (4.59) the voltage/current phasors are given as $\underline{u}_{RST} = \sqrt{\frac{3}{2}} \hat{u}$ and $\underline{i}_{RST} = \sqrt{\frac{3}{2}} \hat{i} e^{j\rho}$ respectively. Note that we introduced the subscript *RST* for these vectors and phasors as to reinforce the fact that these are linked to the supply variables. The reader is reminded of the fact that the phasor concept was introduced in chapter 2. Equation (2.11) as given in that chapter was used to show the relationship that exists between phasors and sinusoidal time dependent waveforms. An observation of equation (2.11) shows the use of an amplitude invariant space vector representation. When dealing with phasors in single phase circuits the real (for cosine functions) or imaginary (for sine functions) space vector component is used in the transformation from time variables to phasors and vice versa.

An example of using space vectors in the form shown by equation (4.59) is given in figure 4.28 for $\omega t = \frac{\pi}{3}$, $\rho = -\frac{\pi}{6}$, together with the corresponding phasor diagram.

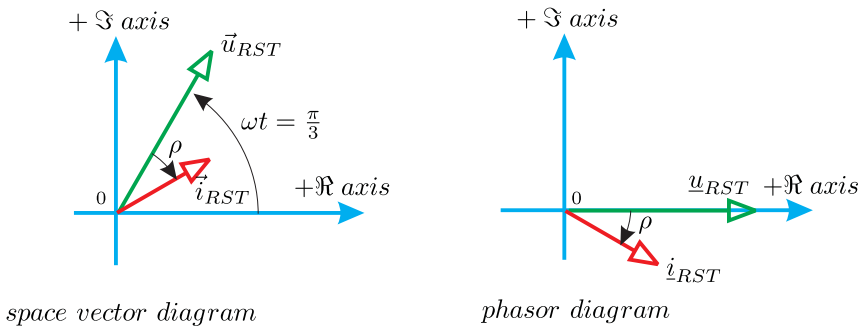


Figure 4.28. Example showing ‘supply’ space vector and corresponding phasor diagram

4.7.1 Use of phasors in three-phase circuits

It is instructive to consider the transformation of a space vector differential equation to phasor format for the R-L type circuit considered in sections 4.6.2 and 4.6.4 for the star and delta connected configuration. The analysis is shown for the star based variables. However, the analysis for the delta case is identical. The only change lies with the change of subscripts from $S123$ to $D123$. The space vector load differential equation for the star connected case is given by equation (4.42). Substitution of $\vec{v}_{S123} = L\vec{i}_{S123}$ gives

$$\vec{u}_{S123} = L \frac{d\vec{i}_{S123}}{dt} + R \vec{i}_{S123} \quad (4.60)$$

where \vec{u}_{S123} , \vec{i}_{S123} represent the voltage/current space vector linked to phase variables of the star configured circuit. The transformation of equation (4.60) to its phasor equivalent form is made using

$$\vec{u}_{S123} = \underline{u}_{S123} e^{j\omega t} \quad (4.61a)$$

$$\vec{i}_{S123} = \underline{i}_{S123} e^{j\omega t} \quad (4.61b)$$

$$\frac{d\vec{i}_{S123}}{dt} = j\omega \underline{i}_{S123} e^{j\omega t} \quad (4.61c)$$

Equation (4.61) shows the conversion required as well as the current space vector differential, which in phasor terms leads to the addition of component $j\omega$. The resultant phasor equation is found by eliminating the time dependent term $e^{j\omega t}$, which leads to

$$\underline{u}_{S123} = j\omega L \underline{i}_{S123} + R \underline{i}_{S123} \quad (4.62)$$

If for example the voltage phasor is known then the current phasor is calculated using

$$\underline{i}_{S123} = \frac{\underline{u}_{S123}}{R + j\omega L} \quad (4.63)$$

The peak phase current amplitude is then found using $\hat{i} = |\underline{i}| \sqrt{\frac{2}{3}}$. The phase angle with respect to the phase voltage is equal to $\rho = -\arctan \frac{\omega L}{R}$.

It is instructive to examine the process of calculating the supply phasor \underline{i}_{RST} on the basis of a given supply phasor according to (4.59a) for the star/delta connected circuit. In both cases the voltage phasor $\underline{u}_{S123}/\underline{u}_{D123}$ must first be derived from the given supply phasor \underline{u}_{RST} . Next, the current phasor $\underline{i}_{S123}/\underline{i}_{D123}$ needs to be calculated using equation (4.63). Finally, the conversion from $\underline{i}_{S123}/\underline{i}_{D123}$ to supply current phasor \underline{i}_{RST} needs to be made.

For the star connected case the relationship between phase and supply vectors (for currents and voltages) is given by equation (4.40). Consequently the relationship between the phasors in a star connected circuit is of the form

$$\underline{u}_{S123} = \underline{u}_{RST} \quad (4.64a)$$

$$\underline{i}_{S123} = \underline{i}_{RST} \quad (4.64b)$$

This means that the calculation of the current phasor from a given voltage phasor is as discussed above, see equation (4.63). A phasor diagram example with $\rho = -\frac{\pi}{3}$ is given in figure 4.29.

For the delta connected case the relationship between phase and supply vectors is given by equations (4.45) and (4.56). The corresponding phasor relationships between the phase and supply based phasors is of the form

$$\underline{u}_{D123} = \sqrt{3} e^{-j\frac{\gamma}{4}} \underline{u}_{RST} \quad (4.65a)$$

$$\underline{i}_{D123} = \frac{1}{\sqrt{3}} e^{-j\frac{\gamma}{4}} \underline{i}_{RST} \quad (4.65b)$$

For the calculation of the current phasor \underline{i}_{D123} use is made of equation (4.63) (with subscript $D123$), in which \underline{u}_{D123} is calculated using equation (4.65a). Once the phasor \underline{i}_{D123} is found equation (4.65b) can be used to find the supply current phasor. The phasor diagram as given by figure 4.29, shows the conversion process with the same circuit model as used for the star connected example.

An important conclusion to make is that the supply current level which will appear for the delta connected case is three times larger than that which will appear in the star connected configuration (provided that the impedances are constant). This is clearly apparent from figure 4.29, where the currents and voltage for the delta connected configuration are scaled as required in comparison

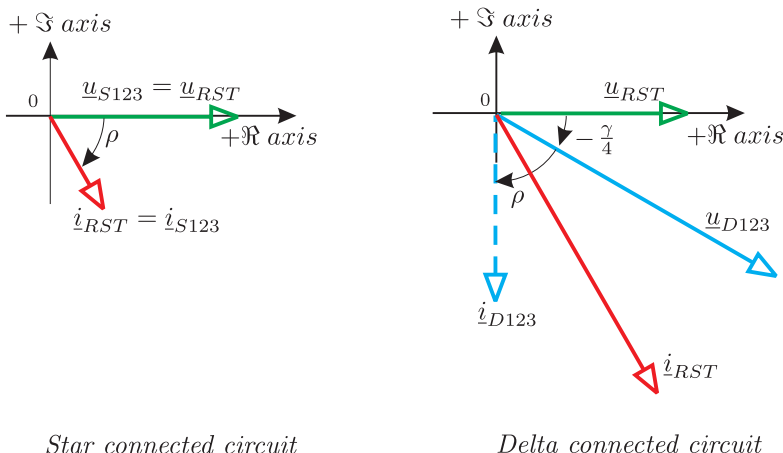


Figure 4.29. Phasor diagram for star and delta R-L circuit

to the star diagram. It is for this reason that grid connected three-phase induction machines are often star configured during the initial start up sequence. Once past the start up phase, the machine phase configuration is changed to delta. This approach reduces the initial peak starting currents in the supply lines. However significant transient peaks still occur just after the Y- Δ reconfiguration. As explained earlier, delta connected machines are commonplace in applications with high phase currents (low supply voltage, high power). Inverter connected machines with phase currents typically less than 100A are usually star configured to avoid circulating phase currents.

It is noted that the process of modelling a delta connected circuit can be avoided if we simply take the delta circuit parameter values, divide these by a factor of three and re-configure the circuit in ‘star’ . However, we loose access to the ‘delta phase variables’ under these circumstances. In applications where the delta connected voltages/currents are to be measured for control purposes, the conversion process as described above would need to be implemented. In any event, it is considered to be of importance to realize that there is a substantial difference between the modelling processes linked to the ‘star’ and ‘delta’ connected circuit.

4.8 Tutorials for Chapter 4

4.8.1 Tutorial 1

In this tutorial the conversion process (*supply* \rightarrow *phase* and *phase* \rightarrow *supply*) for a star connected circuit will be considered. The Simulink model according to figure 4.30 forms the basis for this tutorial. Shown in this figure is a ‘signal builder’ module which provides the supply voltages u_R , u_S , u_T for a period of

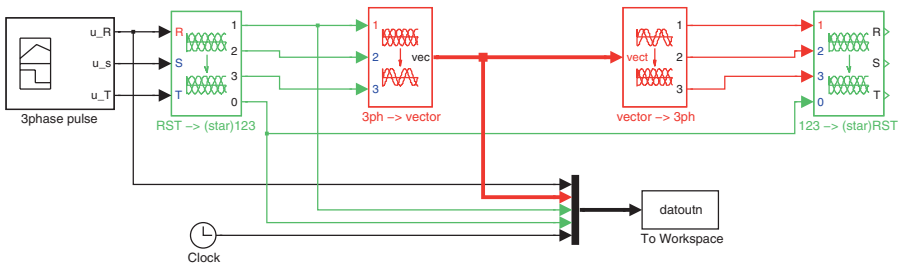


Figure 4.30. Simulink model: Conversion modules for star connected circuits

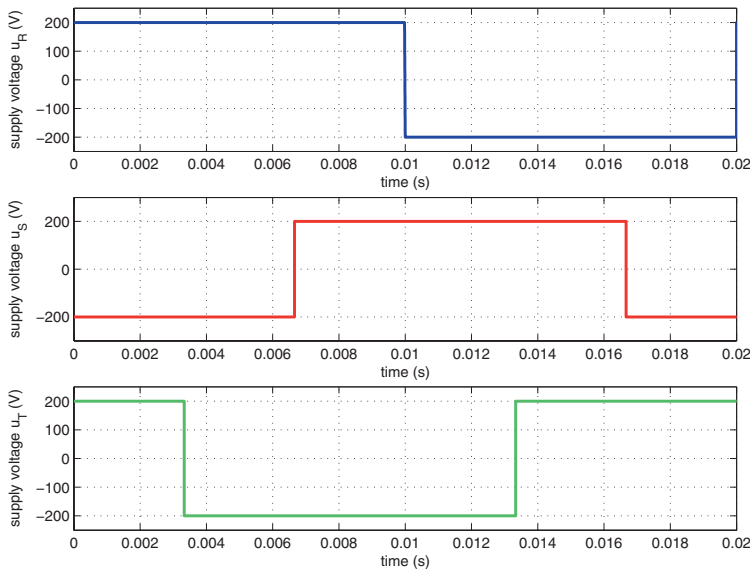


Figure 4.31. Supply voltage waveforms u_R , u_s , u_T

20ms, which is the ‘run’ time for this simulation. Details of the waveform versus time functions to be implemented are given in figure 4.31. It is noted that the set of waveforms used in this tutorial are in fact those which are typically generated by a power electronic converter when used in a so-called ‘six-step’ mode. As a second step in this tutorial provide an implementation of the conversion module ‘ $RST \rightarrow (\text{star})123$ ’ according to the matrix defined by equation (4.4). An example of the output of this conversion is shown in figure 4.32 where the supply voltage waveform u_R is also added for reference purposes. Clearly observable from figure 4.32 is the presence of a non-zero sequence voltage component u_{S0} as calculated with the aid of equation (4.5). The second module to be implemented is the ‘three to two’ phase conversion module identified in

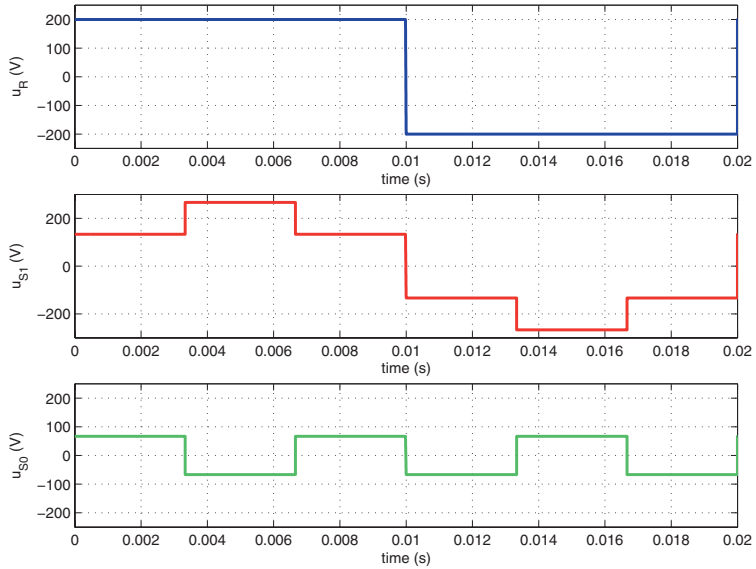
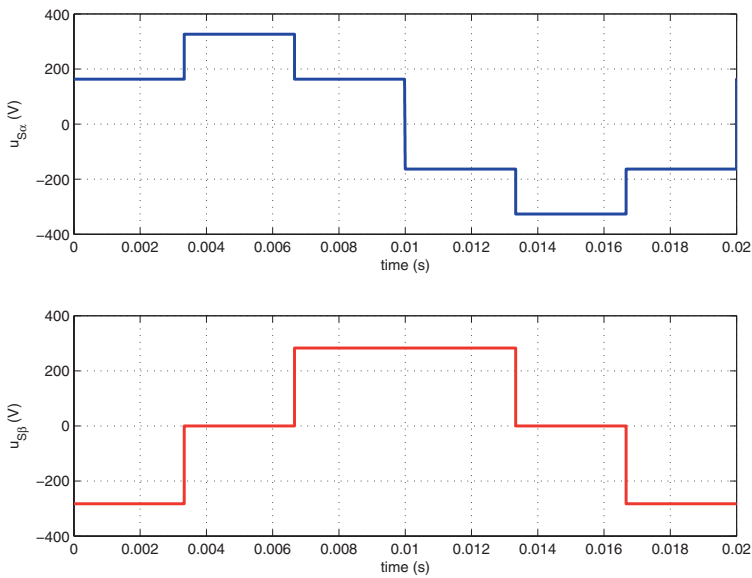
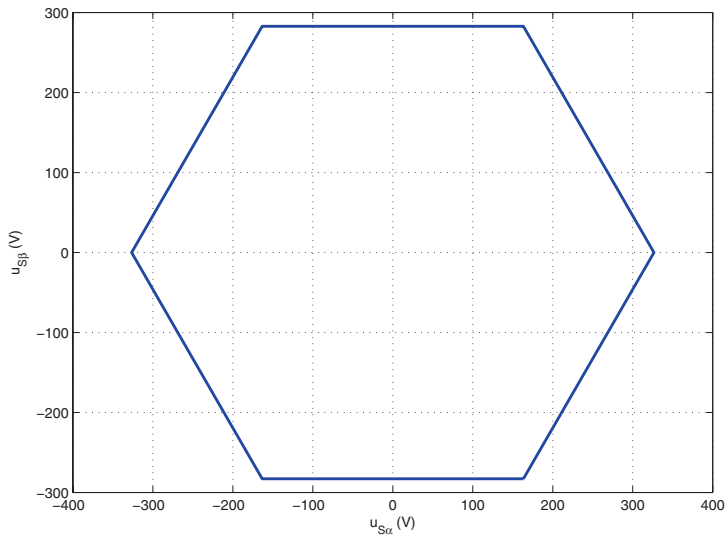


Figure 4.32. Waveforms: u_R , u_{S1} , u_{S0}

figure 4.30 as ‘ $3ph \rightarrow$ vector’. The matrix according to equation (4.31) must be implemented in this case with $C = \sqrt{\frac{2}{3}}$, given that a power invariant notation is assumed. It is helpful to build these conversion modules in Simulink with the aid of a ‘multiplexer’ and two ‘function’ modules. The output of the two function modules can be combined via a ‘de-multiplexer’ module. The real and imaginary components of the space vector \vec{u}_{S123} which should appear as output variables of this module are shown in figure 4.33. A further cross check on the output of this module is given by figure 4.34 which shows the locus of the space vector end point \vec{u}_{S123} versus time for the 20ms duration of this simulation. Note that the shape is that of a hexagon where the vector end point moves from corner to corner which is why this mode of operation is referred to as ‘six step’. It is instructive to carefully consider how the vector end point moves in figure 4.34 in relation to the simulation time. From such an analysis it may be observed that the vector end point changes from hexagon corner to corner whenever a waveform voltage transition in either $u_{S\alpha}(t)$ or $u_{S\beta}(t)$ occurs. Finally, implement the two remaining conversion modules ‘vector \rightarrow 3ph’ and ‘123 \rightarrow (star)RST’ according to equations (4.37) and (4.6) respectively. The output waveforms from these modules can be directly checked against those obtained from the output of the ‘RST \rightarrow (star)123’ module and ‘signal builder’ module which provides the supply voltage waveforms.

An example of an m-file which is able to plot the results from this simulation is given below.

Figure 4.33. Waveforms: $u_{S\alpha}, u_{S\beta}$ Figure 4.34. Waveforms: \vec{u}_{S123} , vector locus diagram

m-file Tutorial 1, chapter 4

```
%tutorial 1, chapter 4
close all
subplot(3,1,1)
```

```

plot(datoutn(:,6),datoutn(:,1))
grid
xlabel('time (s)')
ylabel('u_R (V)')
axis([0 20e-3 -250 250])
subplot(3,1,2)
plot(datoutn(:,6),datoutn(:,4),'r')
xlabel('time (s)')
ylabel('u_{S1} (V)')
axis([0 20e-3 -300 300])
grid
subplot(3,1,3)
plot(datoutn(:,6),datoutn(:,5),'g')
xlabel('time (s)')
ylabel('u_{S0} (V)')
grid
axis([0 20e-3 -250 250])
%%%%%
figure
subplot(2,1,1)
plot(datoutn(:,6),datoutn(:,2))
grid
xlabel('time (s)')
ylabel('u_{S\alpha} (V)')
axis([0 20e-3 -400 400])
subplot(2,1,2)
plot(datoutn(:,6),datoutn(:,3),'r')
xlabel('time (s)')
ylabel('u_{S\beta} (V)')
axis([0 20e-3 -400 400])
grid
figure
plot(datoutn(:,2),datoutn(:,3))
axis equal
axis([-400 400 -300 300])
grid
xlabel('u_{S\alpha} (V)')
ylabel('u_{S\beta} (V)')

```

4.8.2 Tutorial 2

The relationship between supply, phase and space vector variables is considered here for a star connected circuit. This tutorial is similar to the previous tutorial with the notable change that the implementation is undertaken with the aid of Caspoc. A pulse generator is again used which delivers the supply voltages u_R , u_S , u_T as defined by figure 4.31 on page 104. The Caspoc simulation as given in figure 4.35 on page 108 demonstrates the conversion process from supply voltage variables to space vector variables and vice-versa, with and without the presence of the zero sequence voltage variable u_{s0} which is non-zero in this case.

The scopes given in figure 4.35 show the supply, phase and space vector variables as well as the space vector locus. Table 4.1 shows the variables which are linked with the scopes shown in this tutorial.

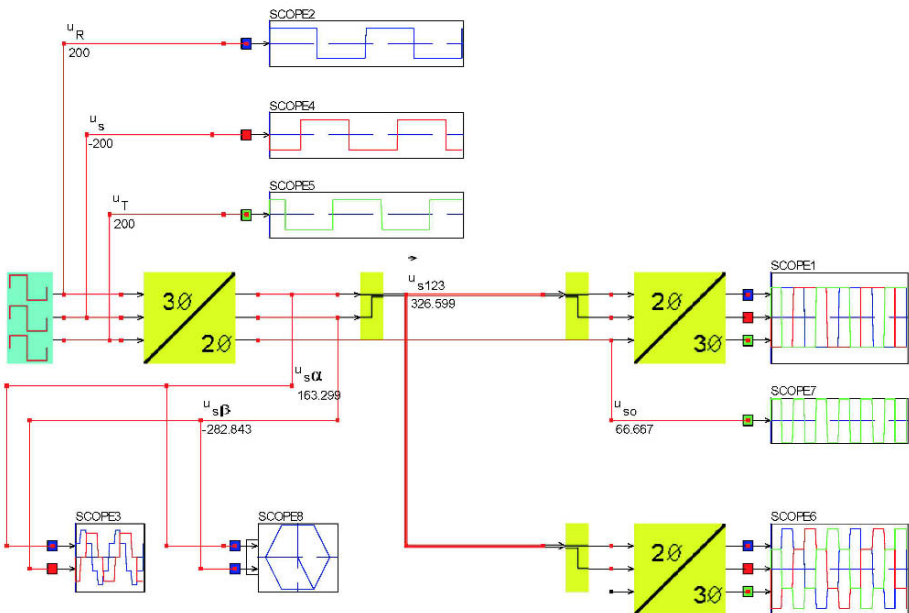


Figure 4.35. Caspoc simulation: space vector example, star connected

Table 4.1. Scope variables

Scope number	Variables
Scope 1	u_R, u_S, u_T
Scope 2	u_R
Scope 3	$u_{S\alpha}, u_{S\beta}$
Scope 4	u_S
Scope 5	u_T
Scope 6	u_{S1}, u_{S2}, u_{S3}
Scope 7	u_{S0}
Scope 8	\vec{u}_{S123}

4.8.3 Tutorial 3

A Simulink implementation of the generic diagram shown in figure 4.19 is considered in this tutorial. The load is represented in this figure by the module $R - L - e - 3\text{ph}$. This module will be used more extensively in subsection 4.8.8. In this tutorial this model is simplified by setting the resistance value to zero and the inductance value to $L = 100\text{mH}$. Furthermore, the ‘sinus’ modules shown in this figure are not implemented. The supply waveforms as used in tutorial 1 (see section 4.8.1) remain unchanged. Add a ‘three to three’ phase conversion module as shown in figure 4.6(a) to convert the supply voltages to

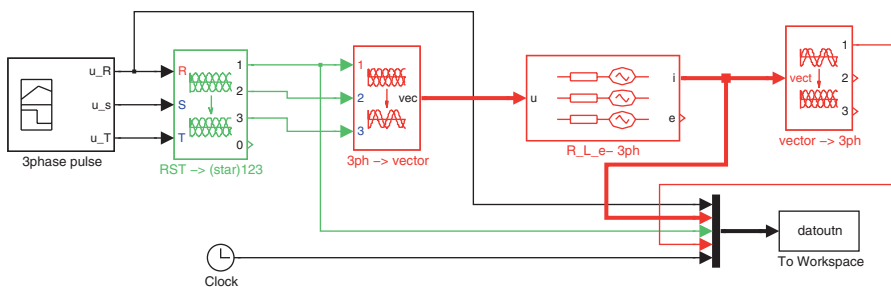


Figure 4.36. Simulink model: star connected circuit

phase voltages. Build this simulation and examine the current waveforms $i_{S\alpha}$, $i_{S\beta}$, i_{S1} . Repeat this exercise after removing the ‘three-phase’ to three-phase’ module used to convert the supply voltages to phase voltages. Explain if there is likely to be a difference in the current output waveforms. Note that for the star connected circuit the phase currents are equal to the supply currents. An example of the current waveforms which should appear in your simulation is given in figure 4.37. Shown are the real and imaginary current space vector components together with the phase/supply current i_{S1} . The phase voltage u_{S1} is also added for reference purposes. Removal of the module ‘ $RST \rightarrow (\text{star})123$ ’ will not change the current waveforms despite the presence of a zero sequence component u_{S0} in the supply voltages. The reason for this is that the space vector components $u_{S\alpha}$, $u_{S\beta}$ are not affected by the presence of a component u_{S0} (see equation (4.39)). The m-file which is able to plot the results of this simulation is as follows

m-file Tutorial 3, chapter 4

```
%tutorial 3, chapter 4
close all
subplot(3,1,1)
plot(datoutn(:,6),datoutn(:,4))
grid
xlabel('time (s)')
ylabel('u_{S1} (V)')
axis([0 20e-3 -400 400])
subplot(3,1,2)
plot(datoutn(:,6),datoutn(:,2),'r')
xlabel('time (s)')
ylabel('i_{S\alpha} (A), i_{S\beta} (A)')
hold on
plot(datoutn(:,6),datoutn(:,3),'b')
axis([0 20e-3 -25 25])
grid
legend('i_{S\alpha}', 'i_{S\beta}')
subplot(3,1,3)
plot(datoutn(:,6),datoutn(:,5),'g')
```

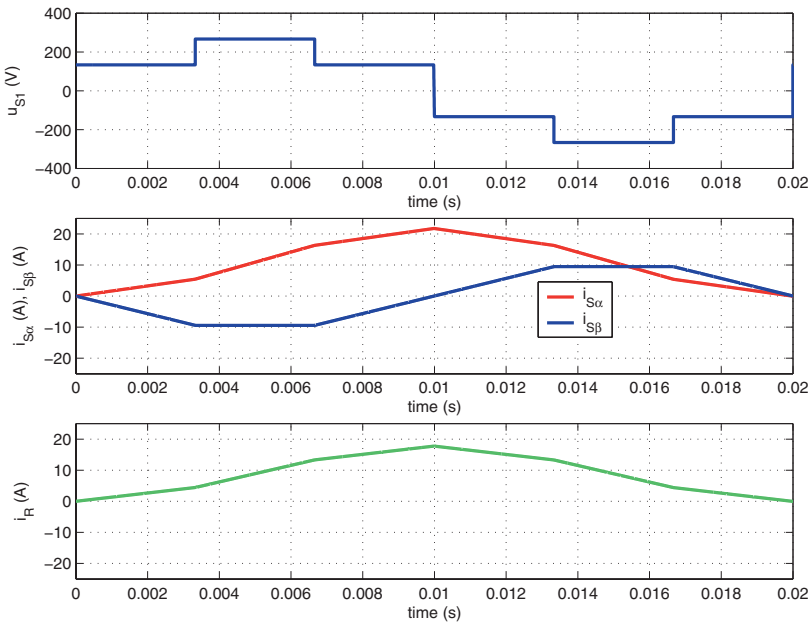


Figure 4.37. Waveforms: u_{S1} , ($i_{S\alpha}$, $i_{S\beta}$), i_{S1}/i_R

```

xlabel('time (s)')
ylabel('i_R (A)')
grid
axis([0 20e-3 -25 25])

```

4.8.4 Tutorial 4

This tutorial considers a Caspoc simulation model of the previous Simulink based tutorial. The input waveforms are the supply voltage versus time functions as shown in figure 4.31. A possible Caspoc model of this problem as given in figure 4.38 shows a set of ‘scope’ modules which display the output variables as discussed in the previous tutorial. Table 4.2 shows the variables which are tied to each scope in figure 4.38.

Table 4.2. Scope variables

Scope number	Variables
Scope 1	i_{S1}, i_{S2}, i_{S3}
Scope 2	$u_{S\alpha}$
Scope 3	$i_{S\alpha}, i_{S\beta}$

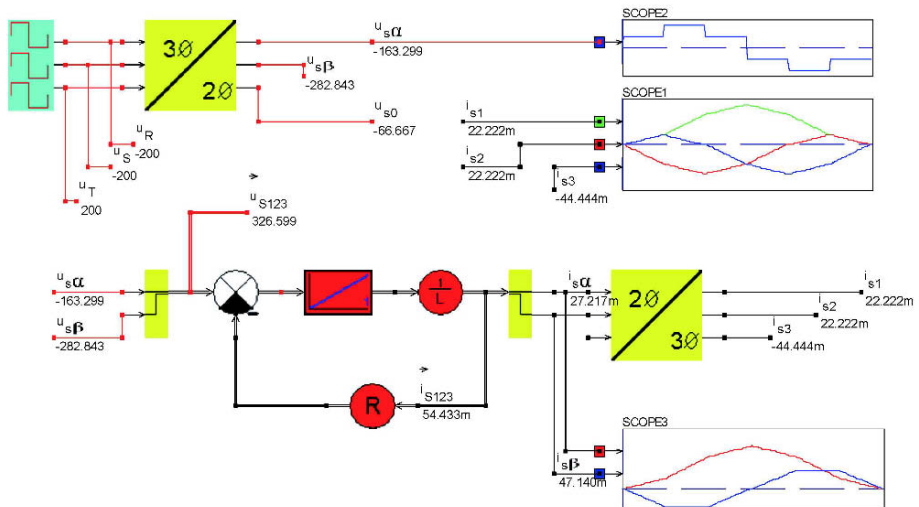


Figure 4.38. Caspoc simulation: space vector example, star connected

4.8.5 Tutorial 5

Tutorial 1 as discussed in subsection 4.8.1 for the ‘star’ configured three-phase circuit is repeated here for the ‘delta’ connected case. This means that the module ‘ $RST \rightarrow (\text{star})123$ ’ (see figure 4.30) must be replaced by a new module ‘ $URST \rightarrow (\text{delta})123$ ’ as shown in figure 4.39, which has a conversion matrix according to equation (4.13). Note that the conversion matrices for supply to phase variables and vice versa are different for voltages and currents. An example of the phase voltage u_{D1} which should appear from this module is given in figure 4.40. The waveforms u_R , u_{S0} which also appear in this figure remain unchanged. The module ‘ $3ph \rightarrow \text{vector}$ ’ is unchanged but the output of this module will be different given the new phase voltage inputs. The space vector \vec{u}_{D123} , formed by the variables $u_{D\alpha}$, $u_{D\beta}$ should be of the form given

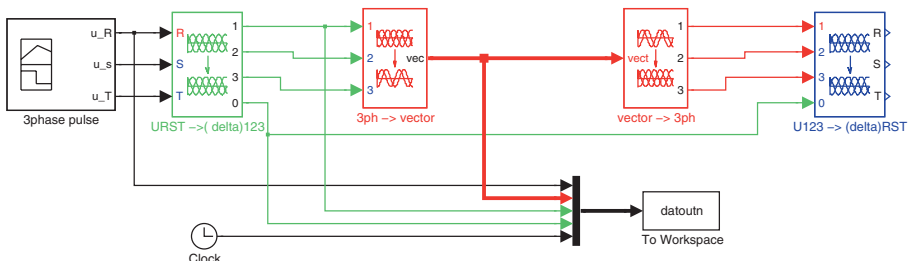


Figure 4.39. Simulink model: Conversion modules for delta connected circuit

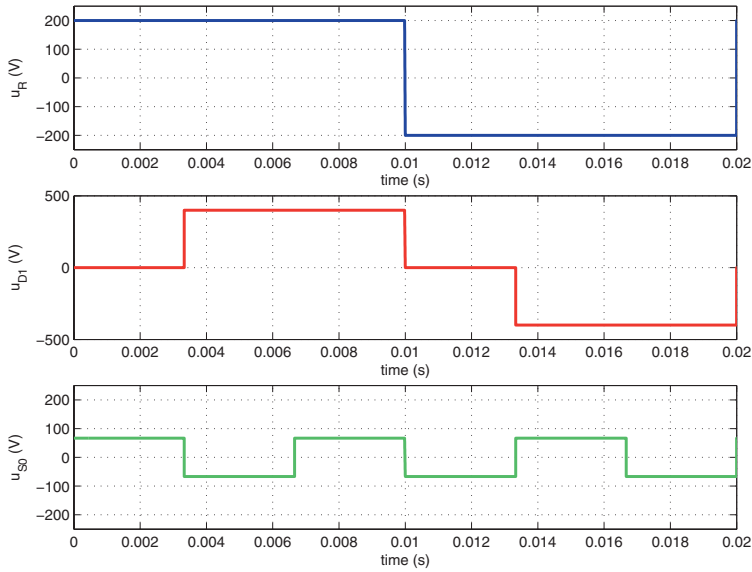


Figure 4.40. Waveforms: u_R , u_{D1} , u_{S0}

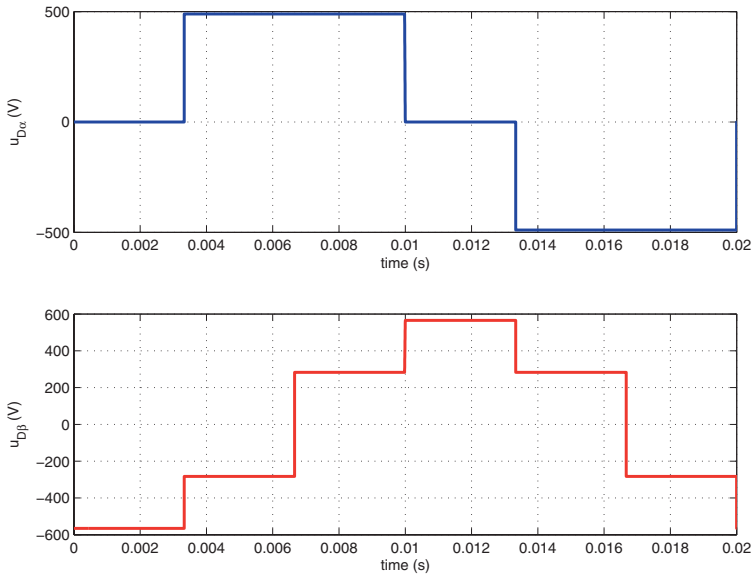


Figure 4.41. Waveforms: $u_{D\alpha}$, u_{Db}

by figure 4.41. A further cross-check on the output of this module can also be made for this case. Figure 4.42 shows the locus of the space vector end point \vec{u}_{D123} versus time for the delta connected case. Note that the shape is again

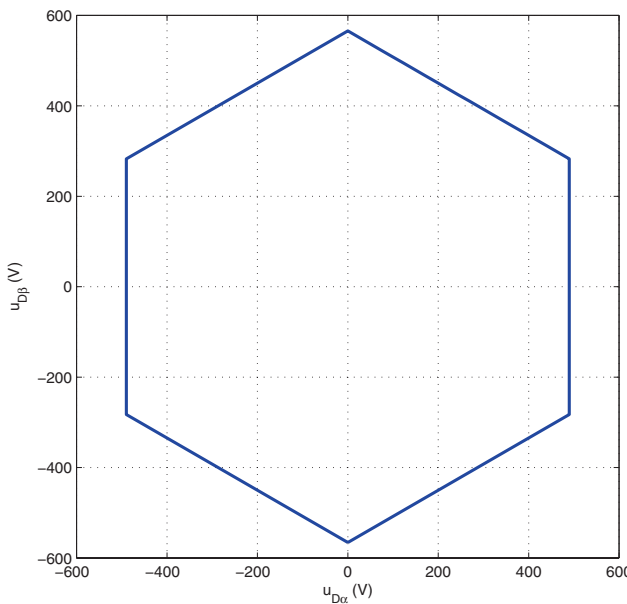


Figure 4.42. Waveforms: $u_{D\alpha}$, $u_{D\beta}$, vector locus diagram

that of a hexagon which is now rotated by an angle of $-\pi/6$. Furthermore, the hexagon is larger by a factor of $\sqrt{3}$ when compared to the previous example (see figure 4.34). The conversion from space vector to phase variables remains unchanged. However, the voltage module ‘123→(star)RST’ must be replaced by a new module ‘U123→(delta)RST’ which has a conversion matrix as given by equation (4.16). The output waveforms from this module should be the supply voltage waveforms according to figure 4.31. The m-file shown below can be used to plot the data obtained from the simulation.

m-file Tutorial 5, chapter 4

```
%tutorial 5, chapter 4
close all
subplot(3,1,1)
plot(datoutn(:,6),datoutn(:,1))
grid
xlabel('time (s)')
ylabel('u_R (V)')
axis([0 20e-3 -250 250])
subplot(3,1,2)
plot(datoutn(:,6),datoutn(:,4),'r')
xlabel('time (s)')
ylabel('u_{D1} (V)')
axis([0 20e-3 -500 500])
grid
subplot(3,1,3)
```

```

plot(datoutn(:,6),datoutn(:,5),'g')
xlabel('time (s)')
ylabel('u_{S0} (V)')
grid
axis([0 20e-3 -250 250])
%%%%%
figure
subplot(2,1,1)
plot(datoutn(:,6),datoutn(:,2))
grid
xlabel('time (s)')
ylabel('u_{D\alpha} (V)')
axis([0 20e-3 -500 500])
subplot(2,1,2)
plot(datoutn(:,6),datoutn(:,3),'r')
xlabel('time (s)')
ylabel('u_{D\beta} (V)')
axis([0 20e-3 -600 600])
grid
figure
plot(datoutn(:,2),datoutn(:,3))
axis equal
axis([-600 600 -600 600])
grid
xlabel('u_{D\alpha} (V)')
ylabel('u_{D\beta} (V)')

```

4.8.6 Tutorial 6

This tutorial considers a Caspoc implementation of the previous Simulink based tutorial. The excitation and parameters are identical to those used in the previous examples. The scope modules as shown in figure 4.43 correspond to a set of output variables as given in table 4.3. In the example as given

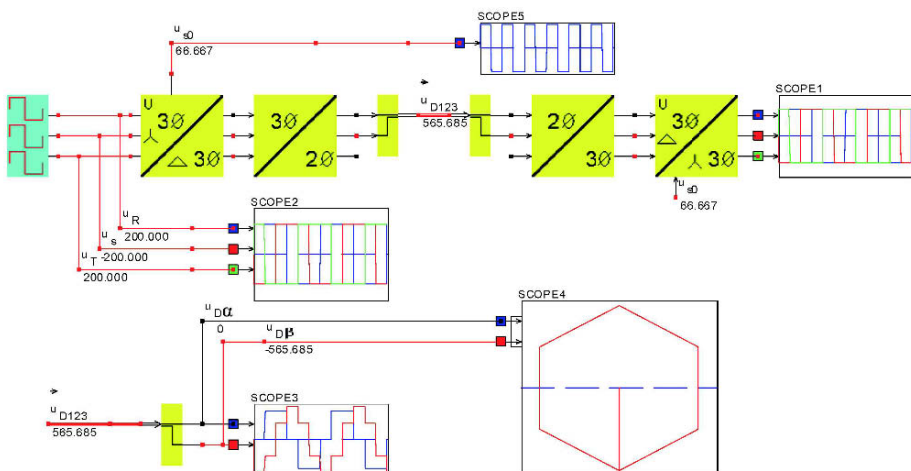


Figure 4.43. Caspoc simulation: space vector example, delta connected

Table 4.3. Scope variables

Scope number	Variables
Scope 1	u_R, u_S, u_T
Scope 2	u_R, u_S, u_T
Scope 3	$u_{D\alpha}, u_{D\beta}$
Scope 4	\vec{u}_{D123}
Scope 5	u_{so}

in figure 4.43, scopes 1 and 2 give the same result because the zero sequence variable u_{so} is also connected (as required) to the three to three phase conversion module tied to scope 1. It is instructive to temporarily remove the zero sequence link between the two three to three phase conversion modules and to rerun the simulation. Under these conditions the output of scopes 1 and 2 will differ because the zero sequence voltage is non-zero in this example.

4.8.7 Tutorial 7

This exercise is concerned with the implementation of the generic diagram according to figure 4.27. The delta connected load is in the form of an ideal inductance value with value $L = 100\text{mH}$, as discussed in section 4.8.3. The revised circuit model as given by figure 4.44 shows the ‘signal builder’ module and conversion modules (as discussed in the previous tutorials) needed to arrive at the voltage space vector \vec{u}_{D123} for the delta connected case. The output from the ‘R-L-e-3ph’ module is the current vector $\vec{i}_{D123} = i_{D\alpha} + j i_{D\beta}$ which must be converted to three-phase currents using a vector to three-phase conversion module. This module is unchanged, but the phase current to RST current module ‘I123 → (delta)RST’ as shown in figure 4.44 must be built with a conversion matrix as defined by equation (4.9). An example of the current waveforms which should appear (with a zero resistance coil) in your simulation is given in figure 4.45. Shown are the real and imaginary current space vector components $i_{D\alpha}, i_{D\beta}$ together with the supply current i_R . The phase voltage u_{D1} is also

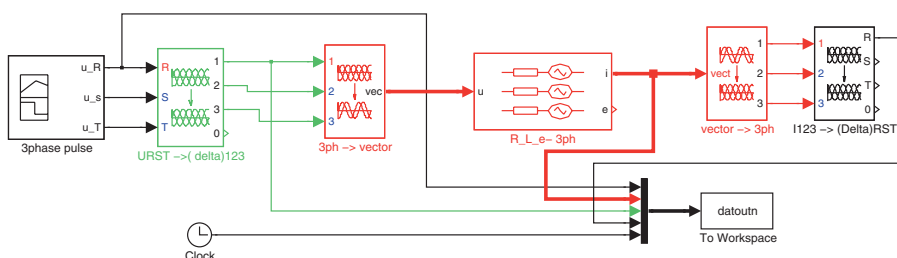


Figure 4.44. Simulink model: delta connected circuit

added for reference purposes. When comparing the supply current i_R waveform according to figure 4.45 against the result obtained with the star connected circuit (see figure 4.37) we see that the latter is three times smaller (as expected). The waveform shape remains unchanged. It is again noted that the process of modelling a delta connected circuit could be avoided if we simply take the delta circuit parameter values, divide these by a factor of three and re-configure the circuit in ‘star’. The m-file which corresponds with the simulation is as follows

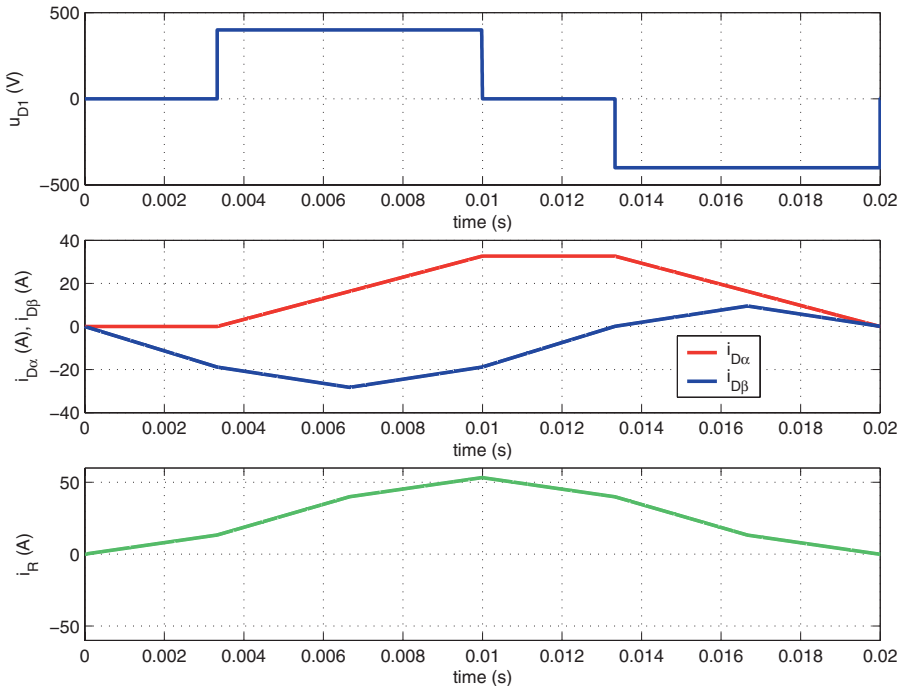


Figure 4.45. Waveforms: u_{D1} , $(i_{D\alpha}, i_{D\beta})$, i_R

m-file Tutorial 7, chapter 4

```
%tutorial 7, chapter 4
close all
subplot(3,1,1)
plot(datoutn(:,6),datoutn(:,4))
grid
xlabel('time (s)')
ylabel('u_{D1} (V)')
axis([0 20e-3 -500 500])
subplot(3,1,2)
plot(datoutn(:,6),datoutn(:,2),'r')
xlabel('time (s)')
ylabel('i_{D\alpha} (A), i_{D\beta} (A)')
hold on
```

```

plot(datoutn(:,6),datoutn(:,3),'b')
axis([0 20e-3 -40 40])
grid
legend('i_{D\alpha}', 'i_{D\beta}')
subplot(3,1,3)
plot(datoutn(:,6),datoutn(:,5),'g')
xlabel('time (s)')
ylabel('i_R (A)')
grid
axis([0 20e-3 -60 60])

```

4.8.8 Tutorial 8

This tutorial is concerned with a phasor analysis of a star configured three-phase circuit connected to a sinusoidal supply. The simulation model as given by figure 4.36 needs to be modified by replacing the ‘signal builder’ module with a three-phase sinusoidal excitation module as shown in figure 4.46. The

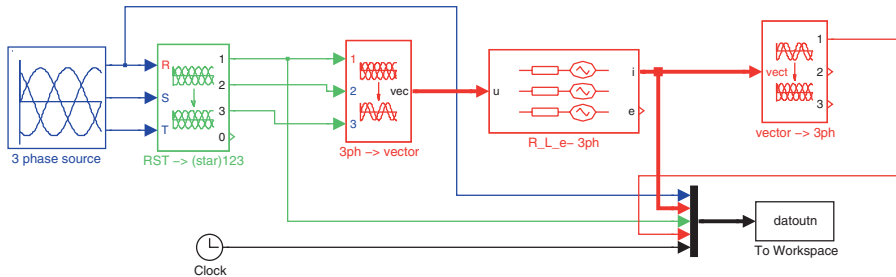


Figure 4.46. Simulink model: star connected circuit, sinusoidal excitation

three-phase supply unit needs to be built and an implementation example of this module is given in figure 4.47(a). The output waveforms should be according to equation (4.19). The sub-module shown is made with three ‘sine’ modules which represent the ‘R,S,T’ supply voltages. The sub-module should have the numerical inputs as given by table 4.4.

Table 4.4. Parameters for three-phase supply unit

Parameters	Value
RMS Supply voltage U_R	220 V
RMS Supply voltage U_S	220 V
RMS Supply voltage U_T	220 V
Supply frequency f	50 Hz
Phase ρ	$\pi/2$ rad

Note that the ‘phase’ entry is set to $\pi/2$ given that our supply voltages are chosen as cosine functions. If we set the ρ parameter to zero the output will be

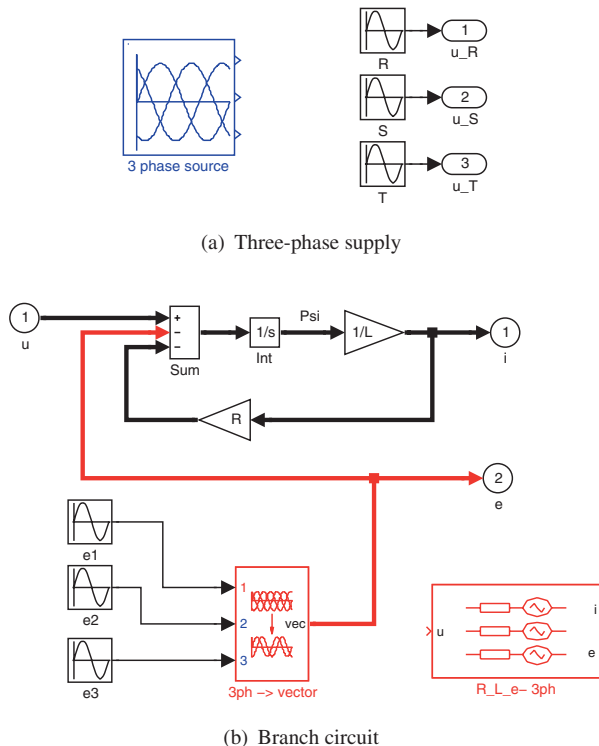


Figure 4.47. Simulink: Supply and branch circuit modules

a sine function, i.e. at $t = 0$ the value of u_R will be zero. In our case its value should be $U_R\sqrt{2}$.

The branch circuit model as shown in figure 4.47(b) (in space vector form) is extended to include an ‘EMF’ three-phase voltage source defined according to equation (4.66).

$$e_1 = E\sqrt{2} \cos(\omega t + \rho_e) \quad (4.66a)$$

$$e_2 = E\sqrt{2} \cos(\omega t + \rho_e - \gamma) \quad (4.66b)$$

$$e_3 = E\sqrt{2} \cos(\omega t + \rho_e - 2\gamma) \quad (4.66c)$$

where the parameters E , ρ_e are set to 100V and $-\frac{\pi}{3}\text{rad}$ respectively. Note that this equation is again built up with ‘sine’ modules which means that an additional phase shift of $\frac{\pi}{2}$ must be added, given that we have chosen cosine functions in this example. Furthermore, the supply angular frequency is set to $\omega = 2\pi f$, with $f = 50\text{Hz}$. Furthermore, a ‘three to two-phase’ conversion module as discussed in section 4.8.1 must be added in order to arrive at the vector \vec{e}_{123} . The remaining parameters for this module are taken to be $R = 10\Omega$, $L = 100\text{mH}$. The results of the simulation which should be run over a period

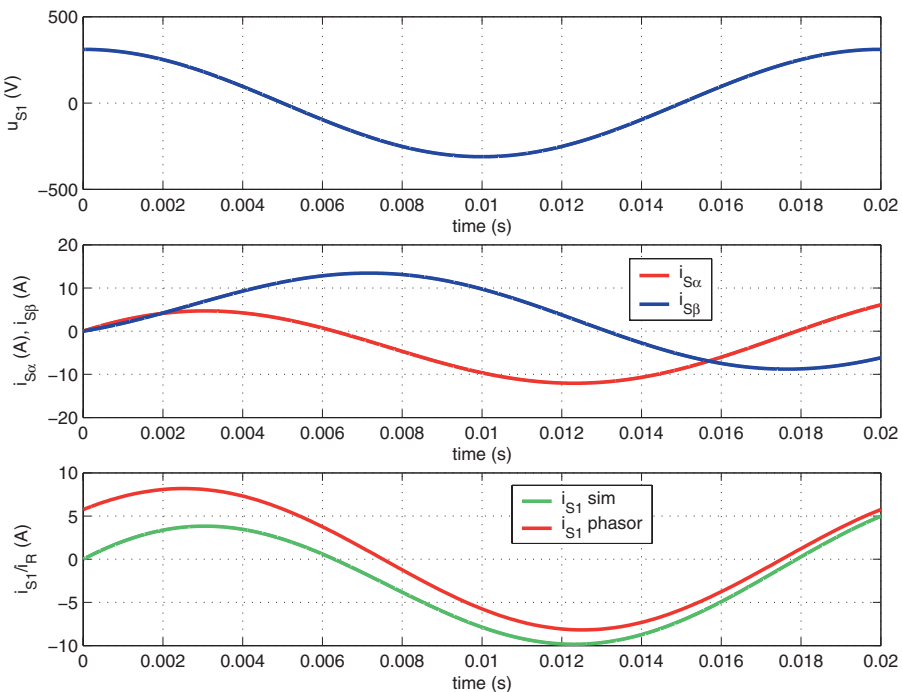


Figure 4.48. Waveforms: $u_{S1}, (i_{S\alpha}, i_{S\beta}), i_{S1}/i_R$

of 20ms, are collected with a ‘To Workspace’ module. An example of the results obtained are given in figure 4.48. Shown in figure 4.48 are the following waveforms: phase voltage u_{S1} (which in this case is also the supply voltage u_R), current vector components $i_{S\alpha}, i_{S\beta}$ and phase/supply current i_{S1} (which is also i_R). The phase/supply current obtained with the simulation ‘ i_{S1} sim’ is shown together with the ‘steady-state’ phase/supply current ‘ i_{S1} phasor’, as obtained via a phasor analysis of the problem at hand. An observation of figure 4.48 learns that the two waveforms converge towards the end of the simulation. This implies that the ‘transient’ components’ present in our dynamic simulation become less significant after approximately one cycle of operation.

On the basis of the approach outlined in section 4.7 build an m-file which allows you to calculate the steady-state current waveform i_{S1} as shown in figure 4.48 with the notation ‘ i_{S1} phasor’. An example of this phasor calculation together with the commands needed to display the results of the simulation are shown in the m-file below.

m-file Tutorial 8, chapter 4

```
%tutorial 8, chapter 4
close all
```

```

subplot(3,1,1)
plot(datoutn(:,6),datoutn(:,4))
grid
xlabel('time (s)')
ylabel('u_{S1} (V)')
axis([0 20e-3 -500 500])
subplot(3,1,2)
plot(datoutn(:,6),datoutn(:,2),'r')
xlabel('time(s)')
ylabel('i_{S\alpha} (A), i_{S\beta} (A)')
hold on
plot(datoutn(:,6),datoutn(:,3),'b')
axis([0 20e-3 -20 20])
grid
legend('i_{S\alpha}', 'i_{S\beta}')
subplot(3,1,3)
plot(datoutn(:,6),datoutn(:,5),'g')
xlabel('time (s)')
ylabel('i_{S1}/i_R (A)')
grid
axis([0 20e-3 -10 10])
%%%%%
%phasor analysis
C=sqrt(2/3); %space vector constant power invariant
U=220; %supply phase voltage RMS
E=100; %EMF phase voltage RMS
rho_e=-pi/3; %EMF phase angle
u_123=3/2*C*U*sqrt(2); %supply phasor
e_p=3/2*C*E*sqrt(2); %emf peak voltage
e_123=e_p*cos(rho_e)+j*e_p*sin(rho_e); %EMF phasor
R=10; %phase resistance
L=100e-3; %phase inductance(H)
w=100*pi; %supply frequency (rad/s)
X=w*L; %load reactance
i_123=(u_123-e_123)/(R+j*X); %current phasor
ip=abs(i_123); %peak value phasor
rho_i=angle(i_123); %phase angle current phasor
i1p=2/(3*C)*ip; %phase/supply current amplitude
%
%%%plot phase current i1 in sub-plot with waveform from simulation
t=[0:.1e-3:20e-3];
i1vt=i1p*cos(w*t+rho_i); % phase current versus time
subplot(3,1,3)
hold on
plot(t,i1vt,'r')
legend('i_{S1}sim', 'i_{S1}phasor')

```

Chapter 5

CONCEPT OF REAL AND REACTIVE POWER

5.1 Introduction

In this chapter the meaning of ‘real’ and ‘reactive’ power are explored for sinusoidal systems. Initially, single phase (so-called two wire) circuits are discussed as to gain an understanding of the energy flow within a circuit configuration that is representative for electrical machines. We will then extend this analysis to three-phase (three wire) circuits. In the final part of this chapter a set of tutorials is introduced to reinforce the concepts discussed.

5.2 Power in single phase systems

The concept of power is introduced with the aid of figure 5.1, which shows a load in the form of an inductance L , resistance R and voltage source u_e in series connection. The voltage source u_e is generally known as the induced voltage in electrical machines. The circuit configuration as described above is representative for electrical machines hence its use here. A current source $i(t)$ is connected to this network. The reason for using a sinusoidal supply current source instead of a supply voltage source is to simplify the mathematical analysis. Application of Kirchhoff’s voltage laws to this circuit shows that the

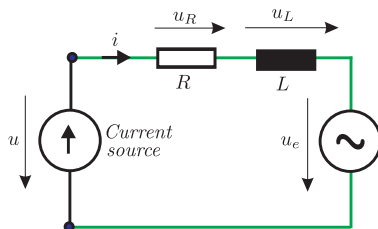


Figure 5.1. $R-L-u_e$ load connected to current source

voltage across the current source can be written as

$$u = u_R + u_L + u_e \quad (5.1)$$

where u_R , u_L , u_e represent the instantaneous voltages across the resistance, inductance and voltage source u_e respectively. If we multiply equation (5.1) with the instantaneous current produced by the current source, the so-called power balance equation appears as shown in equation (5.2).

$$\underbrace{u i}_{p_{in}} = \underbrace{i u_R}_{p_R} + \underbrace{i u_L}_{p_L} + \underbrace{i u_e}_{p_e} \quad (5.2)$$

The instantaneous power, which is a physical quantity, is simply the product of the instantaneous voltage and instantaneous current. If this value is positive then power flows into the circuit element or internal voltage source u_e . With reference to equation (5.2) the term p_{in} refers to the power supplied to the network. For the resistance and inductance the instantaneous power is given as p_R and p_L respectively. The same definition in terms of energy/power flow also applies to the voltage source u_e . For this circuit element energy can for example be converted to mechanical energy. It is noted that for a resistance, energy is dissipated which means that it is given as heat to the environment. Note that energy (Ws=joule) is defined as $\Delta W_e = \int_0^t p(\tau) d\tau$, i.e. in a time-diagram the area underneath the respective power function and the horizontal time line.

It is instructive to discuss these concepts with the aid of an example where we assume a sinusoidal current time function of the form

$$i(t) = \hat{i} \cos \omega t \quad (5.3)$$

The ‘steady-state’ voltage across the current source will be of the form

$$u(t) = \hat{u} \cos(\omega t + \rho) \quad (5.4)$$

In addition we will assume that the voltage across the induced voltage source u_e can be written as

$$u_e(t) = \hat{e} \cos(\omega t + \eta) \quad (5.5)$$

It is convenient at this stage to introduce a phasor representation of the variables $u(t)$, $i(t)$ according to the approach discussed in section 2.5. The variables according to equations (5.3), (5.4) may also be written as

$$i(t) = \Re \left\{ \underbrace{\hat{i}}_i e^{j\omega t} \right\} \quad (5.6a)$$

$$u(t) = \Re \left\{ \underbrace{\hat{u}}_u e^{j\rho} e^{j\omega t} \right\} \quad (5.6b)$$

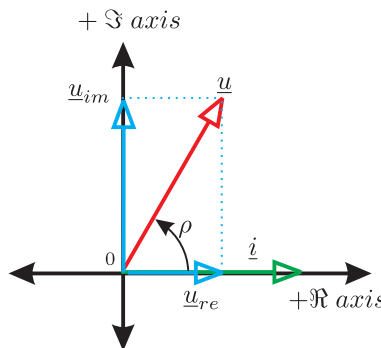


Figure 5.2. Phasor diagram of phasors \underline{i} , \underline{u}

An observation of figure 5.2 learns that we can also represent the voltage phasor in terms of the vector sum of the two phasors $\underline{u}_{re} = \hat{u} \cos \rho$ and $\underline{u}_{im} = j\hat{u} \sin \rho$, i.e. $\underline{u} = \underline{u}_{re} + \underline{u}_{im}$. The phasor \underline{u}_{re} is aligned (in phase) with the current phasor, the other \underline{u}_{im} is orthogonal, i.e. at right angles to \underline{i} . If the nature of the circuit is ‘inductive’ (as shown) the angle ρ will be greater than zero. Alternatively, circuits which exhibit a negative ρ are referred to as being ‘capacitive’. This definition ties in with the fact that the phasor diagram of for example an inductance, corresponds to the case $\rho = \frac{1}{2}\pi$ rad, whereas for a capacitance the angle is equal to $\rho = -\frac{1}{2}\pi$ rad.

The voltage phasor components \underline{u}_{re} , \underline{u}_{im} can also be converted to variables as function of time (by using the transformations given in equation (5.6)) namely

$$u_{re}(t) = \hat{u} \cos \rho \cos \omega t \quad (5.7a)$$

$$u_{im}(t) = -\hat{u} \sin \rho \sin \omega t \quad (5.7b)$$

Note that expression (5.7) may also be written in space vector form as

$$\vec{u}(t) = u_{re}(t) + j u_{im}(t) \quad (5.8)$$

The introduction of phasor components \underline{u}_{re} , \underline{u}_{im} allows us to rewrite the input power equation $p_{in} = i u$ as

$$p_{in} = \underbrace{i u_{re}}_{p_{re}} + \underbrace{i u_{im}}_{p_{im}} \quad (5.9)$$

which shows that the instantaneous input power expression is now defined in terms of two components which with the aid of equations (5.3), (5.7) can also be written as

$$p_{re} = \hat{u} \hat{i} \cos \rho \cos^2 \omega t \quad (5.10a)$$

$$p_{im} = -\hat{u} \hat{i} \sin \rho \cos \omega t \sin \omega t \quad (5.10b)$$

Equation 5.10 can also be rewritten in the form given below

$$p_{re} = \underbrace{\frac{\hat{u}\hat{i}}{2} \cos \rho}_{P} (1 + \cos 2\omega t) \quad (5.11a)$$

$$p_{im} = \underbrace{\frac{\hat{u}\hat{i}}{2} \sin \rho}_{Q} (-\sin 2\omega t) \quad (5.11b)$$

An analysis of equation (5.11a) learns that there is a time-independent term, known as the ‘real power P in ‘watts’ which represents the average power level P of the function p_{re} . In other words, the average power level corresponds to the total amount of energy supplied to the circuit for one cycle period T (the area enclosed by the power function p_{re} and time line) divided by T . Note that the average power level is also present in the function p_{in} given that the average value of the variable p_{im} is zero. The so-called ‘reactive’ power value Q expressed in VA is tied to the energy flow associated with expression (5.11b). Note that this power expression is based on the use of the voltage phasor component, which is at right angles to the current phasor (see figure 5.2). An observation of expression (5.11b) learns that the average power level is zero. The amplitude of the power function p_{im} is known as the reactive power value Q .

The real and reactive power value of the circuit may be written as

$$P = U I \cos \rho \quad \text{W} \quad (5.12a)$$

$$Q = U I \sin \rho \quad \text{VA} \quad (5.12b)$$

where $U = \hat{u}/\sqrt{2}$, $I = \hat{i}/\sqrt{2}$ are the respective RMS values of the voltage/current waveforms of the source connected to the $R-L-u_e$ circuit. The term $\cos \rho$ is referred to as the *power factor*.

It is at this stage helpful to consider a simple numerical example where we assume the current to be of the form $i = \cos \omega t$, where $\omega = 100\pi$ rad/s. The circuit elements are chosen purposely as to arrive at a voltage across the current source which is of the form $u = 2 \cos(\omega t + \rho)$, with $\rho = \pi/3$. Hence, the circuit is ‘inductive’ given that the voltage/time function leads the current/time function. For this example the values of P and Q are according to equation (5.12), equal to $P = 0.5\text{W}$ and $Q = 0.866\text{VA}$ respectively. The input power versus time plot together with its components p_{re} , p_{im} are shown in figure 5.3 for one 20ms cycle of operation. An observation of figure 5.3 shows that the energy flow is towards the circuit for some parts of the cycle (shown in ‘green’) and back to the current source for other parts (shown in ‘red’). There is however, an average energy flow (the difference between the ‘green’ and

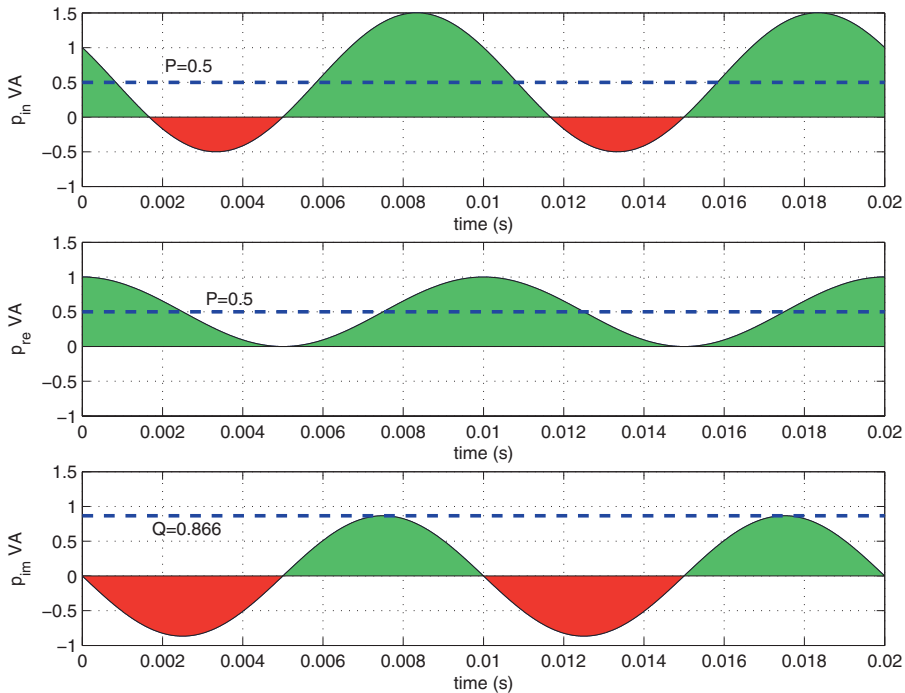


Figure 5.3. Power plot for $R-L-u_e$ circuit, supply side

‘red’ areas) and the power associated with this net energy is known as the ‘real’ power P given in watts as was discussed above.

Also shown in figure 5.3 are the two components p_{re} , p_{im} of the input power function. An observation of this example confirms that the energy linked with the power function p_{re} is precisely the energy supplied to the circuit over one period $T = 20\text{ms}$. The amount of energy supplied (shaded ‘green’ in the power function p_{re}) is equal to P times the cycle time T . The energy linked to the power waveform p_{im} represents the energy which is temporarily stored in the circuit (in either the inductive, capacitive elements or the internal voltage source). This energy oscillates between circuit and supply source (as shown by the ‘green’ and ‘red’ areas which identify the energy direction).

The reactive power value Q is equal to the amplitude of the waveform p_{im} . Note that the value of Q can be positive or negative, in both cases its value remains linked to the amplitude of the energy fluctuations. It is interesting to consider the changes to figure 5.3 for the case $\rho = 0$. Under these circumstances the reactive power level Q is zero, hence there are no energy fluctuations linked to this term. The energy level still fluctuates, but the energy flow is unidirectional, i.e. from supply to circuit. On the other hand, if we choose $\rho = \frac{1}{2}\pi$ the

real power P will be zero in which case the average amount of energy transferred from supply to the circuit is zero. The energy under these circumstances is stored and recovered from the circuit, i.e. for parts of the cycle it flows from source to the circuit and for the other (equal amount) it flows in the opposite direction.

At this point we have considered the power and energy situation when viewed from outside the circuit, i.e. from the source connected to the circuit. We will now consider the energy flow within the circuit itself.

Firstly, we examine the resistive component where the voltage across this element is given as $u_R = i R$, which can also be linked to its phasor representation namely

$$u_R(t) = \Re \left\{ \underbrace{\hat{i} R}_{u_R} e^{j\omega t} \right\} \quad (5.13)$$

The phasor \underline{u}_R is in phase with the current phasor \underline{i} as shown in figure 5.4. The

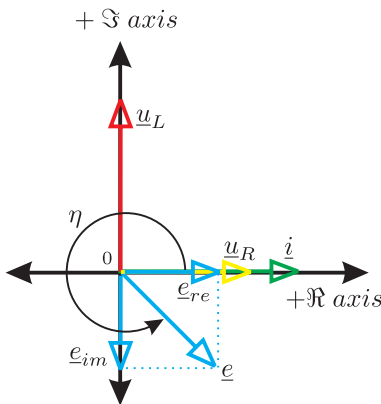


Figure 5.4. Phasor diagram for $R-L-u_e$ circuit, component side

instantaneous power linked to this component is equal to $p_R = i^2 R$, which after substitution of equation (5.3) can (after some manipulation) be written as

$$p_R(t) = \frac{\hat{i}^2 R}{2} (1 + \cos(2\omega t)) \quad (5.14)$$

An important observation from equation (5.14) is that the power p_R is greater than or equal to zero. Furthermore, the real power P_R (which is defined as the average value of $p_R(t)$) is equal to $P_R = I^2 R$, where $I = \hat{i}/\sqrt{2}$ is equal to the RMS value of the current.

We will now consider the inductance L of the circuit. The voltage across this element is given as $u_L = L \frac{di}{dt}$. Substitution of the current expression (5.3) leads to $u_L = -\hat{i} \omega L \sin \omega t$, which can also be written in terms of the phasor

\underline{u}_L linked to this function namely

$$u_L(t) = \Re \left\{ \underbrace{j \hat{i} \omega L}_{\underline{u}_L} e^{j\omega t} \right\} \quad (5.15)$$

Equation (5.15) shows that the voltage phasor \underline{u}_L is orthogonal (at right angles) to the current phasor as shown in figure 5.4. The power linked with this component is given as $p_L = u_L i$, which can also be written as

$$p_L(t) = -\frac{\omega L \hat{i}^2}{2} \sin(2\omega t) \quad (5.16)$$

The first observation to be made from equation (5.16) is that its average value is zero, which is to be expected given that an inductance cannot dissipate energy. Hence energy taken into the device is stored and must (at a later stage) be recovered. The peak value of p_L represents the reactive power Q_L of this component and is equal to $Q = I^2 \omega L$. Note that a similar analysis of this type can also be done for the capacitor in which case the reactive power is taken to be negative and of the form $I^2 \frac{1}{\omega C}$.

Finally, the circuit component u_e is considered, which is of the form given by equation (5.5). The phasor \underline{e} linked to this voltage function is of the form

$$u_e(t) = \Re \left\{ \underbrace{\hat{e} e^{j\eta}}_{\underline{e}} e^{j\omega t} \right\} \quad (5.17)$$

The phasor \underline{e} shown in figure 5.4 (with $\eta = -\pi/4$) can be defined in terms of two phasors \underline{e}_{re} , \underline{e}_{im} (also given in figure 5.4 according to the approach outlined for the voltage phasor (see equation (5.7))). The corresponding voltages are of the form

$$e_{re}(t) = \hat{e} \cos \eta \cos \omega t \quad (5.18a)$$

$$e_{im}(t) = -\hat{e} \sin \eta \sin \omega t \quad (5.18b)$$

$$(5.18c)$$

The introduction of these two voltage components allows us to rewrite the power equation $p^e = i u_e$ as

$$p^e = \underbrace{i e_{re}}_{p_{re}^e} + \underbrace{i e_{im}}_{p_{im}^e} \quad (5.19)$$

which shows that the instantaneous power expression is again defined by two terms, which with the aid of equations (5.3), (5.18) can also be written as

$$p_{re}^e = \hat{e} \hat{i} \cos \eta \cos^2 \omega t \quad (5.20a)$$

$$p_{im}^e = -\hat{e} \hat{i} \sin \eta \cos \omega t \sin \omega t \quad (5.20b)$$

Equation (5.20) can also be rewritten in the form given below

$$p_{re}^e = \underbrace{\frac{\hat{e}\hat{i}}{2} \cos \eta}_{P_e} + \underbrace{\frac{\hat{e}\hat{i}}{2} \cos \eta \cos 2\omega t}_{Q_e} \quad (5.21a)$$

$$p_{im}^e = \underbrace{\frac{\hat{e}\hat{i}}{2} \sin \eta}_{Q_e} (-\sin 2\omega t) \quad (5.21b)$$

Expressions (5.21) clearly show the real and reactive power contributions P_e , Q_e respectively, which are associated with the voltage source u_e .

It is at this stage helpful to return to the numerical example given for the supply side. For example, if we set $\hat{e} = \sqrt{2}/2\text{V}$, $\eta = -\frac{\pi}{4}\text{rad}$, $R = 0.5\Omega$, $\omega L = (\sqrt{3} + 0.5)\Omega$ and $\hat{i} = 1\text{A}$, then a simple phasor analysis of this circuit learns that the voltage across the current supply source will be equal to $u = 2 \cos(\omega t + \pi/3)$, which is the waveform used for the supply example that corresponds to the power/energy figure 5.3. Use of these circuit parameters with equations (5.14), (5.16) and (5.21) leads to the power waveforms and ‘energy’ surfaces as given in figure 5.5. The axis scaling has purposely been chosen to match that of figure 5.3. The energy levels linked with this circuit are again shown, where ‘green’ implies an energy flow into the circuit element and ‘red’ out of an element. For example, in the resistance, energy flow is always into this component, given that this energy is dissipated as heat. The average value of the waveform p_R represents the real power $P_R = 0.25\text{W}$ dissipated in the resistance given our choice of parameter values. For the inductance we observe a pulsating energy flow, which corresponds to a reactive power value of $Q_L = 1.116\text{VA}$.

Finally, we need to consider the voltage source u_e which has two power components, where the first p_{re}^e has an energy flow which must be unidirectional and (for this example) into this element. The average power level with the present parameter values is equal to $P_e = 0.25\text{W}$. A reactive power term is also evident, which in this case was arbitrarily chosen to be capacitive, which corresponds with a negative reactive value of $Q_e = -0.25\text{VA}$. The total real power which is absorbed by the circuit is equal to $P_R + P_e = 0.25 + 0.25 = 0.5\text{W}$, which corresponds to the power $P = 0.5\text{W}$ (supplied by the current source), as shown in figure 5.3.

The reactive component sum is equal to $Q_L + Q_e = 1.116 - 0.25 = 0.866\text{VA}$, which corresponds to the reactive power level of the circuit as shown in figure 5.3. From this analysis we can also observe where the real and reactive power ends up in the circuit. The real power supplied by the source is equally divided between the resistance and voltage source u_e . Furthermore, in this example,

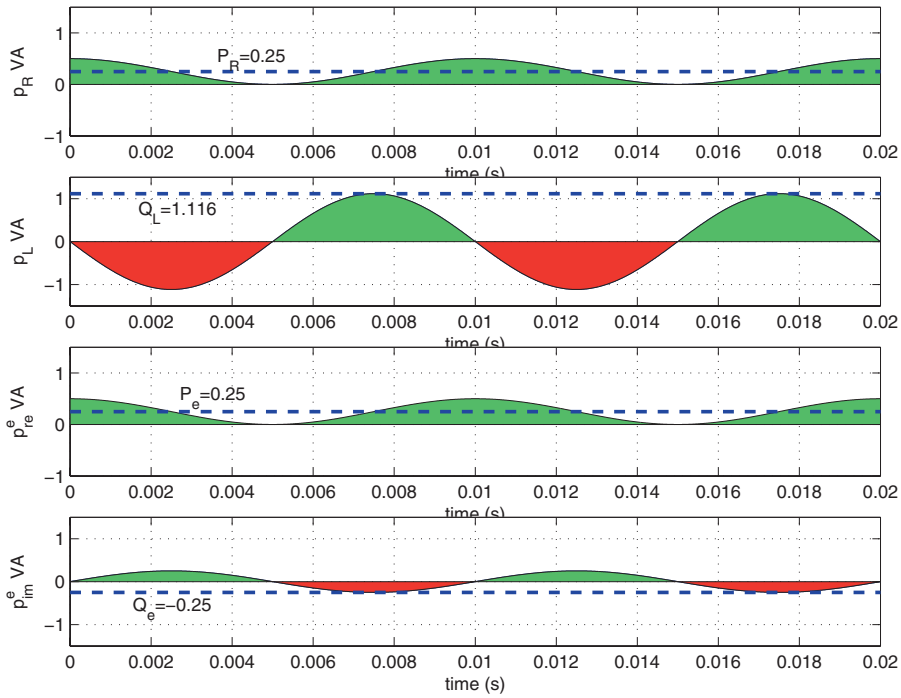


Figure 5.5. Power plot for R , L , e circuit, component side

the analysis shows the total reactive power Q is predominantly linked with that of the inductance. However, a small capacitive component (-0.25/0.866) (0.866VA represents the total reactive power level) is also linked with the voltage source u_e .

5.3 Power in three-phase systems

The approach used to explain the concept of power in single phase systems is extended in this section to three-phase systems. Use will be made of the material presented in chapter 4 in particular with respect to the use of space vectors.

It is helpful to assume a three-phase supply current source of the form

$$i_R = \hat{i} \cos(\omega t) \quad (5.22a)$$

$$i_S = \hat{i} \cos(\omega t - \gamma) \quad (5.22b)$$

$$i_T = \hat{i} \cos(\omega t - 2\gamma) \quad (5.22c)$$

The phase voltages which appear across the respective supply current sources may be written as

$$u_R = \hat{u} \cos(\omega t + \rho) \quad (5.23a)$$

$$u_S = \hat{u} \cos(\omega t + \rho - \gamma) \quad (5.23b)$$

$$u_T = \hat{u} \cos(\omega t + \rho - 2\gamma) \quad (5.23c)$$

The corresponding space vector representation (power invariant notation, see equation (4.26)) of the supply waveforms is in this case given as

$$\vec{u} = \sqrt{\frac{3}{2}} \hat{u} e^{j\rho} e^{j\omega t} \quad (5.24a)$$

$$\vec{i} = \sqrt{\frac{3}{2}} \hat{i} e^{j\omega t} \quad (5.24b)$$

where \hat{u} , \hat{i} represent the peak values of the three phase sinusoidal variables.

The three-phase circuit configuration as described for the single phase is again used here, which means that each phase consists of a series network in the form of a resistance R , inductance L and voltage source u_e which for the three phases 1, 2, 3 is now of the form

$$u_{e1} = \hat{e} \cos(\omega t + \eta) \quad (5.25a)$$

$$u_{e2} = \hat{e} \cos(\omega t + \eta - \gamma) \quad (5.25b)$$

$$u_{e3} = \hat{e} \cos(\omega t + \eta - 2\gamma) \quad (5.25c)$$

which can also be presented in its space vector form

$$\vec{u}_e = \sqrt{\frac{3}{2}} \hat{e} e^{j\eta} e^{j\omega t} \quad (5.26)$$

It is instructive to represent the three-phase network as considered here in its space vector form according to the approach outlined in chapter 4. We will assume for simplicity a ‘star’ connected circuit, given that phase variables are under these conditions equal to supply variables (there is no zero sequence voltage component in this case $u_0 = 0$). The resultant space vector based circuit diagram is of the form shown in figure 5.6. On the basis of figure 5.6 we will examine the power/energy concepts. A suitable starting point is the total

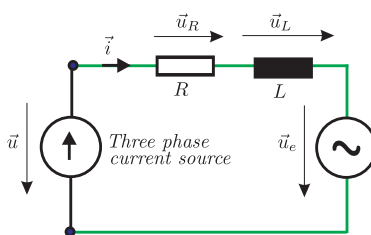


Figure 5.6. Space vector representation of the three-phase circuit

instantaneous input power which is now of the form

$$p_{in} = \underbrace{u_R i_R}_{p_R} + \underbrace{u_S i_S}_{p_S} + \underbrace{u_T i_T}_{p_T} \quad (5.27)$$

in which the instantaneous power for each phase is also shown. The real power in for example the 'R' phase is according to equation (5.12a) equal to $P_R = \frac{\hat{u}\hat{i}}{2} \cos \rho$. The total real power for this system will be three times this amount, on the grounds that the circuit configuration for all three phases is identical, hence the total real power is equal to

$$P = \frac{3\hat{u}\hat{i}}{2} \cos \rho \quad (5.28)$$

Note that this expression can also be written in terms of RMS values namely

$$P = 3UI \cos \rho \quad (5.29)$$

In this case it is helpful to use the form according to equation (5.28), given that it provides a relative easy transition to the space vector form of the power which is of the form

$$P = \Re \left\{ \vec{u} \left(\vec{i}^* \right) \right\} \quad (5.30)$$

Note that the superscript * indicates the conjugate of a vector. The validity of this expression is readily verified upon substitution of equation (5.24), in which case the end result must conform with equation (5.28). Note that it is precisely with the use of power invariant space vectors that we are able to make this conversion smoothly. With amplitude invariant space vectors a factor 3/2 would need to be added.

Equation (5.30) can also be given in terms of its space vector components $\vec{u} = u_\alpha + j u_\beta$ and $\vec{i} = i_\alpha + j i_\beta$, which leads to equation (5.31).

$$P = u_\alpha i_\alpha + u_\beta i_\beta \quad (5.31)$$

The space vector components can also with the aid of the conversion matrix (4.31) be rewritten in terms of phase variables, which (with sinusoidal variables and star connected circuit) also correspond to the supply variables $u_R, u_S, u_T, i_R, i_S, i_T$. After some mathematical manipulation equation (5.32) appears.

$$P = \underbrace{u_R i_R}_{p_R} + \underbrace{u_S i_S}_{p_S} + \underbrace{u_T i_T}_{p_T} \quad (5.32)$$

A comparison between equations (5.32), (5.27) learns that they are identical. The significant conclusion is therefore that the total instantaneous input power of the circuit is equal to the real power, hence

$$P = p_{in} \quad (5.33)$$

Equation (5.33) also states that there is no energy fluctuation present in the waveform p_{in} , given that the average value (as defined by the value P) corresponds to the instantaneous value. This observation is of fundamental importance as it means that the energy flow from supply to source is fully utilized in terms of transport efficiency. This is the fundamental reason why three wire (three-phase) circuits are used for energy conversion processes. A two wire circuit (single phase) cannot realize such an efficient energy transport as can be observed from figure 5.3, waveform $p_{in}(t)$.

For simulation purposes it is helpful to introduce a new building block as given by figure 5.7, which calculates the real power P according to equation (5.31). The input variables are in this case ‘vector’ lines, which means that

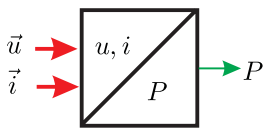


Figure 5.7. Real power module

the voltage and current input lines are given by the variables u_α , u_β and i_α , i_β respectively. The output of this module is the power P . Prior to discussing the concept of reactive power in three-phase systems it is instructive to extend the single phase example according to figure 5.3 for the three-phase case. The same circuit parameters and phase current/voltage parameters are used here, which means that $\hat{i} = 1\text{A}$, $\hat{u} = 2\text{V}$, $\rho = \frac{1}{3}\pi\text{rad}$, $\omega = 100\text{rad/s}$. On the basis of this data the instantaneous power for the three phases can be plotted using equations (5.22), (5.23) and (5.27). The results as given by figure 5.8 also show the energy linked with these waveforms, where ‘green’ is used to identify power into the circuit, whereas ‘red’ depicts an outgoing energy flow.

Figure 5.8 has as expected a constant instantaneous power value, whereas the phase power waveforms have an average value, which corresponds to the phase power $P_{R,S,T}$, calculated using equation (5.12a). The reader could perhaps at this point come to the erroneous conclusion that the reactive power Q for the three-phase circuit is zero given that the input power level is constant. This is *not* the case as will become apparent in the following discussion.

The reactive power in for example the ‘R’ phase is according to equation (5.12b) equal to $Q_R = \frac{\hat{u}\hat{i}}{2} \sin \rho$. The total reactive power for this system will be three times this amount on the grounds that the circuit configuration for all three phases is identical (as mentioned earlier), hence the total reactive power is equal to

$$Q = \frac{3\hat{u}\hat{i}}{2} \sin \rho \quad (5.34)$$

Note that this expression can also be written in terms of RMS values namely

$$Q = 3UI \sin \rho \quad (5.35)$$

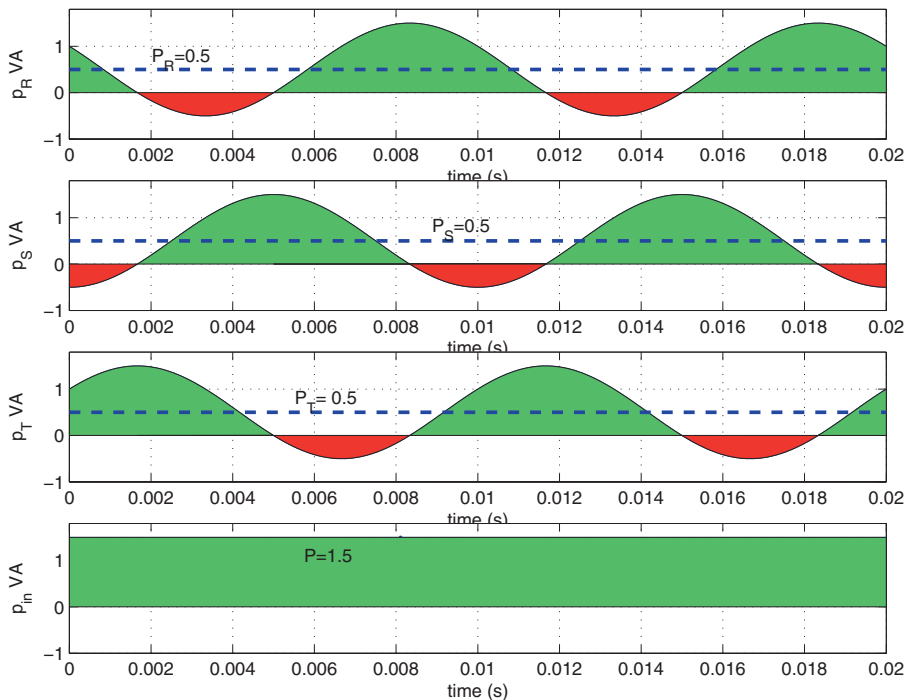


Figure 5.8. Three-phase ‘real’ power plot

In this case it is helpful to use the form according to equation (5.34) for further development, given that it provides a relative easy transition to the space vector format of the reactive power equation namely

$$Q = \Im \left\{ \vec{u} \cdot (\vec{i})^* \right\} \quad (5.36)$$

The validity of this expression is readily verified upon substitution of equation (5.24), in which case the end result must conform with equation (5.34). Note again that it is precisely with the use of power invariant space vectors that we are able to make this conversion smoothly. With amplitude invariant space vectors a factor $\frac{3}{2}$ would need to be added.

Equation (5.36) can also be given in terms of its space vector components \vec{u} , \vec{i} which leads to equation (5.37).

$$Q = u_\beta i_\alpha - u_\alpha i_\beta \quad (5.37)$$

At this point it is convenient to introduce a simulation building block which has as output the reactive power value as defined by equation (5.37). The input variables are in this case ‘vector’ lines which means that the voltage and current input lines are given by the variables u_α , u_β and i_α , i_β respectively. Prior to

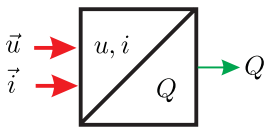


Figure 5.9. Reactive power module

discussing the power/energy flow within the three-phase circuit it is instructive to return to our numerical example used to plot the waveforms given in figure 5.8. The reactive power plot (for one cycle $T = 20\text{ms}$) which corresponds with this example is given by figure 5.10. The parameters used to obtain these results are $\hat{i} = 1\text{A}$, $\hat{u} = 2\text{V}$, $\rho = \frac{\pi}{3}\text{rad}$, $\omega = 100\text{rad/s}$.

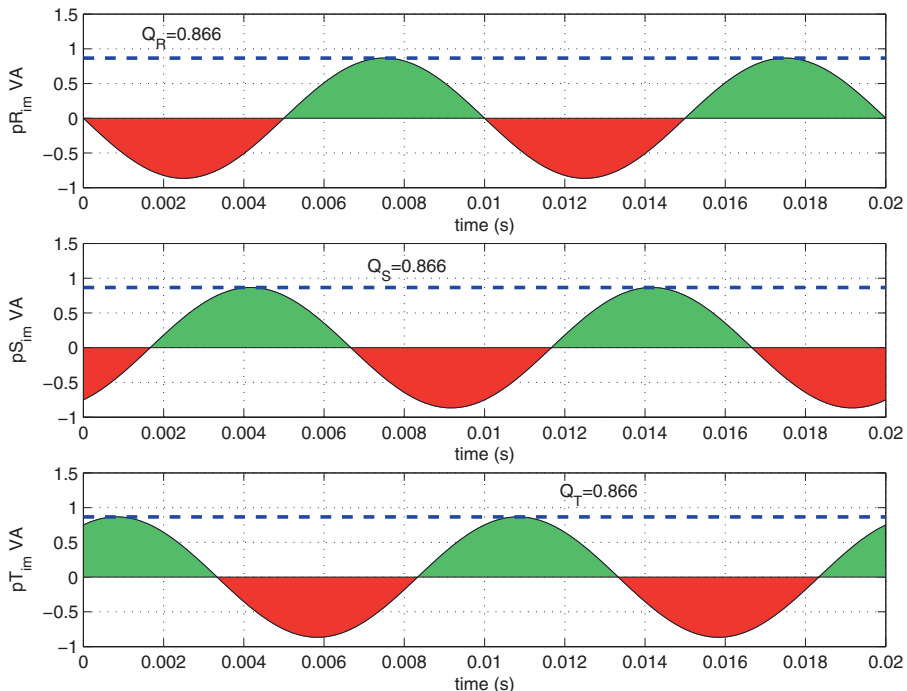


Figure 5.10. Three-phase ‘reactive’ power plot

The reactive power per phase corresponds to the amplitude of the p_{im}^R , p_{im}^S , p_{im}^T waveforms. Note that the instantaneous sum of these three waveforms is zero. The total reactive power of the circuit is defined as the sum of the reactive power per phase contributions, hence this sum is NOT zero but three times the amplitude of the phase contributions.

The approach used to examine the power contributions (for each element of the circuit) is based on the real and reactive power definitions as given by

equations (5.30) and (5.36) respectively. The vector \vec{u} must be replaced by the vector which corresponds to the circuit element under discussion.

For the resistive element the voltage vector is of the form $\vec{u}_R = \vec{i} R$ in which case the total power dissipated is given as

$$P_R = \vec{i} \vec{i}^* R \quad (5.38)$$

The reactive power for the inductance is found by use of the voltage vector $\vec{u}_L = L \frac{d\vec{i}}{dt}$ with equation (5.36), which leads to the reactive power Q_L expression defined as

$$Q_L = \vec{i} \vec{i}^* \omega L \quad (5.39)$$

The real and reactive power contributions linked to the three-phase voltage source u_e are found by using equation (5.26) with equations (5.30), (5.36) which leads to

$$P_e = \Re \left\{ \vec{e} \vec{i}^* \right\} \quad (5.40a)$$

$$Q_e = \Im \left\{ \vec{e} \vec{i}^* \right\} \quad (5.40b)$$

As with the single phase example it is instructive to return to the numerical example given for the three-phase supply side (figures 5.8, 5.10). If we again set $\hat{e} = \sqrt{2}/2V$, $\eta = -\pi/4\text{rad}$, $R = 0.5\Omega$, $\omega L = (\sqrt{3} + 0.5)\Omega$ and $\hat{i} = 1A$ then a space vector analysis of this circuit learns that the voltage across the current supply source will be given by equation (5.24a) with $\hat{u} = 2V$, $\rho = \frac{\pi}{3}\text{rad}$. The real and reactive power contributions as calculated using equations (5.38), (5.39) and (5.40) for these circuit elements is given in table 5.1.

Table 5.1. Real and reactive value for circuit example

Variable	Value
Real power resistance	P_R
Reactive power inductance	Q_L
Real power source u_e	P_e
Reactive power source u_e	Q_e

According to table 5.1 the total real power utilized by the circuit elements is equal to $P_R + P_e = 0.75 + 0.75 = 1.5W$ which is precisely the power level shown in figure 5.8. The reactive power of the circuit is according to table 5.1 equal to $Q_L + Q_e = 3.348 - 0.75 = 2.598\text{VA}$. This value divided by three gives the reactive power contribution per phase as shown in figure 5.10.

At the conclusion of this section it is helpful to introduce a simulation module which has as input a space vector $\vec{x} = x_\alpha + j x_\beta$ and as output the ‘RMS’ value

x. This module is useful for simulations with three-phase sinusoidal systems, where the RMS value linked to a space vector is often of interest. The building block which represents this conversion process is given in figure 5.11.

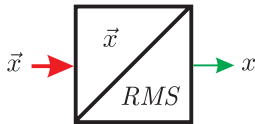


Figure 5.11. Vector to RMS module

The relationship between input and output is found by realizing that the amplitude of the vector is given as $|\vec{x}| = \sqrt{(x_\alpha)^2 + (x_\beta)^2}$. Furthermore, for power invariant type transformations (and sinusoidal waveforms) the RMS phase value is given as $x = \frac{\hat{x}}{\sqrt{2}}$, where $\hat{x} = \sqrt{\frac{2}{3}} |\vec{x}|$. The resultant conversion may also be written as

$$x = \frac{1}{\sqrt{3}} \sqrt{(x_\alpha)^2 + (x_\beta)^2} \quad (5.41)$$

5.4 Phasor representation of real and reactive power

In section 4.7.1 the relationship between phasors and space vectors was discussed. In this section the use of phasors with real and power concepts is considered. According to equation (4.59) the phasor representation of a voltage/current based power invariant space vectors may be written as

$$\vec{u} = \underbrace{\sqrt{\frac{3}{2}} \hat{u} e^{j\rho}}_{\underline{u}} e^{j\omega t} \quad (5.42a)$$

$$\vec{i} = \underbrace{\sqrt{\frac{3}{2}} \hat{i} e^{j\omega t}}_{\underline{i}} \quad (5.42b)$$

The observant reader will have noted that the phasor representation of for example the current is given as $\underline{i} = \sqrt{\frac{3}{2}} \hat{i}$, which is a factor $\sqrt{\frac{3}{2}}$ higher than the phasor representation used for the single phase analysis as given in section 2.5. The reason for this is that we are now dealing with three-phase systems where space vectors are given in a power invariant format.

The calculation of the real power of for example the $R-L-u_e$ circuit is defined by equation (5.30). Substitution of equation (5.42) leads to the phasor based form namely

$$P = \Re \{ \underline{u} (\underline{i})^* \} \quad (5.43)$$

A similar approach for conversion from space vector to phasor format can also be carried out for the reactive power equation (5.36) which gives

$$Q = \Im \{ \underline{u} (\underline{i})^* \} \quad (5.44)$$

Similarly the real and reactive power phasor based equations for the circuit components may be obtained. Use of equations (5.38), (5.39), (5.40) leads to

$$P_R = \underline{i} (\underline{i})^* R \quad (5.45)$$

$$Q_L = \underline{i} (\underline{i})^* \omega L \quad (5.46)$$

$$P_e = \Re \{ \underline{e} (\underline{i})^* \} \quad (5.47)$$

$$Q_e = \Im \{ \underline{e} (\underline{i})^* \} \quad (5.48)$$

5.5 Tutorials for Chapter 5

5.5.1 Tutorial 1

This tutorial is concerned with the energy flow within a resonant circuit connected to a battery source $u_b = 10V$ via a switch S which is closed at time $t = 0$. The resonant period of the circuit, as shown in figure 5.12 is given as $T = 2\pi\sqrt{LC}$. In this example, the period is set to $T = 20ms$. By choosing $L = 100mH$, the C value can be found using $T = 2\pi\sqrt{LC}$ to give the selected T . A simple computation learns that the capacitor value must be set to $C = 101.32\mu F$. Furthermore, we will assume that the capacitor is fully discharged at $t = 0$, hence $u_c(0) = 0$. A Simulink representation of figure 5.12

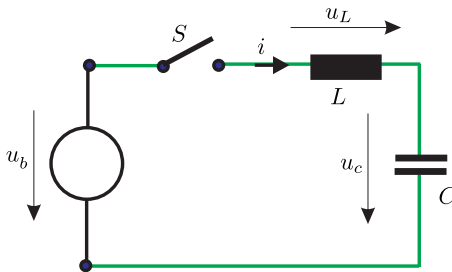


Figure 5.12. Resonant circuit example

is to be made based on the equation set which is linked with this circuit. An example of a Simulink representation of this circuit is given in figure 5.13. The objective of this tutorial is to examine the voltage, current and instantaneous power waveforms of this circuit for the time interval $0 \rightarrow 10ms$, i.e. for one half period cycle $T/2$ after the switch is closed. This means that the ‘run’ time of your simulation must be set to 10ms. Process your results in MATLAB, by writing an m-file to display the results. An example of the results which should appear in terms of the current i , voltage across the capacitor u_c and inductance u_L is given in figure 5.14. The energy flow for this circuit can

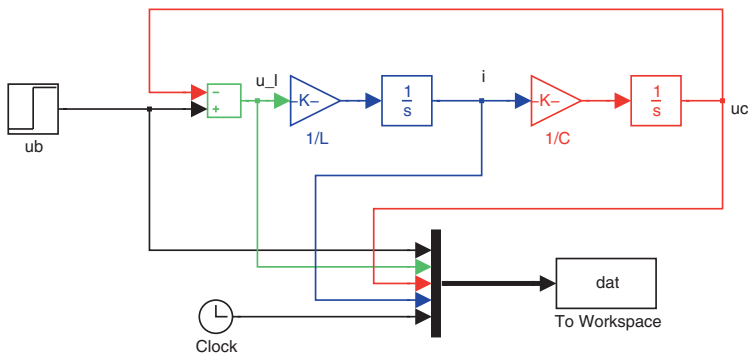


Figure 5.13. Simulink: Resonant circuit model

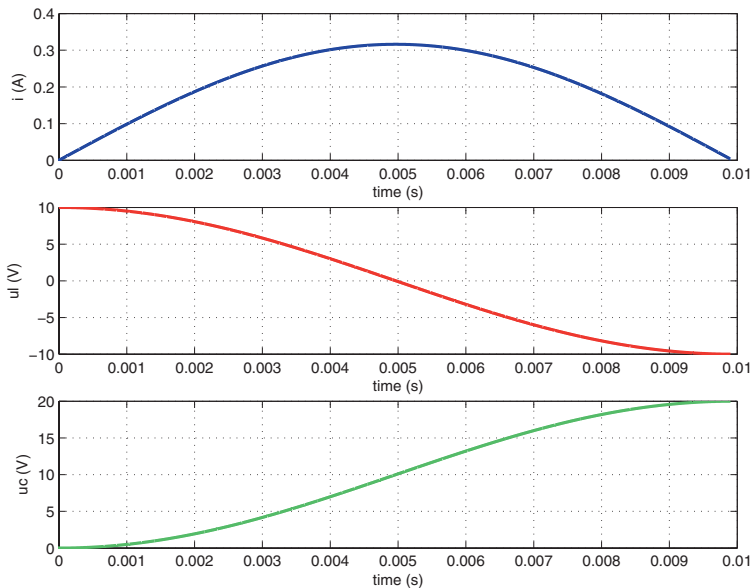


Figure 5.14. Simulink: results $i(t)$, $u_L(t)$, $u_C(t)$

be studied with the aid of the instantaneous power for each of the elements. The power for the battery, inductance and capacitor are of the form $p_s = u_b i$, $p_L = u_L i$ and $p_C = u_C i$ respectively. The power plots for this example are given in figure 5.15 and these show the energy supplied to and from the circuit elements. Areas shaded 'green' correspond to energy supplied to an element, whereas 'red' relates to energy which is recovered. An observation of figure 5.15 learns that during the first quarter ($0 \rightarrow 5\text{ms}$) of the cycle, energy from the battery source is supplied to the capacitor and inductance. During the second part of

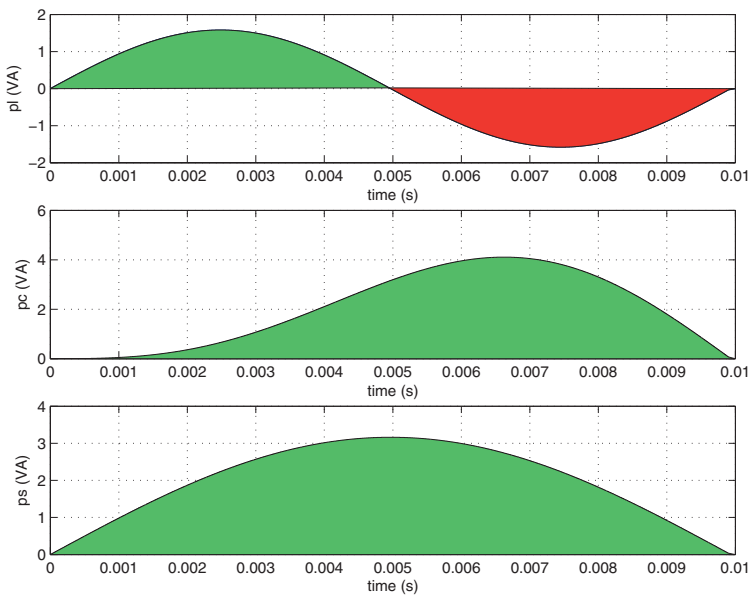


Figure 5.15. Simulink: results $p_L(t)$, $p_c(t)$, $p_s(t)$

the cycle ($5 \rightarrow 10\text{ms}$) the capacitor receives energy from the battery as well as the inductance. An example of an m-file implementation for this tutorial is given below:

m-file Tutorial 1, chapter 5

```
%Tutorial 1, chapter 5
close all
L=100e-3; C=101.32e-6; Ub=10; T=pi*sqrt(L*C);
i=dat(:,4); % current
uc=dat(:,3); % capacitor voltage
ul=dat(:,2); % inductance voltage
% subplot(3,1,1)
t=[dat(:,5); T]; % time
subplot(3,1,1)
plot(dat(:,5),i,'b');
xlabel('time (s)')
ylabel('i(A)')
grid
subplot(3,1,2)
plot(dat(:,5),ul,'r');
xlabel('time(s)')
ylabel('ul (V)')
grid
subplot(3,1,3)
plot(dat(:,5),uc,'g');
xlabel('time (s)')
ylabel('uc (V)')
```

```

grid
%%%%%%%
figure
pl=[ul.*i;0];                                % power inductance
pc=[uc.*i ;0];                                % power capacitance
ps=[Ub*i; 0];                                 % supply power
n=size(t,1);
subplot(3,1,1);
plot(t,pl);
hold on
grid
m=round(n/2);
fill(t(1:m),pl(1:m),'g')
fill(t(m:n),pl(m:n),'r')
xlabel('time(s)')
ylabel('pl (VA)')
%%%%%%
subplot(3,1,2);
plot(t,pc);
fill(t(1:n),pc(1:n),'g')
grid
xlabel('time (s)')
ylabel('pc (VA)')
%%%%%
subplot(3,1,3);
plot(t,ps);
fill(t(1:n),ps(1:n),'g')
grid
xlabel('time (s)')
ylabel('ps (VA)')

```

5.5.2 Tutorial 2

In this tutorial a Caspoc implementation of figure 5.12 is considered. The parameters for this example correspond to those given in the previous tutorial. The Caspoc simulation model as given in figure 5.16 on page 141 is in this case constructed with the aid of ‘circuit’ modules instead of generic modules (as shown in the previous tutorial). Furthermore, the simulation time has been doubled with respect to the first tutorial, i.e. $T = 20$ ms.

5.5.3 Tutorial 3

This tutorial is concerned with an $R-L-u_e$ circuit as given by figure 5.1. However, in this case a voltage source is connected to the load. A Simulink implementation of this circuit configuration, as given in figure 5.17, has an input voltage function $u = \hat{u} \cos(\omega t)$, where $\hat{u} = 220\sqrt{2}$ V, $\omega = 100\pi$ rad/s. The voltage source u_e is given as $e = \hat{e} \cos(\omega t + \zeta)$ were $\hat{e} = 100$, $\zeta = -7\pi/6$. The resistance and inductance value are taken to be $R = 10\Omega$ and $L = 100\text{mH}$ respectively. The $R-L-u_e$ circuit model is implemented in a single sub-module.

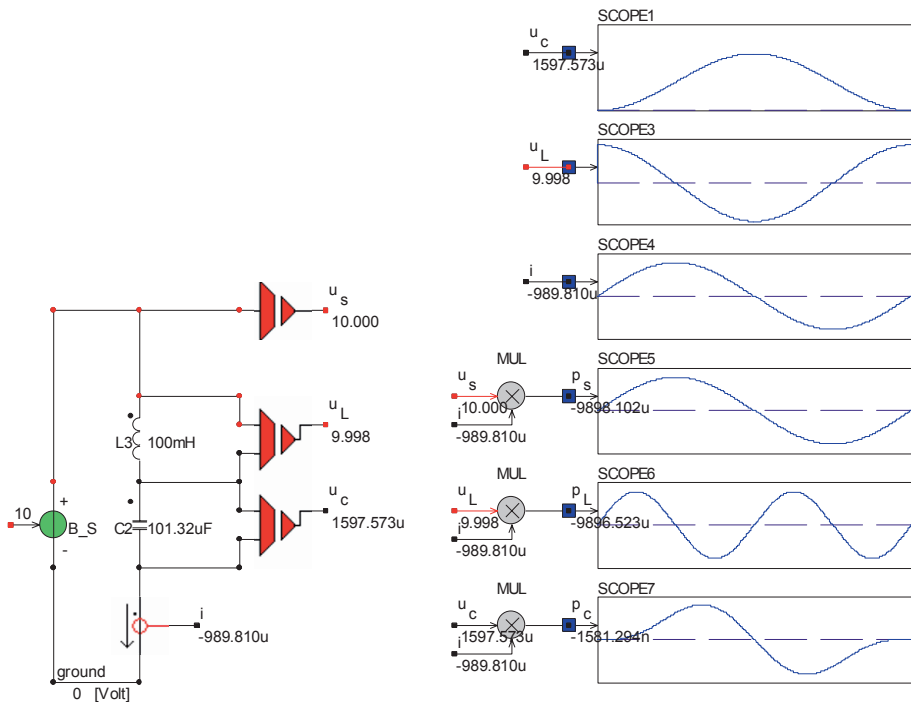
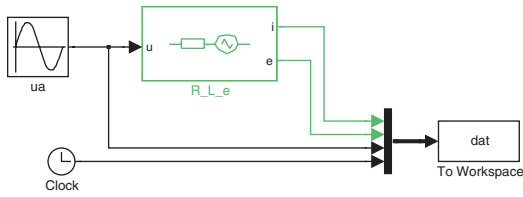


Figure 5.16. Caspoc simulation: resonant circuit

Figure 5.17. Simulink: Single phase $R-L-u_e$ circuit example

Run the simulation for a period of 60ms and plot the voltage/current waveforms u , e and i . An example of the results after running this simulation is given in figure 5.18. The instantaneous power waveforms $p_{in} = u i$ for the circuit and for the voltage source u_e , $p_e = e i$ are given in figure 5.19. The objective of this tutorial is to examine the power linked with the voltage source u_e on the basis that the latter is an unknown quantity. A problem of this type is typical for machines, hence its inclusion here. The input to this problem are the ‘measured’ steady-state current (as observed from the simulation, see figure 5.18), which is equal to $I = 9.29\text{A}$ and the ‘measured’ real power level (taken from figure 5.19) $P = 293\text{W}$.

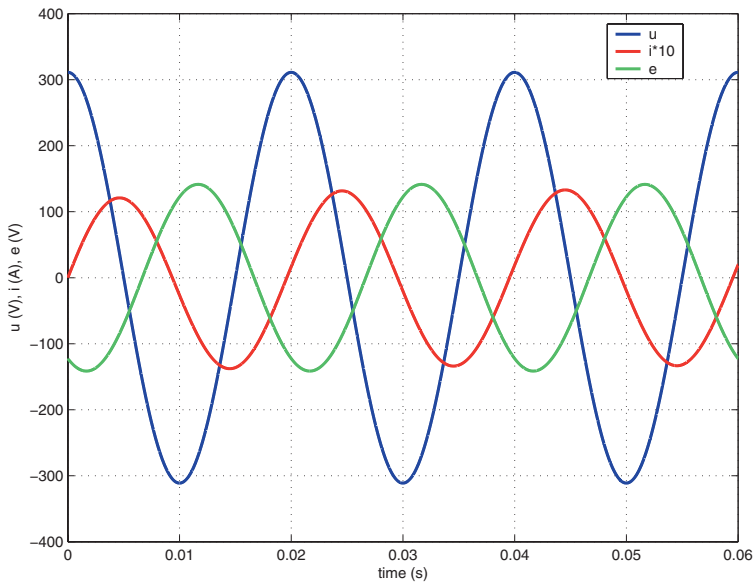


Figure 5.18. Simulink:results u, i, u_e

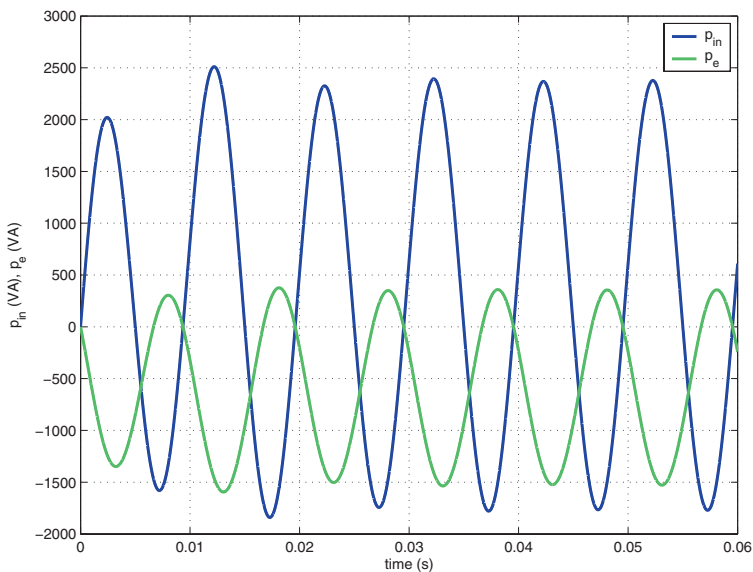


Figure 5.19. Simulink: results p_{in}, p_e

On the basis of the data provided calculate the reactive power Q , Q_L , Q_e of the circuit, the inductance and source u_e respectively. In addition calculate the real power associated with the resistance P_R and u_e source P_e . Finally, calculate on the basis of the Q_e and P_e values the amplitude and phase angle of the u_e source. An example of this calculation together with the m-file used to generate the plots for this tutorial is given at the end of this tutorial. The real and reactive results obtained after running the simulation and corresponding m-file are given in table 5.2.

Table 5.2. Real and reactive values for tutorial 2 example

Variable	Value
Real power resistance	P_R 863.0 W
Reactive power inductance	Q_L 2711.3 VA
Real power source u_e	P_e -570.0 W
Reactive power source u_e	Q_e -688.6 VA

The amplitude and phase of the u_e source are found by taking the ratio of the terms Q_e and P_e which gives the angle $\eta = \arctan(Q_e/P_e)$. Substitution of the values Q_e , P_e as given in table 5.2, gives $\eta = -129^\circ$ which is the angle between the phasors \underline{e} , \underline{i} as shown in the phasor diagram (see figure 5.20). Once the angle η is known, the amplitude of the u_e source can be calculated using equation (5.21) which gives $\hat{e} \approx 96.22 \cdot \sqrt{2}$. The value calculated using this approach compares favourably with the actual value of $100 \cdot \sqrt{2}$ as used for the simulation. The phase angle between the voltage and current phasors was found to be $\rho_i = -81.7^\circ$ and this angle is also shown in the phasor diagram given by figure 5.20.

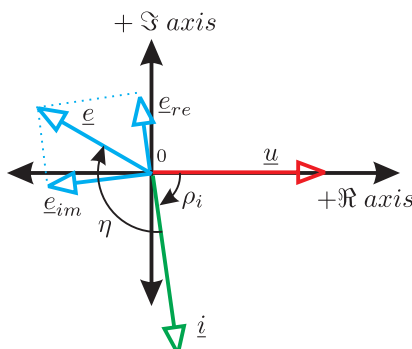


Figure 5.20. Phasor diagram for tutorial 3

Also shown in the phasor diagram are the phasor components \underline{e}_{re} and \underline{e}_{im} used to derive the real and reactive power components P_e and Q_e for the u_e source. Note that these components are in phase and orthogonal to the current phasor, *not* to the voltage phasor.

m-file Tutorial 3, chapter 5

```
%Tutorial 3, chapter 5
%we set E=100; eta=-7*pi/6 assume we don't know these values
%determine real reactive components on the basis of measured
%current
close all
R=10; % resistance
L=100e-3; % inductance
w=100*pi; % frequency in rad/s
%%%%%
t=dat(:,4); u=dat(:,3); i=dat(:,1);
e=dat(:,2); % used to cross check results calculation
%%%%%
plot(t,u);
grid
hold on
plot(t,i*10,'r')
plot(t,e,'g')
legend('u','i*10','e')
ylabel('u (V), i (A), e (V)')
xlabel('time(s)')
%%%%%
%analysis
%measured current
I=9.29;%measured RMS current
U=220; %RMS voltage
%watt meter,
figure
plot(t,u.*i);
grid
hold on
plot(t,e.*i,'g')
legend('p_{in}','p_e')
ylabel('p_{in} (VA), p_e (VA)')
xlabel('time (s)')
P=293; % measured average power
rho_i=acos(P/(U*I)); % phase angle u and i (rad)
%Current lags voltage, i.e inductive circuit
P_R=I^2*R; % dissipated power
P_e=P_P_R; % calculated power in $u_e$
Q=U*I*sin(rho_i);
Q_L=I^2*w*L; % reactive power in inductance
Q_e=Q-Q_L; % calculated reactive power in $u_e$
eta=atan(Q_e/P_e); % phase angle $u_e$, between e,i ,
% solution in third quadrant
eta3=(pi-eta)*180/pi; % result in degrees
E=1/I*sqrt(P_e^2+Q_e^2); % amplitude e source
```

5.5.4 Tutorial 4

The objective of this tutorial is to modify the simulation model given in section 4.8.8 in such a manner as to give the user the option of choosing a star or delta configured $R-L-u_e$ branch circuit. This means that we should be able to examine how the supply power and RMS current changes when the phase configuration is changed. Furthermore, the real and reactive power modules and RMS conversion modules are to be added as shown in figure 5.21. The

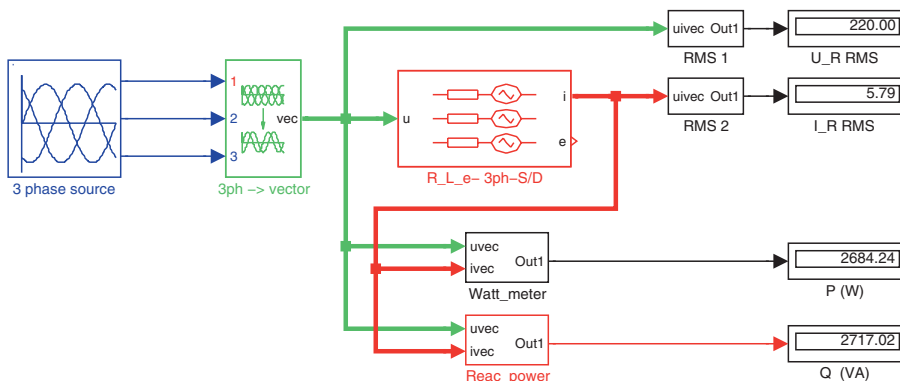


Figure 5.21. Simulink: Three-phase L , R , e circuit example, with star/delta selection

circuit shown in figure 5.21 appears on the surface to be very similar to that given by figure 4.47(b). The difference is that the power and RMS conversion modules according to figures 5.7, 5.9 and 5.11 have been added together with ‘display’ modules to observe the respective values. A set of modules needs to be added which will allow the $R-L-u_e$ space vector based phase circuit to be used in a star or delta configuration. The key is to introduce a menu ‘prompt’ for this sub-module which is linked to a variable ‘ S ’ shown in figure 5.22 within a ‘constant’ module. The output of this module must change with the configuration selected. For example, $S = 1$ for star, $S = 2$ for delta, in which case a switch module can be used for the conversion as shown in figure 5.23. In addition to the use of a switch, a set of conversion modules must be added for the delta connected case, as was discussed in section 4.6.3. The conversion modules for conversions from $\vec{u}_{RST} \rightarrow \vec{u}_{D123}$ and $\vec{i}_{D123} \rightarrow \vec{i}_{RST}$ need to

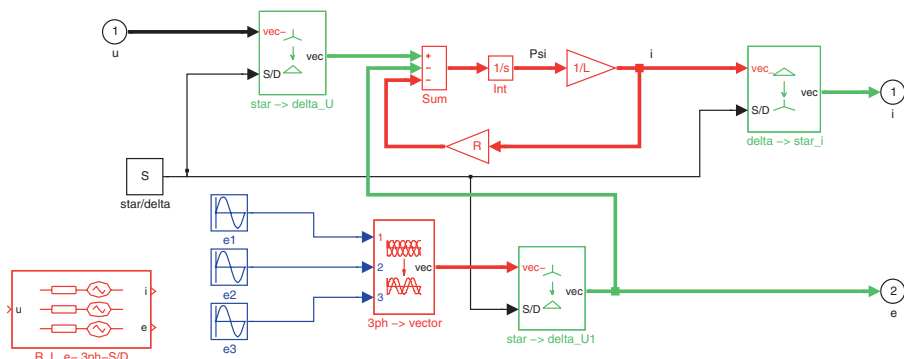
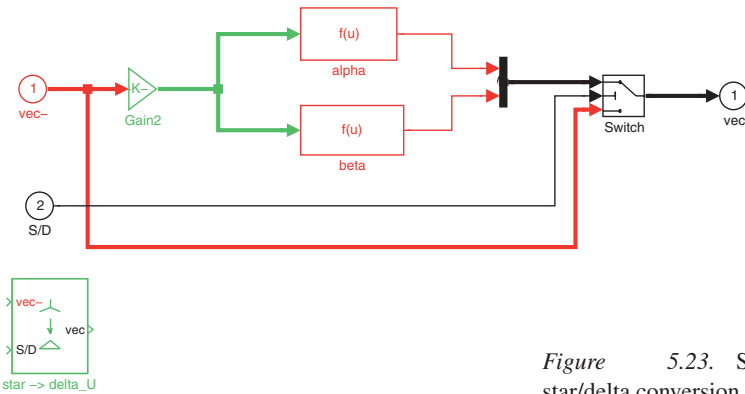


Figure 5.22. Simulink: star/delta circuit model

Figure 5.23. Simulink:
star/delta conversion

be implemented for the delta connected case, as shown in figure 5.23. The ‘function’ modules shown in figure 5.23 are used to realize the vector rotation $\pm\gamma/4$ and $\sqrt{3}$ scaling as required for the current and voltage space vectors. The supply voltage and circuit components remain unchanged when compared to those given in section 4.47(b). Run your simulation with a ‘run’ time of 600ms and observe the results on the numerical display modules for the star and delta configured circuit case. If your circuit is implemented correctly the results according to table 5.3 should appear. The sequel to this tutorial is concerned

Table 5.3. Simulation results tutorial 4

Parameters	Value
RMS Supply current (star)	I_s 5.79 A
RMS Supply current (delta)	I_d 17.36 A
Real power (star)	P_s 2684.2 W
Real power (delta)	P_d 8052.7 W
Reactive power (star)	Q_s 2717.0 VA
Reactive power (delta)	Q_d 8151.0 VA

with verifying the results shown in table 5.3 by way of a phasor analysis (in the form of an m-file) of this problem for the star and delta connected case. The results of this analysis should be the variables and values as given in table 5.3. Note that the values for the delta connected circuit configuration are three times higher than those shown for the star case. An example of an m-file for this problem is given below:

m-file Tutorial 4, chapter 5

```
%Tutorial 4, chapter 5
%%%eta=-pi/3
R=10; % phase resistance
L=100e-3; % phase inductance(H)
```

```

w=100*pi;                                % supply frequency (rad/s)
X=w*L;                                    % load reactance
C=sqrt(2/3);                             % space vector constant power invariant
U=220;                                     % supply phase voltage RMS
E=100;                                     % EMF phase voltage RMS
rho_e=-pi/3;                               % EMF phase angle
u_RST=3/2*C*U*sqrt(2);                   % supply phasor
U=u_RST/sqrt(3);                          % RMS suply
e_p=3/2*C*E*sqrt(2);                    % emf peak voltage
e_RST=e_p*cos(rho_e)+j*e_p*sin(rho_e); % EMF phasor
gamma=2*pi/3;                            % Star/delta choice in circuit module
% phasor analysis=star connected
u_123s=u_RST;% phase vector
e_123s=e_RST;%e phase vector
i_123s=(u_123s-e_123s)/(R+j*X);        % current phasor
ips=abs(i_123s);                         % peak value phasor
rho_is=angle(i_123s);                     % phase angle current phasor
% RMS supply current
Is=ips/sqrt(3);                          % RMS current
Ps=real(u_123s*conj(i_123s));           % real power W
Qs=imag(u_123s*conj(i_123s));           % reactive power VA
%%%%%%%%%%%%%%%%%%%%%%%%%%%%%%%%%%%%%
%Delta connected
u_123d=u_RST*sqrt(3)*(cos(-gamma/2)+j*sin(-gamma/2));    % U_phase phasor
e_123d=e_RST*sqrt(3)*(cos(-gamma/2)+j*sin(-gamma/2));    % e_phase phasor
i_123d=(u_123d-e_123d)/(R+j*X);                      % current phasor
ipd=abs(i_123d);                           % peak value phasor
rho_id=angle(i_123d);                        % phase angle current phasor
%RMS supply current
Id=ipd/sqrt(3)*sqrt(3);                  % RMS current
Pd=real(u_123d*conj(i_123d));            % real power W
Qd=imag(u_123d*conj(i_123d));           % reactive power VA

```

Chapter 6

SPACE VECTOR BASED TRANSFORMER MODELS

6.1 Introduction

This chapter considers an extension of the single phase transformer (ITF) model to a two-phase space vector based version. The introduction of a two phase (ITF) model is instructive as a tool for moving towards the so-called ‘ideal rotating transformer’ ‘IRTF’ concept, which forms the basis of machine models for this book. The reader is reminded of the fact that a two-phase model is a convenient method of representing three-phase systems as was discussed in section 4.6 on page 89. The development from ITF to a generalized two inductance model as discussed for the single phase model (see chapter 3) is almost identical for the two-phase model. Consequently, it is not instructive to repeat this process here. Instead, emphasis is placed in this chapter on the development of a two-phase space vector based ITF symbolic and generic model.

6.2 Development of a space vector based ITF model

The process of moving from a single phase ITF model to a space vector based version is readily done by making use of figure 3.1, which is modified to a two-phase configuration as shown in figure 6.1.

A comparison between the single phase (figure 3.1) and two-phase (figure 6.1) shows that there are now two windings on the primary and two on the secondary side of the transformer. The primary and secondary ‘alpha’ winding pair are orthogonal to the ‘beta’ winding pair. The number of ‘effective’ primary and secondary turns is equal to n_1 and n_2 respectively. Note that the windings are shown in symbolic form in order to show where the winding majorities are located. The primary and secondary phase windings are assumed to be sinusoidally distributed. A discussion on the concept of sinusoidally distributed

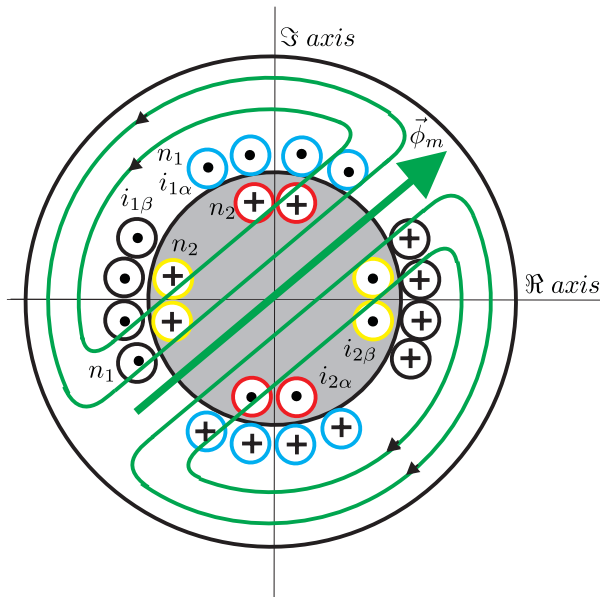


Figure 6.1. Two-phase physical transformer model

windings and ‘effective’ number of turns is given in appendix A. The currents in the primary and secondary windings are defined as $i_{1\alpha}$, $i_{1\beta}$ and $i_{2\alpha}$, $i_{2\beta}$ respectively. A complex plane with a real and imaginary axis is also introduced in figure 6.1. Also shown in this figure is the circuit flux distribution which is linked to a flux space vector $\vec{\psi}_m = \psi_{m\alpha} + j\psi_{m\beta}$. The complex plane is purposely tied to the orientation of the primary windings of the transformer, as can be explained by considering the two-phase model in a single phase form. If we ignore, for the purpose of this discussion, the windings which carry the currents ($i_{1\beta}$, $i_{2\beta}$), then a primary current $i_{1\alpha}$ (formerly i_1 in the single phase model) leads to a primary MMF $n_1 i_{1\alpha}$. This primary MMF must, for reasons discussed in chapter 3, correspond to a secondary MMF $n_2 i_{2\alpha}$, where $i_{2\alpha}$ is now used instead of i_2 (as used in the single phase model). Furthermore, the circuit flux vector $\vec{\psi}_m$ is under these circumstances oriented along the horizontal axis, which is precisely the chosen direction for the ‘real’ axis of the new complex plane in which case $\vec{\psi}_m = \psi_{m\alpha}$.

The relationship between currents and flux-linkages for the two-phase ITF model proceeds along similar lines as discussed for the single phase ITF model. The relationship between the primary and secondary currents is given as

$$n_1 i_{1\alpha} - n_2 i_{2\alpha} = 0 \quad (6.1a)$$

$$n_1 i_{1\beta} - n_2 i_{2\beta} = 0 \quad (6.1b)$$

The primary and secondary flux-linkages are defined as

$$\psi_{1\alpha} = n_1 \phi_{m\alpha} \quad (6.2a)$$

$$\psi_{2\alpha} = n_2 \phi_{m\alpha} \quad (6.2b)$$

$$\psi_{1\beta} = n_1 \phi_{m\beta} \quad (6.2c)$$

$$\psi_{2\beta} = n_2 \phi_{m\beta} \quad (6.2d)$$

Expressions (6.1), (6.2) correspond to the space vector form given in chapter 4.4 where the general notational form $\vec{x} = x_\alpha + jx_\beta$ was introduced. The resultant space vector based ITF equation set is given by (6.3).

$$\vec{u}_1 = \frac{d\vec{\psi}_1}{dt} \quad (6.3a)$$

$$\vec{u}_2 = \frac{d\vec{\psi}_2}{dt} \quad (6.3b)$$

$$\vec{\psi}_2 = \left(\frac{n_2}{n_1} \right) \vec{\psi}_1 \quad (6.3c)$$

$$\vec{i}_1 = \left(\frac{n_2}{n_1} \right) \vec{i}_2 \quad (6.3d)$$

The corresponding symbolic model and generic model of the space vector based ITF is given in figure 6.2. Note that the generic model shown in figure 6.2(b) represents the so-called ‘ITF-flux’ version, which is one of two possible model configurations available (see figure 3.3). One configuration is shown here to demonstrate the transition from single to space vector form. However, both are equally applicable for the space vector based ITF model. The difference

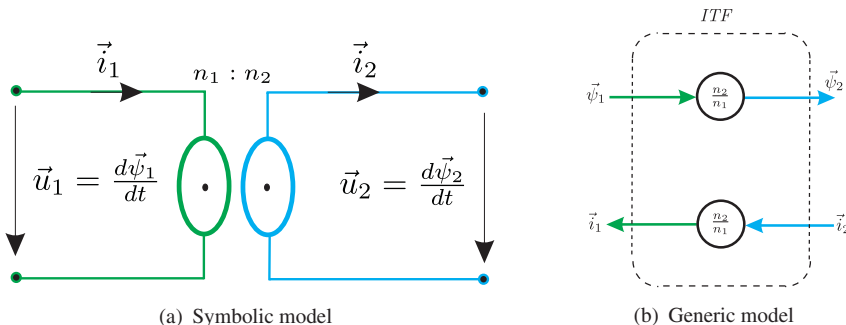


Figure 6.2. Symbolic and Generic space vector based ITF models

between the single and two-phase ITF models lies with the use of ‘vector lines’ (lines which are drawn wider when compared to single phase) which now represent the real and imaginary components. For example, the ‘vector line’ $i_{1\alpha}$, $i_{1\beta}$

represents the vector \vec{i}_1 . The symbolic and generic models as discussed for the single phase ITF based transformer remain unchanged in terms of configuration. Consequently, the ITF based single phase models with its extensions as discussed in chapter 3 are directly applicable here. An alternative symbolic way to represent the space vector ITF (figure 6.2(a) model is given in figure 6.3. In figure 6.3, the ITF is shown in terms of its primary and secondary α, β components.

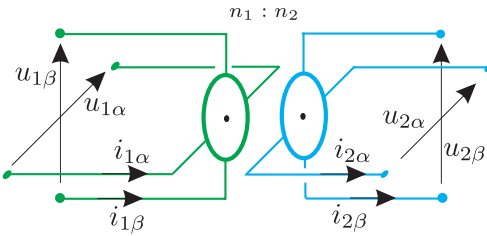


Figure 6.3. Three-dimensional ITF representation

ponents. This representation will be particularly instructive when discussing the so-called IRTF module.

6.2.1 Simplified ITF based transformer example

In this section an application example is given which demonstrates the use of the space vector based ITF model (see figure 6.2). The ITF model is extended by the introduction of a finite magnetizing inductance L_m as discussed in section 3.4 on page 50 for the single phase case. Leakage inductance and winding resistance are ignored in this model. A series configured resistive/inductive load is connected to the secondary winding. The symbolic model of this system as given in figure 6.4 shows the transformer with the load.

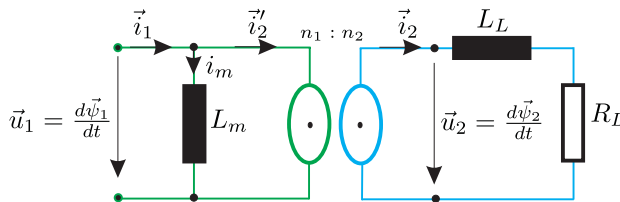


Figure 6.4. Two-phase transformer example with R, L load (space vector model)

The aim is to build a generic model of this system which will be transformed to a Simulink/Caspoc model (see the tutorial at the end of this chapter). As input to the generic model we will assume the primary flux-linkage space vector $\vec{\psi}_1$ rather than the primary supply voltage vector \vec{u}_1 . The reason for doing this is to emphasize the fact that it is the flux-linkage vector, which is central to the behaviour of this type of system. It is noted that generally we are not able to use the flux-linkage as an input vector given that its amplitude will change when

a more complicated transformer model is used (as was discussed earlier, see single phase transformer section 3.6 on page 55).

We will assume that the primary flux-linkage vector is given by

$$\vec{\psi}_1 = \hat{\psi}_1 e^{j\omega t} \quad (6.4)$$

The implementation of equation (6.4) in generic form calls for the introduction of a new building block, namely a ‘polar to cartesian’ conversion module, as indicated in figure 6.5(a). The conversion equation set is derived with the aid of

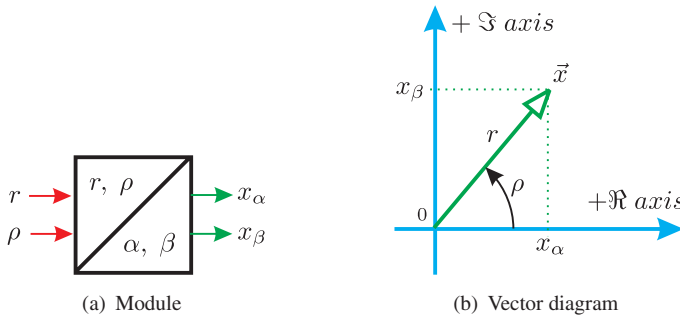


Figure 6.5. Module and vector diagram for polar to cartesian conversion

figure 6.5(b) which tells us that a vector \vec{x} can be either written in its polar form $\vec{x} = r e^{j\rho}$ or cartesian form $\vec{x} = x_\alpha + jx_\beta$. A comparison of these notation forms and observation of figure 6.5(b) gives

$$x_\alpha = r \cos \rho \quad (6.5a)$$

$$x_\beta = r \sin \rho \quad (6.5b)$$

The module according to figure 6.5(a) is directly used to build the generic model shown in figure 6.6.

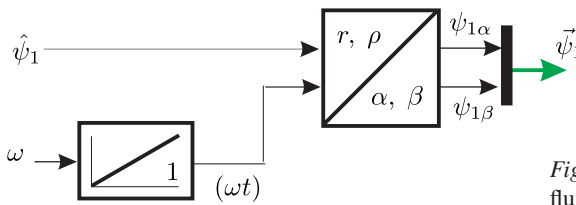


Figure 6.6. Generation of the flux-linkage vector $\vec{\psi}_1$

The model according to figure 6.6 shows the polar to cartesian conversion unit which has as input the amplitude and argument of the space vector $\vec{\psi}_1$. The output represents the real and imaginary components of the flux-linkage vector. These components are then combined via a ‘multiplexer’ to give a single

'vector. In the following the multiplexer will be placed inside the conversion module.

The resultant vector $\vec{\psi}_1$ serves as an input to the generic model of the transformer. The model according to figure 3.9 is directly applicable with the only change being that the load resistance is replaced by a resistance-inductance combination. Furthermore, the reader is reminded of the fact that the generic model is now used in its space vector form, i.e. 'vectors' are now present in the diagram. The generic model of the load is directly taken from the earlier

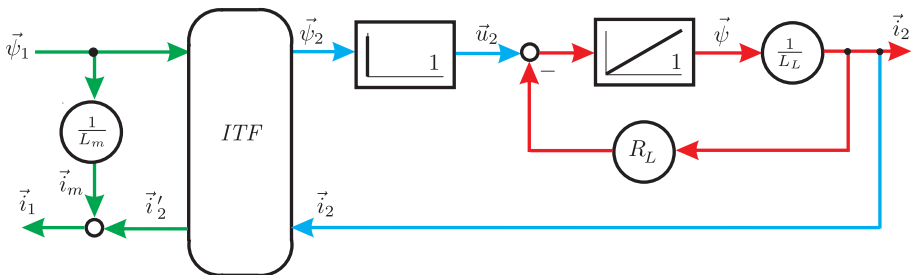


Figure 6.7. Generic ITF based transformer model with load: space vector form

example shown in figure 4.19 given that it represents precisely the resistance-inductance network. In this case, the resistance and inductance values are defined as R_L , L_L .

The model according to figure 6.7 shows a differentiator module which we implement in a different way as to avoid simulation problems. The reader is reminded that the use of differentiator modules in simulations can be problematic and should therefore be avoided where possible. For the tutorial exercise linked with this chapter we need access to the primary voltage vector which is defined by equation (6.3a). Furthermore, the differentiator module shown in figure 6.7 is there to implement equation (6.3b). Both equations differentiate a flux vector which (in this section) in its general form is given as

$$\vec{\psi} = \hat{\psi} e^{j\omega t} \quad (6.6)$$

where $\hat{\psi}$ is (in this example) *not* a function of time. If we differentiate equation (6.6) according to $\vec{u} = d\vec{\psi}/dt$, we find a very simple representation namely $\vec{u} = j\omega\vec{\psi}$. The generic implementation of this alternative 'differentiator' module is shown in figure 6.8.

The generic module according to figure 6.8 is *only* usable when the flux amplitude is constant. This is valid here and consequently the module can be used to implement equations (6.3a) and (6.3b) with the appropriate flux vector.

The gain module shown in figure 6.8 requires some further attention in terms of modelling such a unit. Essentially the gain $j = e^{j\pi/2}$ rotates an input vector

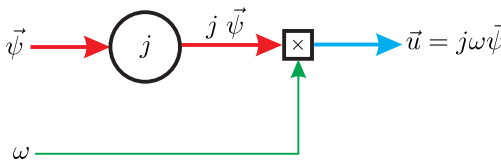


Figure 6.8. Alternative implementation of differentiator module

$\vec{x} = x_\alpha + jx_\beta$ by $\frac{\pi}{2}$ rad (90°). Hence the relation between input and output (for the gain module) vector $\vec{y} = y_\alpha + jy_\beta$ is of the form $\vec{y} = j\vec{x}$, which may also be written in the form given by equation (6.7).

$$\begin{bmatrix} y_\alpha \\ y_\beta \end{bmatrix} = \begin{bmatrix} 0 & -1 \\ 1 & 0 \end{bmatrix} \begin{bmatrix} x_\alpha \\ x_\beta \end{bmatrix} \quad (6.7)$$

In the Simulink environment equation (6.7) is directly usable with a ‘Matrix gain’ type element. In Caspoc an ‘alternative differentiator’ building block is available which conforms directly with figure 6.8.

6.2.2 Phasor analysis of simplified model

The analysis shown here is in fact very similar to that carried out for the three-phase R , L model (see section 4.7.1). Its inclusion here can therefore be seen as a revision exercise applied to the transformer system.

The flux-linkage vector (see equation (6.4)) is the input vector which corresponds with the phasor $\underline{\psi}_1 = \hat{\psi}_1$. The remaining phasors are found using the phasor based equation set of this system which is of the form

$$\underline{u}_1 = j\omega \underline{\psi}_1 \quad (6.8a)$$

$$\underline{u}_2 = j\omega \underline{\psi}_2 \quad (6.8b)$$

$$\underline{\psi}_2 = \left(\frac{n_2}{n_1} \right) \underline{\psi}_1 \quad (6.8c)$$

$$\underline{i}'_2 = \left(\frac{n_2}{n_1} \right) \underline{i}_2 \quad (6.8d)$$

$$\underline{i}_1 = \underline{i}'_2 + \underline{i}_m \quad (6.8e)$$

$$\underline{i}_m = \frac{\underline{\psi}_1}{L_m} \quad (6.8f)$$

$$\underline{u}_2 = (R_L + j\omega L_L) \underline{i}_2 \quad (6.8g)$$

The reader is advised to look carefully at equation (6.8) in terms of identifying where the various terms come from. Look carefully at the generic diagram (figure 6.7), which in fact represents the space vector based equation set for the system under consideration.

We will now proceed with the analysis to find the unknown phasors. The input voltage phasor is found using equation (6.8a) with $\underline{\psi}_1 = \hat{\psi}_1$ which gives

$\underline{u}_1 = j\omega \hat{\psi}_1$. The secondary flux-linkage vector is found using (6.8c) which gives $\underline{\psi}_2 = \frac{n_2}{n_1} \hat{\psi}_1$. This vector in turn allows us to find (with the aid of equation (6.8b)) the secondary voltage phasor namely $\underline{u}_2 = j\omega \frac{n_2}{n_1} \hat{\psi}_1$. We are now able to find the load current phasor with the aid of equation (6.8g) which yields

$$\underline{i}_2 = \frac{\underline{u}_2}{R_L + j\omega L_L} \quad (6.9)$$

The load current phasor on the secondary side corresponds with a current phasor (known as the primary referred secondary current phasor) \underline{i}'_2 on the primary side of the ITF which is calculated using equations (6.9) and (6.8d). Finally, the primary current is calculated by making use of equation (6.8e) and equation (6.8f) with $\underline{\psi}_1 = \hat{\psi}_1$. Two phasor diagrams are given in figure 6.9 for the case $n_2/n_1 = 0.5$.

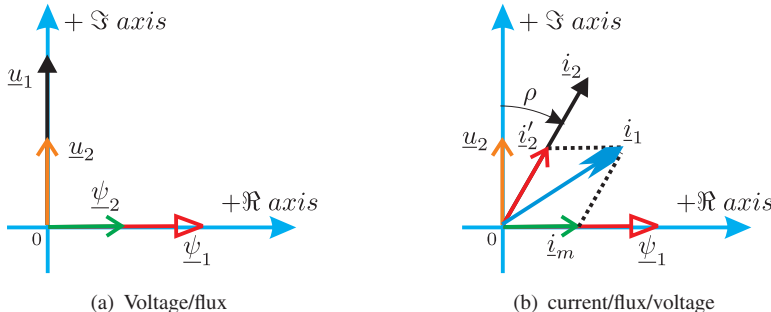


Figure 6.9. Phasor diagrams for transformer with R, L load

An observation of figure 6.9(a) learns that the primary flux-linkage is aligned with the real axis. This can be expected given that the primary flux-linkage has no imaginary component. The secondary flux-linkage phasor must be aligned with the primary phasor and its amplitude is reduced by a factor 0.5 which corresponds to the arbitrarily chosen winding ratio. The voltages are $\frac{\pi}{2}$ rad rotated forward with respect to their flux phasors. The secondary current phasor \underline{i}_2 , as shown in figure 6.9(b), lags the secondary voltage phasor by an angle $\rho = -\arctan(\omega L_L / R_L)$ as may be deduced from equation (6.9). The primary referred secondary current must be in phase with the secondary current phasor and its value is reduced by a factor 0.5 given our choice of winding ratio. Adding, in vector terms, the primary referred secondary current \underline{i}'_2 and the magnetizing current phasor (which must be in phase with the primary flux-linkage phasor) yields the primary current phasor \underline{i}_1 , as may be observed from figure 6.9(b).

6.3 Two-phase ITF based generalized transformer model

The use of a space vector type notation allows us to take any single phase symbolic or generic model (as developed in chapter 3) and use it in a two-phase system context.

The single-phase transformer development to include magnetizing inductance and leakage is therefore equally applicable to two-phase systems. Likewise, the resultant two inductance model as given by figure 3.15 is readily converted to a space vector form as indicated in figure 6.10. The correspond-

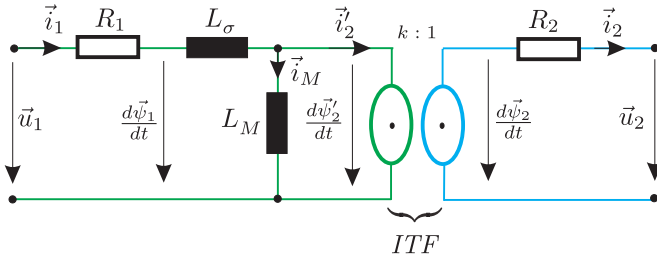


Figure 6.10. Four parameter, space vector based transformer model

ing generic diagram of this transformer is similar to the single-phase version, with the change that scalar lines are replaced by vector lines, i.e. the lines in figure 6.10 now represent two variables. The equation set which corresponds with figure 6.10 is as follows

$$\vec{u}_1 = \vec{i}_1 R_1 + \frac{d\vec{\psi}_1}{dt} \quad (6.10a)$$

$$\vec{\psi}_1 = \vec{i}_1 L_\sigma + \vec{\psi}'_2 \quad (6.10b)$$

$$\vec{\psi}'_2 = L_M \vec{i}_M \quad (6.10c)$$

$$\frac{d\vec{\psi}_2}{dt} = \vec{u}_2 + \vec{i}_2 R_2 \quad (6.10d)$$

$$\vec{\psi}'_2 = k \vec{\psi}_2 \quad (6.10e)$$

$$\vec{i}_2 = k \vec{i}'_2 \quad (6.10f)$$

6.3.1 Space vector transformer example

This example is concerned with the generic implementation of the symbolic model given in figure 6.11. The model according to figure 6.11 is basically the general model as shown in figure 6.10 with a load resistance R_L connected to the secondary winding. Furthermore, the secondary phase windings are connected in delta while the primary windings are star configured. The load resistance R_L as shown in figure 6.10 represents in three-phase terms a delta connected symmetrical load where each load phase consists of a resistance R_L .

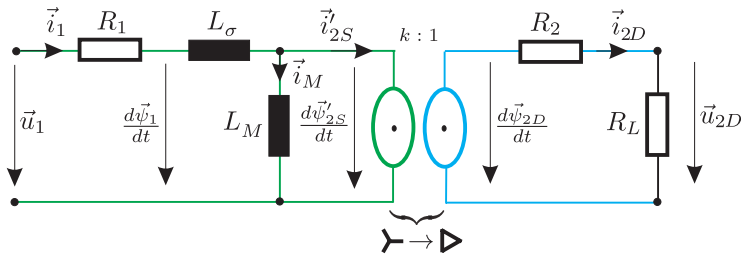


Figure 6.11. Symbolic model, transformer example

The *star*→*delta* symbol underneath the ITF module identifies the presence of a winding connection change between primary and secondary. No such notation is normally shown with the ITF module if the winding configuration between secondary and primary is unchanged. Equation set (6.10) is applicable to this example where the subscripts *S* and *D* need to be added (as given in figure 6.11) to identify secondary star/delta space vectors. Furthermore, an additional equation must be added to equation set (6.10) namely

$$\vec{u}_{2D} = \vec{i}_{2D} R_L \quad (6.11)$$

where R_L represents the load resistance. The primary windings are taken to be connected to a three-phase sinusoidal grid with angular frequency ω , which in space vector form corresponds to a vector $\vec{u}_1 = \hat{u}_1 e^{j\omega t}$. An example of a generic diagram based on equations (6.10) and (6.11) which can be used for dynamic simulation purposes is given in figure 6.12. The diagram according

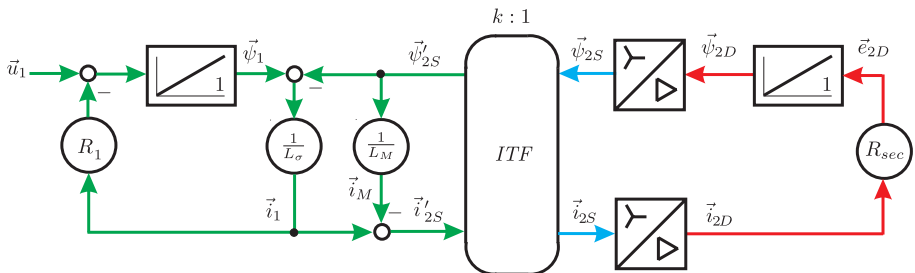


Figure 6.12. Generic model, transformer example

to figure 6.12 uses an *ITF-current* (because the primary current is designated as an input) module. In addition, a star/delta and delta/star conversion module are required for this example. The first conversion $\vec{\psi}_{2D} \rightarrow \vec{\psi}_{2S}$ uses the ‘voltage’ conversion equation (4.48), while the second conversion $\vec{i}_{2S} \rightarrow \vec{i}_{2D}$ uses equation (4.56). A voltage vector $\vec{e}_{2D} = \frac{d\vec{\psi}_{2D}}{dt}$ is introduced on the secondary

side of the model, given that the input to the integrator (on the secondary side) is equal to $\vec{e}_{2D} = R_{\text{sec}} \vec{i}_{2D}$, where $R_{\text{sec}} = R_2 + R_L$.

6.3.2 Phasor analysis of generalized model

The model according to figure 6.11 can also use phasors. Such an analysis may, in some cases, be useful if it is sufficient to consider the model under steady-state conditions. In other instances a phasor analysis is useful as means of verifying the steady-state results obtained with a dynamic simulation model.

In this example, the aim is to calculate the phasors $|i_1|$, $|i_{2D}|$, $|\psi_1|$ and $|\psi_{2D}|$ which represent the output variables from the dynamic simulation. The excitation to the model is the phasor u_1 which is linked with the space vector representation $\vec{u}_1 = u_1 e^{j\omega t}$. The supply vector amplitude is \hat{u}_1 , hence $u_1 = \hat{u}_1$. The calculation of the primary current phasor i_1 is similar to the approach discussed for the single phase transformer. This approach makes use of a primary referred model as shown in figure 6.13.

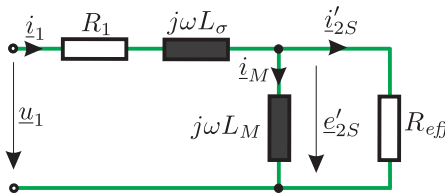


Figure 6.13. Primary referred phasor model of transformer with load

The components which represent the primary resistance, leakage inductance and magnetizing inductance are readily identifiable. Also shown is a component R_{eff} , which is the effective ‘primary referred’ load resistance. Its value is of the form given by equation (6.12).

$$R_{\text{eff}} = \frac{1}{3} k^2 \underbrace{(R_L + R_2)}_R \quad (6.12)$$

Equation (6.12) can be made plausible by realizing that the total secondary resistance R must be transformed from a delta to a star equivalent form, which according to section 4.7.1 is possible by multiplying the impedance by a factor $\frac{1}{3}$. Furthermore, equation (6.12) shows a factor k^2 , where k represents the ITF winding ratio. This factor as introduced for the single phase models is required to ‘refer’ a secondary impedance to the primary side.

The primary current phasor i_1 is found using $i_1 = u_1 / Z_1$, where Z_1 represents the input impedance. Once the current is found, the phasor ψ_1 can be calculated using $\psi_1 = (u_1 - i_1 R_1) \frac{1}{j\omega}$. The calculation of the secondary current is more elaborate as it requires access to the phasor e_{2D} . The process of calculating this phasor is initiated by determining the phasor e'_{2S} , which according to figure 6.13 can be found using $e'_{2S} = u_1 - i_1 R_1 - j\omega L_\sigma i_1$.

The phasor $\underline{e}_{2S} = j\omega \underline{\psi}_{2S}$ is found using $\underline{e}_{2S} = \underline{e}'_{2S} \frac{1}{k}$ and this phasor must be transformed to the delta form (see equation (4.65a)) with $\underline{e}_{2D} = \underline{e}_{2S} \sqrt{3} e^{-j\gamma/4}$. Once this phasor is found the flux-linkage phasor $\underline{\psi}_{2D}$ and secondary current phasor \underline{i}_{2D} can be calculated according to $\underline{\psi}_{2D} = \underline{e}_{2D} \frac{1}{j\omega}$ and $\underline{i}_{2D} = \underline{e}_{2D} \frac{1}{R_L + R_2}$.

6.4 Tutorials for Chapter 6

6.4.1 Tutorial 1

This tutorial is concerned with implementing the generic model given by figure 6.7. The load which is connected to the secondary winding is formed by an inductance $L_L = 1\text{mH}$ and resistance $R_L = 0.4\Omega$. As input to the model a flux-linkage space vector $\vec{\psi}_1$ is assumed which is taken to be of the form $\vec{\psi}_1 = \hat{\psi}_1 e^{j\omega t}$, where $\hat{\psi}_1 = 1.25\text{Wb}$ and $\omega = 2\pi 50 \text{ rad/s}$. The ITF winding ratio is taken to be $\frac{n_1}{n_2} = 5$. Furthermore, the magnetizing inductance is set to $L_m = 1.5\text{H}$. Leakage inductance and winding resistances are ignored.

Build a polar to cartesian converter module by making use of ‘Fcn’ functions. Add a ‘mux’ so that the output of the converter is a vector (select ‘wide non scalar lines’ to make your simulation more readable) with components $\psi_{1\alpha}$, $\psi_{1\beta}$. Use a ‘constant’ module to generate the ω (electrical frequency in rad/s) value and add an integrator which will give as output the variable ωt . Check your work by using a ‘XY’ scope module, with axis values $x_{\min} = -1.5$, $x_{\max} = 1.5$, $y_{\min} = -1.5$, $y_{\max} = 1.5$. Under simulation parameters select a ‘fixed step’ type ‘solver’ with step size $1\text{e-}3\text{s}$. Solver type should be ‘ode4’. Run the simulation for 1s and observe the result, which should be a circle with a radius equal to 1.25. Maintain the solver settings and run time as given above for the rest of the tutorial.

Add a set of modules which will generate the voltage space vector $\vec{u}_1 = j\omega \vec{\psi}_1$ as shown in figure 6.8. You will need to use a multiplier and gain module with gain j . The latter is realized in Simulink by using a ‘Matrix gain’ module. Select ‘Matrix gain K*u’ within this module and set the gain to $[0 \ -1; 1 \ 0]$. Build using a ‘Fcn’ module, a building block which allows you to calculate the RMS value of the three-phase waveforms which correspond to a vector \vec{x} . Connect the output of the ‘vector to RMS converter’ to a ‘display module’ (see ‘sinks library’) so that the RMS primary voltage value can be shown.

Add an *ITF-flux* module, magnetizing inductance L_m and a series of modules which will allow you to calculate the secondary voltage vector $\vec{u}_2 = j\omega \vec{\psi}_2$, where $\vec{\psi}_2$ is the output vector from the ITF module. Use two vector to RMS converters with display units to show the RMS secondary voltage and RMS primary current values. Furthermore, build two additional sub-modules which are able to calculate the real and reactive power values $P(\text{W})$ and $Q(\text{Var})$ respectively.

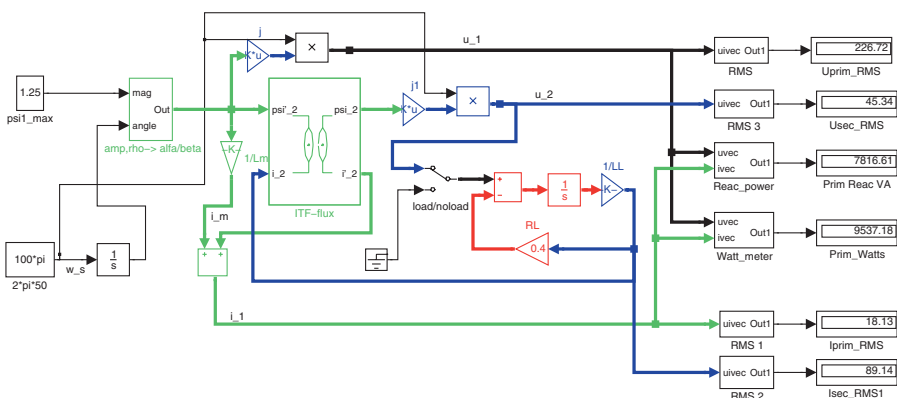


Figure 6.14. Simulink model of transformer with load

The last step is concerned with testing our transformer under load and no-load conditions. Add a ‘manual’ load/noload switch which enables you to connect/disconnect the load. An example of a Simulink model which corresponds to the generic model in question is given in figure 6.14. Run the simulation and record the six display values. Repeat the exercise for the no-load case.

The values which should appear on the display modules for the variables under discussion are given in table 6.1.

Table 6.1. Simulation results transformer no-load/load

Parameters		no-load	load
RMS Primary voltage	U_{prim}	226.72 V	226.72 V
RMS Secondary voltage	U_{sec}	45.34 V	45.34 V
RMS Primary current	I_{prim}	0.48 A	18.13 A
RMS Secondary current	I_{sec}	0.00 A	89.14 A
Real Primary power	P_{prim}	0.00 W	9537.18 W
Reactive Primary power	Q_{prim}	327.25 VA	7816.61 VA

6.4.2 Tutorial 2

A Caspoc implementation of the generic model given by figure 6.7 is considered in this tutorial. The simulation model as given in figure 6.15 represents the simplified transformer model connected to a resistive/inductive load. The parameters and excitation are according to those discussed in the previous tutorial. The simulation results (given with each variable) as shown in figure 6.15 at the completion of the simulation run (when steady-state operating conditions have been reached) match those given by table 6.1 (load column).

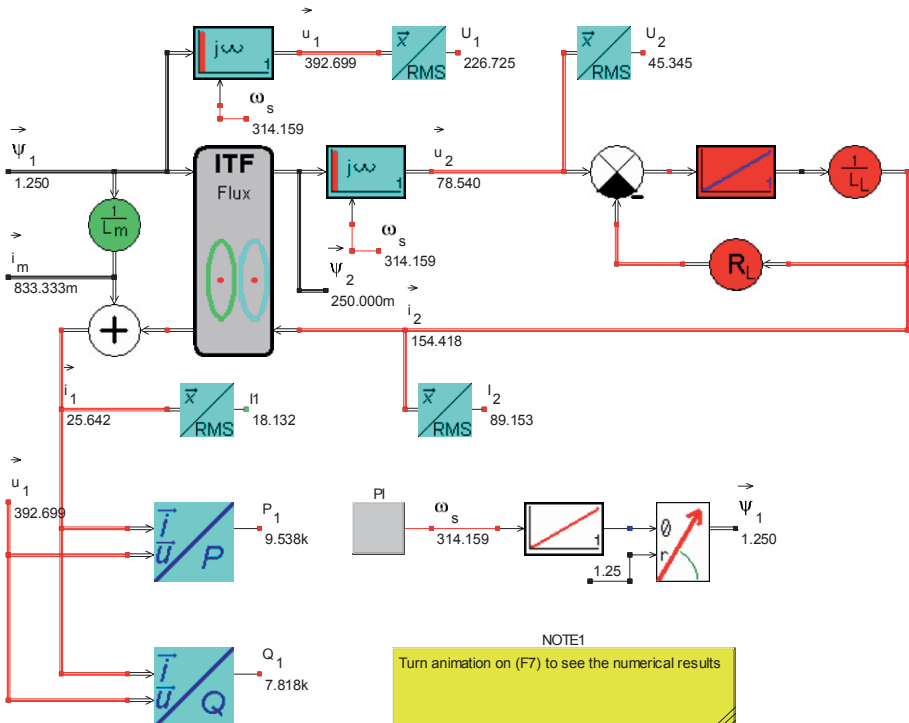


Figure 6.15. Caspoc simulation: simplified transformer model

6.4.3 Tutorial 3

A phasor analysis should be carried out of the transformer configuration as discussed in the previous two tutorials, to verify the simulation results obtained via the six display units shown in figure 6.14. The input for this analysis is taken to be the flux phasor $\psi_1 = 1.25\text{Wb}$. On the basis of this phasor we can calculate the remaining phasors ψ_2 , u_1 , u_2 , i_m , i_2 , i_1 . In addition, the real and reactive power value can be calculated. The exercise should be carried out for the no-load (means no $R-L$ network connected to the secondary of the transformer) and load situation. A MATLAB file must be written for this exercise. An example of such an m-file is as follows:

m-file Tutorial 3, chapter 6

```
%Tutorial 3, chapter 6
ps11_hat=1.25; % primary flux amplitude
ps11=ps11_hat; % primary flux phasor
k=5; % n1/n2=5 winding ratio
Lm=1.5; % magnetizing inductance
w=2*pi*50; % frequency rad/s
%%%%%%%%%%%%%
```

```

u1=j*w*psi1_hat; % primary supply voltage phasor
U1=abs(u1)/sqrt(3); % primary RMS voltage
psi2=1/k*psi1; % secondary flux phasor
u2=j*w*psi2; % secondary voltage phasor
U2=abs(u2)/sqrt(3); % secondary RMS voltage
%
%%%%%no-load case
im=psi1/Lm; % magnetizing current phasor
i1n=im; % no secondary current
I1n=abs(i1n)/sqrt(3); % primary current no-load
Pn=real(u1*conj(i1n)); % primary real power
Qn=imag(u1*conj(i1n)); % primary reactive power
%%%%%
%%%%% load case
LL=1e-3; % load inductance
RL=0.4; % load resistance
i2=u2/(RL+j*w*LL); % secondary load current phasor
I2=abs(i2)/sqrt(3); % secondary RMS current
i2r=i2/k; % primary referred current phasor
i1=im+i2r; % primary current phasor load
I1=abs(i1)/sqrt(3); % primary current load
P=real(u1*conj(i1)); % primary real power (load)
Q=imag(u1*conj(i1)); % primary reactive power (load)

```

The results after running the m-file should match closely with those given in table 6.1.

6.4.4 Tutorial 4

A Simulink implementation of the example outlined in section 6.3.1 is considered in this tutorial. A three-phase supply source as given in figure 4.47(a) is to be used, with an RMS phase voltage of $U_1 = 220V$ and angular supply frequency of $\omega = 2\pi f$ rad/s, where $f = 50\text{Hz}$. The primary and secondary winding resistances are set to $R_1 = 10\Omega$ and $R_2 = 5\Omega$ respectively. The leakage and magnetizing inductance are equal to $L_\sigma = 10\text{mH}$ and $L_M = 300\text{mH}$ respectively, while the load resistance of the delta connected load is set to $R_L = 20\Omega$. An ITF winding ratio of $k = 2$ is assumed.

The simulation is to be run for a period of 0.4s, using a ‘step-size’ of 10^{-5}s and ‘solver’ ode4. Outputs of the simulation should be the vectors \vec{i}_1 , \vec{i}_{2D} , $\vec{\psi}_1$ and $\vec{\psi}_{2D}$. An example of a possible implementation of this problem is given in figure 6.16. The modules used in this example for the conversion of supply voltages to space vector format and those used for the star/delta conversions have been discussed in chapter 4. A ‘To Workspace’ module has been added to plot the results in the form of the absolute value versus time of the vectors \vec{i}_1 , \vec{i}_{2D} , $\vec{\psi}_1$ and $\vec{\psi}_{2D}$. Figures 6.17 and 6.18 show the current and flux plots which should appear after running your simulation.

The results show the presence of a transient in the current and flux waveforms after the transformer has been connected to the supply. A detailed observation of the results given show that the steady-state currents and steady-state flux values

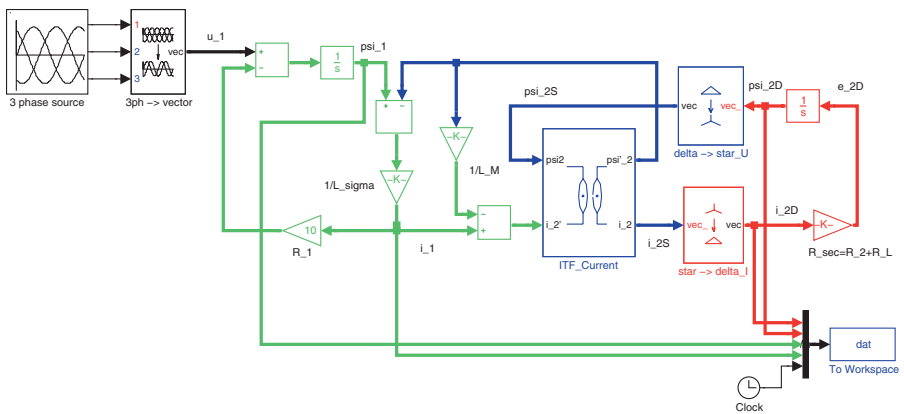


Figure 6.16. Simulink model of transformer with resistive load

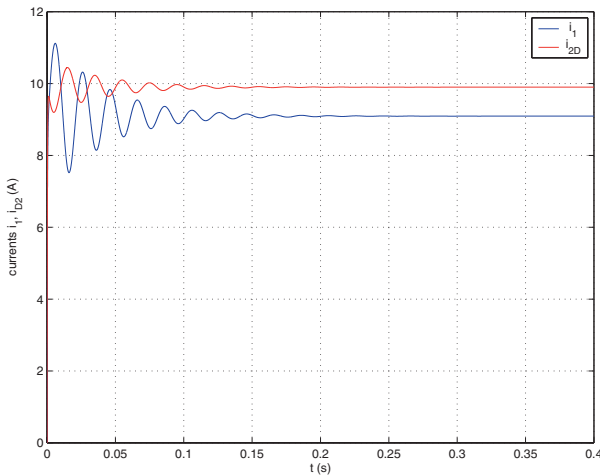


Figure 6.17. Simulink results: primary and secondary currents, $|\vec{i}_1|$, $|\vec{i}_{2D}|$

are equal to $|\vec{i}_1| = 9.09\text{A}$, $|\vec{i}_{2D}| = 9.90\text{A}$ and $|\vec{\psi}_1| = 0.94\text{Wb}$, $|\vec{\psi}_{2D}| = 0.79\text{Wb}$ respectively.

The m-file to plot the results shown in figure 6.18 is as follows

m-file Tutorial 4, chapter 6

```
%Tutorial 4, chapter 6
close all
%plot file
L_sig=10e-3; % leakage inductance
L_M=300e-3; % magnetizing inductance
R_1=10; % primary resistance
```

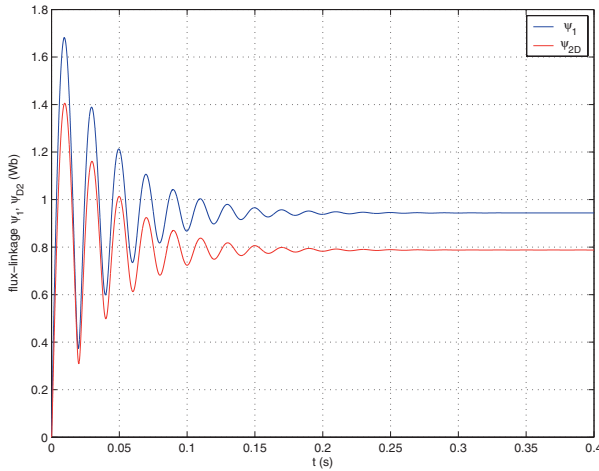


Figure 6.18. Simulink results: primary and secondary flux-linkage, $|\vec{\psi}_1|$, $|\vec{\psi}_{2D}|$

```
R_2=5; % secondary resistance
R_1=20; % load resistance
k=2; % winding ratio ITF
gamma=2*pi/3;
%plot data
i2Da=dat(:,1); i2Db=dat(:,2); psi2Da=dat(:,3); psi2Db=dat(:,4);
psi1a=dat(:,5); psi1b=dat(:,6); i1a=dat(:,7); i1b=dat(:,8);
t=dat(:,9); i1=sqrt(i1a.^2+i1b.^2);
plot(t,i1); grid; hold on
i2D=sqrt(i2Da.^2+i2Db.^2); plot(t,i2D,'r')
xlabel('t (s)')
ylabel('currents i_1, i_{2D} (A)')
legend('i_1', 'i_{2D}')
figure
psi1=sqrt(psi1a.^2+psi1b.^2); psi2D=sqrt(psi2Da.^2+psi2Db.^2);
plot(t,psi1,'b')
grid
hold on
plot(t,psi2D,'r')
xlabel('t (s)')
ylabel('flux-linkage \psi_1, \psi_{2D} (Wb)')
legend(' \psi_1', '\psi_{2D}')
```

6.4.5 Tutorial 5

This tutorial is concerned with a Caspoc implementation of the full transformer model with resistive load as represented by figure 6.12. The excitation and parameter set correspond to those given in the previous tutorial. Likewise, the results as shown in the Caspoc model (see figure 6.19) match those presented in figure 6.17 and figure 6.18.

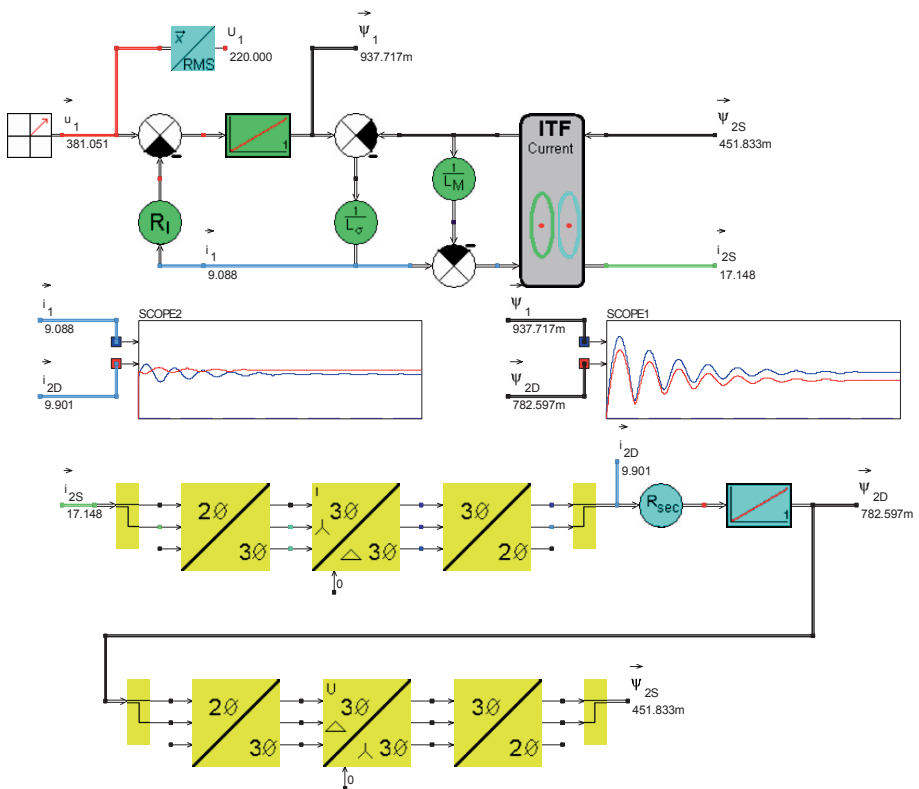


Figure 6.19. Caspoc simulation: transformer with resistive load

6.4.6 Tutorial 6

The aim of this tutorial is to undertake a phasor analysis, as discussed in section 6.3.2, to confirm the steady-state results obtained with the dynamic model discussed in the previous two tutorials. The phasor analysis is to be given in the form of an m-file. An example of an m-file which shows this analysis is given at the end of this tutorial. The results in the form of the variables $|i_1|$, $|i_{2D}|$, $|\psi_1|$ and $|\psi_{2D}|$ should match (within 1 %) with the steady-state results obtained from the dynamic simulation.

m-file Tutorial 6, chapter 6

```
%Tutorial 6, chapter 6
close all
%parameters
L_sig=10e-3; % leakage inductance
L_M=300e-3; % magnetizing inductance
R_1=10; % primary resistance
R_2=5; % secondary resistance
R_l=20; % load resistance
```

```
k=2;                                % winding ratio ITF
%phasor analysis
U=220;                               % RMS phase voltage
w=100*pi;                            % angular freq
u_1=U*sqrt(3);                       % phasor amplitude
X_sig=j*w*L_sig;                     % magnetizing reactance
X_M=j*w*L_M;                         % leakage reactance
Rt=R_2+R_1;                           % sum load resistance
Rtref=k^2*Rt/3;                      % delta load/3,star, and referred
Zp=Rtref*X_M/(Rtref+X_M);           % XM/Rtref
Z1=R_1+X_sig+Zp;                     % total prim. impedance
i_1ph=u_1/Z1;                         % primary current phasor
i_1=abs(i_1ph);                      % abs value primary current
e_1ph=u_1-i_1ph*R_1;                 % primary flux phasor
psi_1=abs(e_1ph);                     % abs value primary flux
e2rSph=u_1-i_1ph*(R_1+X_sig);       % phasor secondary side (star)
e2Sph=e2rSph/k;                      % secondary flux phasor(delta)
e2Dph=e2Sph*sqrt(3)*(cos(-gamma/4)+j*sin(-gamma/4));
psi_2Dph=e2Dph/(j*w);                % secondary flux phasor(delta)
psi_2D=abs(psi_2Dph);                % abs value secondary flux
i_2Dph=e2Dph/Rt;                     % secondary current phasor
i_2D=abs(i_2Dph);                   % abs value secondary current
```

Chapter 7

INTRODUCTION TO ELECTRICAL MACHINES

7.1 Introduction

This chapter considers the basic working principles of the so-called ‘classical’ set of machines. This set of machines represents the asynchronous (induction), synchronous, DC machines, and variable reluctance machines. The latter will be discussed in the book ‘Advanced Electrical Drives’ currently under development by the authors of this book. Of these classical machines, the asynchronous machine is most widely used in a large range of applications. Note that the term ‘machine’ is used here, which means that the unit is able to operate as a motor (converting electrical power into mechanical power) or as a generator (converting mechanical power into electrical power). The machine can be fed via a power electronic converter or connected directly to an AC or DC supply.

Central to this chapter is the development of an ‘ideal rotating transformer’, which is in fact a logical extension of the two-phase ITF module discussed in chapter 6. We will then look to the conditions required for producing constant torque in an electrical machine. This in turn will allow us to derive the principle of operation for the three classical machine types. A general model concept will be introduced at the end of this chapter which forms the backbone of the machine models discussed in this book.

7.2 Ideal Rotating Transformer (IRTF) concept

The fundamental building block for rotating machines used in this book is the IRTF module which is directly based on the work by A. Veltman [Veltman, 1994] which is directly derived from the two-phase space vector ITF concept given in figure 6.1. The new IRTF module, shown in figure 7.1, differs in two points. Firstly, the inner (secondary) part of the transformer is assumed to be able to

rotate freely with respect to the outer (primary) side. The airgap between the two components of this model remains infinitely small. Secondly, the number of ‘effective’ turns on the primary and secondary winding are assumed to be equal, i.e. $n_1 = n_2 = n$. Furthermore, the windings are (like the ITF) taken to be sinusoidally distributed (see appendix A). This implies that the winding representation as shown in figure 7.1 is only symbolical as it shows where the majority of conductors for each phase are located. In the future the primary and secondary will be referred to as the stator and rotor respectively. A second

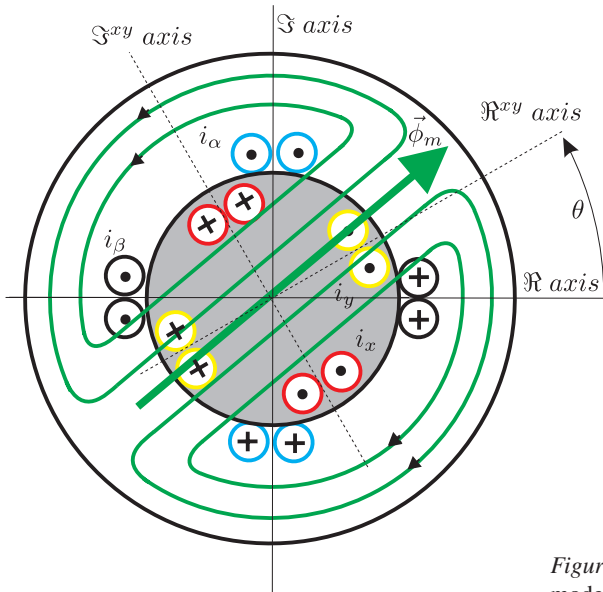


Figure 7.1. Two-phase IRTF model

complex plane (in addition to the stator based complex plane) with axis \Re^{xy} , \Im^{xy} is introduced in figure 7.1 which is tied to the rotor. Note the use of the superscript xy which indicates that a vector is represented in rotor coordinates. For a stationary coordinate system, as used on the stator side, we sometimes use the superscript $\alpha\beta$. However, in most cases this superscript is omitted to simplify the mathematical expressions. Hence, no superscript implies a stationary coordinate based vector.

The angle between the stationary and rotating complex plane is given as θ and this is in fact the machine shaft angle of rotation (relative to the stationary part of the motor). If the angle of rotation θ is set to zero then the IRTF module is reduced to the two-phase ITF concept (with $n_1 = n_2$) as given by figure 6.1. The symbolic representation of the IRTF module as given in figure 7.2 shows similarity with the ITF module (see figure 6.2(a)).

The IRTF is a three-port unit (stator circuit, rotor circuit and machine shaft). In figure 7.2 a symbolic shaft (shown in ‘red’) is introduced which is physically

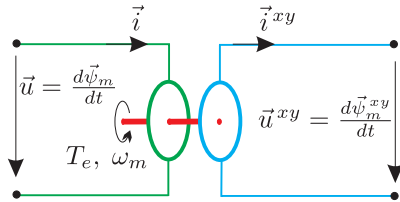


Figure 7.2. Symbolic IRTF representation

connected to the rotor circuit and appears via the stator circuit on the outside of the machine.

The flux linked with the stator and rotor is equal to $\vec{\psi}_m = n\vec{\phi}_m$ and can be expressed in terms of the components seen by each winding namely

$$\vec{\psi}_m = \psi_{m\alpha} + j\psi_{m\beta} \quad (7.1a)$$

$$\vec{\psi}_m^{xy} = \psi_{mx} + j\psi_{my} \quad (7.1b)$$

An illustration of the flux-linkage seen by the rotor and stator winding is given in figure 7.3(a). The relationship between the stator and rotor oriented flux-

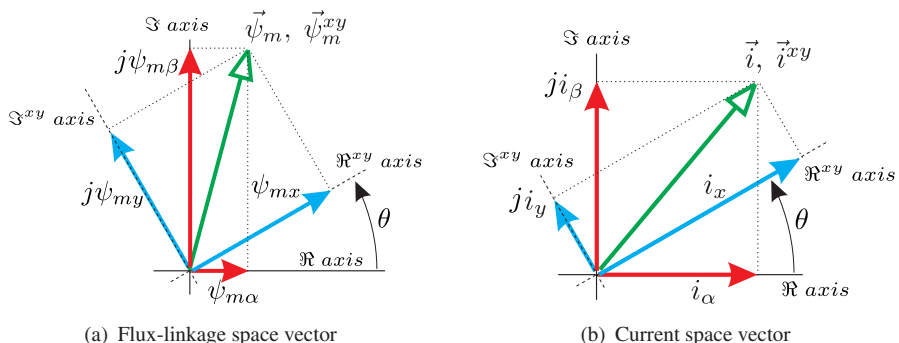


Figure 7.3. Flux-linkage and current space vector diagrams

linkage space vectors is given as

$$\vec{\psi}_m^{xy} = \vec{\psi}_m e^{-j\theta} \quad (7.2)$$

The relationship between the rotor and stator oriented current space vectors as shown in figure 7.3(b) can be written as

$$\vec{i} = \vec{i}^{xy} e^{j\theta} \quad (7.3)$$

Figure 7.3 emphasizes the fact that there is only one single flux-linkage and one current space vector present in the IRTF. The components of these vectors can be projected onto a rotating or stationary complex reference frame. The relationship between for example the variables i_α, i_β and i_x, i_y, θ of equation (7.3)

can also be written as

$$\begin{bmatrix} i_\alpha \\ i_\beta \end{bmatrix} = \begin{bmatrix} \cos \theta & -\sin \theta \\ \sin \theta & \cos \theta \end{bmatrix} \begin{bmatrix} i_x \\ i_y \end{bmatrix} \quad (7.4a)$$

The symbolic diagram of figure 7.2 can also be shown in terms of its space vector components as was done for the ITF case (see figure 6.3). The result, given in figure 7.4, shows that the rotor side of the IRTF now rotates *with* the rotor shaft given that it is physically attached to it. The energy balance for the

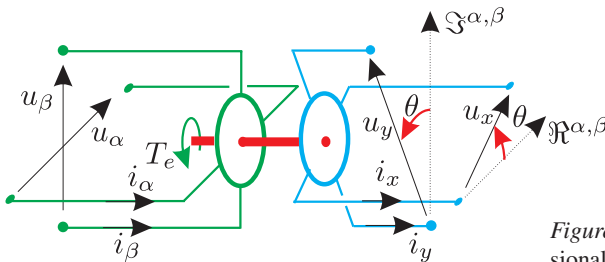


Figure 7.4. Three-dimensional IRTF representation

IRTF module is found by making use of the power expressions (5.30), (5.33) which are directly linked with the incremental energy $dW = pdt$. The input (stator) power p_{in} for the IRTF module is of the form

$$p_{in} = \Re \left\{ \vec{u} (\vec{i})^* \right\} \quad (7.5)$$

Note that \vec{u} and \vec{i} are taken to be time dependent complex numbers as indicated by equation (5.8) on page 123. Equation (7.5) can with the aid of $\vec{u} = \frac{d\vec{\psi}_m}{dt}$ be expressed in terms of the stator (input) incremental energy

$$dW_{in} = \Re \left\{ d\vec{\psi}_m (\vec{i})^* \right\} \quad (7.6)$$

Similar to the ITF, the IRTF is defined with a positive electrical and positive (rotor) electrical ‘power out’ convention (see figure 3.4). Unlike the ITF, the IRTF has a second output power component formed by the product of the shaft torque T_e (Nm) and shaft speed ω_m (rad/sec). If this product is positive the machine is said to operate as a motor. The total (mechanical plus electrical) output power is now of the form

$$p_{out} = \Re \left\{ \vec{u}^{xy} (\vec{i}^{xy})^* \right\} + T_e \omega_m \quad (7.7)$$

The incremental mechanical and electrical output energy linked with the rotor side of the IRTF can with the aid of $\vec{u}^{xy} = \frac{d\vec{\psi}_m^{xy}}{dt}$ be written as

$$dW_{out} = \Re \left\{ d\vec{\psi}_m^{xy} (\vec{i}^{xy})^* \right\} + T_e d\theta \quad (7.8)$$

The overall IRTF incremental energy balance can with the aid of equations (7.6) and (7.8) and use of the energy conservation law be written as

$$\Re \left\{ d\vec{\psi}_m (\vec{i})^* \right\} - \Re \left\{ d\vec{\psi}_m^{xy} (\vec{i}^{xy})^* \right\} = T_e d\theta \quad (7.9)$$

The left hand side of equation (7.9) shows the electrical incremental energy IRTF components. In equation (7.9), the term $d\vec{\psi}_m^{xy}$ may be developed further using equation (7.2) and the differential ‘chain rule’, which leads to

$$d\vec{\psi}_m^{xy} = e^{-j\theta} d\vec{\psi}_m - j\vec{\psi}_m e^{-j\theta} d\theta \quad (7.10)$$

Multiplication of equation (7.10) by the vector $(\vec{i}^{xy})^* = \vec{i}^* e^{j\theta}$ (see equation (7.3)) gives

$$d\vec{\psi}_m^{xy} (\vec{i}^{xy})^* = d\vec{\psi}_m \vec{i}^* - j\vec{\psi}_m \vec{i}^* d\theta \quad (7.11)$$

Substitution of equation (7.11) into equation (7.9) leads to the following expression for the electromechanical torque on the rotor.

$$T_e = \Re \left\{ j\vec{\psi}_m \vec{i}^* \right\} \quad (7.12)$$

Equation (7.12) can with the aid of expression $\Re \left\{ j\vec{a}\vec{b}^* \right\} = \Im \left\{ \vec{a}^*\vec{b} \right\}$ be rewritten as

$$T_e = \Im \left\{ \vec{\psi}_m^* \vec{i} \right\} \quad (7.13)$$

Hence, the torque acting on the rotor is at its maximum value in case the two vectors $\vec{\psi}_m, \vec{i}$ as shown in figure 7.3, are perpendicular with respect to each other. Under these circumstances the torque is directly related to the product of the rotor radius and the Lorentz force. The latter is proportional to the magnitudes of the flux and current vectors. The generic diagram of the IRTF module that corresponds to the symbolic representation shown in figure 7.2 is based on the use of equations (7.2), (7.3) and (7.13). The IRTF generic module as given in figure 7.5(a) is shown with a stator to rotor coordinate flux conversion module and rotor to stator current conversion module. The two coordinate conversion modules can also be reversed as shown in figure 7.5(b). The IRTF version used is application dependent as will become apparent at a later stage. The torque computation is not affected by the version used. Nor for that matter is the torque affected by the choice of coordinate system. The rotor angle θ required for the IRTF module must be derived from the mechanical equation-set of the machine which is of the form

$$T_e - T_l = J \frac{d\omega_m}{dt} \quad (7.14a)$$

$$\omega_m = \frac{d\theta}{dt} \quad (7.14b)$$

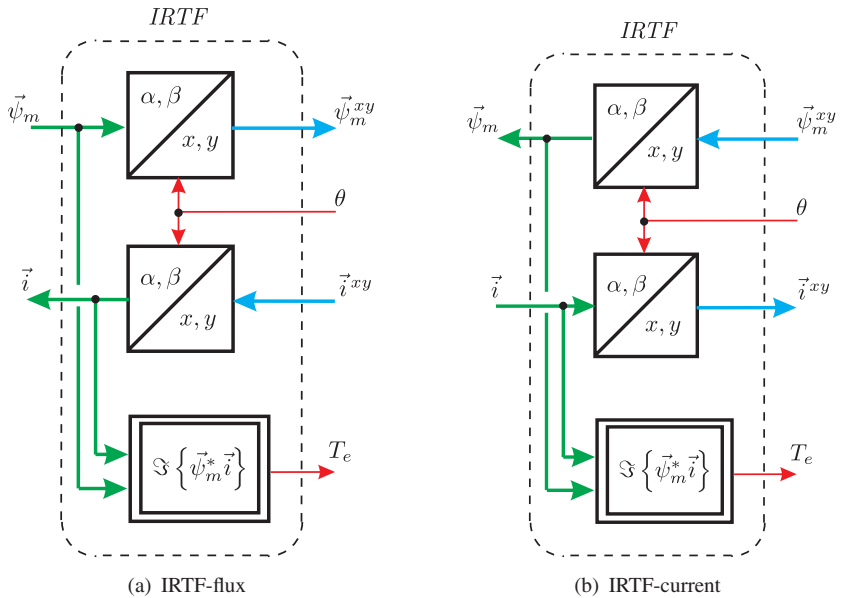


Figure 7.5. Generic representations of IRTF module

with T_l and J representing the load torque and inertia of the rotor/load combination respectively (as discussed in section 1.4.2). Finally, it is noted that the IRTF has a unity winding ratio, which implies that an inductance component (unlike a resistive component) may be moved from one side to the other without having to change its value.

7.2.1 IRTF example

The IRTF module forms the backbone to the electrical machine concepts presented in this book. Consequently, it is particularly important to fully understand this concept. In the example given here we will discuss how stator currents and torque can be produced in the event that stator windings are connected to a voltage source and the rotor windings to a current source as shown in figure 7.6. In the discussion to come we will make use of figure 7.1 in a stylized form for didactic reasons. Furthermore, we will assume that we can hold the motor shaft at any desired position. The voltage source shown in fig-

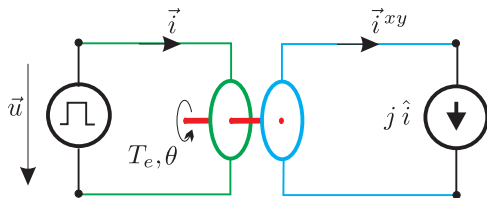


Figure 7.6. IRTF module connected to voltage and current source

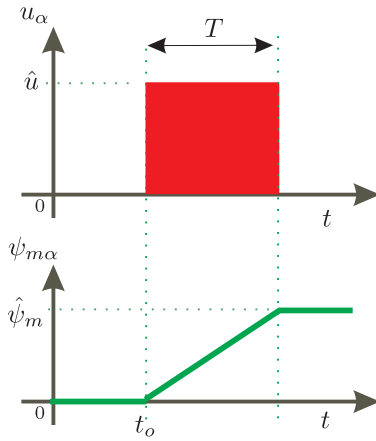


Figure 7.7. Voltage excitation and flux-linkage for the α winding

ure 7.6 delivers a pulse to the α winding at $t = t_o$ as shown in figure 7.7. The flux-linkage $\psi_{m\alpha}$ versus time waveform which corresponds with the applied pulse is also shown in figure 7.7. The β stator winding is short circuited with condition $\psi_{m\beta} = 0$. We will consider events after $t = t_o + T$ in which case a flux distribution will be present in the IRTF where the majority of the flux is concentrated along the $\Re^{\alpha,\beta}$ axis as shown in figure 7.8(a). Furthermore, the flux-linkage value will be equal to $\psi_{m\alpha} = \hat{\psi}_m$. The corresponding space vector representation will be of the form $\vec{\psi}_m = \hat{\psi}_m$.

We would like to realize a rotor excitation of the form $\vec{i}^{xy} = j\hat{i}$, which implies that the y rotor winding must carry a current $i_y = \hat{i}$. We have omitted for didactic reasons the x winding from figure 7.8 because this winding is not in use (open circuited). We will now examine the IRTF model and corresponding space vector diagrams for the excitation conditions indicated above and three rotor positions. For each case (rotor position) we will assume that the rotor is initially set to the required rotor position after which the stator and rotor excitation as discussed above is applied. The aim is to provide some understanding with respect to the currents which will occur on the stator side and the nature of torque production based on first principles. To assist us with this discussion two ‘contours’ namely x and y are introduced in figure 7.8 which are linked to the rotating complex plane. These contours are helpful in determining the currents which must appear on the stator side. If we assume that such a contour represents a flux tube then there would need to be a corresponding resultant MMF within the contour in case the latter would contain some form of magnetic reluctance. The magnetic reluctance of the IRTF model is zero (infinite permeability material and infinitely small airgap), hence the MMF ‘seen’ inside either contour must always be zero.

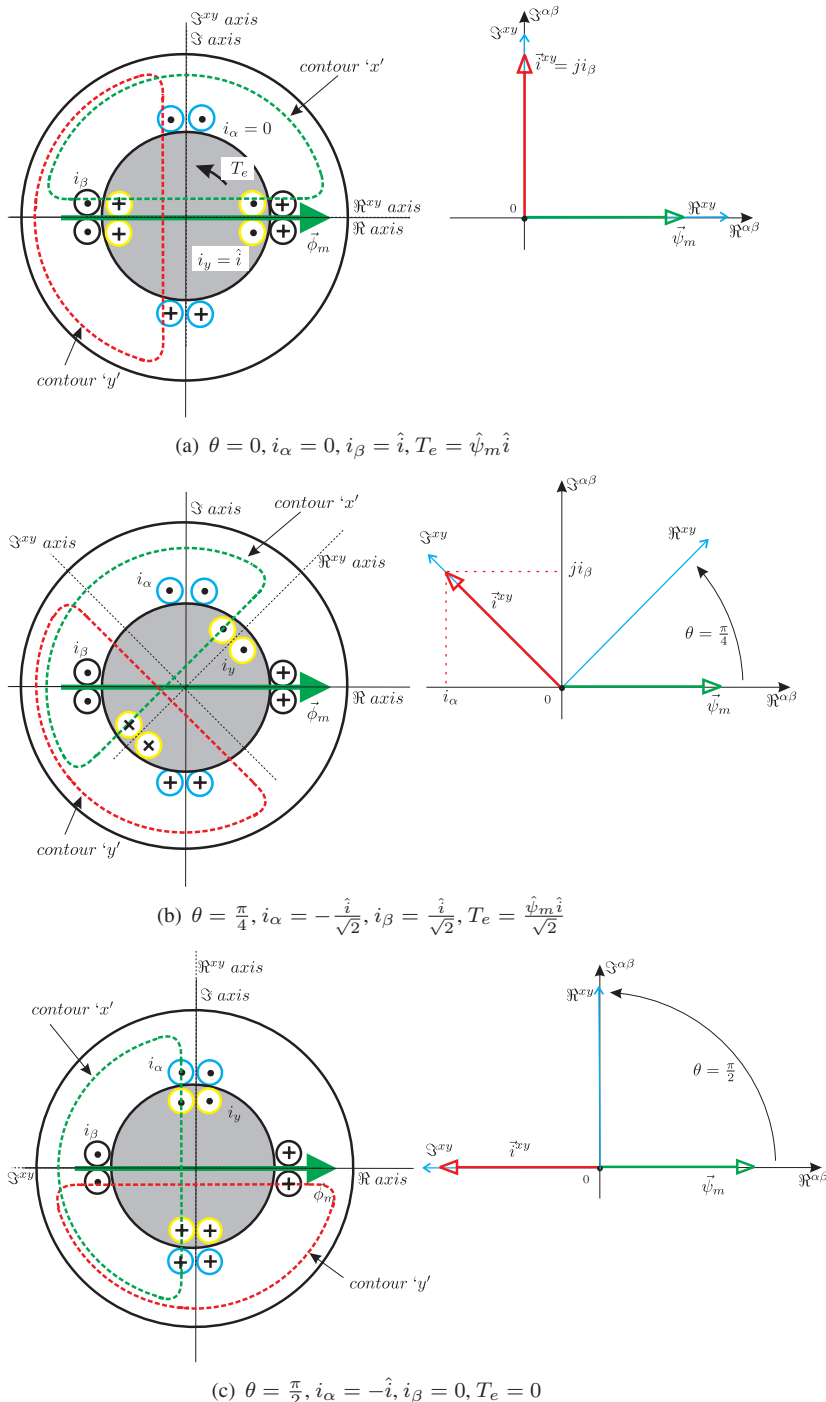


Figure 7.8. IRTF Symbolic model and space vector diagrams, for: $\theta = 0, \theta = \frac{\pi}{4}$ and $\theta = \frac{\pi}{2}$

- Rotor position $\theta = 0$: if we consider the x contour in figure 7.8(a), then it coincides with the flux distribution that exists in the model. The MMF seen by this contour is equal to ni_α . The excited rotor winding cannot contribute (given both halves are in the contour) to this contour. Hence, the current i_α must be zero. By observing the y contour and the MMF ‘seen’, we note the presence of the imposed rotor current $i_y = \hat{i}$. The number of winding turns on rotor and stator are equal, hence a stator current $i_\beta = \hat{i}$ (with the direction shown) must appear in the short-circuited β coil to ensure that the zero MMF condition with this contour is satisfied. The space vector representation of the current and flux as given in figure 7.8(a), shows that they are $\frac{\pi}{2}$ radian apart. Note (again) that there is *only one* set of space vectors and their components may be projected onto either the rotor or stator complex plane. The torque according to equation (7.13) will under these circumstances (with the current vector leading the flux vector) equal to $T_e = \hat{\psi}_m \hat{i}$. From first principles (see figure 1.9) we note that forces will be exerted on the rotor winding in case the latter carries a current and is exposed to a magnetic field. In this case the flux and flux density distributions are at their highest level along the α axis (see appendix A). The y winding carries a current in the direction shown and this will cause a force on the individual conductors of the y rotor winding and thus a corresponding torque in the anti-clockwise (positive) direction.
- Rotor position $\theta = \frac{\pi}{4}$: if we consider the x contour in figure 7.8(b), then we note that a MMF due to the α winding would be less than ni_α . The reason for this is that the contour also encloses part of α winding which gives a negative MMF contribution to the total MMF. The resultant MMF is found by integrating equation (A.9) over the angle range $\pi/4 \rightarrow \pi, -\pi \rightarrow -3\pi/4$ and comparing the outcome of this integral with the integral over the range $0 \rightarrow \pi$. This analysis will show that the MMF is reduced by a factor $1/\sqrt{2}$ (when compared to the previous case) hence the resultant MMF of the α winding is equal to $ni_\alpha/\sqrt{2}$. The same x contour also encloses part of the β winding and its MMF contribution is equal to $ni_\beta/\sqrt{2}$. There are no other contributions, hence the sum of these two MMF’s is of the form $ni_\alpha/\sqrt{2} + ni_\beta/\sqrt{2} = 0$ because the MMF in the contour must be zero. From this analysis it follows that, for the given angle, the currents must be in opposition, i.e. $i_\alpha = -i_\beta$. If we now consider the MMF enclosed by the y contour we note that the α will contribute a MMF component $-ni_\alpha/\sqrt{2}$ (now negative because the other side of this winding), while the β will contribute a component $ni_\beta/\sqrt{2}$. Furthermore, the y winding will add a component $n\hat{i}$. The resultant MMF (the sum of these three contributions), gives together with the condition $i_\alpha = -i_\beta$, the required stator currents $i_\alpha = -\hat{i}/\sqrt{2}, i_\beta = \hat{i}/\sqrt{2}$ respectively. The space vector representation shown in

figure 7.8(b) confirms the presence of the two current components. Note also that the angle between the current and flux vectors is equal to $\frac{3\pi}{4}$ radian. The torque according to equation (7.13) will under these circumstances be equal to $T_e = \hat{\psi}_m \hat{i} / \sqrt{2}$. The torque must be less (than the previous case) because a number of the conductors of the y winding now ‘see’ a flux density value which is in opposition to that seen by the majority of the conductors.

- Rotor position $\theta = \frac{\pi}{2}$: if we consider the x contour in figure 7.8(c), then we can conclude that the current i_β must be zero (the other winding cannot contribute, given both halves are in the contour). The reason for this is that the MMF seen by this contour must be zero. By observing the y contour and the MMF ‘seen’ by this contour we note the presence of the rotor current $i_y = \hat{i}$. The number of winding turns on rotor and stator are equal, hence a stator current $i_\alpha = -\hat{i}$ must appear to ensure that the zero MMF condition with this contour is satisfied. The space vector representation of the current and flux as given in figure 7.8(c) shows that they are π radian apart. The torque according to equation (7.13) will under these circumstances be equal to $T_e = 0$. From first principles we note that half the conductors of the y winding will experience a force in opposition to the other half, hence the net torque will be zero.

7.3 Conditions required to realize constant torque

The ability of a machine to produce a torque which has a non-zero average component is of fundamental importance. In this section we will consider the conditions under which electrical machines are able to produce a constant (time independent) torque. For this analysis it is sufficient to re-consider the model according to figure 7.6. The rotor is again connected to a current source which in this case is assumed to be of the form $\hat{i} e^{j(\omega_r t + \rho_r)}$, where ω_r represents the angular velocity of this vector *relative* to the rotor of the IRTF. The ITF current \vec{i}^{xy} is therefore of the form

$$\vec{i}^{xy} = \hat{i} e^{j(\omega_r t + \rho_r)} \quad (7.15)$$

The stator is connected to a three-phase sinusoidal voltage source such that the voltage vector is taken to rotate at a constant angular velocity ω_s . The corresponding flux vector $\vec{\psi}_m$ can then be found using $\vec{u} = \frac{d\vec{\psi}_m}{dt}$ which will in general terms result in a rotating flux vector of the form

$$\vec{\psi}_m = \hat{\psi}_m e^{j\omega_s t} \quad (7.16)$$

The rotor angle θ is a function of rotor speed ω_m and load angle ρ_m and is (for constant speed operation) defined as

$$\theta = \omega_m t + \rho_m \quad (7.17)$$

The importance of the angle variable ρ_m will be discussed at a later stage. The

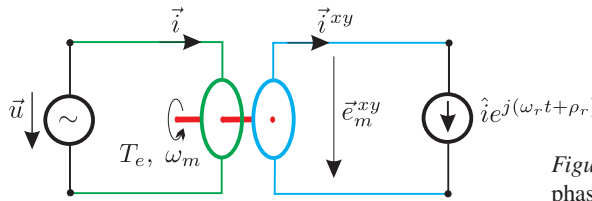


Figure 7.9. Simplified two-phase, machine model

induced voltage on the rotor side in figure 7.9 is in this case $\vec{e}_m^{xy} = \frac{d\vec{\psi}_m^{xy}}{dt}$, which with the aid of equations (7.16), (7.2) and (7.17) may also be written as

$$\vec{e}_m^{xy} = \frac{d\vec{\psi}_m^{xy}}{dt} = e^{j((\omega_s - \omega_m)t - \rho_m)} \frac{d\hat{\psi}_m}{dt} + j(\omega_s - \omega_m) \vec{\psi}_m^{xy} \quad (7.18)$$

in which the term $\frac{d\hat{\psi}_m}{dt}$ is taken to be zero given that a quasi-steady-state operation is assumed, i.e. we assume that the flux amplitude $\hat{\psi}_m$ is constant. On the basis of this assumption equation (7.18) reduces to

$$\vec{e}_m^{xy} = j(\omega_s - \omega_m) \vec{\psi}_m^{xy} \quad (7.19)$$

The torque produced by this machine is found using equation (7.13). Further mathematical handling of this torque equation and use of equations (7.16) (in rotor coordinates), (7.2) and (7.17) leads to

$$T_e = \Im \left\{ \hat{\psi}_m \hat{i} e^{j((\omega_r + \omega_m - \omega_s)t + \rho_r + \rho_m)} \right\} \quad (7.20)$$

where it is emphasized that the angle variables ρ_r , ρ_m shown in equation (7.20) are not a function of time. Equation (7.20) is of prime importance as it shows that a time independent torque value is obtained in case the following speed condition is met

$$\omega_s = \omega_m + \omega_r \quad (7.21)$$

If the speed condition, according to equation (7.21) is satisfied, then the torque expression is reduced to

$$T_e = \hat{\psi}_m \hat{i} \sin(\rho_r + \rho_m) \quad (7.22)$$

Equations (7.21), (7.22) and (7.19) are useful in terms of explaining the basic classical machine concepts as will be done in the next three chapters. Prior to considering how these expressions are applied for the three types of machines it is instructive to look at the vector diagram given in figure 7.10 which corresponds to machine configurations discussed in this section. The diagram shows

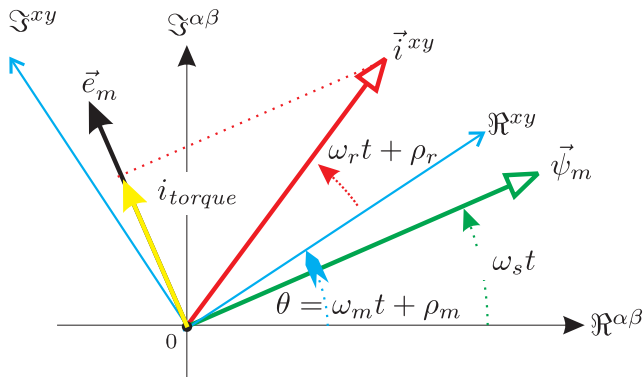


Figure 7.10. Space vector diagram for machine model

the stationary complex plane ($\Re^{\alpha\beta}$, $\Im^{\alpha\beta}$) and the rotating (with constant rotor speed ω_m) rotor coordinate frame which is displaced by an angle $\theta = \omega_m t + \rho_m$ with respect to the former. Also shown in the diagram is the rotating (with angular speed ω_s) flux vector $\vec{\psi}_m$, which is caused by the presence of the three-phase voltage supply connected to the stator. Finally, the current vector \vec{i}^{xy} is shown which rotates at an angular speed ω_r *relative to the rotating reference frame*. This means that this vector rotates at a speed $\omega_r + \omega_m$ relative to the stator based (stationary) reference frame.

In the example shown, the current vector leads (we assume positive direction as anti-clockwise) the flux vector. This combination of the two vectors corresponds to a positive torque condition as will be shown below. A time independent torque will be realized if the angle between the current and flux vectors remains constant. This is the case when condition (7.21) is met. Furthermore, we also assume that the magnitude of the two vectors is constant. If condition (7.21) is met, the angle between the two vectors is equal to the sum of ρ_m and ρ_r . In the example shown, the sum of these two angles is taken to be positive, which according to equation (7.22) gives a positive torque, i.e. the machine acts as a motor. The induced voltage vector \vec{e}_m (written here in stator coordinates) is orthogonal to the flux vector. The projection of the current vector on this voltage vector shown as $i_{torque} = \hat{i} \sin(\rho_r + \rho_m)$ (see figure 7.10), is according to equation (7.22) proportional to the torque, provided the condition as given by equation (7.21) is met. The largest motor torque value, equal to $\hat{T}_e = \hat{\psi}_m \hat{i}$, which can be delivered is realized when the rotor current vector leads the flux vector by $\frac{\pi}{2}$ rad, in phase with the voltage $\frac{d\psi_m}{dt}$. We will use this diagram again in the next three chapters in different forms consistent with the three main types of machines in use today. A tutorial at the end of this chapter is given to reinforce the concepts discussed in this section.

7.3.1 IRTF extension to ‘multi-pole’ representation

Up to now we have considered magnetic structures which have two magnetic poles, like for example the bar magnet given in figure 1.10(a). The flux distribution (shown symbolically) of such a magnet is very similar to that shown in figure 7.11(a) which is in fact a simplified version of figure 7.1, given that the rotor windings are not shown for didactic reasons. These rotor windings are however essential to the correct functioning of the IRTF, i.e. to balance the currents as discussed in section 7.2.1. The model according to figure 7.11(a) has two magnetic poles or one pole-pair ($p=1$). Most electrical machines tend to have more than one pole-pair given that a more efficient winding configuration can be realized in for example a four-pole ($p = 2$) machine. The flux distribution which will occur in a four-pole machine is shown (symbolically) in figure 7.11(b). The corresponding four-pole (sinusoidally distributed) phase

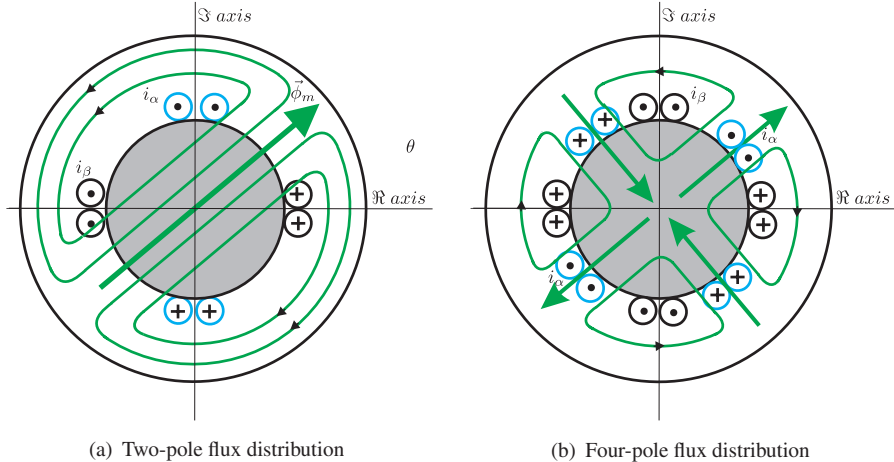


Figure 7.11. Two and four-pole flux distributions

windings shown symbolically in figure 7.11(b) are markedly different when compared to the two-pole case. In the latter case the majority of α windings are located on the imaginary axis. Furthermore, the angle between the phase winding halves is equal to π rad (see figure 7.11(a)). In addition, the two phase windings are mechanically displaced by an angle of $\frac{\pi}{2}$ rad (90°). In the four-pole case the angle between phase winding halves is reduced to $\frac{\pi}{4}$ rad. In addition, each phase winding now has the majority of its sinusoidally distributed windings at four locations as shown in figure 7.11(b). Furthermore, the two phase windings are now mechanically displaced (with respect to each other) by an angle of $\frac{\pi}{4}$ rad.

This change in winding configuration has important implications for the so-called rotational speed (see appendix A for more details on this concept). For

example, in the two-pole machine we can rotate the resultant magnetic field by an angle of $\frac{\pi}{2}$ radians by way of a voltage excitation sequence of the two stator windings over a given time. When we apply the same excitation sequence to the four-pole machine, a magnetic field rotation of $\frac{\pi}{4}$ radians would occur. Vice versa if we move from a multi-pole to a two-pole model we need to double (when starting from a four-pole model) the rotor angle. The process of modelling the behaviour of a multi-pole machine with a two-pole IRTF model can thus be initiated by introducing (as a first step) a ‘gain’ module with gain p to the rotor angle input side of the IRTF model.

The torque per ampère produced by the multi-pole machine will increase when a larger number of pole pairs is used. A qualitative explanation of this statement is as follows: in the two-pole machine as shown in fig 7.11(a) a set of current carrying conductors is positioned along the circumference where the flux is at its highest level. This in turn causes a force on these conductors and consequently a torque on the rotor. In the four-pole model as shown in figure 7.11(b), there are four high flux concentration areas (magnetic poles), which implies that we can double the number of current carrying conductors (with half the cross-sectional area, given that the total available area for the windings remains unchanged) hence the torque produced per ampère on the rotor will be *doubled* when compared to the two-pole case. This leads to the important conclusion that a (second) gain module, with gain p , must be added to the torque output of a two-pole generic IRTF model. Note that changing the number of poles does not affect the rated torque of the machine, given that the latter is constrained by the rotor-volume, as was discussed in section 1.7 on

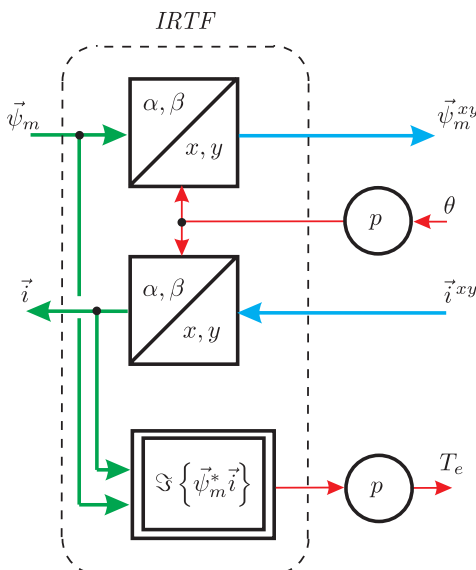


Figure 7.12. Use of IRTF module for multi-pole pair models

page 22. Figure 7.12 shows the two additional gain modules which must be added to the IRTF module (figure 7.5(a)), in order to use the IRTF concept for multi-pole models.

7.4 General machine model

In this section we will consider the two-phase machine model which has two n_s turn stator windings and two n_r turn rotor windings. The motor concept as shown in figure 7.13 is very similar to the two-phase ITF based transformer with finite airgap (see figure 6.1) in case the rotor angle is set to zero. This ITF configuration was used to arrive at the two-inductance ITF based symbolic transformer model with leakage and magnetizing inductance as indicated in figure 6.10. Note that figure 6.10 also shows the primary and secondary coil resistances. The extension to a rotating rotor, i.e. with variable θ calls for the introduction of the two-phase IRTF module as discussed in the previous section.

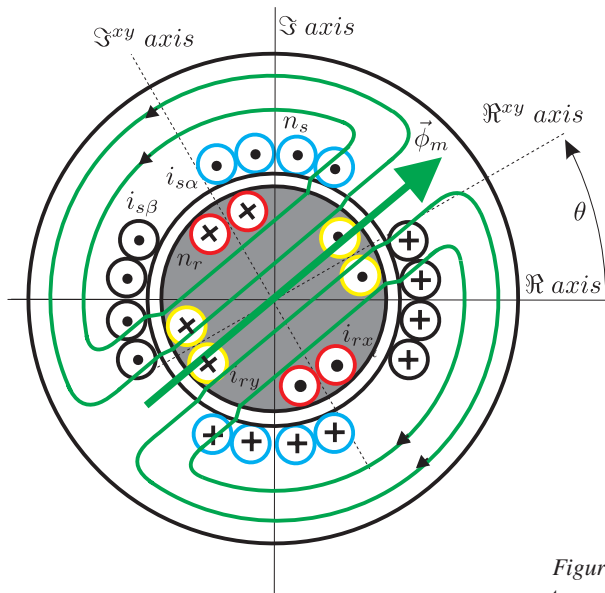


Figure 7.13. Generalized two-phase machine model

The resultant two-inductance model (with zero coil resistance at this stage) of the generalized machine is given in figure 7.14. The parameters shown in figure 7.14 are found using equation (7.23).

$$k^r = \kappa \sqrt{\frac{L_s}{L_r}} \quad (7.23a)$$

$$L_M = \kappa^2 L_s \quad (7.23b)$$

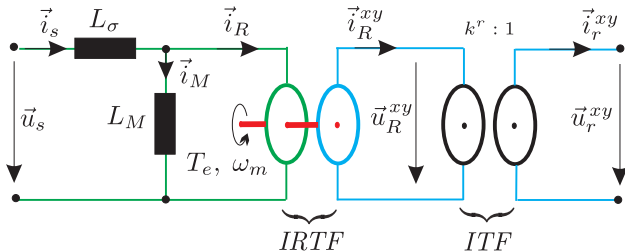


Figure 7.14. Symbolic generalized two-phase, IRTF/ITF machine model

$$L_\sigma = L_s (1 - \kappa^2) \quad (7.23c)$$

with

$$\begin{aligned} L_r &= L_{\sigma r} + \left(\frac{n_r}{n_s} \right)^2 L_m \\ L_s &= L_{\sigma s} + L_m \end{aligned}$$

where κ is given by equation 3.20 which leads to

$$\kappa = \sqrt{1 - \frac{L_{\text{stator short-circuit}}}{L_{\text{stator open-circuit}}}} \quad (7.25)$$

with

$$\begin{aligned} L_{\text{open-circuit}}^{\text{stator}} &= L_s \\ L_{\text{short-circuit}}^{\text{stator}} &= L_{\sigma s} + \frac{L_m L'_{\sigma r}}{L_m + L'_{\sigma r}} \end{aligned}$$

where $L'_{\sigma r} = \left(\frac{n_s}{n_r} \right)^2 L_{\sigma r}$.

The equation set (7.23) and equation (7.25) follow directly from the ITF based equation set (3.23) and equation (3.20) where primary and secondary parameters are replaced by stator and rotor based quantities. The extension of the model to include stator and rotor resistance is similar to the ITF module. At this point, the rotor resistance R_R is introduced, which is the rotor resistance R_r as referred to the primary side of the ITF, i.e. between the IRTF and ITF modules (see figure 7.14). The value of R_R is equal to

$$R_R = (k^r)^2 R_r \quad (7.27)$$

where R_r represents the actual rotor resistance. For machine analysis it is often sufficient to consider the IRTF module with referred rotor variables \vec{u}_R^{xy} , \vec{i}_R^{xy}

which implies that the ITF module is omitted. For those cases where the rotor is connected to an external source it is important to include the ITF module.

The resultant four parameter model as indicated in figure 7.15 (two resistance values and two inductance values) forms the basic concept which will be used in the following chapters to examine with the aid of simulation models a range of classic motor configurations as they exist today. Given the importance of this model it is instructive to summarize the underlying considerations namely:

- Linear magnetic material stator/rotor
- No magnetic losses
- Sinusoidal distributed windings
- Two-pole motor
- Four parameter model: rotor parameter referred

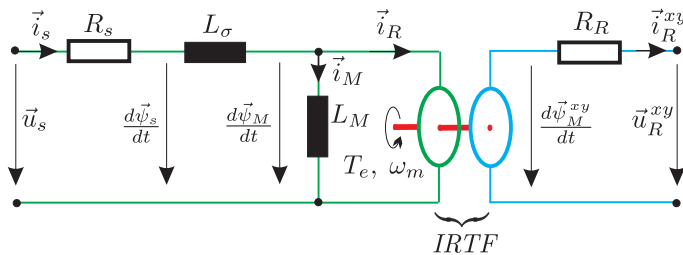


Figure 7.15. Symbolic generalized two-phase, four parameter machine model

The corresponding equation set for the model according to figure 7.15 is of the form

$$\vec{u}_s = \vec{i}_s R_s + \frac{d\vec{\psi}_s}{dt} \quad (7.28a)$$

$$\vec{\psi}_s = \vec{\psi}_M + \vec{i}_s L_\sigma \quad (7.28b)$$

$$\frac{\vec{\psi}_M}{L_M} = \vec{i}_s - \vec{i}_R \quad (7.28c)$$

$$\vec{u}_R^{xy} = -\vec{i}_R^{xy} R_R + \frac{d\vec{\psi}_M^{xy}}{dt} \quad (7.28d)$$

$$\vec{i}_R = \vec{i}_R^{xy} e^{j\theta} \quad (7.28e)$$

$$\vec{\psi}_M^{xy} = \vec{\psi}_M e^{-j\theta} \quad (7.28f)$$

$$T_e = \Im \left\{ \vec{\psi}_M^* \vec{i}_R \right\} \quad (7.28g)$$

It is noted that the magnetizing inductance L_M can be placed to either side of the IRTF. If L_M is placed on the rotor side, the IRTF module will calculate the torque with the aid of vectors $\vec{\psi}_M, \vec{i}_s$ which gives

$$T_e = \Im \left\{ \vec{\psi}_M^* \vec{i}_s \right\} \quad (7.29)$$

This expression is found upon substitution of equation (7.28c) into (7.28g).

The complete set of equations in (7.28) can for the purpose of numerical simulation be rewritten in the following form:

$$\vec{\psi}_s = \int \left(\vec{u}_s - \vec{i}_s R_s \right) dt \quad (7.30a)$$

$$\vec{\psi}_M^{xy} = \int \left(\vec{u}_R^{xy} + \vec{i}_R^{xy} R_R \right) dt \quad (7.30b)$$

$$\vec{\psi}_M = \vec{\psi}_M^{xy} e^{j\theta} \quad (7.30c)$$

$$\vec{i}_s = \frac{\vec{\psi}_s - \vec{\psi}_M}{L_\sigma} \quad (7.30d)$$

$$\vec{i}_R = \vec{i}_s - \frac{\vec{\psi}_s}{L_M} \quad (7.30e)$$

$$\vec{i}_R^{xy} = \vec{i}_R e^{-j\theta} \quad (7.30f)$$

7.5 Tutorials for Chapter 7

7.5.1 Tutorial 1

This tutorial is aimed at providing a better understanding of the IRTF module. As a first step a Simulink model of the IRTF module must be built. The Simulink implementation follows the generic version given in figure 7.5(a). An example of possible implementation is given in figure 7.16, where the IRTF sub-module ‘x/y → alpha/beta’ performs the conversion $\vec{i} = \vec{i}^{xy} e^{j\theta}$. A Simulink implementation of this module is given in figure 7.17. As a first step, build this module and derive the equation set required for the ‘fcn’ functions. The conversion $\vec{\psi}_m^{xy} = \vec{\psi}_m e^{-j\theta}$ is carried out with the module developed above. However, an additional gain module with gain -1 must be introduced. Finally, the torque produced by the machine is given as $T_e = \Im \left\{ \vec{\psi}_m^* \vec{i} \right\}$, which requires the use of the vector components $\psi_{m\alpha}, \psi_{m\beta}, i_\alpha, i_\beta$. Further development of the torque equation leads to an expression which can be used in a ‘fcn’ module to generate the torque. Build all three modules for the IRTF module and place the entire system into a single ‘IRTF’ sub-module as shown in figure 7.16.

In the second part of this tutorial a numerical implementation of the example as discussed in section 7.2.1 is considered. The simulation, as given in figure 7.18, shows the IRTF module developed in the first part of this tutorial. The flux vector which is the input on the stator side is of the form $\vec{\psi}_m = 1.25 \text{Wb}$,

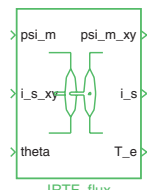
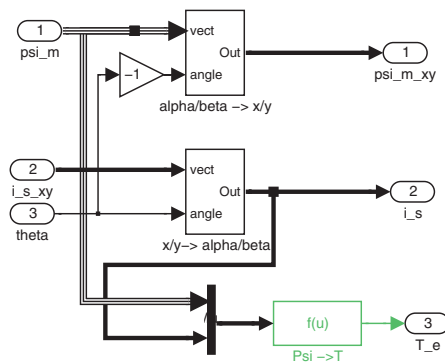


Figure 7.16. Simulink model of IRTF module

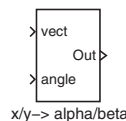
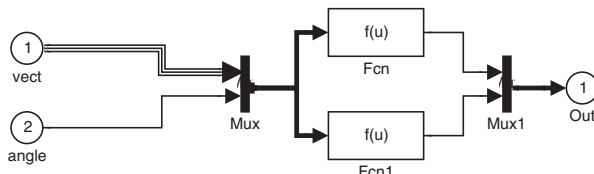


Figure 7.17. Simulink model of IRTF conversion module

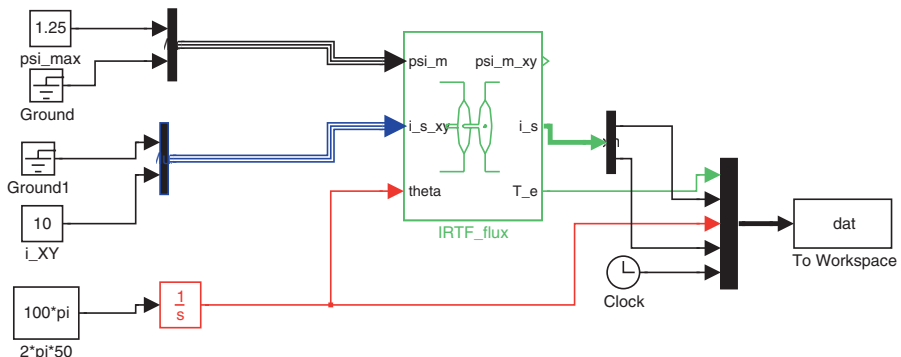


Figure 7.18. Simulink model of IRTF Simulation

this is a scalar, i.e. no imaginary component. The rotor side is connected to a current source (as shown in figure 7.6) and we assume that the vector is equal to $\vec{i}^{xy} = j10A$, i.e. imaginary component only. The rotor angle is provided via an integrator which in turn has as input the angular frequency $2\pi 50$ rad/sec, hence if we run the simulation for 20ms the rotor will have moved one full rotation. For this reason we will set the ‘run time’ for our simulation to 20ms. Furthermore, in the dialog box ‘simulation parameters’, set the solver type to ‘fixed step’, ‘ode4’.

To observe the result we will use the MATLAB Workspace and the data in the form of an array named ‘dat’ will be generated when the simulation is run. Input to the ‘dat’ module are the stator currents (both components), the time, rotor angle and of course the torque. A set of MATLAB commands needs to be given to display the data. Below an example of such a file.

m-file Tutorial 1, chapter 7

```
%Tutorial 1, chapter 7
close all;
plot(dat(:,3),dat(:,2),'r'); % i_alpha as function of rotor angle
grid; % puts grid in place
hold on; % allows to add more plots in one figure
plot(dat(:,3),dat(:,4),'g'); % i_beta as function of rotor angle
plot(dat(:,3),dat(:,1),'b'); % torque as function of rotor angle
axis([ 0 2*pi -15 15]); % redefines axis for figure
xlabel('rotor angle radian');
ylabel('stator current and torque')
legend('i_{\alpha}', 'i_{\beta}', 'Torque');
```

Examine the results produced carefully to determine if the IRTF module is working correctly. To assist you with this task it is helpful to look carefully at the example given in section 7.2.1.

The output produced after running your simulation and m-file should look like those given in figure 7.19.

7.5.2 Tutorial 2

This tutorial considers a Caspoc simulation implementation of the previous tutorial. The simulation as shown in figure 7.20 is a direct generic implementation of the symbolic model given in figure 7.6. The results are shown with the aid of ‘scope’ units and numerical values. The latter are shown underneath the variables. It is noted that the scalar variable which is linked to a vector \vec{x} is in fact the amplitude, i.e. $|\vec{x}|$. Furthermore, the values displayed in the simulation model are the values which appear at that point in time when the simulation is stopped.

The variables and corresponding colour code as shown on the scope modules are given in table 7.1. In this simulation the scope variables are chosen to be

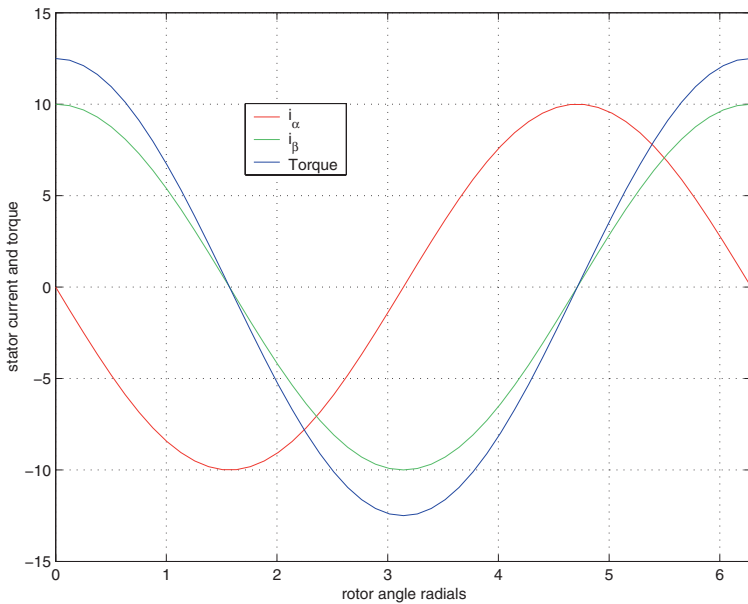


Figure 7.19. Simulink results of IRTF simulation

a function of time, where the duration of the simulation is set to coincide with one period of shaft rotation (20ms in this example). The results as given in

Table 7.1. Scope variables

Scope number	color	Variables
Scope 1	blue red green	T_e i_α i_β
Scope 2	blue red	ψ_{mx} ψ_{my}

scope 1 are directly comparable to those given in figure 7.19. The difference being (as discussed above) that in the latter case the variables are shown with respect to the rotor angle.

7.5.3 Tutorial 3

The IRTF example discussed in tutorial 1 is modified to explore how a constant (time independent) torque value can be obtained (see section 7.3). The revised Simulink model as given in figure 7.21, shows the IRTF-flux module with inputs $\vec{\psi}_m = \hat{\psi}_m e^{j\omega_s t}$, $\vec{i}^{xy} = \hat{i} e^{j(\omega_r + \rho_r)}$. The simulation model is directly

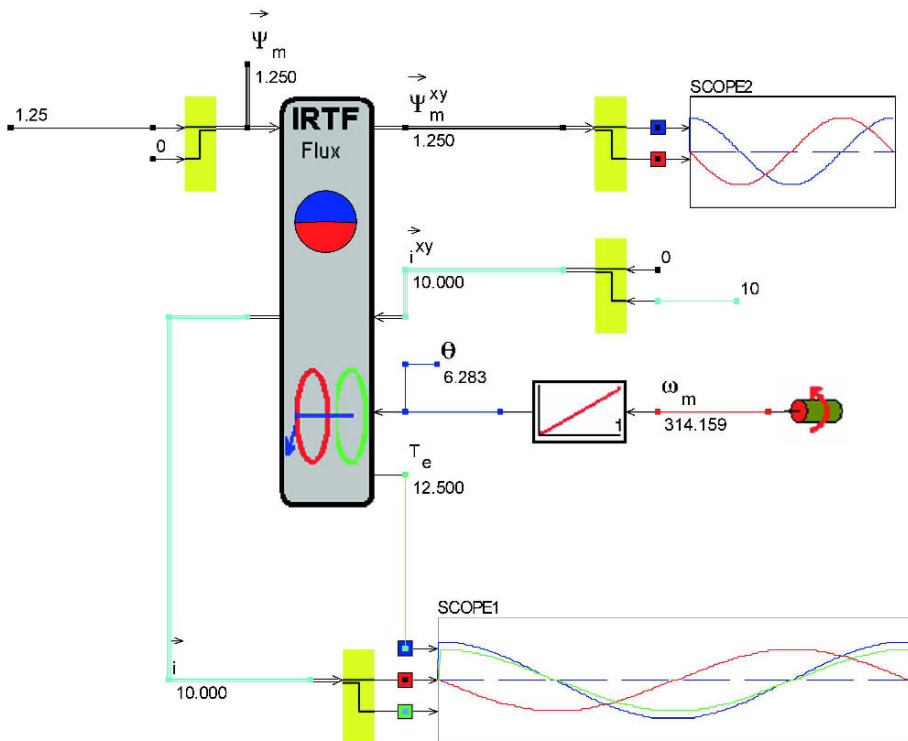


Figure 7.20. Caspoc simulation: IRTF model verification

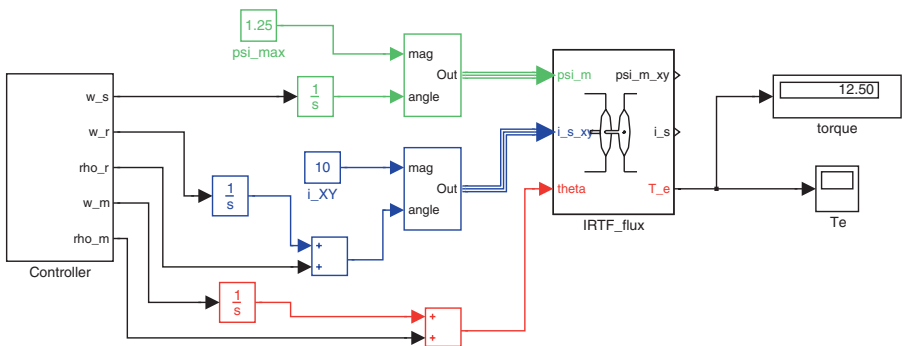


Figure 7.21. Simulink model: speed condition model

based on the symbolic model given in figure 7.21 with the important change that the voltage source is replaced with a ‘flux’ source $\vec{\psi}_m$.

The amplitudes for the flux and current vectors are arbitrarily set to $\hat{\psi}_m = 1.25\text{Wb}$ and $\hat{i} = 10\text{A}$ respectively, which results in a peak torque value of

$\hat{T}_e = 12.5\text{Nm}$. The generation of the flux vector for the IRTF module is realized with the aid of a polar to cartesian conversion module, as shown in figure 6.6. A similar approach is also used for the generation of the current vector \vec{i}^{xy} with the minor change that a phase angle input ρ_r must be added as shown in figure 7.21.

The ‘controller’ module sets the variables ω_s , ω_m , ω_r (rad/s) and angles ρ_r , ρ_m (rad) for the simulation. The controller inputs are taken to the rotational speed (rpm) variables n_s , n_m , n_r (rpm) which correspond to the angular frequencies given above. The controller multiplies these variables with a factor $2\pi/60$. In addition, the user must set values for the angles ρ_r , ρ_m (rad). As with the previous tutorial the shaft angle, speed and load angle are defined by the user and taken to be of the form $\theta = \omega_m t + \rho_m$. The torque T_e produced by the machine (IRTF module) is examined using a ‘scope’ and ‘display’ module.

The ‘scope’ module is used to verify that the torque is indeed time independent, while the display module is added to show directly the torque as a numerical value.

The aim is to choose the controller variables in such a manner as to ensure that the machine delivers a constant torque level equal to the maximum value of 12.5Nm.

Four cases are considered which reflect the basic operation of electrical machines. Run your simulation for a ‘run’ time of 1s and time step of 10^{-4}s , using the ode4 solver. Note that controller variables must be chosen in accordance with equations (7.21) and (7.22). In the latter case the sum of the two angles ρ_r , ρ_m (rad) must be equal to $\pi/2$ rad because the aim is to set the output torque to its maximum value, i.e. $T_e = \hat{T}_e$. Observe the output of your simulation for the following cases:

Table 7.2. Case studies

machine type	n_s (rpm)	n_m (rpm)	n_r (rpm)	ρ_r (rad)	ρ_m (rad)
Synchronous	3000	3000	0	π	$-\pi/2$
Asynchronous	3000	2000	1000	$\pi/2$	0
DC brush	0	3000	-3000	$\pi/2$	0
DC brushless	3000	3000	0	$\pi/2$	0

7.5.4 Tutorial 4

This tutorial considers a Caspoc implementation of the previous Simulink based tutorial. The Caspoc simulation model as shown in figure 7.22 contains a set of ‘UPDOWN’ modules which enable the user to alter the variables ω_s , ω_m , ω_r and ρ_m , ρ_r . Changing these variables allows the user to verify the conditions

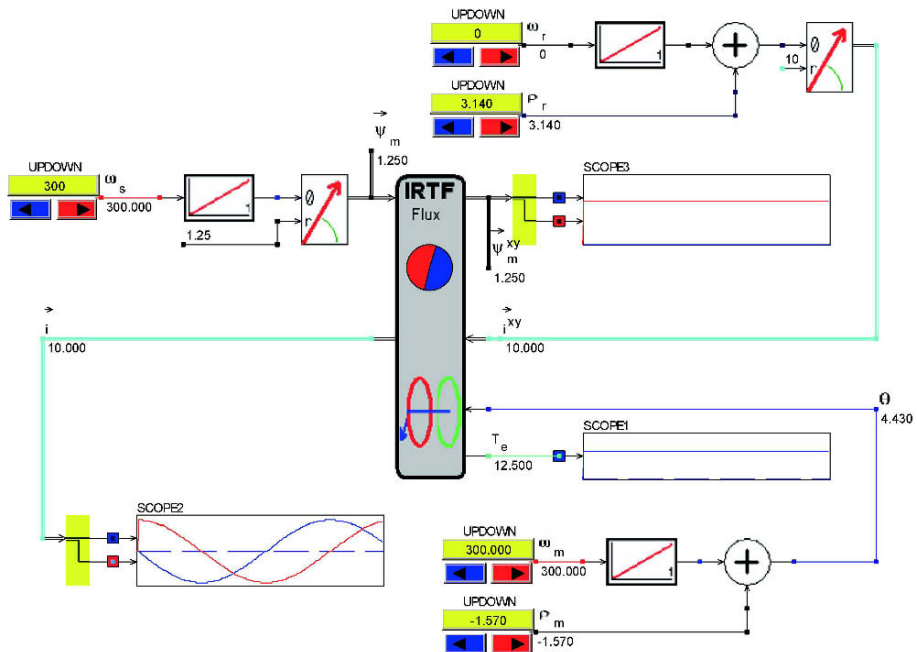


Figure 7.22. Caspoc simulation: IRTF model, speed condition verification

under which a constant torque output from the IRTF can be achieved. The rotational frequencies values are slightly different (for the sake of convenience) when compared to the Simulink based example. The Caspoc simulation can be set up for multiple simulations, which implies that the simulation is restarted after the selected simulation period (20ms in this example) has been reached. The ‘scope’ modules shown in figure 7.22 are tied to a set of variables as listed in table 7.3.

Table 7.3. Scope variables

Scope number	color	Variables
Scope 1	blue	T_e
Scope 2	blue	i_α
	red	i_β
Scope 3	blue	ψ_{mx}
	red	ψ_{my}

The example shown in figure 7.22 corresponds to the ‘synchronous machine’ example as given in table 7.2, with the difference that the rotational frequencies ω_s , ω_m are now set to 300rad/s instead of 100π rad/s as used in the Simulink based example.

Chapter 8

VOLTAGE SOURCE CONNECTED SYNCHRONOUS MACHINES

8.1 Introduction

The synchronous machine has traditionally been used for power generation purposes. For motor applications (when mains connected) its use is ideal when the operating speed must remain constant, i.e. independent of load changes. Starting up however needs special measures.

Modern drives often use a converter which gives us more flexibility in terms of controlling the machine and enable the machine to self-start. The synchronous machine when used with a converter has become an important player in the field of drives.

In this chapter we will look at the basic operation of the synchronous machine, where we will apply the theory of the previous chapter in general and section 7.3 on page 178 in particular.

8.2 Machine configuration

The machine has a non-rotating component known as the stator which is shown in figure 8.1. The stator consists of a ‘frame’ within which a laminated stator core stack is positioned. This core has a series of slots which house the three-phase windings of the machine. Of these windings the so-called active sides (named thus because these are responsible for the energy conversion) are distributed appropriately in the core slots. The stator-coil end-winding-parts are at each end of the core stack as shown in figure 8.1. The three-phase windings will, when connected to a three-phase supply source, produce a rotating magnetic field which is, as was discussed in the previous chapter, an essential requirement for producing constant torque. More details on machines and rotating fields are given in Bödefeld [Bödefeld and Sequenz, 1962] or Hughes [Hughes, 1994]. Note that the same stator is also used when discussing

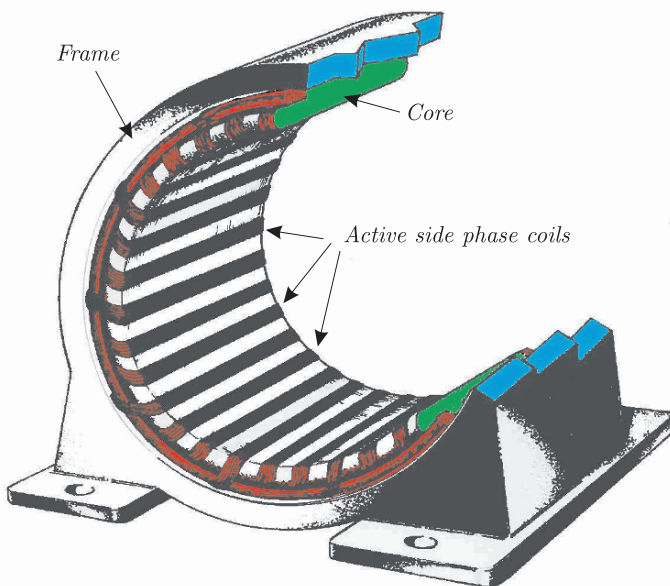


Figure 8.1. Stator of three-phase synchronous machine

the asynchronous/induction machine. The rotor configuration for the synchronous machines may take on several forms. A very simple configuration as shown in figure 8.2 conveys the basic structure. A more extensive discussion on the machine structure is given by Hughes [Hughes, 1994]. Shown in figure 8.2 is a rotor in the form of a single coil (referred to as the field winding) with sides *A* and *B* which are connected to sliprings 1 and 2 respectively. These copper sliprings are linked to a set of brushes which in turn are connected to a stationary DC power supply. The use of the slipring/brush combination allows

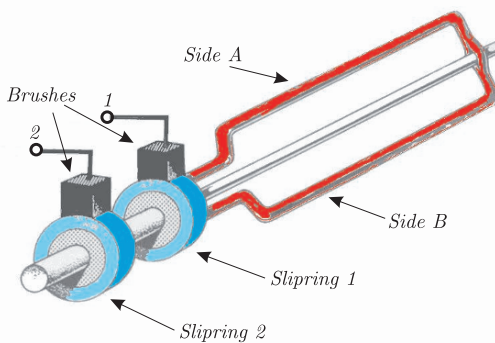


Figure 8.2. Simple rotor for synchronous machine

us to excite a rotating rotor coil with a DC ‘field’ current via a stationary source. Note that this rotor can be replaced by a permanent magnet which means that the slipring/brush combination is then avoided. However, the excitation can under these circumstances not be varied. Such machines belong to the class of so-called ‘Brushless DC machines’.

8.3 Operating principles

The synchronous machine with a slipring/brush combination is, as was discussed in the previous section, fed on the rotor side with a DC field current. This implies that the current \vec{i}^{xy} (as introduced in section 7.3 on page 178) is given by equation (7.15) with $\omega_r = 0$, hence $\vec{i}^{xy} = \hat{i} e^{j\rho_r}$. A choice remains with respect to the angle ρ_r ; its value can be taken to be zero or π rad. The latter choice amounts to reversing the polarity of the DC current source shown in figure 7.9. This option is chosen here for reasons which will become apparent shortly, hence $\vec{i}^{xy} = -\hat{i}$. The magnitude of the current \hat{i} is in context of synchronous machines more commonly known as the field current i_F , i.e. $\vec{i}^{xy} = -i_F$. On the basis of the speed condition (see equation (7.21), with $\omega_r = 0$) constant torque operation is only possible when the shaft speed is equal to the rotational speed ω_s of the rotating flux vector produced by the three-phase stator winding. The term ‘synchronous machine’ reflects this type of operation, i.e. rotor speed synchronized to the rotating field. The torque produced by this machine can be calculated using equation (7.22) on page 179 with, $\vec{i}^{xy} = -i_F$, $\rho_r = \pi$ which yields

$$T_e = -\hat{\psi}_M i_F \sin(\rho_m) \quad (8.1)$$

If a mechanical load is applied to the machine the load angle ρ_m will be non-zero. This explains why this angle is referred to as the ‘load angle’. When a load is applied, the rotor will lag behind the magnetic field ($\rho_m < 0$), which leads to a positive torque value that matches the applied load. The load angle can for a given load torque be modified by varying the amplitude of the field or rotor current. The maximum torque \hat{T}_e that can be delivered by this machine is reached when the load angle reaches $\frac{\pi}{2}$ rad. Speed changes are implemented by changing the stator frequency ω_s , which nowadays require the use of a power electronic converter with the machine.

The general space vector diagram according to figure 7.10 reduces to the form shown in figure 8.3 given the present choice of rotor excitation. Several interesting observations can be made with respect to figure 8.3. Firstly, the current vector \vec{i}^{xy} is tied to the negative real axis of the rotor given that the rotor is fed with a DC current i_F . Secondly, the vectors $\vec{\psi}_m$, \vec{i} are stationary with respect to each other. The angle between the two can and will vary depending on the load torque. For example, an increase in the load torque will see the rotor slip back momentarily (in the clockwise direction) so that the machine adjusts

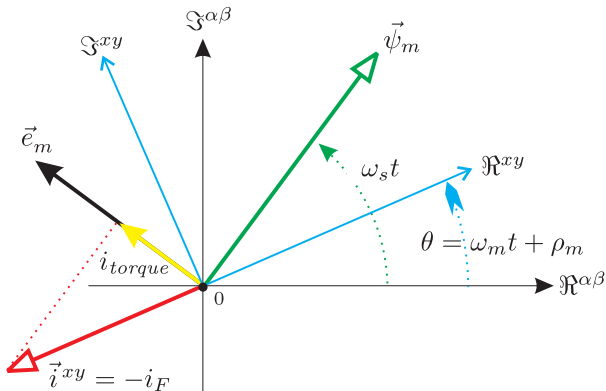


Figure 8.3. Space vector diagram for synchronous machine, motoring operation shown $\rho_m < 0$

its torque T_e to match the load torque T_l . As indicated above the highest torque (known as the ‘pull out’ torque) that can be delivered by the machine is equal to $\hat{T}_e = \hat{\psi}_m i_F$. The machine will stall (or rotate uncontrolled in the opposite direction) when a load torque above this value is applied. In this situation, the two vectors will no longer be stationary with respect to each other, i.e. the machine will deliver a pulsating torque with zero average value. Also shown in figure 8.3 is the voltage vector \vec{e} (which is equal to the supply voltage vector \vec{u}) which leads the flux vector by $\pi/2$. The projection of the current onto this vector shown as i_{torque} in figure 8.3 is proportional to the torque.

If the option $\rho_r = 0$ would have been selected then the field current would be aligned with the positive real axis. Under the circumstances shown in figure 8.3 the torque would be negative, hence the rotor would rotate until the current vector would be diametrically opposite its present position.

8.4 Symbolic model

The model to be discussed is based on the simplified generalized model as given in figure 7.15 which in this case is configured to operate as a synchronous machine. The symbolic model of the machine is given in figure 8.4. The rotor resistance is purposely omitted in figure 8.4 given that the rotor winding is connected to a current source i_F with the new polarity, as discussed above. The stator resistance and leakage are also not included in this model. The equation set which corresponds to figure 8.4 is found using Kirchhoff’s law which gives

$$\vec{u}_s = \frac{d\vec{\psi}_M}{dt} \quad (8.2a)$$

$$\vec{\psi}_M = L_M (\vec{i}_s + i_F e^{j\theta}) \quad (8.2b)$$

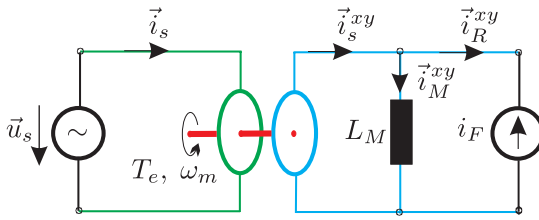


Figure 8.4. Synchronous machine, zero resistance and leakage inductance

$$T_e - T_l = J \frac{d\omega_m}{dt} \quad (8.2c)$$

$$\omega_m = \frac{d\theta}{dt} \quad (8.2d)$$

Note that in this equation set the flux vector $\vec{\psi}_M$ (see equation (8.2b)) is given in its stator based form. This expression is in fact found by using Kirchhoff's current law on the rotor side which gives $\vec{\psi}_M^{xy} = L_M (\vec{i}_s^{xy} - \vec{i}_R^{xy})$, where $\vec{i}_R^{xy} = -i_F$.

A rotating magnetizing flux vector $\vec{\psi}_M = \hat{\psi}_M e^{j\omega_s t}$ is established as a result of the machine being connected to a three-phase grid with angular frequency ω_s .

8.4.1 Generic model

A generic representation of the (two-pole) synchronous machine in its present form is given in figure 8.5. The model follows directly from equation (8.2). Central to this model is the IRTF sub-module which is represented by figure 7.5(a). The load torque is provided by a sub-module $T_l(\omega_m)$, which has been configured to deliver a quadratic torque speed characteristic $T_l = k_l \left(\frac{\omega_m}{\omega_m^R} \right)^2$ where ω_m^R is set to ω_s (rad/sec). The value of the constant k_l is set by the user. The initial speed of the machine is set to $\omega_m = \omega_s$ (rad/sec), which corresponds to the rotational speed of the flux vector $\vec{\psi}_M$.

8.5 Generalized symbolic model

The model discussed in section 8.4 was given in its simplified form, i.e. without stator resistance and leakage inductance. The rotor resistance was also not included but this is of less importance, given that we assume a current source connected to the rotor. The complete model (without rotor resistance) shown in figure 8.6, is applicable for so-called 'non-salient' machines, which generally do not carry any damper windings (short-circuited windings on the rotor). Salient machines show different L_M values for the x and y direction. The equation set which corresponds to this machine is given by equation (8.3).

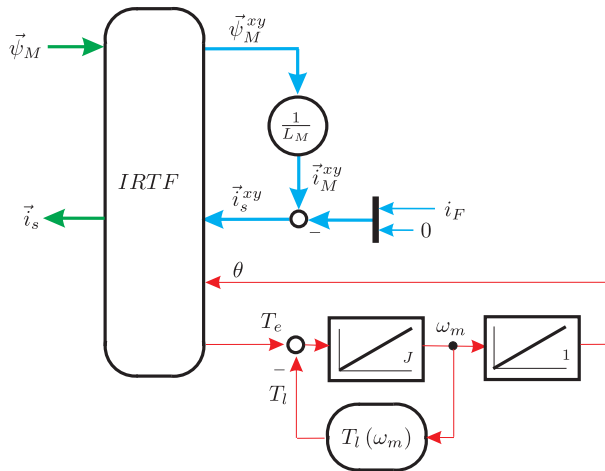


Figure 8.5. Generic representation of a voltage source connected synchronous machine, corresponding to figure 8.4

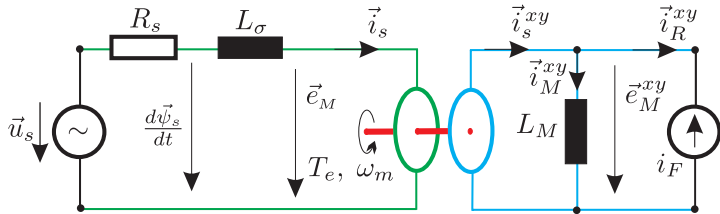


Figure 8.6. Synchronous machine

$$\vec{u}_s = \vec{i}_s R_s + \frac{d\vec{\psi}_s}{dt} \quad (8.3a)$$

$$\vec{\psi}_s = \vec{i}_s L_\sigma + \vec{\psi}_M \quad (8.3b)$$

$$\vec{e}_M^{xy} = \frac{d\vec{\psi}_M^{xy}}{dt} \quad (8.3c)$$

$$\vec{\psi}_M^{xy} = L_M (\vec{i}_s^{xy} + i_F) \quad (8.3d)$$

$$T_e - T_l = J \frac{d\omega_m}{dt} \quad (8.3e)$$

$$\omega_m = \frac{d\theta}{dt} \quad (8.3f)$$

The symbolic model according to figure 8.6 can also be redrawn in the form given by figure 8.7. The difference between the two models lies in the positioning of the magnetizing inductance L_M which is now on the stator side. The

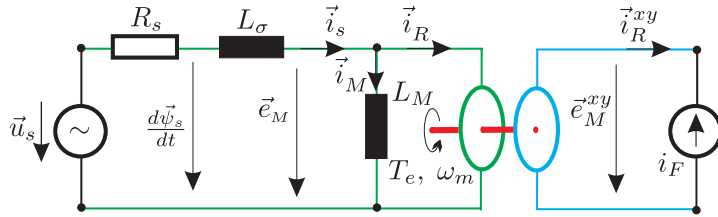


Figure 8.7. Revised synchronous machine model

revised model allows use to move towards a generic model where we are able to group the two inductances L_σ and L_M . To realize this it is helpful to introduce the flux $\psi_F = L_M i_F$. This allows us to rewrite equation (8.3d) (in its stator coordinate based form) in the form given by equation (8.4).

$$\vec{\psi}_M = L_M \vec{i}_s + \psi_F e^{j\theta} \quad (8.4)$$

Substitution of equation (8.4) into equation (8.3b) leads to equation (8.5), which for completeness contains the complete set needed to derive a generic model of this machine.

$$\vec{u}_s = \vec{i}_s R_s + \frac{d\vec{\psi}_s}{dt} \quad (8.5a)$$

$$\vec{\psi}_s = \vec{i}_s \underbrace{(L_\sigma + L_M)}_{L_s} + \psi_F e^{j\theta} \quad (8.5b)$$

$$\vec{e}_R = \frac{d(\psi_F e^{j\theta})}{dt} \quad (8.5c)$$

$$T_e - T_l = J \frac{d\omega_m}{dt} \quad (8.5d)$$

$$\omega_m = \frac{d\theta}{dt} \quad (8.5e)$$

In equation (8.5b) the sum of the two inductances known as the stator inductance L_s appears as intended. Furthermore, the voltage vector \vec{e}_R is introduced, given that the vector \vec{e}_M is no longer directly available as a result of using the parameter L_s .

8.5.1 Generic model

The generic model of the non-salient synchronous machine without damper-winding is directly found using equation (8.5). An example of implementation as given in figure 8.8, shows that the ‘IRTF-flux’ model is replaced with an ‘IRTF-current’ model (see figure 7.5(b)). Observation of figure 8.8 learns that

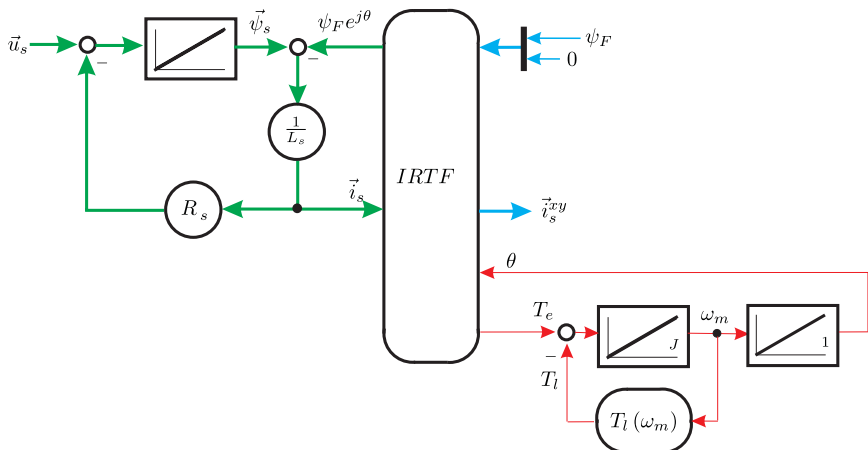


Figure 8.8. Full generic synchronous machine model, corresponding to model in figure 8.7

the IRTF module has as ‘inputs’ the flux vector $\vec{\psi}_F^{xy} = (\psi_F, 0)$ and stator current vector $\vec{i}_s = (i_{s\alpha}, i_{s\beta})$.

The mechanism through which a stator current will occur is readily shown using this generic model. Note that the reasoning presented here differs from that given in section 8.3, given the way in which the IRTF module is now used. Both approaches to describing machine operation must of course give the same result. For simplicity we will ignore the stator resistance in this discussion. If we assume that the stator is connected to a three-phase sinusoidal supply then this leads to a rotating stator flux vector $\vec{\psi}_s$. The rotor winding carries a current i_F which corresponds to a flux vector ψ_F . If we assume that the rotor rotates at the same speed as the stator flux field then the rotor and stator flux vectors will move at the same speed. If we initially assume that the magnitude of both vectors is equal and aligned then no stator current will be present. Under these circumstances the vector into the gain module $1/L_s$ (see figure 8.8) is zero, hence the current \vec{i}_s will be zero.

If, for example, we increase the rotor current then the rotor flux will increase and a stator current component will occur which will lead the voltage vector by $\frac{\pi}{2}$ radians. No torque will be realized under these circumstances.

If we return to our initial conditions (flux vectors equal magnitude and aligned) then the application of a mechanical load will momentarily cause the rotor to slow down, until an angle between the two flux vectors occurs. The difference vector between the two vectors is proportional to the stator current. Hence, a current vector will occur which means that the machine will produce a torque to counteract the new load torque (after transient effects have died down following the load torque change).

8.6 Steady-state characteristics

In this section we look to the steady-state performance of the synchronous machine in case we connect the stator windings to a three-phase sinusoidal source. This implies that the stator phase voltage equals the grid voltage with its fixed amplitude and frequency. We also assume the shaft speed to run at synchronous speed, although different shaft angles are possible with respect to the rotating field in the stator. Consequently the torque and field current are the only independent variables left at this stage. Steady-state analysis provides insight with regard to the trajectory of the stator current vector and load angle when either of these independent variables is varied.

The approach taken is to consider the simplified model first and develop the so-called ‘Blondel diagram’ and torque angle curves on the basis of the phasor equation set applicable to this model. This model is then extended to a full machine model. Synchronous operation is assumed which means that the condition $\omega_s = \omega_m$ is met. The stator is connected to a three-phase sinusoidal voltage supply which is represented by the space vector \vec{u}_s . Up to now we have chosen the flux vector of the form $\vec{\psi}_M = \hat{\psi}_M e^{j\omega_s t}$ which corresponds to a supply vector $\vec{u}_s = j\omega_s \hat{\psi}_M e^{j\omega_s t}$. The corresponding phasor representations are according to equation (4.59) of the form $\underline{\psi}_M = \hat{\psi}_M$ and $\underline{u}_s = j\omega_s \hat{\psi}_M$.

The phasor diagrams which are linked to AC machines, will be discussed in line with the general convention where the supply voltage phasor is chosen along the real axis, i.e. $\underline{u}_s = \hat{u}_s$. With our present choice of flux vector the voltage phasor is along the imaginary axis. If we redefine (for the purpose of examining the steady-state performance only) the relationship between space vectors and phasors as,

$$\vec{x} = \underline{x} e^{j(\omega_s t + \frac{\pi}{2})} \quad (8.6)$$

then the flux and voltage phasor will be of the form $\underline{\psi}_M = \hat{\psi}_M e^{-j\frac{\pi}{2}}$ and $\underline{u}_s = \omega_s \hat{\psi}_M$ respectively, i.e. rotated clockwise so that the voltage phasor is real, as preferred for steady-state analysis.

8.6.1 Steady-state characteristics, simplified model

The steady-state characteristics of the non-salient synchronous machine are studied with the aid of figure 8.5. The magnetizing flux vector $\vec{\psi}_M$ will also rotate at the same speed but will lag the voltage vector \vec{u}_s by $\frac{\pi}{2}$ radians. This vector is derived from the voltage vector using $\vec{u}_s = \frac{d\vec{\psi}_M}{dt}$, or $\underline{u}_s = j\omega_s \underline{\psi}_M$ in phasor form.

The basic characteristics of the machine relate to the stator current of the machine in phasor form and the torque load angle curve. The flux phasor $\underline{\psi}_M$ according to equation (8.4) can, with the aid of equations (8.6) and (7.17) (with

$\omega_m = \omega_s$) be written as

$$\underline{\psi}_M = L_M \left(\underline{i}_s + i_F e^{j(\rho_m - \frac{\pi}{2})} \right) \quad (8.7)$$

The current \underline{i}_s can with the aid of equation (8.7) and expression $\underline{\psi}_M = \frac{\hat{u}_s}{j\omega_s}$, be written as

$$\underline{i}_s = \frac{\hat{u}_s}{j\omega_s L_M} - i_F e^{j(\rho_m - \frac{\pi}{2})} \quad (8.8)$$

Equation (8.8) can also be represented in terms of an equivalent circuit as given by figure 8.9. Equation (8.8) may also be rewritten in the following form

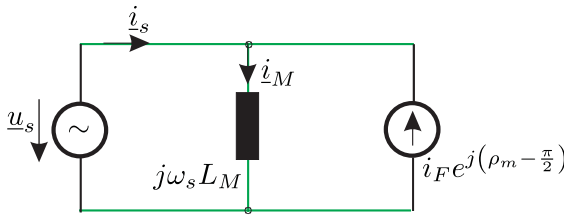


Figure 8.9. Simplified synchronous machine, phasor based model

$$\underline{i}_s = \underbrace{\frac{\hat{u}_s}{j\omega_s L_M}}_{i_{s1}} - \underbrace{\frac{\hat{u}_s k_F e^{j\rho_m}}{j\omega_s L_M}}_{i_{s2}} \quad (8.9)$$

in which the factor k_F is defined as

$$k_F = \frac{\omega_s L_M i_F}{\hat{u}_s} \quad (8.10)$$

which can also be written in the form given by equation (8.11).

$$k_F = \frac{L_M i_F}{\hat{\psi}_M} \quad (8.11)$$

If the value of k_F is greater than 1 the machine is said to be operating under ‘over-excited’ conditions. For k_F value less than 1 a so-called ‘under-excited’ machine operating condition is present.

The current phasor \underline{i}_s can be plotted as a function of the load angle ρ_m with i_F as parameter. This type of diagram as given in figure 8.10, shows the two current components according to equation (8.9) together with lines of constant output power p_{out} . These output power curves are found by making use of the energy balance equation, which for the current machine with zero stator resistance is of the form

$$\Re \{ \underline{u}_s \underline{i}_s^* \} = p_{out} \quad (8.12)$$

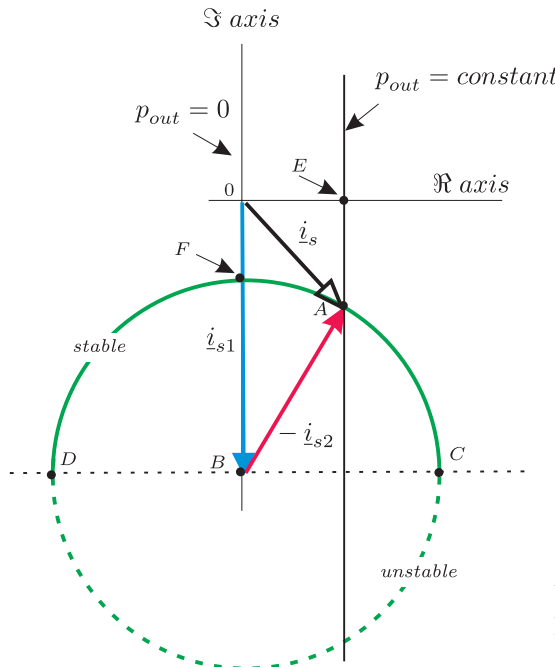


Figure 8.10. Blondel diagram of synchronous machine with $R_S = 0$, $\rho_m < 0$ and $k_F < 1$

where $p_{out} = T_e \omega_m$. The power balance states that the output power is in this case equal to the input power. This expression may be reduced to

$$\hat{u}_s \Re \{\underline{i}_s^*\} = p_{out} \quad (8.13)$$

where use is made of $\underline{u}_s = \hat{u}_s$. Equation (8.13) shows that lines of constant output power are represented by vertical lines in figure 8.10. It is noted that for a given shaft speed the output power is proportional to the output torque.

The diagram according to figure 8.10 is known as a ‘Blondel’ diagram and is particularly useful for identifying a range of operating situations. In particular the user is able to gain insight as to how, for example, changes to the load torque or field current will affect the stator current and power factor. A number of these are itemized as follows.

- Motor operation is realized in the first and fourth quadrant of the complex plane.
- Generator operation is achieved if the current vector end point ‘A’ is located in the second or third quadrant of the complex plane.
- When the load angle is changed a circle will appear which represents the stator current end point trajectory. The circle radius is proportional to the current i_F , where point B represents the case for $i_F = 0$. In case the

load torque is zero and $i_F > 0$, the operating point will be located at for example point F . As the load torque is increased ($\rho_m < 0$) the motoring region is entered and the output power will increase. The horizontal distance from the operating point to the zero power line determines the output power level. The larger this distance, the higher the output power. This means that motor operation with a current phasor end point positioned at C gives the highest output power level achievable for a given field current. This operating point also represents the limit for stable motor operation. If the load torque is increased beyond this value, then the load angle is increased (in absolute terms) further, which leads to a smaller rather than larger output torque. The motor will now loose synchronization with the grid. A similar reasoning is also applicable for generator operation in which case the limit of stable operation is identified by point D . The entire operating trajectory for unstable operation is also shown in figure 8.10.

- For a given output power level at for example point A it is possible to change the excitation current as to minimize the stator current amplitude. This is achieved at point E which corresponds to unity power factor. Under these conditions the machine will be over-excited, i.e. $k_F > 1$.
- The Blondel diagram according to figure 8.10 is shown with $k_F = 0.7$. The current end point trajectory from point $A \rightarrow E$ is realized in case k_F is increased (by changing i_F) to the value 1.06 while maintaining a constant output power level.

In addition to using the Blondel diagram it is desirable to have access to a cartesian type diagram in the form of the output power/load angle diagram. This type of diagram is readily obtained by making use of for example equations (8.1) and (8.11), with $p_{out} = T_e \omega_s$, $\hat{\psi}_M = \hat{u}_s / \omega_s$, which leads to the following output power expression

$$p_{out} = -\frac{\hat{u}_s^2 k_F}{\omega_s L_M} \sin \rho_m \quad (8.14)$$

This expression can be further developed by introducing a normalization factor $\frac{\hat{u}_s^2}{\omega_s L_M}$ which gives

$$p_{out}^n = -k_F \sin \rho_m \quad (8.15)$$

A graphical representation of equation (8.15) is shown in figure 8.11 with $k_F = 0.7$. The parameters used here are identical to those used for figure 8.10. This means that a number of operating points given in the Blondel diagram can also be shown here for comparison purposes. A second torque/load angle curve is included in figure 8.11 which represents the case $k_F = 1.06$ which as was

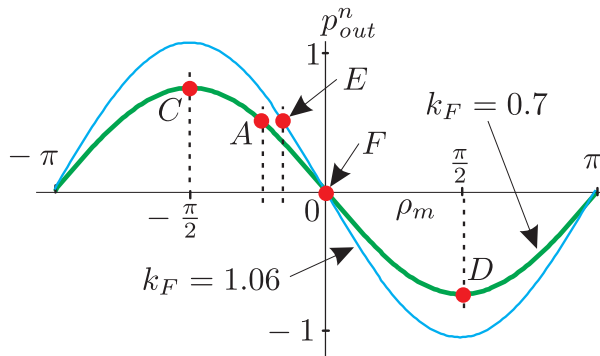


Figure 8.11. Normalized output power versus load angle curves, with $R_s = 0$

discussed earlier allows operation with unity power factor. Several interesting observations can be made with respect to the output power versus load angle diagram.

- The power versus load angle curves are radial symmetrical
- The stable operating range of load angles corresponds to region $C - D$. The concept of so-called ‘stable’ operation is readily illustrated by considering operation at for example point A . If the mechanical load power is increased, the machine can respond by producing more output power which in turn leads to a more negative load angle. If this example is carried out for operation at for example point C , then an increase in load power cannot be met by increase in machine output power, in which case de-synchronization will occur.

8.6.2 Steady-state characteristics, full model

In reality machines have a finite stator resistance and stator inductance. It is therefore necessary to consider the Blondel diagram and load torque/angle curves for the more general case.

The Blondel diagram is found by making use of equation set (8.5), which may be converted to phasor form using equations (8.6) and (7.17) (with $\omega_m = \omega_s$), which leads to equation (8.16).

$$\underline{u}_s = i_s R_s + j\omega_s \underline{\psi}_s \quad (8.16a)$$

$$\underline{\psi}_s = L_s \underline{i}_s + \underline{\psi}_F e^{j(\rho_m - \frac{\pi}{2})} \quad (8.16b)$$

Elimination of the flux phasor $\underline{\psi}_s$ from equation (8.16), leads to the following current phasor expression.

$$\underline{i}_s = \frac{\hat{u}_s (1 - k_F e^{j\rho_m})}{R_s + j\omega_s L_s} \quad (8.17)$$

Expression (8.17) may also be presented in terms of a circuit representation as given in figure 8.12. A normalization of equation (8.17) is again introduced

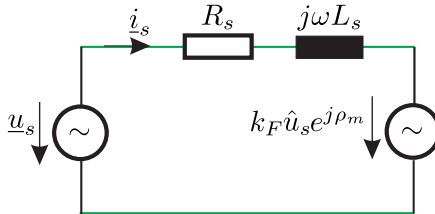


Figure 8.12. Synchronous phasor based machine model

which is of the form

$$\underline{i}_s^n = \frac{\underline{i}_s}{\left(\frac{\hat{u}_s}{R_s}\right)} \quad (8.18)$$

where the term $\left(\frac{\hat{u}_s}{R_s}\right)$ is referred to as the ‘base’ value. The resultant normalized expression as given by (8.19) shows the presence of two components $\underline{i}_{s1}^n, \underline{i}_{s2}^n$

$$\underline{i}_s^n = \underbrace{\frac{1}{1 + j \frac{j\omega_s L_s}{R_s}}}_{\underline{i}_{s1}^n} - \underbrace{\frac{k_F e^{j\rho_m}}{1 + j \frac{j\omega_s L_s}{R_s}}}_{\underline{i}_{s2}^n} \quad (8.19)$$

The excitation factor k_F as defined by equation (8.10) is expressed in its more general form (in terms of $\psi_F = L_M i_F$) as given by equation (8.20).

$$k_F = \frac{\omega_s \psi_F}{\hat{u}_s} \quad (8.20)$$

A graphical representation of equation (8.19) as given in figure 8.13 on page 207, shows the two current components together with curves of (normalized) constant output power p_{out}^n . The speed is kept quasi-constant while the load angle is able to vary. The curves of constant torque, i.e. constant output power are found using the energy balance equation

$$\Re \{\underline{u}_s \underline{i}_s^*\} - \Re \{\underline{i}_s \underline{i}_s^*\} R_s = p_{out} \quad (8.21)$$

In this case, a dissipative term is introduced which was not present in the previous energy equation (8.12). Expression (8.21) can be written in a more simplified normalized form which after some mathematical handling gives

$$\left(x - \frac{1}{2}\right)^2 + y^2 = \left(\frac{1}{4} - p_{out}^n\right) \quad (8.22)$$

with

$$x = \Re \{\underline{i}_s^n\}$$

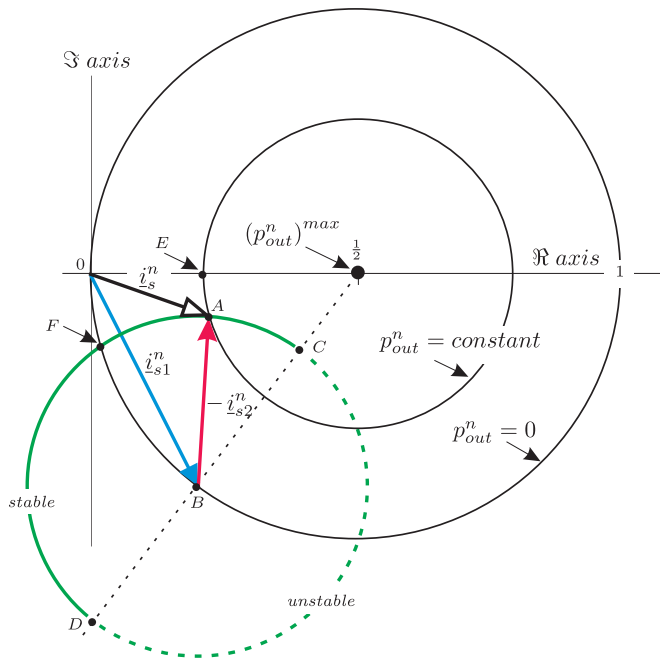


Figure 8.13. Blondel diagram of synchronous machine with $R_s > 0$, $\rho_m < 0$ and $k_F < 1$

$$\begin{aligned} y &= \Im\{i_s^n\} \\ p_{out}^n &= \frac{p_{out}}{\frac{\hat{u}_s^2}{R_s}} \end{aligned}$$

Equation (8.22) states that we are able to represent circles of constant output power in the complex plane as well as the normalized stator current. These circles are centered on the \Re axis with coordinates $(\frac{1}{2}, 0)$ and radius $\sqrt{\frac{1}{4} - p_{out}^n}$. This implies that the zero output power circle has a radius of $\frac{1}{2}$. Furthermore, the machine has a maximum (per unit) output power level $(p_{out}^n)^{\max} = \frac{1}{4}$ which in figure 8.13 is found at coordinates $(\frac{1}{2}, 0)$ of the complex plane. It is noted that for a given shaft speed the output power is proportional to the output torque. The general Blondel diagram with $R_s > 0$ as given by figure 8.13 has a number of interesting operating points which are itemized below.

- If the field current i_F is set to zero (point B) then the stator current will be positioned on the zero output power circle.
- Motor operation is present within the circle constrained by $p_{out}^n = 0$.
- For a given field current (and corresponding k_F value) and variable load angle a circle will appear which represents the stator current endpoint tra-

jectory. The radius of this circle is proportional to the current i_F . When the load torque is zero the operating point will be located at point F . As load torque is increased, the motoring region is entered and the output power will increase. The distance from the operating point to the maximum output power point $(p_{out}^n)^{max}$ determines the output power level. The shorter this distance the higher the output power. This means that operation with a current phasor end point positioned at C gives the highest output power level achievable for the given field current. This operating point also represents the limit for stable operation.

- For a given output power level at for example point A , it is possible to change the excitation to minimize the stator current. This is achieved at point E which corresponds to unity power factor.
- The Blondel diagram according to figure 8.13 is shown with $k_F = 0.7$ and $\frac{\omega_s L_s}{R_s} = 1.96$. The current end point trajectory can be made to intersect with the maximum power point in case k_F is increased to the value 1.1.
- Lines of constant power are represented as circles in this case which have their center at coordinates $\left(\frac{1}{2}, 0\right)$.

The output power/load angle diagram is found using equation (7.28g) and equation (8.19) in its non-normalized general form. An observation of the generic diagram (figure 8.8) learns that the IRTF module now calculates the torque using the flux vector $\psi_F e^{j\theta}$ and current vector \vec{i}_s . Both vectors can be converted to phasor form using equations (8.6) and (7.17) (with $\omega_m = \omega_s$), which leads to equation (8.24).

$$T_e = \Re \left\{ j\psi_F \vec{i}_s e^{-j\rho_m} \right\} \quad (8.24)$$

The output power, defined as $p_{out} = T_e \omega_m$ is then found using equations (8.24) and (8.19), in non-normalized form. The output power expression in a normalized form is given by equation (8.25)

$$p_{out}^n = -\frac{4k_F}{\sqrt{1 + \left(\frac{\omega_s L_s}{R_s}\right)^2}} \left\{ \sin \left(\rho_m + \gamma - \frac{\pi}{2} \right) - k_F \sin \left(\gamma - \frac{\pi}{2} \right) \right\} \quad (8.25)$$

where $\gamma = \arctan \left(\frac{\omega_s L_s}{R_s} \right)$. The normalization used in equation (8.25) is of the form

$$p_{out}^n = \frac{p_{out}}{p_{out}^{max}} \quad (8.26)$$

where

$$p_{out}^{max} = \frac{\hat{u}^2}{4R_s} \quad (8.27)$$

A graphical representation of equation (8.25) as function of the load angle ρ_m is shown in figure 8.14 with $k_F = 0.7$ and $\frac{\omega_s L_s}{R_s} = 1.96$.

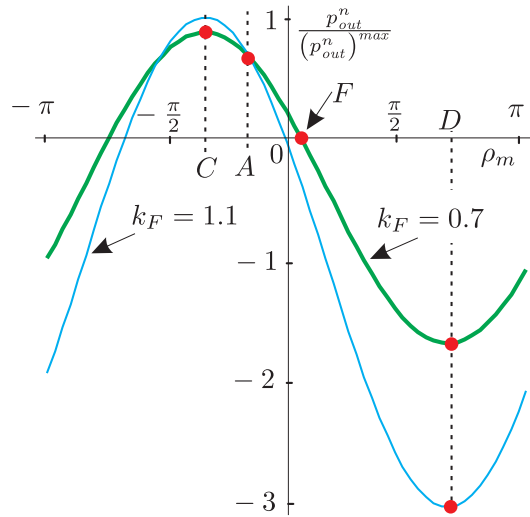


Figure 8.14. Normalized output power versus load angle curves

The parameters used here are identical to those used for figure 8.13. This means that a number of operating points given in the Blondel diagram can also be shown here for comparison purposes. A second torque/load angle curve is included in figure 8.14 that represents the case $k_F = 1.1$ which as was discussed earlier, allows operation at the maximum power point.

Several interesting observations can be made with respect to the output power versus load angle diagram.

- The peak values for motor and generator operation are generally not equal. Equality of the peak values is achieved in case the term $\frac{\omega_s L_s}{R_s} \rightarrow \infty$. This is readily apparent for the zero resistance case (figure 8.11).
- Zero load angle does generally not correspond to zero output power. Only for $k_F = 1$ is this the case.
- The stable operating range of load angle corresponds to region $C - D$.

8.7 Tutorials for Chapter 8

8.7.1 Tutorial 1

This tutorial considers a three-phase IRTF based synchronous machine in its simplified form, i.e. no stator resistance, rotor resistance or leakage inductance. The aim is to build a Simulink model of this machine in accordance with the

generic model given in figure 8.5. This model can be used to examine the steady-state characteristics of this simplified machine. An example of such a Simulink model is given in figure 8.15. The machine in question has a magnetizing

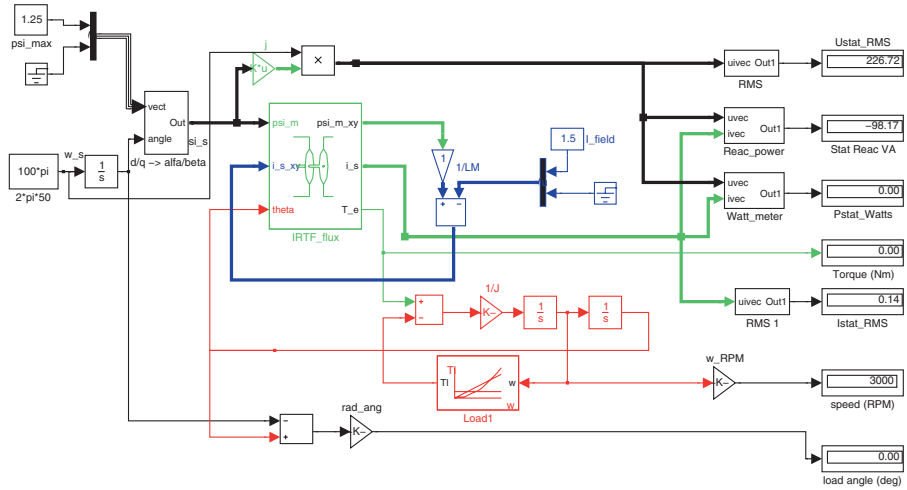


Figure 8.15. Simulink model of synchronous machine

inductance of $L_M=1\text{H}$, and an inertia of $J = 0.00001 \text{kgm}^2$. The rotor is connected to a DC current source which provides a current i_F . Furthermore, a rotating magnetizing flux vector $\vec{\psi}_M$ is assumed which is the result of connecting the machine on the stator side to a three-phase sinusoidal voltage source. The use of a rotating flux vector is in line with the approach taken in the previous tutorial on space vector transformers (see section 6.4.1 on page 160). The machine is connected to a mechanical load via which the load torque can be altered under motor operation. We will now consider some of the modules shown in figure 8.15 in more detail.

The module $d/q - \alpha/\beta$ shown in figure 8.15 has an output/input relationship of the form

$$\vec{\psi}_M = \vec{\psi}_M^{dq} e^{j\rho} \quad (8.28)$$

The output vector $\vec{\psi}_M = \psi_{M\alpha} + j\psi_{M\beta}$ is in stationary coordinates while the input vector $\vec{\psi}_M^{dq} = \psi_{Md} + j\psi_{Mq}$ is given in a general ‘dq’ coordinate frame, which for the IRTF module will be rotating, i.e. ‘dq’ is then ‘xy’. Comparing real and imaginary components of equation (8.28) gives the relationship between the output variables $\psi_{M\alpha}, \psi_{M\beta}$ and input variables $\psi_{Md}, \psi_{Mq}, \theta$. Select ‘wide non-scalar lines’ to make your simulation more readable. The incoming flux vector is $\vec{\psi}_M^{dq} = \hat{\psi}_M + j0$, where $\hat{\psi}_M=1.25\text{Wb}$. The angle $\rho = \omega_s t$ is produced

in exactly the same way as discussed in tutorial 6.4.1. Check your work by using a ‘XY’ scope module with axis values $x_{min}=-1.5$, $x_{max}=1.5$, $y_{min}=-1.5$, $y_{max}=1.5$. Under simulation parameters select a ‘fixed step’ type ‘solver’ with step size 1e-3. Solver type should be ‘ode4’. Note: maintain this solver setting and run time value for the rest of the tutorial.

Run the simulation for 1s and observe the result, which should be a circle with a radius of 1.25, given that the flux vector is of the form $\vec{\psi}_M = 1.25 e^{j100\pi t}$.

Add a module which will generate the voltage space vector $\vec{u}_s = j \omega_s \vec{\psi}_M$ which is based on the model given in figure 6.8. You will need to use a multiplier and gain module with gain j . The latter is realized in Simulink by using a ‘Matrix gain’ module. Select Matrix gain K*u within this module and set the gain to $[0 -1; 1 0]$. Build using a ‘fcn’ module a building block which allows you to calculate the RMS value of the three-phase waveforms which corresponds to a vector \vec{x} . Connect the output of the vector \vec{u}_s via an RMS converter to a ‘Display module’ (see ‘sinks library’), which will give the RMS stator voltage value.

The value on this display follows from the flux amplitude and frequency, namely $\hat{u}_s = \hat{\psi}_M \omega_s$, where \hat{u}_s represents the amplitude of the voltage vector. The readout value is therefore equal to $U_s = \omega_s \hat{\psi}_M / \sqrt{3}$, which in numerical terms is equal to $U_s = 1.25 \cdot 100\pi / \sqrt{3} = 226.7V$.

The IRTF module as developed in section 7.5.1 on page 186 is directly applicable to this tutorial. The magnetizing current component $\vec{i}_M^{xy} = \vec{\psi}_M^{xy} / L_M$ must also be added in order to calculate the primary current vector \vec{i}_s^{xy} . This vector is given as $\vec{i}_s^{xy} = \vec{i}_M^{xy} - i_F$.

It is helpful to also add a series of modules which will allow you to show the torque, rotational speed (rpm) and load angle. The latter is the angle between the shaft and flux vector, its value is shown in degrees, i.e. you need to convert from radians to degrees (factor $180/\pi$). If a mechanical load is applied then a NEGATIVE load angle will occur. In addition to the above, use a vector to RMS converter with display unit to show the RMS stator current value.

We will also need to add two additional sub-modules which will give us the stator real and reactive power values known as $P(W)$ and $Q(VA)$ respectively. The inputs to these modules will be the space vectors \vec{u}_s , \vec{i}_s .

The last part of this tutorial is concerned with the load side of the machine. The generic diagram (figure 8.5) shows the implementation of the mechanical equation set which links load torque T_l , shaft torque T_e and inertia J with the shaft speed ω_m and rotor angle θ . Figure 8.15 shows how the mechanical equation set is implemented in Simulink. Note that the integrator which has as output the shaft speed (integrator which follows the gain module $1/J$), must have its initial condition set to $\omega_s = 100\pi$ rad/s. This means that the simulation starts with the machine rotating at synchronous speed. The load torque module is to be built in a general form given that its use is not restricted to this tutorial.

The module is to be built as a ‘sub-module’ where the user can select a ‘constant’, ‘linear’ or ‘quadratic’ load torque versus speed characteristic. The relationship between load torque and speed is therefore of the form

$$T_l = T^{ref} \quad (8.29a)$$

or

$$T_l = k_{L1}\omega_m \quad (8.29b)$$

or

$$T_l = \begin{cases} \text{if } \omega_m \geq 0 & k_{L2}\omega_m^2 \\ \text{if } \omega_m < 0 & -k_{L2}\omega_m^2 \end{cases} \quad (8.29c)$$

where $k_{L1} = T^{ref} / \omega^{ref}$, $k_{L2} = T^{ref} / (\omega^{ref})^2$. In this example we can use the quadratic load curve as given by equation (8.29c). The value for ω^{ref} must be set to 100π , while T^{ref} is a variable which must be adjusted in this tutorial. This variable is in fact the steady-state load torque value. An example of an implementation of equation (8.29a) in Simulink is given in figure 8.16. Figure 8.16

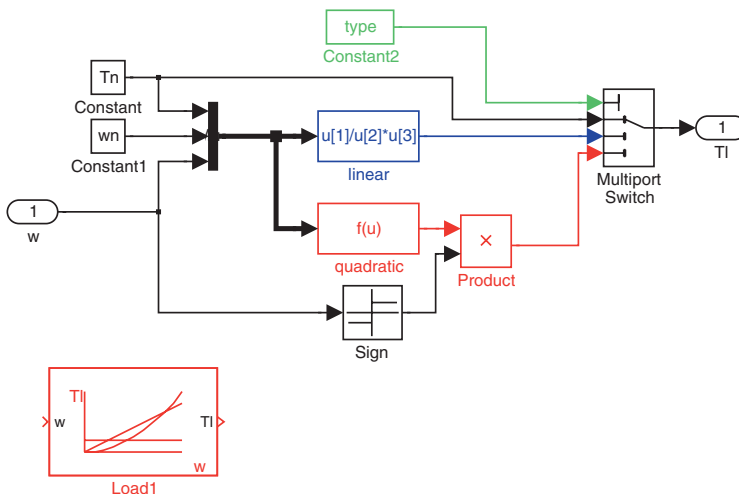


Figure 8.16. Simulink model: load torque module

shows the use of a ‘multi-switch’ selection module, which is controlled by the variable ‘type’, which has a value linked to the selected load/speed curve. The ‘constant’ modules ‘Tn’, ‘wn’ are constants which represent the variables T^{ref} , ω^{ref} respectively.

8.7.2 Tutorial 2

This tutorial is concerned with using the Simulink model as developed in the previous tutorial. The model will be used to examine the steady-state behaviour of the machine operating as a motor under no-load conditions.

Set the load torque to zero, i.e. $T^{ref}=0\text{Nm}$ in your load torque module. Set the field current to $i_F=1.25\text{A}$ and run your simulation with a ‘run’ time of 1s and ‘stepsize’ of 1ms.

Change the field current value to 1A and rerun the simulation. Observe the result on the display modules and confirm these results via a steady-state phasor analysis in the form of an MATLAB file. The results which should appear on the display modules for the two simulation runs is given in table 8.1. The m-file

Table 8.1. Simulation results synchronous machine: no-load

Parameters	$i_F = 1.25 \text{ A}$	$i_F = 1.00 \text{ A}$
RMS Stator voltage	U_s	226.72 V
RMS Stator current	I_s	0.00 A
Real Stator power	P_s	0.00 W
Reactive stator power	Q_s	0.00 VA
Load angle	ρ_m	0.00 °
Shaft speed	ω_m	3000.00 rpm
		3000.00 rpm

as given below, shows the phasor analysis for this problem. The file must be run for the two i_F current values in order to obtain the results shown in table 8.1.

m-file Tutorial 2, chapter 8

```
%Tutorial 2, chapter 8
%steady-state analysis
LM=1;
ws=2*pi*50;
psiM_hat=1.25;
psiM_ph=-j*psiM_hat;
iM_ph=psiM_ph/LM;
us_ph=j*ws*psiM_ph;
U_s=abs(us_ph)/sqrt(3);
T_e=0;
iF=1.;
rho_m=-asin(T_e/(psiM_hat*iF));
rho_mD=rho_m*180/pi;
rh=rho_m*pi/2;
is_ph=iM_ph-iF*(cos(rh)+j*sin(rh)); % stator current phasor calculation
I_s=abs(is_ph)/sqrt(3); % RMS value phase current
P=real(us_ph*conj(is_ph)); % real stator power
Q=imag(us_ph*conj(is_ph)); % reactive stator power
wm=ws; % shaft speed rad/s
nm=wm*60/(2*pi); % shaft speed rad/s
```

8.7.3 Tutorial 3

This tutorial considers the steady-state behaviour of the model as discussed in tutorials 1 and 2 under varying load conditions. For this example, maintain a field current value of 1A and vary the load torque. The maximum load torque which our machine can handle is 1.25Nm. Explain where this value comes from.

Answer: the peak flux level is $\hat{\psi}_M=1.25\text{Vs}/\text{rad}$, the field current is $i_F=1\text{A}$, which according to equation (8.1), gives a maximum torque of 1.25Nm. Change the load torque in ten steps in the range 0 to 1.25Nm and record (after doing a simulation run for each STEP) the following data from the display modules: load angle ρ_m , shaft torque T_e , RMS stator current, real and reactive stator power.

The data as given in table 8.2 should appear from your simulation.

Table 8.2. Simulation results Synchronous machine: no-load→load

$T_e(\text{Nm})$	$\rho_m (\text{ }^\circ)$	$P_s (\text{W})$	$Q_s (\text{VA})$	$I_s (\text{A})$
0.0	0	0	98.14	0.14
0.125	-5.74	39.27	100.14	0.16
0.250	-11.54	78.54	106.11	0.19
0.375	-17.46	117.81	116.26	0.24
0.50	-23.58	157.08	130.96	0.30
0.625	-30.00	196.35	150.79	0.36
0.750	-36.87	235.62	176.71	0.43
0.875	-44.43	274.89	210.43	0.51
1.00	-53.13	314.16	255.25	0.60
1.125	-64.16	353.43	319.43	0.70
1.250	-89.29	392.67	485.98	0.92

Build an m-file which will display the data from your simulation in the form of four sub-plots: $T_e(\rho_m)$, $I_s(\rho_m)$, $P_s(\rho_m)$, $Q_s(\rho_m)$. In addition, plot the current phasor \underline{i}_s in the form of a ‘Blondel’ diagram. Note that the angle between the current and voltage phasor can be calculated using your real and reactive power readings. Add to these plots the results as calculated via a steady analysis. Show these calculations in the same m-file.

An example of the results which should appear from this m-file is given in figures 8.17, and 8.18. Also shown (not to scale) in figure 8.18 by way of reference, is the stator voltage phasor \underline{u}_s . Clearly noticeable from figure 8.18 is that the locus of the stator current phasor \underline{i}_s is part of a circle which has its center at 0, -1.25A. An example of an m-file implementation is given below.

m-file Tutorial 3, Chapter 8

```
%Tutorial 3, Chapter 8
%Tutorial synchronous machine-simplified model
```

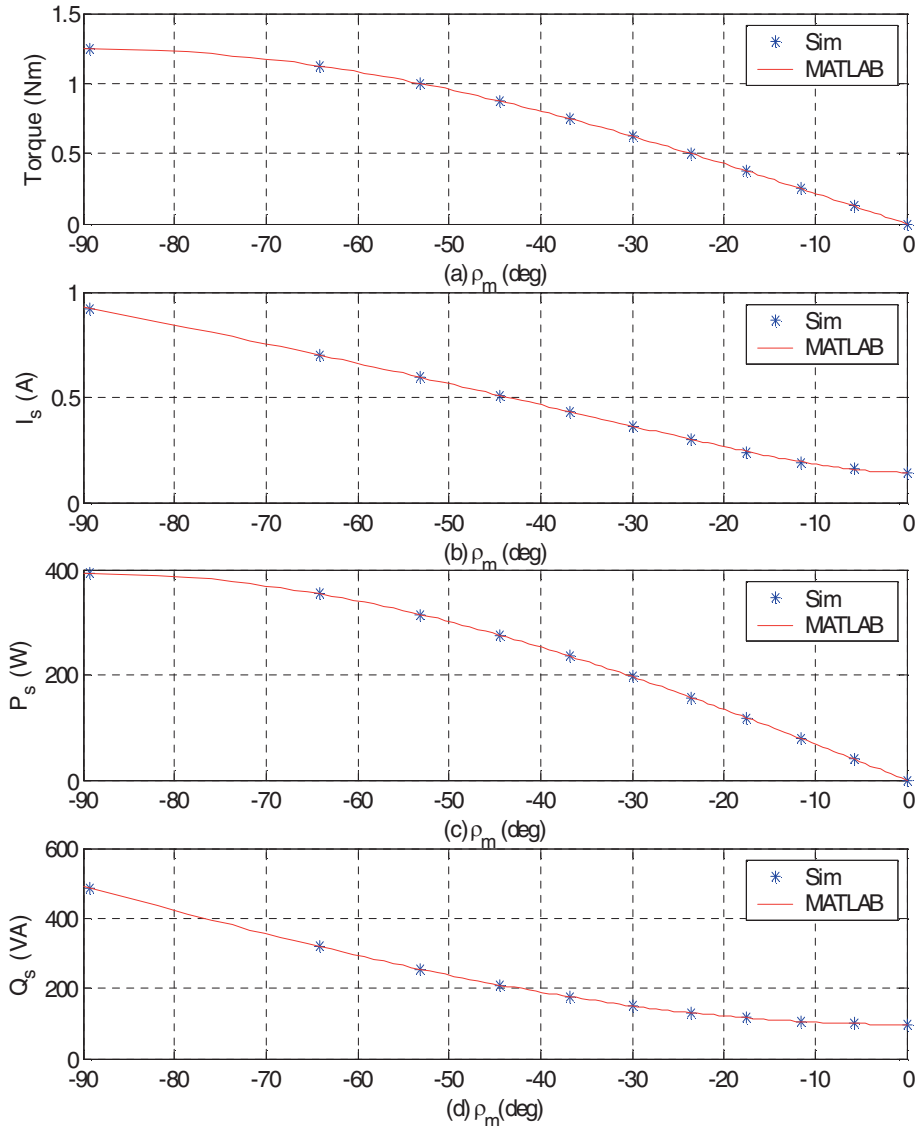


Figure 8.17. Simulink/MATLAB result: $T_e(\rho_m)$, $I_s(\rho_m)$, $P_s(\rho_m)$, $Q_s(\rho_m)$

```
%steady-state analysis
clear all
close all
LM=1;
ws=2*pi*50;
psiM_hat=1.25;
psiM_ph=-j*psiM_hat;
iM_ph=psiM_ph/LM;
% Magnetizing inductance
% frequency rad/s
% flux vector amplitude
% input flux phasor
% magnetizing current
```

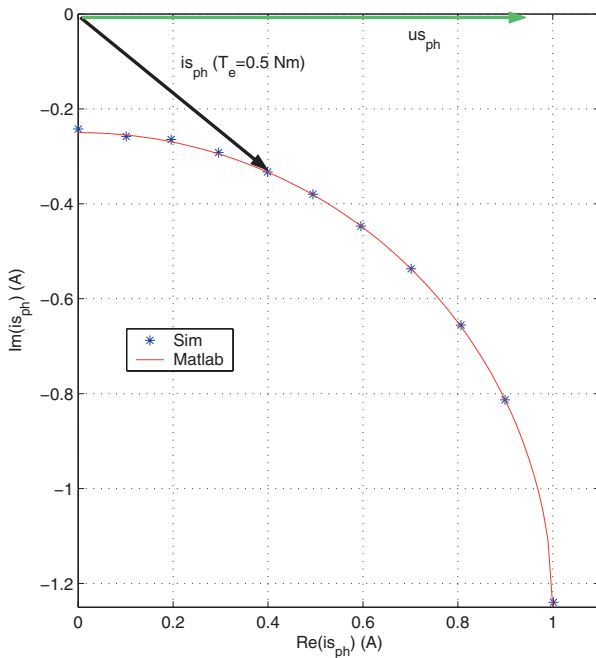


Figure 8.18. Simulink/MATLAB result: Blondel diagram

```

us_ph=j*ws*psiM_ph; % stator voltage phasor
U_s=abs(us_ph)/sqrt(3); % RMS value phase voltage
%%% Data Simulink
Te=[0:1.25/10:1.25]; % selected load torque values
%measured, from display, load angle (deg)
rhoM=[0 -5.74 -11.54 -17.46 -23.58 -30.00...
      -36.87 -44.43 -53.13 -64.16 -89.29];
%measured, from display, real power (W)
PM=[0 39.27 78.54 117.81 157.08 196.35...
      235.62 274.89 314.16 353.43 392.67];
%measured, from display, reactive power (VA)
QM=[98.17 100.14 106.11 116.26 130.96 150.79...
      176.71 210.43 255.25 319.43 485.98];
%measured, from display, RMS stator current (A)
IM=[0.14 0.16 0.19 0.24 0.30 0.36 0.43 0.51 0.60 0.70 0.92];
%%% display measured results
figure (1)
subplot(4,1,1)
plot(rhoM,Te,'*')
grid
xlabel('(\alpha) \rho_m (deg)')
ylabel('Torque (Nm)')
subplot(4,1,2)
plot(rhoM,IM,'*')

```

```

grid
xlabel(' (b) \rho_m (deg)')
ylabel('I_s (A)')
xlabel(' \rho_m (deg)')
subplot(4,1,3)
plot(rhoM,PM,'*')
grid
ylabel('P_s (W)')
xlabel(' (c) \rho_m (deg)')
subplot(4,1,4)
plot(rhoM,QM,'*')
grid
ylabel('Q_s (VA)')
xlabel(' (d) \rho_m(deg)')
%%%%%%%plot Blondel diagram
rhos=atan(-QM./PM); Is_phM=IM*sqrt(3).* (cos(rhos)+j*sin(rhos));
ISRE=real(Is_phM); ISIM=imag(Is_phM);
figure(2)
plot(ISRE,ISIM,'*')
grid
%%%%%%%Add theoretical results phasor analysis to plots
T_e=[0:1.25/100:1.25]; % Te values for analysis
if=1.0;% field current
rho_m=-asin(T_e/(psiM_hat*iF)); % load angle rad
rho_mD=rho_m*180/pi; % load angle in degrees
%%%%%plot results
figure(1)
subplot(4,1,1)
hold on
plot(rho_mD, T_e,'r')
legend('Sim','MATLAB')
%%%%%
rh=rho_m-pi/2;
is_ph=iM_ph-iF*(cos(rh)+j*sin(rh)); % stator current
% phasor calculation
I_s=abs(is_ph)/sqrt(3); % RMS value phase current
subplot(4,1,2)
hold on
plot(rho_mD, I_s,'r')
legend('Sim','MATLAB')
%%%%%
P=real(us_ph*conj(is_ph)); % real stator power
subplot(4,1,3)
hold on
plot(rho_mD, P,'r')
legend('Sim','MATLAB')
Q=imag(us_ph*conj(is_ph)); % reactive stator power
subplot(4,1,4)
hold on
plot(rho_mD, Q,'r')
legend('Sim','MATLAB')
%%%%%Blondel diagram
figure(2)
hold on
isRE=real(is_ph); isIM=imag(is_ph);
figure(2)
plot(isRE,isIM,'r')

```

```

axis equal
axis([0 1.1 -1.25 0])
legend('Sim','MATLAB')
xlabel('Re(is_{ph}) (A)')
ylabel('Im(is_{ph}) (A)')

```

8.7.4 Tutorial 4

This tutorial is an extension of the previous tutorial. However, in this case constant torque operation is assumed while varying the field current. Set the load torque to 0.5Nm and vary the field current in the range of 0.5 to 2.25A with an incremental step of 0.25A. At each incremental step, run your simulation and record the RMS stator current, stator reactive power and load angle. Plot these variables versus the field current.

The data as shown in table 8.3 should appear from your simulation.

Table 8.3. Simulation results synchronous machine: $i_F \in [0.5, \dots, 2.25]A$

$i_F(A)$	$I_s(A)$	$Q_s(VA)$	ρ_m°
0.5	0.60	373.06	-53.13
0.75	0.42	241.73	-32.23
1.0	0.30	130.96	-23.58
1.25	0.23	25.81	-18.66
1.50	0.26	-76.84	-15.47
1.75	0.35	-178.16	-13.21
2.00	0.47	-278.66	-11.54
2.25	0.60	-378.62	-10.24

Build an m-file which will display the data from your simulation in the form of three sub-plots: $I_s(i_F)$, $Q_s(i_F)$, $\rho_m(i_F)$. In addition, plot the stator current phasor \underline{i}_s in the form of a ‘Blondel’ diagram.

Add to these plots the results as calculated via a steady-state (phasor) analysis. Show these calculations in the same m-file. An example of the results which should appear from this m-file is given in figures 8.19, and 8.20.

The stator voltage phasor \underline{u}_s is again added to the Blondel diagram shown in figure 8.20. An important observation which can be made from figure 8.20 is that the reactive power can be controlled by varying the field current, *without* affecting the output power of the machine. Indeed, the reactive power can be changed from inductive $Q > 0$ (stator current phasor lags the voltage phasor) to capacitive $Q < 0$ (stator current leads the voltage phasor). An example of an m-file implementation for this tutorial is given below:

m-file Tutorial 4, Chapter 8

```

%Tutorial 4, Chapter 8
%Tutorial synchronous machine-simplified model

```

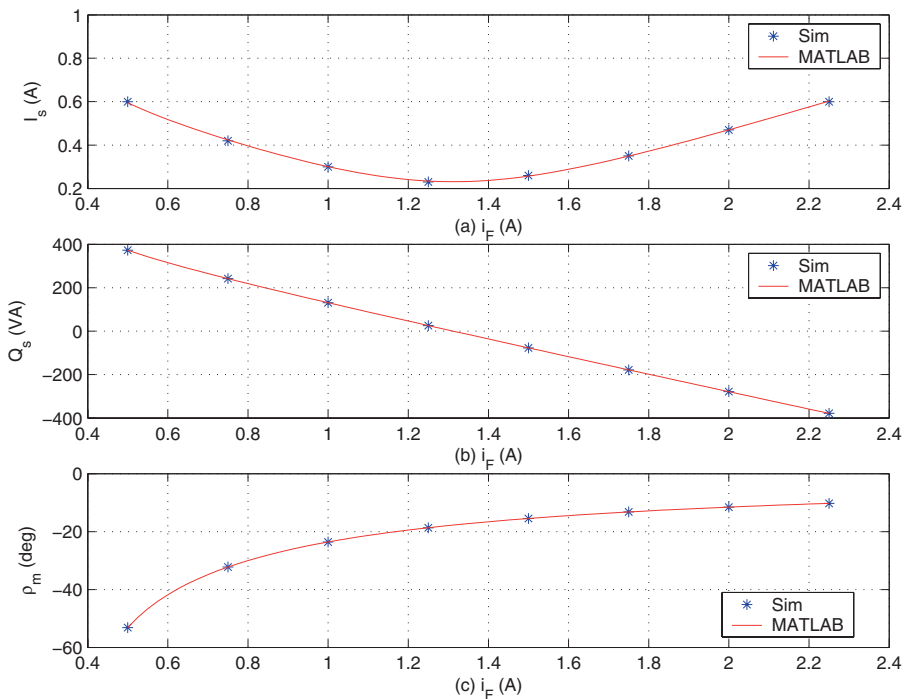


Figure 8.19. Simulink/MATLAB result: I_s (i_F), Q_s (i_F), ρ_m (i_F)

```
%steady-state analysis: constant torque
close all
LM=1; % Magnetizing inductance
ws=2*pi*50; % freqeuncy rad/s
psiM_hat=1.25; % flux vector amplitude
psiM_ph=-j*psiM_hat; % input flux phasor
iM_ph=psiM_ph/LM; % magnetizing current
us_ph=j*ws*psiM_ph; % stator voltage phasor
U_s=abs(us_ph)/sqrt(3); % RMS value phase voltage
%%%%%Data Simulink
TeM=0.5; %torque
iF=[0.5:0.25:2.25]; % selected field current values
%measured, from display, load angle (deg)
rhoM=[-53.13 -32.23 -23.58 -18.66 -15.47 -13.21 -11.54 -10.24];
%measured, from display, real power (W)
PM=157.08;
%measured, from display, reactive power (VA)
QM=[373.06 241.73 130.96 25.81 -76.84 -178.16 -278.66 -378.62];
%measured, from display, RMS stator current (A)
IM=[0.60 0.42 0.30 0.23 0.26 0.35 0.47 0.60];
%%%%%display measured results
figure (1)
subplot(3,1,1)
```

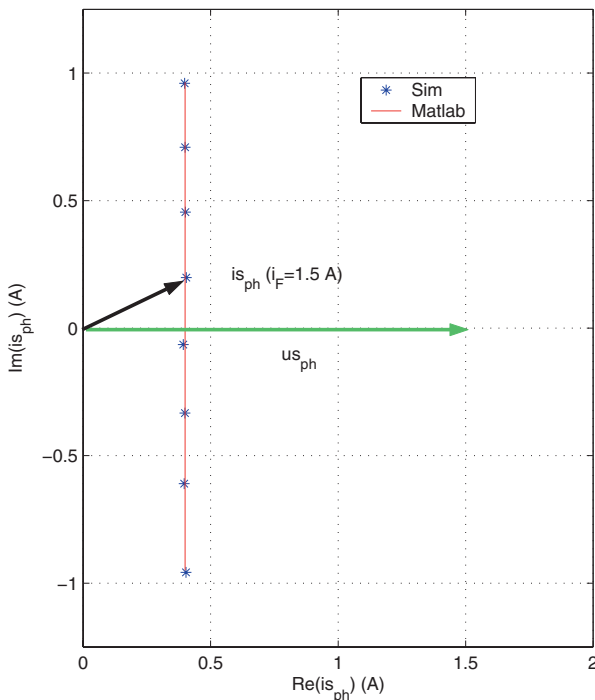


Figure 8.20. Simulink/MATLAB result: Blondel diagram, constant torque $T_e = 0.5\text{Nm}$

```

plot(iFM,IM,'*')
grid
xlabel('(a) i_F (A)')
ylabel('I_s (A)')
subplot(3,1,2)
plot(iFM,QM,'*')
grid
ylabel('Q_s (VA)')
xlabel('(b) i_F (A)')
subplot(3,1,3)
plot(iFM,rhoM,'*')
grid
ylabel('\rho_m (deg)')
xlabel('(c) i_F (A)')
%%%plot Blondel diagram
rhos=atan(-QM./PM); Is_phM=IM.*sqrt(3).*(cos(rhos)+j*sin(rhos));
ISRE=real(Is_phM); ISIM=imag(Is_phM); figure(2)
plot(ISRE,ISIM,'*')
grid
%%%Add theoretical results phasor analysis to plots
%Constant torque T=0.5 Nm
iF=[0.5:0.025:2.25]; % field current values for analysis
T_e=0.5;% Torque
rho_m=-asin(T_e./(psiM_hat.*iF)); % load angle rad
rho_mD=rho_m*180/pi; % load angle in degrees

```

```

rh=rho_m-pi/2;
is_ph=iM_ph-iF.*((cos(rh)+j*sin(rh));% stator current phasor calculation
I_s=abs(is_ph)/sqrt(3); % RMS value phase current
P=real(us_ph*conj(is_ph)); % real stator power
Q=imag(us_ph*conj(is_ph)); % reactive stator power
%%%plot results
figure(1)
subplot(3,1,1)
hold on
plot(iF, I_s,'r')
legend('Sim', 'MATLAB')
%%%%%%%%%%%%%
subplot(3,1,2)
hold on
plot(iF, Q,'r')
legend('Sim', 'MATLAB')
%%%%%%%%%%%%%
subplot(3,1,3)
hold on
plot(iF, rho_mD,'r')
legend('Sim', 'MATLAB')
%%%%%%%%%%%%%
figure(2)
hold on
isRE=real(is_ph); isIM=imag(is_ph);
figure(2)
plot(isRE,isIM,'r')
axis equal
axis([0 2 -1.25 1.25])
legend('Sim','MATLAB')
 xlabel('Re(is_{ph}) (A)')
 ylabel('Im(is_{ph}) (A)')

```

8.7.5 Tutorial 5

This tutorial considers a Caspoc implementation of the simplified synchronous machine model as represented by figure 8.5. The Caspoc simulation model as given in figure 8.21, shows the IRTF module together with an ‘alternative differentiator’ model (identified by way of the $j\omega$ in the differentiator module which calculates the voltage vector \vec{u}_s). The model parameters used in this tutorial are given in tutorial 1. Furthermore, the tutorial exercises as presented in the previous tutorials of this chapter can be directly carried out with this simulation. In addition, the Caspoc simulation contains a display module ‘scope 2’ which together with the module ‘ab-dq’ gives a Blondel representation of the stator current. By altering the load torque or field current the reader is able to observe the impact of these changes in the Blondel diagram and other output variables shown in figure 8.5.

8.7.6 Tutorial 6

The aim of this tutorial is to analyze the operation of a general synchronous machine model under load and a given shaft speed. A three-phase sinusoidal

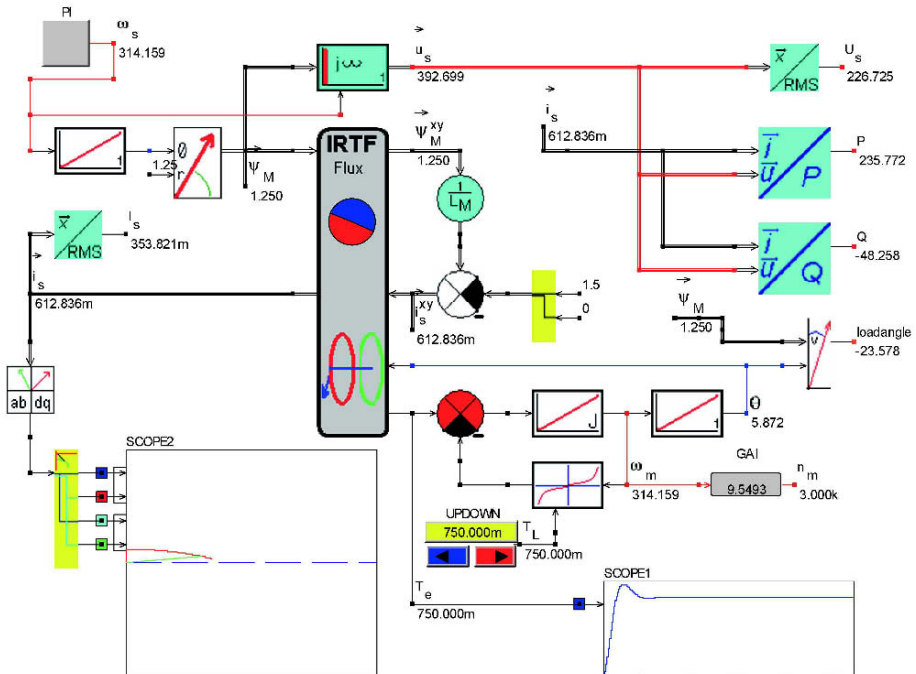


Figure 8.21. Caspoc simulation: synchronous machine, simplified model

variable frequency/ voltage source is required because it is assumed that the machine is at standstill at the start of the simulation. This means that a frequency and supply voltage ramp function will need to be implemented in order to achieve steady-state synchronous operation at a given speed. The practical alternative is to accelerate the machine mechanically (as a generator) to its required speed and then connect the stator windings to the three-phase supply. This process, referred to as synchronization, must be done carefully to ensure that the phase voltages from machine and supply are in phase and equal in magnitude before the connection is made.

For this example a four-pole permanent magnet machine is considered [Mohan, 2001] with the set of parameters as given in table 8.4.

The generic model according to figure 8.8 can be directly implemented in terms of a Simulink model as shown in figure 8.22. The Simulink IRTF submodule for this example needs to be version: *IRTF-current* (see figure 7.5(b)). The reason for this is that a stator based current vector and rotor based flux vector are to be used as inputs. Furthermore, a four-pole machine model is assumed, which means that two additional gain modules need to be added to the IRTF unit as discussed in section 7.3.1 on page 181. The machine in question was designed for operation at 6000rpm, however in this tutorial example two lower shaft

Table 8.4. Parameters for PM Synchronous motor

Parameters		Value
Stator inductance	L_s	1.365 mH
Stator resistance	R_s	0.416 Ω
PM flux amplitude	ψ_F	0.166 Wb
Inertia	J	3.4e-4 kgm ²
Pole pairs	p	2
Initial rotor speed	ω_m^o	0 rad/sec

Table 8.5. Speed, frequency and phase voltages synchronous machine

f_s (Hz)	n_m (rpm)	$U_s(V)$
40	1200	$40/\sqrt{3}$
60	1800	$60/\sqrt{3}$
200	6000	$200/\sqrt{3}$

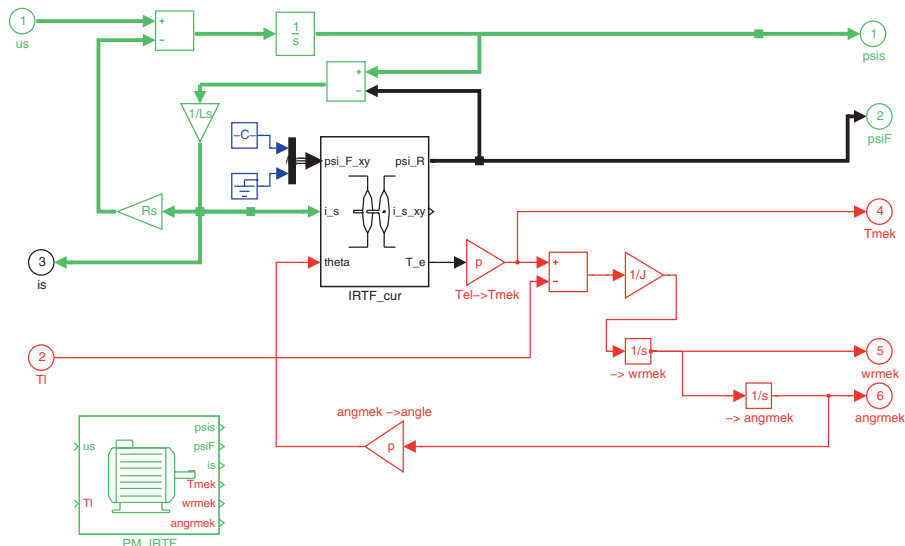


Figure 8.22. Simulink model: synchronous machine

speeds are used, for reasons to be discussed at a later stage. The relationship between RMS phase voltages, shaft speed and excitation frequencies for the two frequencies/shaft speeds considered here are given in table 8.5. Also shown in this table for comparison reasons is the rated speed/frequency entry.

The simulation model as given in figure 8.23 on page 224, shows the ‘star’ configured machine, which is connected to a variable frequency/voltage source.

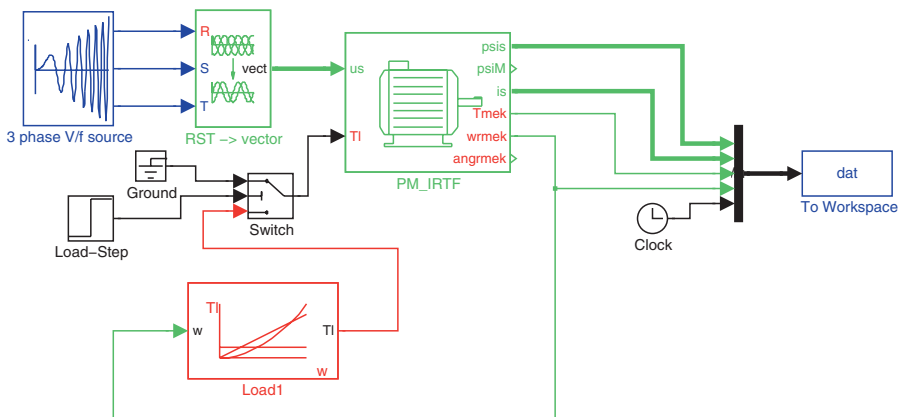


Figure 8.23. Simulink model: synchronous machine connected to V/f source

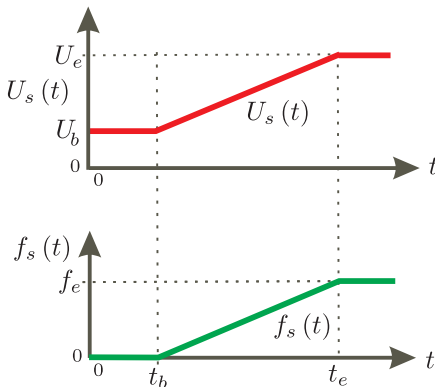


Figure 8.24. Simulation sequence for $U_s(t)$ and $f_s(t)$

The simulation sequence for the variables $U_s(t)$ and $f_s(t)$ is given in figure 8.24. with $U_b=7V$ and $t_b=25ms$. The values of t_e , f_e , U_e are linked with the selected steady-state frequencies $f_s=40, 60Hz$ as shown by table 8.6. The values shown are chosen to maintain the same voltage to frequency ratio during startup for both chosen steady-state excitation frequencies 40, 60Hz.

Table 8.6. startup settings, synchronous machine

f_e (Hz)	t_e (ms)	U_e (V)
40	200	$40/\sqrt{3}$
60	309	$60/\sqrt{3}$

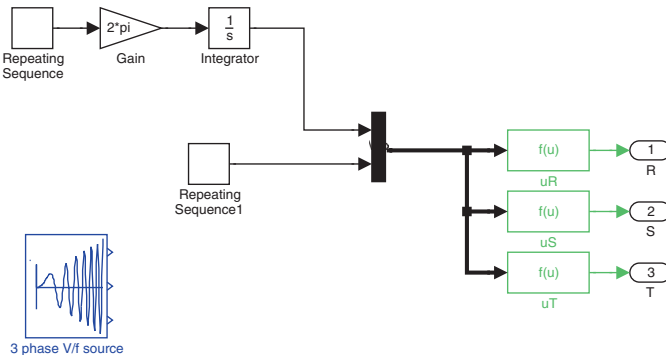


Figure 8.25. Simulink model:V/f three-phase excitation source

The modules which provide the three-phase excitation waveforms are shown in figure 8.25 on page 225. The two ‘repeating sequence’ modules implement the excitation condition as defined by figure 8.24. The inputs for these two modules are in the form of two ‘input’, ‘output’ arrays namely $[0 \ t_b \ t_e \ 0.5]$, $[0 \ 0 \ f_e \ f_e]$, for the ‘top’ module and $[0 \ t_b \ t_e \ 0.5]$, $[U_b \ U_b \ U_e \ U_e]$ for the ‘bottom’ module, as shown in figure 8.25. The entry 0.5 in these arrays represents the ‘run’ time of the simulation. The values for the array variables are given above.

The output waveforms which are generated by the three function modules are of the form

$$u_R = U_s \sqrt{2} \cos(2\pi f_s t) \quad (8.30a)$$

$$u_S = U_s \sqrt{2} \cos\left(2\pi f_s t - \frac{2\pi}{3}\right) \quad (8.30b)$$

$$u_T = U_s \sqrt{2} \cos\left(2\pi f_s t - \frac{4\pi}{3}\right) \quad (8.30c)$$

The load module shown in figure 8.23 as discussed in section 8.15, is used with a quadratic load torque/speed curve. The torque reference must be set to $T^{ref}=3.2\text{Nm}$, while the shaft speed reference $\omega^{ref} = \frac{2\pi n_s}{60} \text{ rad/s}$ must be chosen to match the frequency f_s being considered (see table 8.6). A switch also shown in figure 8.23, is used to disconnect the load torque at time mark $t=400\text{ms}$, which will allow us to examine the effect of suddenly disconnecting the load from the motor.

The dynamic simulation model according to figure 8.23 must be run for the two frequency cases considered. After each run, the magnitude of the stator current vector, shaft speed and torque are to be plotted as a function of time. An example of the results which should appear for these variables is given in figures 8.26, 8.27 and 8.28. An observation of these simulation results reveal some interesting details namely

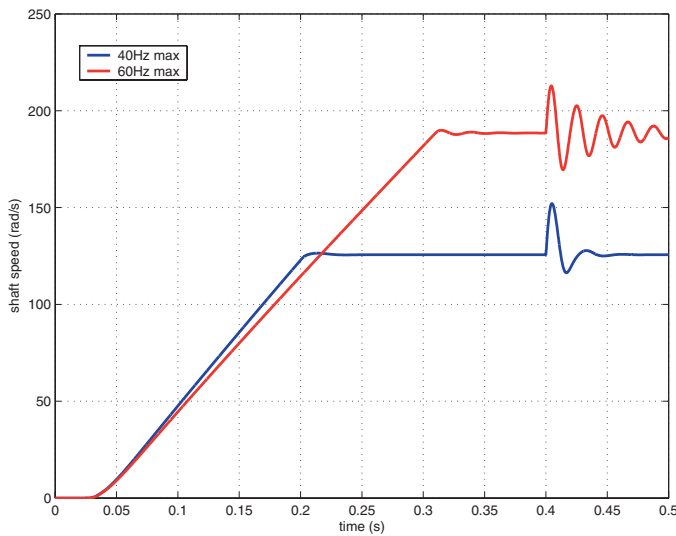


Figure 8.26. Simulink results: shaft speed, $\omega_m (t)$ rad/s

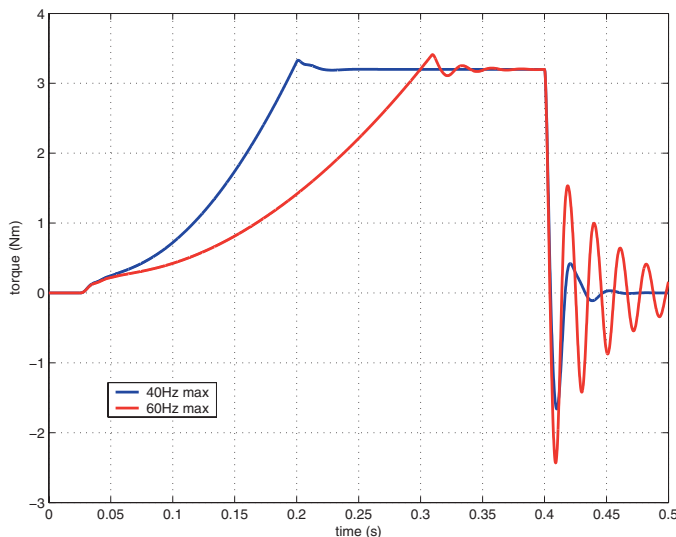


Figure 8.27. Simulink results: torque , $T_e (t)$ Nm

- The machine accelerates to the synchronous speed from standstill as required.
- The transition from load to no-load causes an oscillation in the speed, torque and current. These oscillations become more severe when the supply

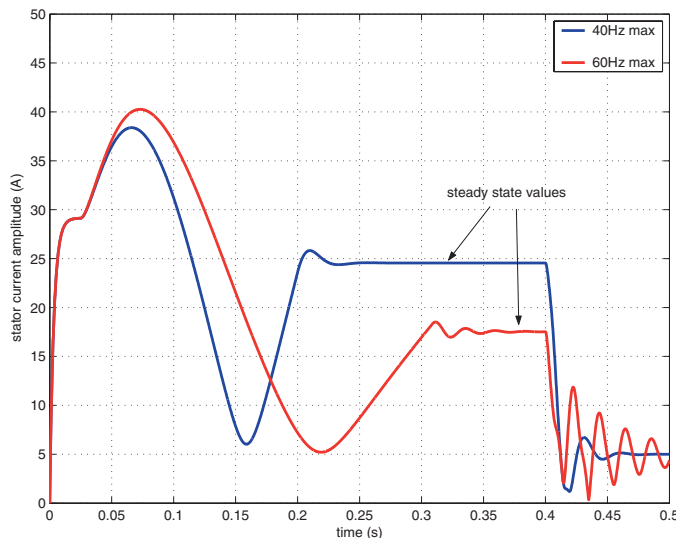


Figure 8.28. Simulink results: stator current magnitude, $|\vec{i}_s|(t)$ A

frequency/voltage is increased from 40Hz to 60Hz. Increasing the supply frequency/voltage to 200Hz is not possible under the current conditions. More advanced control techniques, or additional damping need to be implemented to achieve stable operation.

- The steady-state stator current amplitudes, under load, are equal to 24.5, 17.5A for the 40, 60Hz case studies respectively.

The m-file required to process the data from the simulation is as follows

m-file Tutorial 6, chapter 8

```
%Tutorial 6, chapter 8
%plot file for simulation data
wm=dat(:,6); % shaft speed rad/s
Te=dat(:,5); % shaft torque Nm
iss=sqrt(dat(:,3).^2+dat(:,4).^2); % current amplitude vector is
t=dat(:,7); %time vector
%%%%%
%plot data
close all
plot(t,wm)
xlabel('time (s)')
ylabel('shaft speed (rad/s)')
grid
figure
plot(t,Te)
xlabel('time (s)')
ylabel('torque (Nm)')
grid
```

```

figure
plot(t,is)
xlabel('time (s)')
ylabel('stator current amplitude (A)')
grid
axis([0 0.5 0 50])

```

8.7.7 Tutorial 7

This tutorial is concerned with a Caspoc simulation of the full synchronous machine as represented by the generic diagram shown in figure 8.8 on page 200. The machine parameter and excitation conditions are identical to those described in the previous Simulink based tutorial. Figure 8.29 shows the

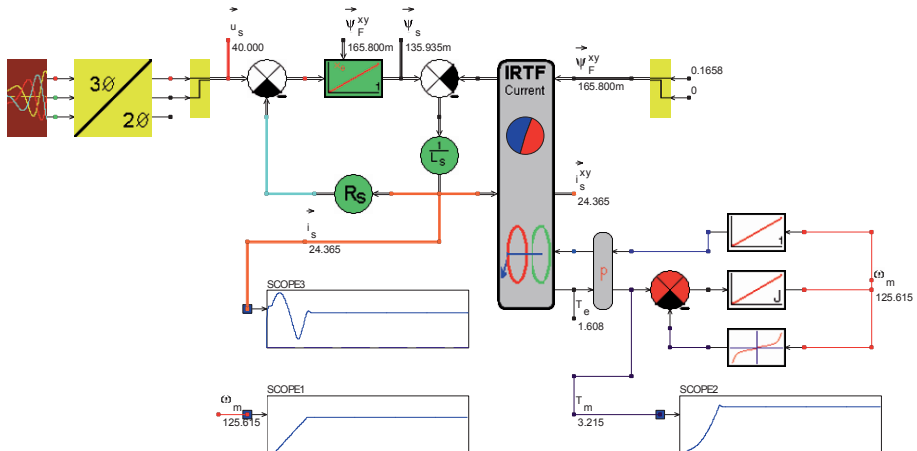


Figure 8.29. Caspoc simulation: synchronous machine, full model

Caspoc simulation model for the ‘40Hz’ case described in the previous tutorial. The stator based integrator module has a second input x_o which allows the user to specify the initial output state of the integrator. In this example the integrator should be set to $\vec{\psi}_F = (\psi_F \ 0)$ which implies that the initial stator flux vector is defined as $\vec{\psi}_s(0) = \vec{\psi}_F$. Consequently the flux error signal used in conjunction with the inductance module $1/L_s$ to calculate the stator current will be equal to zero at $t = 0$.

The ‘scope’ modules display (as function of time) the stator current amplitude $|\vec{i}_s(t)|$ (scope3), shaft speed (scope1) and shaft torque (scope2). As with previous Caspoc simulations the amplitude of the variables (as they appear when the simulation is stopped) are also shown.

8.7.8 Tutorial 8

It is instructive to examine the steady operation of the PM machine by way of a phasor analysis according to the theory presented in section 8.6.2. On the basis of this theory calculate the stator current magnitude for the machine under load with the two frequencies used for the dynamic simulation. Show your calculation in the form of an m-file. The results obtained from the MATLAB analysis should agree with the steady-state simulation values (obtained via Simulink/Caspoc) given earlier. In addition, use this m-file to plot the output power versus speed curve (see equation (8.25)) as shown in figure 8.14, with the parameters and variables given in table 8.4 and table 8.5 respectively. Note that the voltages given in table 8.5 represent phase (RMS) values. This means that the variable U_s must be multiplied by a factor $\sqrt{3}$ (because a power invariant space vector representation is used) in order to arrive at the space vector and corresponding phasor amplitude. An example of the results obtained are shown in figure 8.30. The m-file given below shows the steady-state analysis linked with this problem.

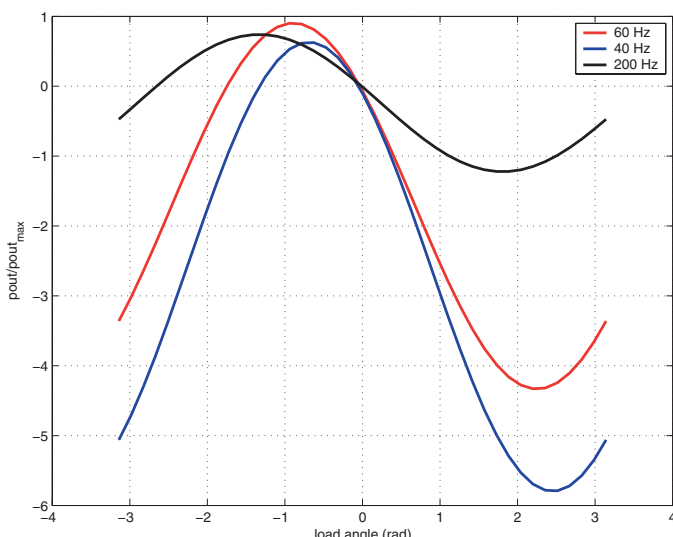


Figure 8.30. Simulink/MATLAB result: $p_{out}^n (\rho_m)$, 40, 60, 200Hz

m-file Tutorial 8, chapter 8

```
%Tutorial 8, chapter 8
%steady-state analysis under load 40, 60 and 200 Hz
clear all
close all
T_e=3.2;                                % load torque
Ls=1.365e-3;                             % stator inductance (H)
```

```

Rs=0.416; % stator resistance
psiF=0.0957*sqrt(3); % amplitude PM flux phasor

f(1)=40; % 40 case 1 , 60, case 2
f(2)=60;
f(3)=200
us_ph(1)=40; % amplitude voltage phasor 40 Hz case
us_ph(2)=60; % amplitude voltage phasor 60 Hz case
us_ph(3)=200; % amplitude voltage phasor 200 Hz case
rhom=[-pi:pi/20:pi];
isA=[];
pnA=[];
for i=1:3,
    freq=f(i);
    us_hat=us_ph(i); % amplitude voltage phasor
    ws=2*pi*freq; % stator frequency
    %% calculate load angle using Te(rho_m) eqn in theory
    wm= ws/2 ; % shaft speed 4-pole machine
    p_out=T_e*wm; pM_out=us_hat^2/(4*Rs);
    pN_out=p_out/pM_out; % normalized output power
    sig=ws*Ls/Rs; % electrical time constant machine
    gamma=atan(sig); kF=ws*psiF/us_hat;
    term1=kF*sin(gamma-pi/2)-pN_out/(4*kF)*sqrt(1+sig^2);
    rho_m=-gamma+pi/2+asin(term1); % load angle in use.
    %calculate current phasor
    is_ph=us_hat*(1-kF*(cos(rho_m)+j*sin(rho_m)))/(Rs+j*ws*Ls);
    is_hat=abs(is_ph);
    isA=[isA;is_hat];
    %% check powfig
    pn=-4*kF/sqrt(1+sig^2)*(sin(rhom+gamma-pi/2)-kF*sin(gamma-pi/2));
    pnA=[pnA;pn];
end
%plot results
pnD=pnA(1,:);
isAmpl1=isA(1)
plot(rhom,pnD,'b')
grid
hold on
pnD=pnA(2,:);
isAmpl2=isA(2)
plot(rhom,pnD,'r')
pnD=pnA(3,:);
isAmpl3=isA(3)
plot(rhom,pnD,'k')
legend('40 Hz','60 Hz', '200 Hz')
xlabel('load angle (rad)')
ylabel('normalized output power')

```

Chapter 9

VOLTAGE SOURCE CONNECTED ASYNCHRONOUS (INDUCTION) MACHINES

9.1 Introduction

The induction machine is by far the most commonly used machine around the globe. Induction machines consume approximately one third of the energy used in industrialized countries. Consequently this type of machine has received considerable attention in terms of its design and handling.

The induction machine is one of the older electric machines with its invention being attributed to Tesla, then working for Westinghouse, in 1888. However, as with most great inventions there were many contributors to the development of this machine. The fundamental operation principle of this machine is based on the magnetic induction principle discovered by Faraday in 1831.

In this chapter we will look at this type of machine in some detail. As with the synchronous machine a simple symbolic and generic diagram will be discussed, which in turn is followed by a more extensive dynamic model of this type of machine. Finally, a steady-state analysis will be discussed where the role of the machine parameters will become apparent.

9.2 Machine configuration

The stator with its three-phase winding as given in figure 8.1 on page 194, is used to develop a rotating magnetic field in exactly the same way as realized with the synchronous machine.

The rotor of an induction machine usually consists of a steel laminated rotor stack as shown in figure 9.1. The metal shaft is through the centre of this stack. The rotor stack is provided with slots around its circumference which house the rotor bars of the so-called squirrel cage. This cage, which consists of rotor bars attached to end rings, is also shown (without the rotor stack) in figure 9.1. The cage can be copper or die-cast in aluminium [Hughes, 1994].

A recent development in this context has been the introduction of a copper coating on the rotor designed to replace the traditional cage concept. In some cases aluminium fan blades are attached to the end rings to serve as a fan for cooling the rotor. The cage acts as a three-phase sinusoidally distributed short-circuited winding which has a finite rotor resistance [Hughes, 1994]. The number of turns of these equivalent rotor windings can be chosen at random, in which case it is prudent to set the number of turns equal to that of the stator, i.e. $n_r = n_s$. This simplifies the equation set (7.23) which corresponds with the symbolic generalized two-phase machine model.

Some induction machines have a wound rotor provided with a three-phase winding where access to the three-phases is provided via brushes/slirings (similar to the type used for the synchronous machine). This type of machine known as a ‘slirring’ machine, allows us to influence the rotor circuit e.g. to alter the rotor resistance (and therefore the operating characteristics) by adding external rotor resistance.

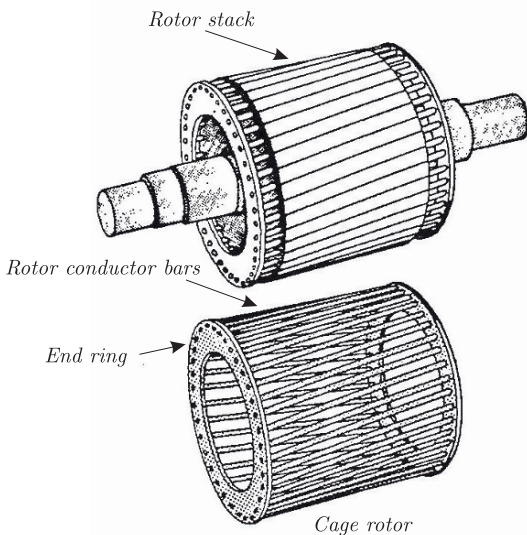


Figure 9.1. Cage rotor for asynchronous machine

The squirrel cage type rotor is very popular given its robustness and is widely used in a range of industrial applications.

9.3 Operating principles

The principles are again discussed with the aid of section 7.3 on page 178. This type of machine has no rotor excitation hence the current source shown in figure 7.9 is removed and the rotor is connected to a resistance R_r . This resistance is usually the resistance of the rotor winding itself. The rotor current is in this case determined by the induced voltage \vec{e}_m^{xy} and the rotor resistance

R_r , which with the aid of equation (7.19) on page 179 leads to

$$\vec{i}^{xy} = \frac{j(\omega_s - \omega_m)}{R_r} \vec{\psi}_m^{xy} \quad (9.1)$$

The corresponding torque produced by this machine is found using equations (7.13) and (7.16) together with equation (9.1), which gives

$$T_e = \frac{\hat{\psi}_m^2}{R_r} (\omega_s - \omega_m) \quad (9.2)$$

In which $\hat{\psi}_m$ is the magnitude or peak value of the flux vector. The term $(\omega_s - \omega_m)$ is referred to as the ‘slip’ rotational frequency and is in fact the rotor rotational frequency ω_r . The term ‘asynchronous’ follows from the operating condition that torque can only be produced when the rotor speed is *not* synchronous with the rotating field. This condition is readily observed from equations (9.1), and (9.2) which state that there is no rotor current and hence no torque in case $\omega_r = (\omega_s - \omega_m) = 0$. When the machine is operating under no-load conditions, the shaft speed will in the ideal case be equal to ω_s . When a load torque is applied the machine speed reduces and the voltage $|\vec{e}_m|$ increases, because the slip rotational frequency ω_r increases. A higher voltage $|\vec{e}_m|$ leads to a higher rotor current component i_{torque} (see figure 9.2), which acts together with the flux vector to produce a torque to balance the load torque.

Additional insight into the operation principles of this machine is obtained by making use of the space vector diagram shown in figure 9.2. The diagram stems from the generalized diagram (see figure 7.10). The generalized diagram has been redrawn to correspond to the induction machine operating under motoring conditions, i.e. the rotational speed $0 < \omega_m < \omega_s$. Shown in figure 9.2 is the rotating flux vector $\vec{\psi}_m$ which is responsible for the (in the rotor) induced

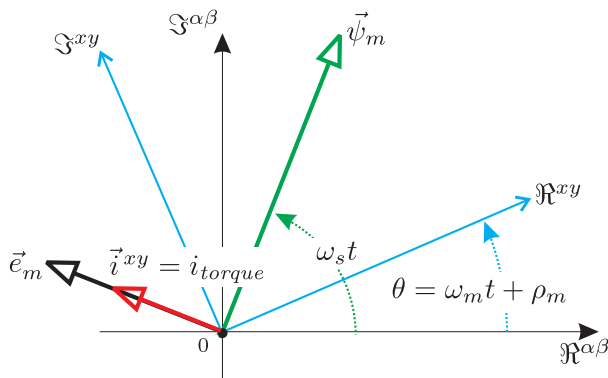


Figure 9.2. Space vector diagram for asynchronous machine

voltage, represented by the vector \vec{e}_m . Observe that both vectors \vec{e}_m and \vec{i} (given here in stator coordinates) rotate synchronous with the flux vector. Hence the current and flux vector shown in this example are orthogonal and stationary with respect to each other, which is the optimum situation in terms of torque production. It is noted that the current vector \vec{i}^{xy} rotates with respect to the rotor at a speed $\omega_s - \omega_m$. The rotor rotates at speed ω_m , hence the current vector \vec{i} has an angular frequency (with respect to the stator) of ω_s . When a higher load torque is applied the machine slows down which means that the induced voltage in the rotor increases, which in turn leads to a higher rotor current and larger torque to match the new load torque.

9.4 Symbolic model, simplified version

The equations of the model according to figure 7.15 is considered here without the presence of leakage inductance, magnetizing inductance or stator resistance. The revised model as given in figure 9.3, shows that the rotor windings are short-circuited, hence the resistance present in this circuit is the rotor resistance R_R . A rotating magnetizing flux vector $\vec{\psi}_M = \hat{\psi}_M e^{j\omega_s t}$ is assumed as input for our model. This rotating field is established as a result of the machine being connected to a three-phase voltage supply with angular frequency ω_s (rad/sec). The equation set which corresponds with figure 9.3 is of the form

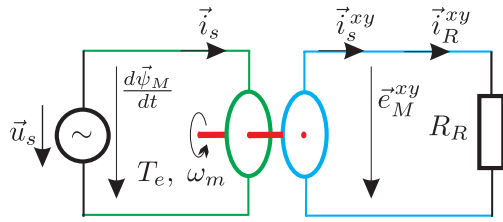


Figure 9.3. Voltage source connected asynchronous machine, simplified version

$$\vec{e}_M^{xy} = \frac{d\vec{\psi}_M}{dt} \quad (9.3a)$$

$$\vec{i}_R^{xy} = \frac{\vec{e}_M^{xy}}{R_R} \quad (9.3b)$$

$$\vec{i}_s^{xy} = \vec{i}_R^{xy} \quad (9.3c)$$

$$T_e - T_l = J \frac{d\omega_m}{dt} \quad (9.3d)$$

$$\omega_m = \frac{d\theta}{dt} \quad (9.3e)$$

9.4.1 Generic model

The generic representation of the asynchronous machine in its present form is given in figure 9.4. The IRTF and load torque sub-modules are identical

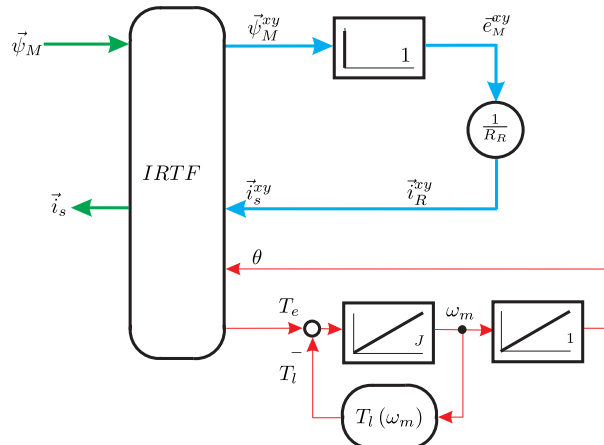


Figure 9.4. Generic representation of simplified asynchronous machine model corresponding to figure 9.3 with mechanical load

to those used for the synchronous machine (see figure 8.5). This means that the IRTF model calculates the torque on the basis of the flux vector provided from the stator side and the stator current vector which has been created on the rotor side, i.e. use is made of an ‘IRTF-flux’ module. The model according to figure 9.4 uses a differentiator to generate the induced voltage vector from the flux vector. From a didactic perspective this is useful as it shows the mechanism of torque production and the formation of the stator current vector. However, in simulations the use of a differentiator is not preferred given that such models are prone to errors. It will be shown that we can in most cases avoid the use of differentiators. In the tutorial at the end of this chapter a steady-state type analysis will be considered which is based on figure 9.4. In that case the differentiator function is created with an alternative ‘differentiator’ module (see figure 6.8).

9.5 Generalized symbolic model

The symbolic and generic model of the simplified machine version as discussed in the previous section, provides a basic understanding.

To be able to understand the behaviour of the machine it is important to consider a more general symbolic model as given in figure 9.5. This new model represents a reoriented version of the generalized machine shown in figure 7.15, given that the magnetizing inductance has been relocated to the rotor side.

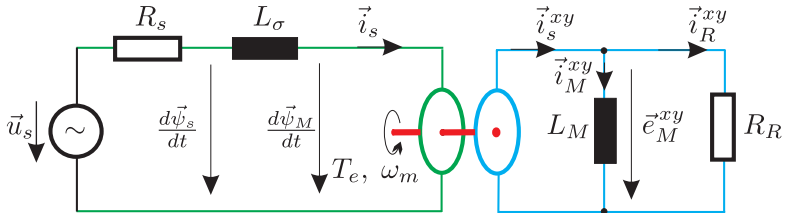


Figure 9.5. Generalized asynchronous (induction) machine model

The equation set which corresponds to figure 9.5 is of the form

$$\vec{u}_s = R_s \vec{i}_s + \frac{d\vec{\psi}_s}{dt} \quad (9.4a)$$

$$\vec{\psi}_s = L_\sigma \vec{i}_s + \vec{\psi}_M \quad (9.4b)$$

$$\vec{i}_M^{xy} = \vec{i}_s^{xy} - \vec{i}_R^{xy} \quad (9.4c)$$

$$\vec{\psi}_M^{xy} = L_M \vec{i}_M^{xy} \quad (9.4d)$$

$$\vec{e}_M^{xy} = \frac{d\vec{\psi}_M^{xy}}{dt} \quad (9.4e)$$

$$\vec{e}_M^{xy} = R_R \vec{i}_R^{xy} \quad (9.4f)$$

The torque for this machine is given by equation (7.28g) which with the aid of equation (9.4b) can also be written as

$$T_e = \Im \left\{ \vec{\psi}_s^* \vec{i}_s \right\} \quad (9.5)$$

In the sequel to this section the conversion from a three- to a two-inductance machine model as discussed in section 7.4 is reconsidered. The reason for this is that a number of textbooks and machine manufacturers define squirrel cage machine models in terms of the parameters: $L_{\sigma s}$, $L_{\sigma r}$, L_m and R_r as introduced in equation (7.23). Furthermore, the assumption of a unity turns ratio $n_s = n_r$ is made (as discussed in the introduction to this chapter). The calculation of the parameters L_M , L_σ and R_R as required in for example equation (9.4), proceeds with the aid of equation (7.23) and equation (7.27).

9.5.1 Generic induction machine model

The development of a generic dynamic model as shown in figure 9.6(a) on page 237 (with zero stator resistance) is directly based on equation (9.4). This generic diagram builds directly on the simplified model given in figure 9.4. The model shown in figure 9.6(a) also contains a differentiator model which is undesirable for dynamic simulations. An improved representation of the generic model according to figure 9.6(a) is possible which avoids the use of a

numerically undesirable differentiator. This model as shown in figure 9.6(b) is preferable for dynamic simulation of induction machines for reasons mentioned above. However, the model becomes untenable when considering a hypothetical machine without leakage inductance or infinite rotor resistance.

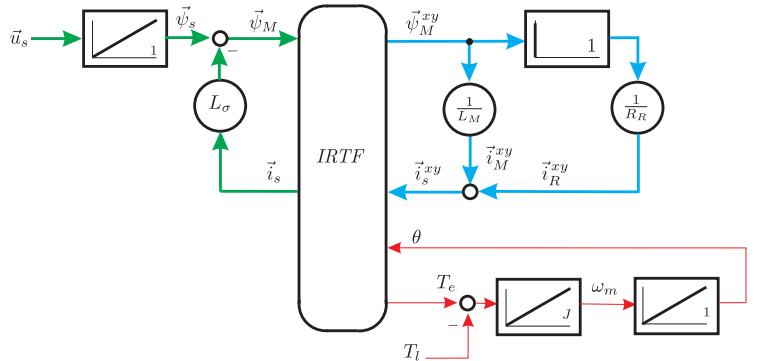
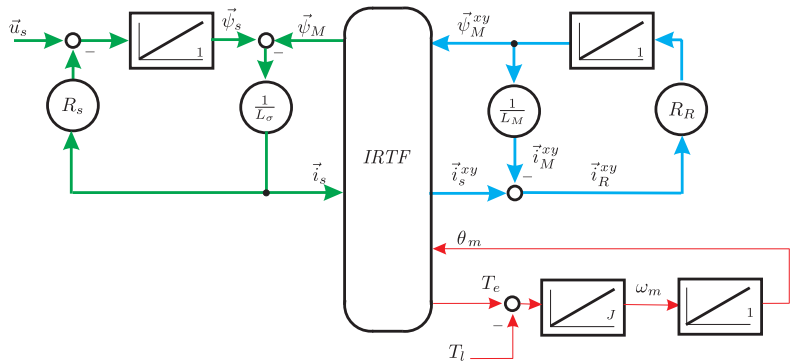
(a) Differentiator based dynamic model without R_s (b) Integrator based dynamic model with R_s

Figure 9.6. Generic asynchronous (induction) machine dynamic models corresponding to figure 9.5

9.6 Steady-state analysis

The steady-state characteristics of the asynchronous machine are studied with the aid of figure 9.5. The stator is again connected to a three-phase sinusoidal supply which is represented by the space vector $\vec{u}_s = \hat{u}_s e^{j\omega_s t}$, hence $\underline{u}_s = \hat{u}_s$. The basic characteristics of the machine relate to the stator current end point locus of the machine in phasor form (when varying the shaft speed) and the torque speed curve. To arrive at a phasor type representation the space vector equations must be rewritten in terms of phasors. For example, the rotor flux on

the stator and rotor side of the IRTF are of the form

$$\vec{\psi}_M = \underline{\psi}_M e^{j\omega_s t} \quad (9.6a)$$

$$\vec{\psi}_M^{xy} = \underline{\psi}_M e^{j(\omega_s t - \theta)} \quad (9.6b)$$

where θ is equal to $\omega_m t$ (constant speed). Use of equations (9.4) and (9.6) leads to the following phasor based equation set for the machine

$$\underline{u}_s - \underline{\epsilon}_M = \underline{i}_s R_s + j\omega_s L_\sigma \underline{i}_s \quad (9.7a)$$

$$\underline{\epsilon}_M = j\omega_s \underline{\psi}_M \quad (9.7b)$$

$$\underline{\epsilon}_M^{xy} = j(\omega_s - \omega_m) \underline{\psi}_M \quad (9.7c)$$

$$\underline{i}_R = \frac{\underline{\epsilon}_M^{xy}}{R_R} \quad (9.7d)$$

$$\underline{\psi}_M = L_M (\underline{i}_s - \underline{i}_R) \quad (9.7e)$$

Elimination of the flux phasor from equations (9.7b) and (9.7c) leads to an expression for the airgap EMF on the stator and rotor side of the IRTF namely

$$\underline{\epsilon}_M^{xy} = \underline{\epsilon}_M s \quad (9.8)$$

where ‘s’ is known as the slip of the machine and is (for a two-pole machine) given by

$$s = 1 - \frac{\omega_m}{\omega_s} \quad (9.9)$$

The slip according to equation (9.9) is simply the ratio between the rotor rotational frequency $\omega_r = \omega_s - \omega_m$ (as apparent on the rotor side of the IRTF) and the stator rotational frequency ω_s . Three important slip values are introduced namely

- Zero slip: $s = 0$, which corresponds to synchronous speed operation, i.e. $\omega_m = \omega_s$.
- Unity slip: $s = 1$, which corresponds to a locked rotor, i.e. $\omega_m = 0$.
- Infinite slip: $s = \pm\infty$, which according to equation (9.9) corresponds to infinite shaft speed or zero rotational stator frequency (DC excitation). This slip value is for $\omega_s \neq 0$ not practically achievable but this operating point is of relevance, as will become apparent at a later stage.

The rotor current phasor may be conveniently rewritten in terms of the slip parameter by making use of equations (9.7d) and (9.8) which gives

$$\underline{i}_R = \frac{\underline{\epsilon}_M}{\left(\frac{R_R}{s}\right)} \quad (9.10)$$

The rotor current is according to equation (9.10) determined by the ratio of the airgap EMF \underline{e}_M and a slip dependent resistance $\left(\frac{R_R}{s}\right)$. At slip zero its value will be ∞ , which corresponds to zero current as is expected at synchronous speed, given that the rotor EMF on the rotor side \underline{e}_M^{xy} will be zero. At standstill ($s = 1$) its value is simply R_R .

The development of the basic machine characteristics in the form of the stator current phasor as function of slip and the torque/slip curve are presented on a step by step basis. This implies that gradually more elements of the model in figure 9.5 are introduced in order to determine their impact on the machine characteristics. The key elements which affect the operation of the machine in steady-state are the rotor resistance R_R and the leakage inductance L_σ . We will initially consider the machine with zero stator resistance, infinite magnetizing inductance and firstly without leakage inductance.

9.6.1 Steady-state analysis with zero leakage inductance and zero stator resistance

A model with zero leakage inductance and zero stator resistance can be represented by figure 9.6(a), assuming $L_\sigma = 0$. Observation of figure 9.6(a) and phasor equation set (9.7), (9.8) and (9.10) learns that the stator current phasor and EMF vector are given as $\underline{i}_s = \underline{i}_R$ and $\underline{e}_M = \hat{u}_s$ respectively. Furthermore, the stator current phasor as function of the slip may be written as

$$\underline{i}_s = \frac{\hat{u}_s}{\left(\frac{R_R}{s}\right)} \quad (9.11)$$

An observation of equation (9.11) learns that the phasor current can be calculated using the equivalent circuit shown in figure 9.7. The steady-state torque may

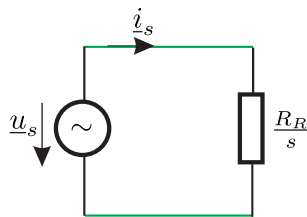


Figure 9.7. Equivalent circuit of an asynchronous machine with zero stator impedance and voltage source in steady-state

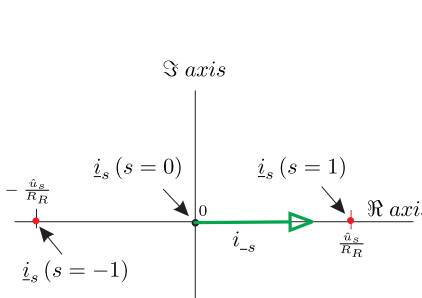
be found using equation (7.28g) where the space vector variables are replaced by the equivalent phasor quantities. This implies that the torque is of the form

$$T_e = \Im \left\{ \underline{\psi}_M^* \underline{i}_s \right\} \quad (9.12)$$

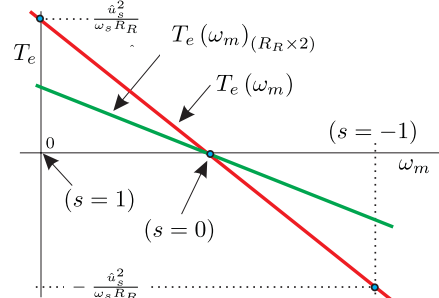
Use of equations (9.11) and (9.7b) with (9.12) leads to the following torque slip expression for the machine in its current simplified form

$$T_e = \frac{\hat{u}_s^2 s}{\omega_s R_R} \quad (9.13)$$

A graphic illustration of the stator current phasor and torque versus speed characteristic is given in figure 9.8. The current phasor will in this case be either



(a) Stator current phasor



(b) Torque versus speed

Figure 9.8. Steady-state characteristics of voltage source connected asynchronous machine with $R_s = 0$, $L_\sigma = 0$ and $L_M = \infty$, according to figure 9.7

in phase or π rad out of phase, with respect to the supply phasor $\underline{u}_s = \hat{u}_s$. The ‘in phase’ case will occur under motoring conditions, i.e. T_e and ω_m have the same polarity. It is noted that a torque sign change will always occur at $s = 0$, while a shaft speed reversal will take place at $s = 1$. This means that motor operation is confined to the slip range $0 \leq s \leq 1$. Note that generation (in for example wind turbine applications) starts when the slip becomes negative.

Shown in figure 9.8(a) are three current phasor end points which correspond to the slip conditions $s = -1, 0, 1$. The torque versus speed curve as given in figure 9.8(b) is according to equation (9.13) a linear function of which the gradient is determined by (among others) the rotor resistance R_R . The effect of doubling this resistance value on the torque speed curve is also shown in figure 9.8(b) by way of a ‘green’ line. Increasing the rotor resistance leads to a torque/speed curve which is less ‘stiff’, i.e. as a result of a certain mechanical load variation, the shaft speed will vary more.

9.6.2 Steady-state analysis with leakage inductance

The simplified R_R -based model (figure 9.7) is now expanded by adding the leakage inductance parameter L_σ . Under these revised circumstances the current phasor can according to equation (9.7) be written as

$$\underline{u}_s - \underline{e}_M = j\omega_s L_\sigma \underline{i}_s \quad (9.14)$$

The stator current is also defined by equation (9.10) given that $\underline{i}_R = \underline{i}_s$. Substitution of this expression into equation (9.14) gives

$$\underline{i}_s = \frac{\hat{u}_s}{\frac{R_R}{s} + j\omega_s L_\sigma} \quad (9.15)$$

The equivalent circuit which corresponds with equation (9.15) is shown in figure 9.9. The steady-state torque is found using equation (9.12) which requires

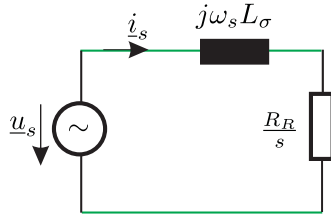


Figure 9.9. Equivalent circuit of an asynchronous machine ($R_s = 0$, $L_\sigma > 0$) and voltage source in steady-state

access to the stator current phasor \underline{i}_s as defined by equation (9.15). The magnetizing flux $\underline{\psi}_M$ is found using equation (9.7a) with $R_s = 0$ and equation (9.7b) which gives

$$\underline{\psi}_M = \frac{\hat{u}_s}{j\omega_s} - L_\sigma \underline{i}_s \quad (9.16)$$

Subsequent evaluation of equations (9.15) and (9.16) with equation (9.12) gives after some manipulation the following expression for the steady-state torque

$$T_e = \frac{\hat{u}_s^2}{\omega_s} \frac{\frac{R_R}{s}}{\left(\frac{R_R}{s}\right)^2 + (\omega_s L_\sigma)^2} \quad (9.17)$$

In order to gain an understanding of the torque versus slip function it is helpful to introduce a normalized form of equation (9.17) namely

$$T_e^n = 2 \frac{\frac{s}{\hat{s}}}{1 + \left(\frac{s}{\hat{s}}\right)^2} \quad (9.18)$$

The normalization introduced is of the form $T_e^n = \frac{T_e}{\hat{T}_e}$ where $\hat{T}_e = \frac{\hat{u}_s^2}{2\omega_s^2 L_\sigma}$.

Furthermore, a parameter $\hat{s} = \frac{R_R}{\omega_s L_\sigma}$ is introduced which is known as the pull-out slip value. Note that the pull-out slip \hat{s} is *not* a peak value of the slip s itself, rather it refers to the slip values $s = \pm \hat{s}$ where the highest attainable torque or so-called ‘pull-out’ torque values of the machine are reached for the model discussed here. It is helpful to recall that the slip is defined as $s = \frac{\omega_r}{\omega_s}$, which means that the highest attainable torque and corresponding pull-out slip value is reached when the rotor angular frequency $\omega_r = \frac{R_R}{L_\sigma}$. The extremes

of equation (9.18) as function of the slip s may be found by differentiation of said expression with respect to the slip and by zeroing the result. Alternatively, the normalized torque/slip function can be examined for two slip regions as indicated in equation (9.19)

$$\text{for } |s| \ll \hat{s} \quad T_e^n \simeq 2 \frac{s}{\hat{s}} \quad (9.19a)$$

$$\text{for } |s| \gg \hat{s} \quad T_e^n \simeq 2 \frac{\hat{s}}{s} \quad (9.19b)$$

The intersection of the two torque/slip functions indicated in equation (9.19) leads to the following two slip values, which correspond to a maximum and minimum torque value of \hat{T}_e and $-\hat{T}_e$ respectively.

$$s = \pm \hat{s} \quad (9.20)$$

A normalization of the stator current phasor (equation (9.15)) is also helpful in terms of understanding the slip dependency. The normalized stator current phasor $\underline{i}_s^n = \underline{i}_s / \left(\frac{\hat{u}_s}{\omega_s L_\sigma} \right)$ can with the aid of equation (9.15) and $\hat{s} = \frac{R_R}{\omega_s} L_\sigma$ be written as

$$\underline{i}_s^n = \frac{\frac{s}{\hat{s}}}{1 + j \frac{s}{\hat{s}}} \quad (9.21)$$

A graphical representation of the normalized stator current locus versus slip is given in figure 9.10(a) with $\hat{s} = \frac{1}{2}$. It should be kept in mind that the selected pull-out slip value of 0.5 was chosen to clearly show the low and high slip regions given in equation (9.19). In reality the pull-out slip values of squirrel cage based machines are considerably smaller. The stator current locus is circular as was determined by Heyland in 1894, hence these diagrams are commonly referred to as ‘Heyland diagrams’. The process of verifying that the locus is a circle may be initiated by introducing the variables $x = \Re\{\underline{i}_s^n\}$, $y = \Im\{\underline{i}_s^n\}$ in equation (9.21) which leads to

$$x + jy = \frac{\xi}{1 + j\xi} \quad (9.22)$$

with $\xi = \frac{s}{\hat{s}}$. Equating the real and imaginary terms in equation (9.22) gives

$$x = \xi(y + 1) \quad (9.23a)$$

$$0 = y + \xi x \quad (9.23b)$$

Eliminating the slip dependent term ξ in equation 9.23 gives the following expression

$$x^2 + \left(y + \frac{1}{2} \right)^2 = \left(\frac{1}{2} \right)^2 \quad (9.24)$$

which indeed represents a circle with its origin at $(0, -\frac{1}{2})$ and radius $\frac{1}{2}$.

A graphical representation of the normalized torque versus shaft speed is given in figure 9.10(b) for the slip range $-1 \leq s \leq 1$ and $\hat{s} = \frac{1}{2}$ ('blue' curve). A second torque/slip curve is also shown ('green' curve) which corresponds to a machine which has a rotor resistance value that is 1.5 times larger than the first. Some interesting observations may be drawn from the basic characteristics

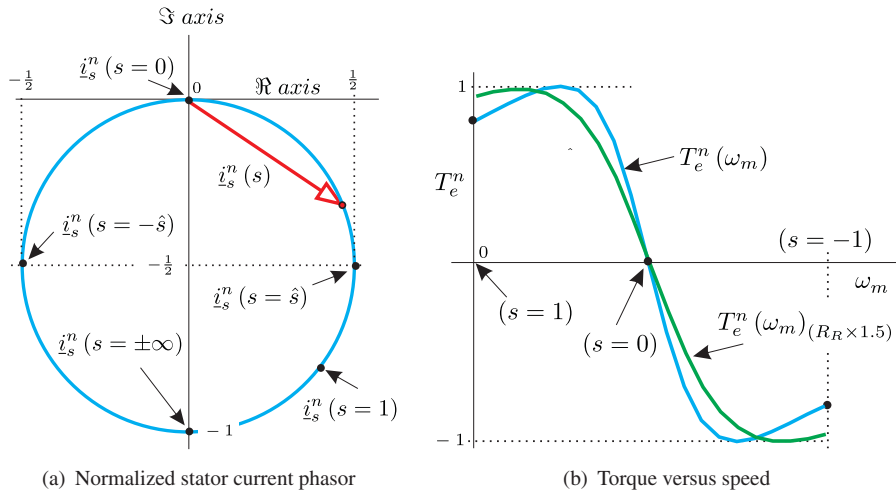


Figure 9.10. Steady-state characteristics of voltage source connected asynchronous machine with $R_s = 0$, $L_\sigma > 0$ and $L_M = \infty$, according to figure 9.9

according to figure 9.10 namely

- The introduction of leakage inductance has a significant impact on the characteristics of the machine as may be concluded by comparing figure 9.10 with figure 9.8.
- Variations of the rotor resistance R_R affect among others the value of the pull-out slip value \hat{s} and the gradient of the torque/speed curve in the low slip region. The peak torque \hat{T}_e is *not* affected by these changes. For a 'slipring' type induction machine it is possible to vary the rotor resistance by prudently adding external resistance to improve the starting torque.
- The peak torque value is dependent on the ratio $\frac{\hat{u}_s}{\omega_s}$. If this ratio is kept constant the torque/speed curves may be moved horizontally along the horizontal axis by changing ω_s without affecting the peak torque value. Such drives are known as 'V/f' drives. Note that the pull-out slip value is inversely proportional to ω_s , which means that the peak (motoring) torque is found at an ω_m value which is R_R/L_σ (rad/s) lower than the synchronous value $\omega_m = \omega_s$. In practical V/f drives, provision needs to be made to

compensate for the change in ψ_s due to the voltage drop across the stator resistance. In the present model configuration the stator resistance is set to zero.

- The Heyland diagram shows motor and generator regions. In addition it shows how the phase angle between voltage phasor $\underline{u}_s = \hat{u}_s$ and stator current phasor changes as function of the slip. For low slip operation the power factor (for the machine in its present form) approaches unity.

The machine model with leakage inductance and rotor resistance represents the basic model in terms of showing the fundamental operating principles of the machine.

9.6.3 Steady-state analysis with leakage inductance and stator resistance

The machine model with leakage inductance and rotor resistance is now extended to include stator resistance. The terminal equation according to (9.14) must be revised and is now of the form

$$\underline{u}_s - \underline{e}_M = (R_s + j\omega_s L_\sigma) \underline{i}_s \quad (9.25)$$

Use of equation (9.25) and $\underline{i}_R = \underline{i}_s$ with equation (9.10) gives

$$\underline{i}_s = \frac{\hat{u}_s}{\left(R_s + \frac{R_R}{s} \right) + j\omega_s L_\sigma} \quad (9.26)$$

The equivalent circuit which corresponds with equation (9.26) is shown in figure 9.11. A normalization of the stator current according to $\underline{i}_s^n = \underline{i}_s / \left(\frac{\hat{u}_s}{\omega_s L_\sigma} \right)$,

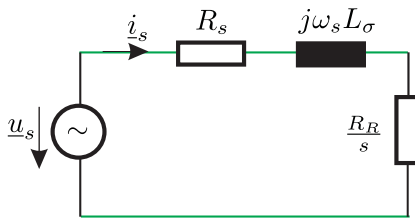


Figure 9.11. Equivalent circuit of an asynchronous machine with both R_s and L_σ , voltage source, steady-state

as introduced to obtain equation (9.21), is also applied to equation (9.26) which gives, with pull-out slip \hat{s} as defined on page 241

$$\underline{i}_s^n = \frac{\frac{\hat{s}}{\hat{s}}}{\left(1 + r \frac{\hat{s}}{\hat{s}} \right) + j \frac{\hat{s}}{\hat{s}}} \quad (9.27)$$

where the parameter r is introduced which is defined according to equation (9.28) namely

$$r = \frac{R_s}{R_R} \hat{s} \quad (9.28)$$

Note that equation (9.27) reverts back to equation (9.21) in case the stator resistance is set to zero. The Heyland diagram for the revised machine is again a circle as may be deduced by evaluation of equation (9.27) and by introducing the variables $x = \Re\{i_s^n\}$, $y = \Im\{i_s^n\}$, as was discussed for the previous case.

In this case the circle in the complex plane is again centered at $(0, -\frac{1}{2})$ and has again a radius of $\frac{1}{2}$ as may be observed from figure 9.12(a). The circle has not changed in size or position relative to the origin of the complex plane when compared to the previous case (see figure 9.10(a)). The various operating regions on the circle have changed. For example, the motor operating region $0 \leq s \leq 1$ is now confined to a smaller section of the circle. In other words the non-linear slip scale along the circle has changed as a result of adding the stator resistance to the model. Furthermore, the infinite slip point has moved into the fourth quadrant. This means that the torque slip curve will no longer be symmetrical with respect to the zero slip point, as will become apparent shortly.

The torque versus slip equation of the revised machine is calculated with the aid of equations (9.12), (9.7b) and (9.10) with $i_R = i_s$. Note that this condition is still applicable, given that the magnetizing inductance L_M is still assumed to be infinite at this stage. This means that the torque can be written as $T_e = \frac{|i_s|^2}{\omega_s} \frac{R_R}{s}$ which after substitution of equation (9.26) gives

$$T_e = \frac{\hat{u}_s^2}{\omega_s} \frac{\frac{R_R}{s}}{\left(R_s + \frac{R_R}{s}\right)^2 + (\omega_s L_\sigma)^2} \quad (9.29)$$

Normalization of equation (9.29) as undertaken for the previous case (equation (9.18)) leads to

$$T_e^n = 2 \frac{\frac{s}{\hat{s}}}{\left(1 + r \frac{s}{\hat{s}}\right)^2 + \left(\frac{s}{\hat{s}}\right)^2} \quad (9.30)$$

A graphical representation of equation (9.30) as function of shaft speed ω_m with $\frac{R_s}{R_R} = 1$ (which corresponds to $r = \frac{1}{2}$), with $\hat{s} = \frac{1}{2}$, as used previously is given in figure 9.12(b). The torque characteristic shown in figure 9.12(b) has, as may be expected, a maximum and minimum value which correspond to the slip values

$$s = \pm \frac{\hat{s}}{\sqrt{1 + r^2}} \quad (9.31)$$

It is emphasized that the slip values which correspond to the peak torque values (as given by equation (9.31)) are in this new model no longer equal to the pull-out slip values \hat{s} . The new pull-out slip values according to equation (9.31) are found by differentiation of equation (9.30) with respect to the slip and setting

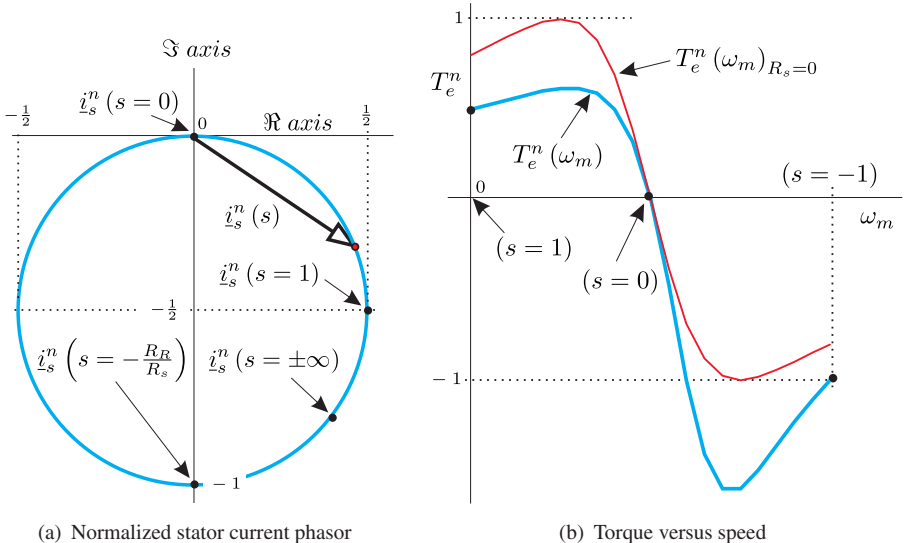


Figure 9.12. Steady-state characteristics of voltage source connected asynchronous machine with $R_s > 0$ (in blue), $L_\sigma > 0$ and $L_M = \infty$, according to figure 9.11

the result to zero. The peak torque values which correspond to the pull-out slip values given in equation (9.31) are equal to

$$T_{e+}^n = \frac{1}{\sqrt{1+r^2} + r} \quad (9.32a)$$

$$T_{e-}^n = \frac{-1}{\sqrt{1+r^2} - r} \quad (9.32b)$$

Equation (9.32) confirms the earlier statement that the two peak torque values indicated in figure 9.12(b) will differ in value when the value of the stator resistance is non-zero.

9.6.4 Steady-state analysis with leakage inductance, stator resistance and finite magnetizing inductance

The development of the asynchronous machine model is completed by adding the magnetizing inductance L_M . The Heyland diagram for this revised model is found by making use of equation (9.7) which leads to the following expression for the phasor based stator current

$$i_s = \frac{\hat{u}_s \left(\frac{R_R}{s} + j\omega_s L_M \right)}{j\omega_s L_M \frac{R_R}{s} + (R_s + j\omega_s L_\sigma) \left(\frac{R_R}{s} + j\omega_s L_M \right)} \quad (9.33)$$

The equivalent circuit which corresponds with equation (9.33) is shown in figure 9.13. A normalization of expression (9.33) is again introduced which

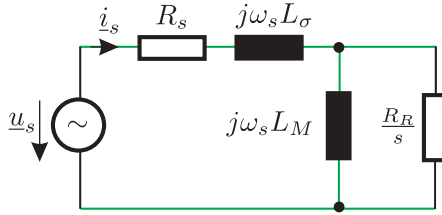


Figure 9.13. Equivalent circuit of an asynchronous machine with L_σ , R_s and L_M , voltage source, steady-state version of dynamic model in figure 9.5

is again of the form $\underline{i}_s^n = \underline{i}_s / \left(\frac{\hat{u}_s}{\omega_s L_\sigma} \right)$. Furthermore, the parameters $\hat{s} = \frac{R_R}{\omega_s L_\sigma}$, $r = \frac{R_s}{R_R} \hat{s}$ are again introduced together with a new parameter $l = \frac{L_\sigma}{L_M}$. Use of these parameters with equation (9.33) leads to

$$\underline{i}_s^n = \frac{\frac{s}{\hat{s}} - jl}{(1 + r \frac{s}{\hat{s}} + l) + j(\frac{s}{\hat{s}} - lr)} \quad (9.34)$$

An indication of its validity can be obtained by setting $l = 0$ which corresponds to the case $L_M \rightarrow \infty$, in which case equation (9.34) is reduced to expression (9.27). A similar exercise can be undertaken with equation (9.34) for the case $r = 0, l = 0$, which corresponds to infinite magnetizing inductance and zero stator resistance. The Heyland diagram is found by introducing the variables $x = \Re \{ \underline{i}_s^n \}$, $y = \Im \{ \underline{i}_s^n \}$ in equation (9.34) and eliminating the slip dependency. Subsequent mathematical handling along the lines indicated in the previous section shows, that the Heyland diagram is a circle with midpoint coordinates (x_c, y_c) and radius r_c which are defined as follows

$$\begin{aligned} x_c &= \frac{r l}{1 + l (1 + r^2)} \\ y_c &= -\frac{\left(\frac{1}{2} + l\right)}{1 + l (1 + r^2)} \\ r_c &= \frac{\frac{1}{2}}{1 + l (1 + r^2)} \end{aligned}$$

An example of the Heyland diagram for the complete machine model is shown in figure 9.14(a) for the case $\hat{s} = \frac{1}{2}$, $r = \frac{1}{2}$ and $l = \frac{1}{5}$. The parameters values \hat{s} , r are identical to the values introduced previously for the sake of comparison. The value $l = \frac{1}{5}$ is chosen considerably higher than those normally encountered (typical values for l would be in the order of 0.05 or smaller) in machines in order to demonstrate the impact on the diagram when compared to the cases $r = 0, l = 0$ and $r > 0, l = 0$ which are also shown in figure 9.14(a) for comparative purposes.

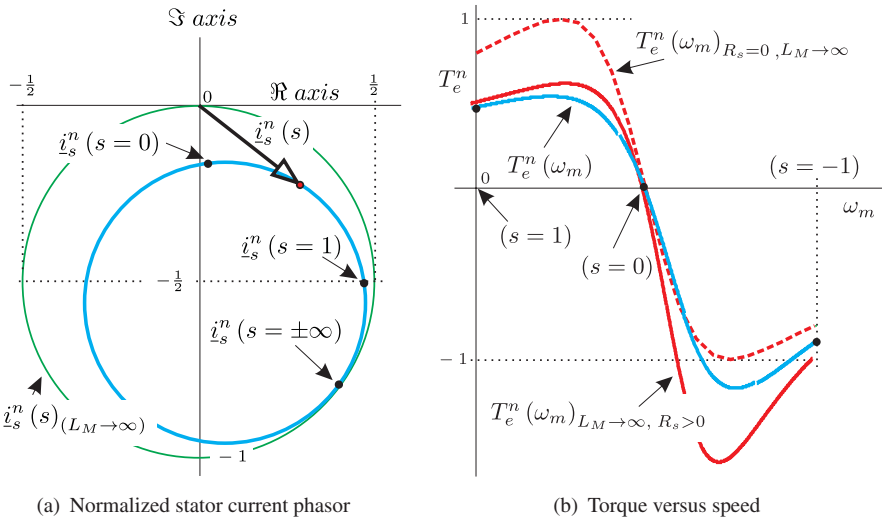


Figure 9.14. Steady-state characteristics of voltage source connected asynchronous machine, complete model (in blue) according to figure 9.13

Also indicated in figure 9.14(a) are the normalized stator current phasor end points which correspond with the three key slip points: $s = 0$, $s = 1$, $s = \pm\infty$ as calculated using equation (9.34) with the present choice of parameters \hat{s} , r and l . A comparison between the two Heyland circles shows that the introduction of magnetizing inductance reduces the radius of the circle and also causes its midpoint to move to the right and downwards. At synchronous speed ($s = 0$) the stator current will in this case no longer be zero but is instead determined by the stator resistance R_s and the sum of the magnetizing reactance $\omega_s L_M$ and leakage reactance $\omega_s L_\sigma$, i.e. under these circumstances $\frac{R_R}{s} \rightarrow \infty$.

The task of finding the torque versus shaft speed characteristic is initiated by making use of equations (9.10) and (9.7) which leads to an expression for the flux phasor $\underline{\psi}_M$ namely

$$\underline{\psi}_M = \frac{\underline{i}_s \frac{R_R}{s} L_M}{\frac{R_R}{s} + j\omega_s L_M} \quad (9.36)$$

Use of equation (9.12) with expression (9.36) gives the following steady-state torque equation

$$T_e = |\underline{i}_s|^2 \frac{\omega_s L_M^2 \frac{R_R}{s}}{\left(\frac{R_R}{s}\right)^2 + (\omega_s L_M)^2} \quad (9.37)$$

Substitution of the stator current expression (9.33) into equation (9.37) gives after some considerable mathematical manipulation the following normalized

torque expression

$$T_e^n = 2 \frac{\frac{s}{\hat{s}}}{(1 + r \frac{s}{\hat{s}} + l)^2 + (\frac{s}{\hat{s}} - l r)^2} \quad (9.38)$$

The normalization introduced is identical to that used in the previous cases namely $T_e^n = \frac{T_e}{\hat{T}_e}$, with $\hat{T}_e = \frac{\hat{u}_s^2}{2\omega_s^2 L_\sigma}$. Furthermore, the parameters \hat{s} , r and l , as defined for equation (9.34) are also introduced in equation (9.38). The torque versus speed characteristic as shown ('blue' curve) in figure 9.14(b) has a maximum and minimum value which correspond to the slip values

$$s = \pm \hat{s} \sqrt{\frac{(l r)^2 + (1 + l)^2}{1 + r^2}} \quad (9.39)$$

The peak torque values which correspond to the pull-out slip values given in equation (9.39) are of the form

$$T_{e+}^n = \frac{1}{\sqrt{((lr)^2 + (1 + l)^2)(1 + r^2) + r}} \quad (9.40a)$$

$$T_{e-}^n = \frac{-1}{\sqrt{((lr)^2 + (1 + l)^2)(1 + r^2) - r}} \quad (9.40b)$$

Two additional torque speed curves have been added to figure 9.14(b) which correspond to the cases $r = 0$, $l = 0$ and $r > 0$, $l = 0$. It is noted that in most practical cases the influence of magnetizing inductance on the Heyland diagram and on the torque speed curve is marginal, given the relatively small value of l , i.e. the magnetizing inductance L_M is much larger than the leakage inductance L_σ .

9.7 Tutorials for Chapter 9

9.7.1 Tutorial 1

This tutorial considers a three-phase IRTF based asynchronous (induction) machine in its simplified form, i.e. no stator resistance R_s or magnetizing inductance L_M . The aim is to build a Simulink model of this machine, which is in accordance with the generic model given in figure 9.6(a) (without L_M , R_s). The influence of leakage inductance will also be examined (in tutorial 2), hence the Simulink model will need to be adapted to accommodate this component. An implementation of the generic model in its present form is given in figure 9.15.

The model in its present form is *not* designed for dynamic analysis, given that the differentiator module in the generic diagram has been replaced by an

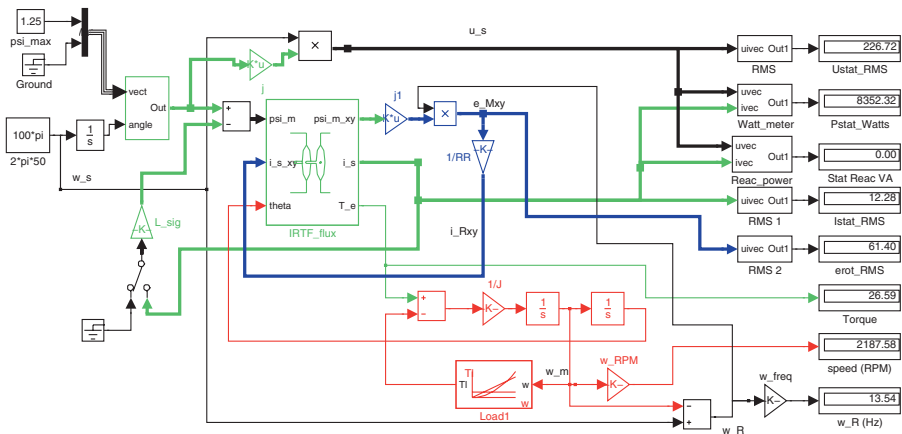


Figure 9.15. Simulink model of asynchronous machine

alternative ‘differentiator’ module (see figure 6.8) which is only usable for quasi-steady-state conditions. The aim of this example is to examine the steady-state characteristics, hence the use of numerical display modules, as well as RMS, and real/reactive power modules as introduced in earlier tutorials. The machine in question has an inertia of $J = 0.001\text{kgm}^2$. The leakage inductance L_σ plays a key role and the model according to figure 9.15 is in a form which allows operation with and without this component, hence the introduction of a ‘manual switch’ (see figure 9.15). In this tutorial the switch is placed to the ‘left’, given that we will exclude the influence of leakage inductance in this tutorial.

A rotating stator flux vector $\vec{\psi}_s$ with angular frequency $\omega_s = 100\pi \text{ rad/s}$ and amplitude $\psi_s = 1.25\text{Wb}$ is assumed as an input to this model. This means that the integrator with output $\vec{\psi}_s$ (see figure 9.6(a)) can be omitted in this tutorial. The generation of the vector $\vec{\psi}_s$ in Simulink is described in section 8.7.1. The machine is connected to a mechanical load with a quadratic torque speed curve, where we are able to vary the load torque (so we can achieve motor operation) value.

Under ‘simulation parameters’ select a ‘fixed step’ type ‘solver’ with step size 10^{-4} . Solver type should be ‘ode4’. Run the simulation for 0.1 s and observe the results by way of the values on the display modules. Maintain this solver setting and run time value for the rest of the tutorial.

The operation of the model is to be examined for two values of the rotor resistance namely $R_R = 5\Omega$ and $R_R = 10\Omega$. Set the reference speed $\omega^{ref} = 100\pi$ in the load torque module. Change the load torque T^{ref} (in the load torque module) in five steps in the range 0 to 30 Nm and record (after doing a simulation run for each step) the data from the display modules. Note that the machine

shaft speed will be at that point where the load torque speed curve $T_l(\omega_m)$ and machine torque speed curve $T_e(\omega_m)$ intersect. An example of the results which should appear on the displays is given in table 9.1. The load torque reference value T^{ref} used with the load torque sub-module is also given in this table. Note that the reactive power display reading should be zero ($Q_s = 0$), while the RMS stator voltage reading will remain constant at $U_s = 226.72\text{V}$. Re-run your

Table 9.1. Simulation results asynchronous machine $R_R = 5 \Omega$: load → no-load

T^{ref} (Nm)	n_m (rpm)	T_e (Nm)	I_s (A)	P_s (W)	E_M (V)	f_r (Hz)
30	2408.92	19.34	8.93	6076.78	44.67	9.85
20	2556.27	14.52	6.71	4561.94	33.54	7.40
10	2744.29	8.37	3.86	2628.87	19.32	4.26
5	2861.04	4.55	2.10	1428.65	10.50	2.32
0	3000.00	0	0	0	0	0

simulation for the case where the rotor resistance is doubled, i.e. $R_R = 10 \Omega$. For this example change the load torque T^{ref} (in the load torque module) in five steps in the range 0 to 50 Nm. The results which should appear on the display are given by table 9.2.

Table 9.2. Simulation results asynchronous machine $R_R = 10 \Omega$: load → no-load

T^{ref} (Nm)	n_m (rpm)	T_e (Nm)	I_s (A)	P_s (W)	E_M (V)	f_r (Hz)
50	1844.66	18.90	8.73	5938.94	87.31	19.26
30	2100.86	14.71	6.80	4621.94	67.95	14.99
20	2288.64	11.64	5.38	3656.71	53.76	11.86
10	2556.27	7.26	3.35	2280.97	33.54	7.40
5	2744.29	4.18	1.93	1314.43	19.32	4.26
0	3000.00	0	0	0	19.32	0

Build an m-file which will display the data from your simulations in the form of three sub-plots $T_e(n_m)$, $I_s(n_m)$, $P_s(n_m)$. An example of the results which should appear is given in figure 9.16. Also shown in figure 9.16 (continuous lines) are the results obtained via a steady analysis of the model in its current form. The m-file, which contains the steady-state analysis and the required code to plot the results obtained from the Simulink model, is as follows:

m-file tutorial 1, chapter 9

```
%tutorial 1, chapter 9
close all
clear all
%steady-state analysis
```

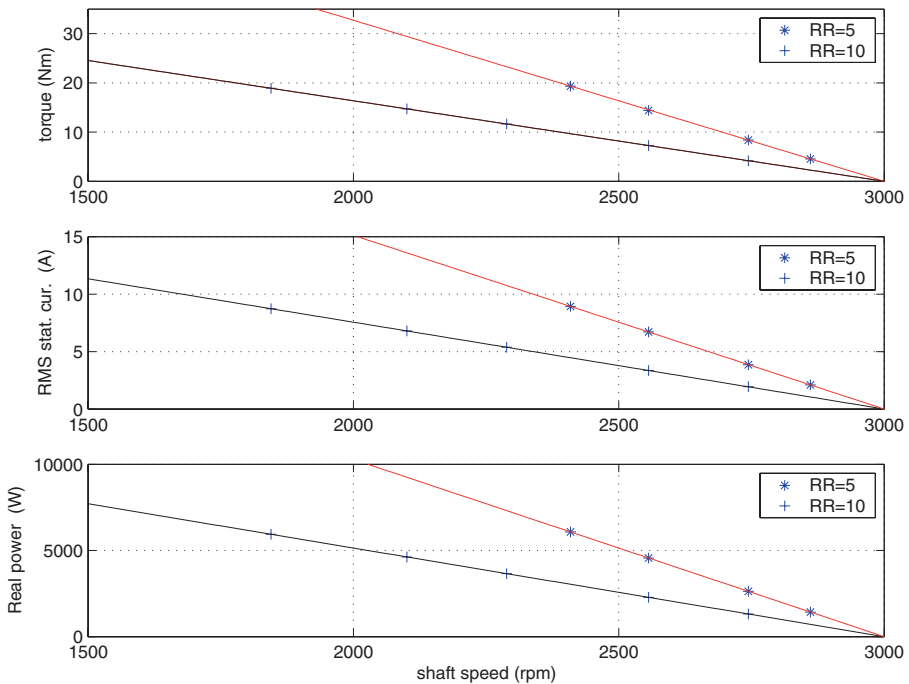


Figure 9.16. Simulink/MATLAB result: T_e (n_m), I_s (n_m), P_s (n_m), $R_R = 5, 10\Omega$, $L_\sigma = 0$

```

psis_ph=-j*1.25; % stator flux vector
ws=100*pi;%stator frequency rad/s
us_ph=j*ws*psis_ph; % voltage phasor (assumed real)
Us=abs(us_ph)/sqrt(3); % stator voltage RMS
nm=[0:10:3000]; % selected speed range
wm=2*pi*nm/60; % shaft speed rad/s
slip=(ws-wm)/ws; % slip calculation
wr=ws-wm; % slip frequency
fr=wr/(2*pi); % rotor freq Hz
P_a=[]; Te_a=[]; I_sa=[];
for j=1:2
    RR=5*j;
    is_ph=us_ph./(RR./slip); % stator current phasor
    I_s=abs(is_ph)/sqrt(3); % RMS value phase current
    I_sa=[I_sa;I_s];
    P=real(us_ph*conj(is_ph)); % real stator power
    P_a=[P_a;P];
    Te=imag(conj(psis_ph)*is_ph); % torque
    Te_a=[Te_a;Te];
end
%show simulink results
%with RR=5, zero leakage inductance
nm1=[2408.92 2556.27 2744.29 2861.04]; % shaft speed
Te1=[19.34 14.52 8.37 4.55]; % torque
Is1=[8.93 6.71 3.86 2.10]; % RMS stator current
Ps1=[6076.78 4561.94 2628.87 1428.65]; % real power

```

```

Qs1=[0 0 0 0]; % reactive power
ER1=[44.67 33.54 19.32 10.50]; % RMS, rotor induced voltage
%%%%%%%%%%%%%
%with RR=10, zero leakage inductance
nm2=[1844.66 2100.86 2288.64 2556.27 2744.29];
Te2=[18.90 14.71 11.64 7.26 4.18];
Is2=[8.73 6.80 5.38 3.35 1.93];
Ps2=[5938.94 4621.94 3656.71 2280.97 1314.43];
Qs2=[0 0 0 0];
ER2=[87.31 67.95 53.76 33.54 19.32];
%plot Simulink results
figure(1)
subplot(3,1,1)
plot(nm1,Te1,'*')
grid
hold on
plot(nm2,Te2,'+')
legend('RR=5','RR=10')
plot(nm,Te_a(1,:),'r')
plot(nm,Te_a(2,:),'k')
axis([1500 3000 0 35])
ylabel('torque(Nm)')
subplot(3,1,2)
plot(nm1,Is1,'*')
grid
hold on
plot(nm2,Is2,'+')
legend('RR=5','RR=10')
plot(nm,I_sa(1,:),'r')
plot(nm,I_sa(2,:),'k')
axis([1500 3000 0 15])
ylabel('RMS stat.cur. (A)')
subplot(3,1,3)
plot(nm1,Ps1,'*')
grid
hold on
plot(nm2,Ps2,'+')
legend('RR=5','RR=10')
plot(nm,P_a(1,:),'r')
plot(nm,P_a(2,:),'k')
axis([1500 3000 0 10000])
ylabel('Real power(W)')

```

9.7.2 Tutorial 2

This tutorial considers the simplified machine model as given in tutorial 1 with the presence of leakage inductance. The model according to figure 9.15 has already been configured to allow operation with leakage inductance. Setting the manual switch shown in figure 9.15 to the ‘right’ changes the model as to include the leakage inductance. Observation of the generic diagram given in figure 9.6(a) learns that in this case the stator flux vector must be reduced by a term $L_\sigma \vec{i}_s$, hence the use of an additional ‘summation’ unit and ‘gain’ module with gain $L_\sigma = \frac{\pi}{80}$ H. The rotor resistance is set to $R_R = 5\Omega$ in this tutorial. Note that the introduction of the term $L_\sigma \vec{i}_s$ to the model will introduce

an ‘algebraic loop’ in the model, which normally is not desired. In this case the presence of the ‘loop’ does not affect the operation, only a warning (in the MATLAB Workspace) is given. The presence of an ‘algebraic loop’ in this specific case is accepted, given the didactic value of using the model in its current form.

Repeat the simulation exercise described in tutorial 1 with ten load reference torque T^{ref} steps in the range of $1000 \rightarrow 0$ Nm. An example of the data which should appear after running this simulation (after each load step) is given in table 9.3. On the basis of the data given in table 9.3 generate four sub-plots

Table 9.3. Simulation results asynchronous machine $R_R = 5 \Omega$, $L_\sigma = \frac{\pi}{80} \text{ H}$: load→no-load

T^{ref} (Nm)	n_m (rpm)	T_e (Nm)	I_s (A)	P_s (W)	Q_s (VA)	E_M (V)
1000	369.29	15.15	16.68	4760.36	10299.87	83.41
200	878.93	17.17	15.94	5393.19	9408.48	79.72
100	1301.94	18.83	14.94	5916.81	8263.42	74.71
70	1590.66	19.68	13.91	6182.47	7166.30	69.57
60	1726.55	19.87	13.29	6243.31	6539.08	66.46
50	1888.55	19.81	12.40	6224.90	5690.40	62.00
30	2284.33	17.39	9.32	5464.44	3216.46	46.61
20	2503.43	13.93	6.95	4375.32	1786.92	34.74
10	2734.06	8.31	3.93	2609.29	570.73	19.63
5	2859.34	4.54	2.11	1426.96	165.08	10.56
0	3000.00	0.00	0.00	0.00	0.0	0.00

which represent the relationships $T_e(n_m)$, $I_s(n_m)$, $P_s(n_m)$, $Q_s(n_m)$. An example of the results which should appear is given in figure 9.17. Also shown in figure 9.17, in the form of continuous lines, are the results from the steady-state analysis. The m-file given at the end of this tutorial shows the steady-state calculations, together with the MATLAB code required to plot the results from table 9.3.

A plot of the stator current phasor end point versus slip can also be made using the data given in table 9.3. On the basis of the real and reactive power, table entries and stator current data, plot the current phasor for the shaft speed values shown in table 9.3.

The solution to this problem is as follows: the angle between the voltage and current phasor is given as $\rho_s = -\arctan(Q_s/P_s)$ (the negative sign is introduced because the phasor current lags the voltage phasor). The current phasor magnitude $|i_s|$ is found using $|i_s| = I_s\sqrt{3}$. The result which should appear is given in figure 9.18 together with the supply voltage phasor \underline{u}_s (not to scale). The m-file given below also shows the code required for plotting this current phasor (as obtained via Simulink and steady-state analysis) over the required speed range.

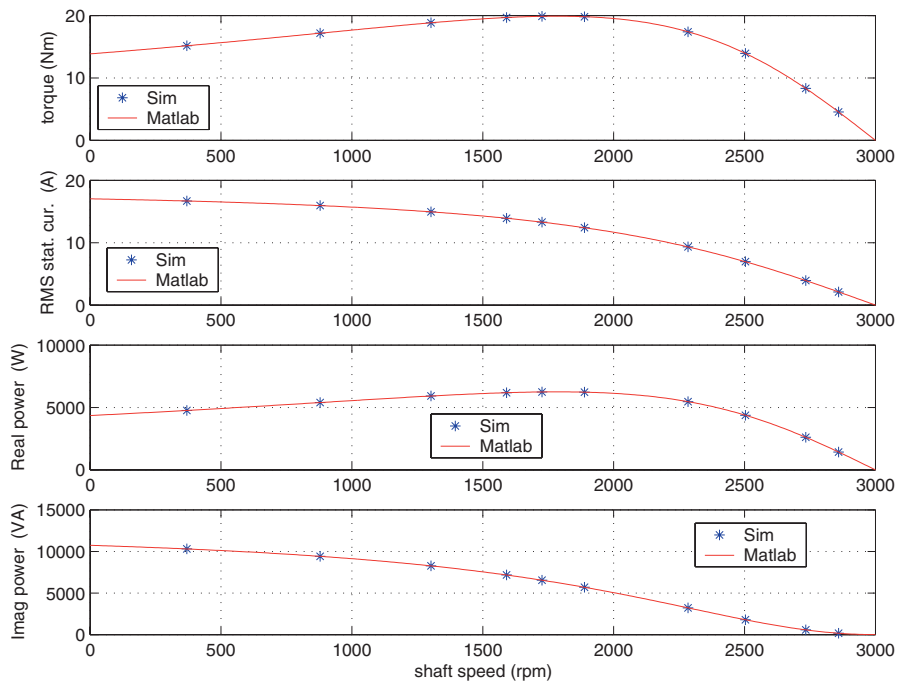


Figure 9.17. Simulink/MATLAB result: T_e (n_m), I_s (n_m), P_s (n_m), Q_s (n_m), $R_R = 5\Omega$, $L_\sigma = \frac{\pi}{80} H$

m-file Tutorial 2, chapter 9

```
%Tutorial 2, chapter 9
close all
clear all
psis_ph=-j*1.25;
ws=100*pi;%stator frequency rad/s
us_ph=j*ws*psis_ph;
Us=abs(us_ph)/sqrt(3);
RR=5;
L_sig=pi/80;
nm=[0:10:3000];
wm=2*pi*nm/60;
slip=(ws-wm)/ws;
wr=ws-wm;
fr=wr/(2*pi);
is_ph=us_ph./(RR./slip+j*ws*L_sig);
I_s=abs(is_ph)/sqrt(3);
P=real(us_ph*conj(is_ph));
Q=imag(us_ph*conj(is_ph));
Te=imag(conj(psis_ph)*is_ph);
psiM_ph=psis_ph-L_sig*is_ph;
e_ph=j*wr.*psiM_ph;
E=abs(e_ph)/sqrt(3);
%
```

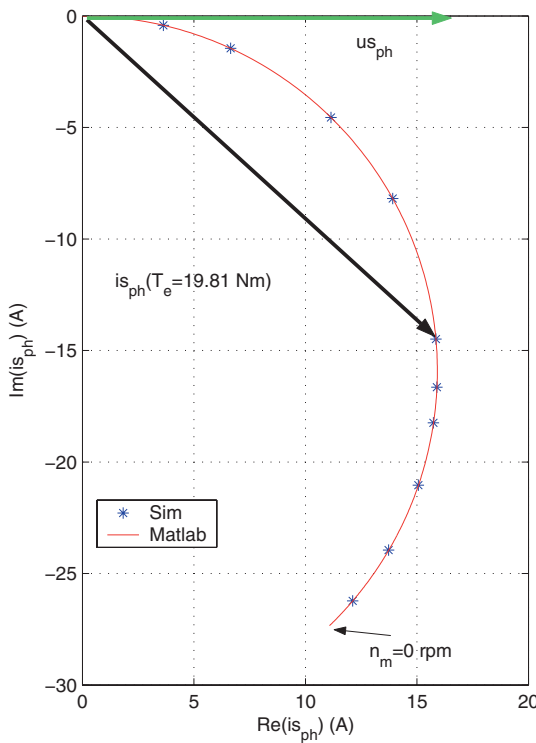


Figure 9.18. Simulink/MATLAB result: Heyland diagram, speed range 3000 → 0rpm

```
%with RR=5 and leakage inductance Lsig=pi/80
nm3=[369.29 878.93 1301.94 1590.66 1726.55 1888.55 2284.33 ...
2503.43 2734.06 2859.34];
Te3=[15.15 17.17 18.83 19.68 19.87 19.81 17.39 13.93 8.31 4.54];
Is3=[16.68 15.94 14.94 13.91 13.29 12.40 9.32 6.95 3.93 2.11];
Ps3=[4760.36 5393.19 5916.81 6182.37 6243.31 6224.90 5464.44 ...
4375.32 2609.29 1426.96];
Qs3=[10299.87 9408.48 8263.42 7166.30 6539.08 5690.40 3216.46 ...
1786.92 570.73 165.08];
ER3=[83.41 79.72 74.71 69.57 66.46 62.00 46.61 34.74 19.63 4.54];
%%%%%
%plot Simulink results
subplot(4,1,1)
plot(nm3,Te3,'*')
grid
hold on
plot(nm,Te,'r')
ylabel('torque (Nm)')
legend('Sim','Matlab',0)
subplot(4,1,2)
plot(nm3,Is3,'*')
grid
hold on
plot(nm,I_s,'r')
ylabel('RMS stat. cur. (A)')
```

```

legend('Sim','Matlab',0)
subplot(4,1,3)
plot(nm3,Ps3,'*')
grid
hold on
plot(nm,P,'r')
ylabel('Real power (W)')
legend('Sim','Matlab',0)
subplot(4,1,4)
plot(nm3,Qs3,'*')
grid
hold on
plot(nm,Q,'r')
ylabel('Imag power (VA)')
legend('Sim','Matlab',0)
%%% plot Heyland diagram
figure(2)
rhos=-atan(Qs3./Ps3);
isR=sqrt(3)*Is3.*cos(rhos);
isI=sqrt(3)*Is3.*sin(rhos);
plot(isR,isI,'*')
hold on
plot(real(is_ph),imag(is_ph),'r')
axis equal
grid
axis ([0 20 -30 0])
xlabel('Re(is_{ph})(A)')
ylabel('Im(is_{ph})(A)')
legend('Sim','Matlab')

```

9.7.3 Tutorial 3

In this tutorial a Caspoc simulation is considered of the generic model as shown in figure 9.4. The parameters and excitation conditions used in this tutorial are given in tutorial 1 of this chapter. Figure 9.19 on page 258 shows the Caspoc simulation model where ‘alternative’ differentiator modules are used instead of ‘standard’ differentiator modules which may cause simulation problems. The model in its present form does not contain leakage inductance or magnetizing inductance, hence the reactive power module output as shown in figure 9.19, should be zero.

9.7.4 Tutorial 4

This tutorial is concerned with a start up sequence of an induction machine when the latter is connected to a three-phase voltage supply. The first part of this tutorial is concerned with the development of a general IRTF based dynamic model of the machine which does not use any differentiators. The second part of the tutorial is concerned with analyzing this model when connected to the three-phase supply source. In addition a load torque module (as developed for previous simulations) is to be connected.

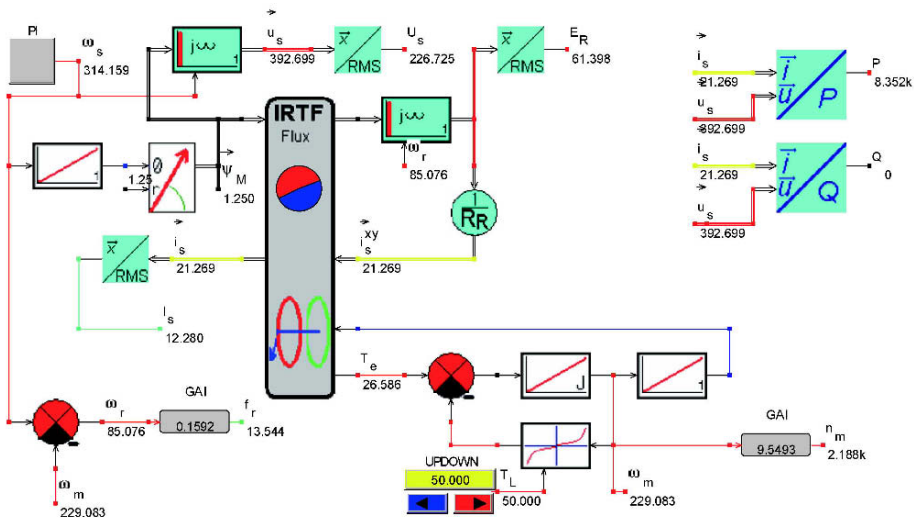


Figure 9.19. Caspoc simulation: asynchronous machine, simplified model

Central to the development of this simulation diagram is the generic model given by figure 9.6(b). The IRTF module shown in this diagram is an ‘IRTF-current’ type unit, given that the stator current vector is selected as an input. Furthermore, it is instructive to expand this IRTF unit to suit multi-pole machines as discussed in section 7.3.1. A Simulink interpretation along the lines discussed above is given in figure 9.20.

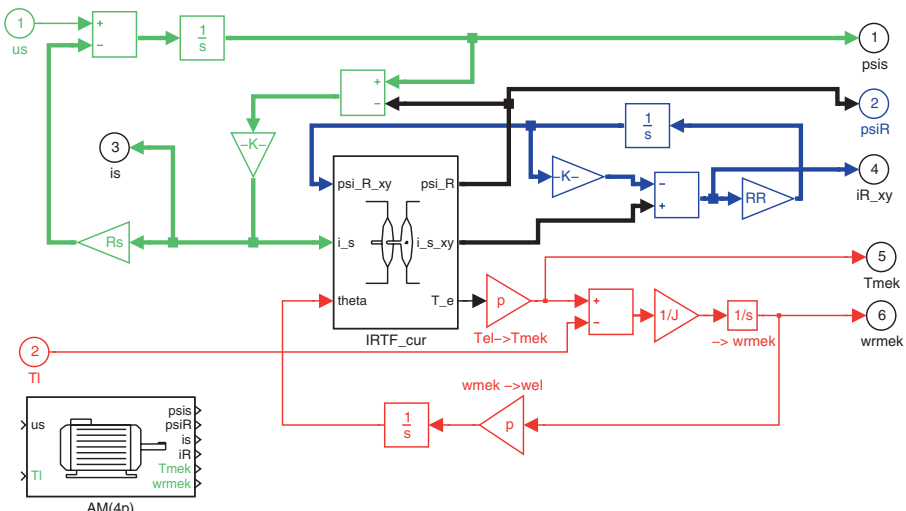


Figure 9.20. Simulink model: asynchronous machine

A 2.2kW, 2-pole machine is assumed with the set of parameters as given in table 9.4.

Table 9.4. Parameters for AC induction machine

Parameters	Value
Leakage inductance	L_σ 11.93 mH
Stator resistance	R_s 6.9 Ω
Rotor resistance	R_R 2.7 Ω
Magnetizing inductance	L_M 335.0 mH
Inertia	J 0.005 kgm^2
Pole pairs	p 1
Initial rotor speed	ω_m^o 0 rad/sec

The RMS phase voltage and frequency of the three-phase supply are taken to be 220V and 50Hz respectively. The three-phase supply as given in figure 4.47(a) is directly applicable for this example. Use a ‘three-phase to two-phase’ conversion module to generate the voltage vector \vec{u}_s . Connect a load module (see equation (8.29a)) to the machine model. This module must be configured with a quadratic load speed curve and parameters $T^{ref} = 7.3\text{Nm}$, $\omega^{ref} = 2\pi \frac{2850}{60} \text{rad/s}$. A Simulink implementation of the machine connected to mechanical load and three-phase supply is given in figure 9.21. Under ‘simu-

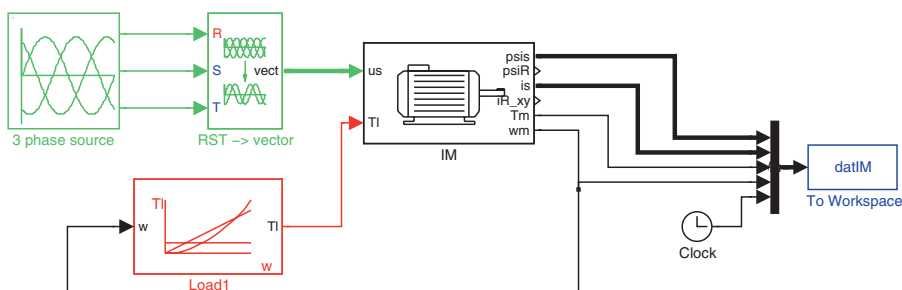


Figure 9.21. Simulink model: Mains connected asynchronous motor

lation parameters’ select a ‘fixed step’ type ‘solver’ with step size 10^{-3} , solver type should be ‘ode4’. Run the simulation for 0.4 s and add a ‘To Workspace’ module as to allow the results to be processed in MATLAB. The results which should be plotted for a time period $0 \rightarrow 0.4\text{s}$ are $|\vec{\psi}_s|$, $|\vec{i}_s|$, T_e and ω_m .

Build an m-file which enables you to show the results of the simulations in the form of four sub-plots. An example of such an m-file is given at the end of this tutorial.

The results from your simulation should be in accordance with those given in figure 9.22.

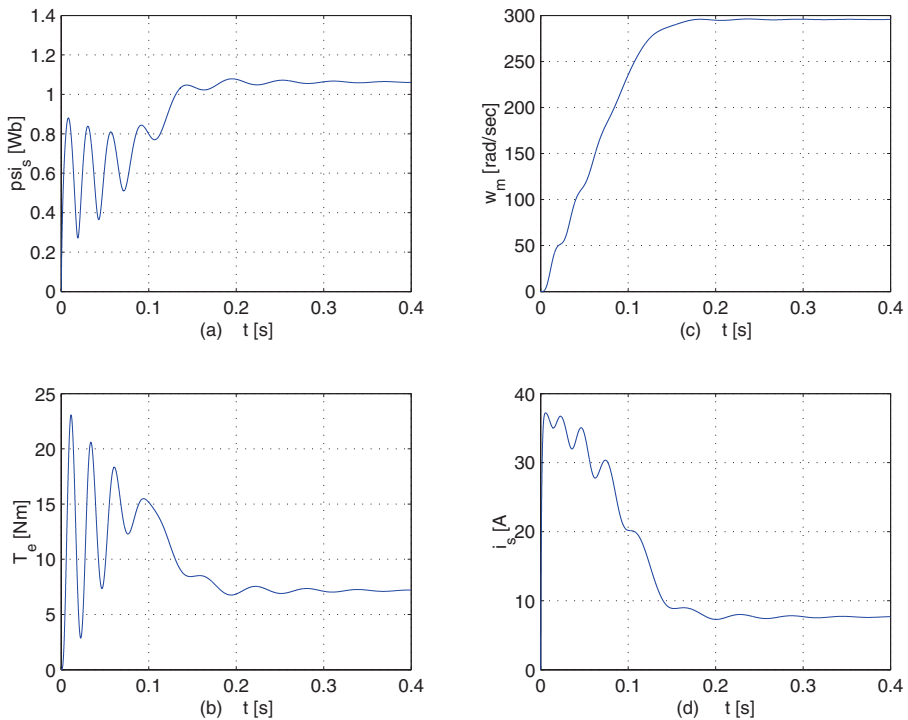


Figure 9.22. Simulink results: Mains connected asynchronous machine

m-file Tutorial 4, chapter 9

```
%Tutorial 4, chapter 9
%calculates plots for AC motor simulation
%mains connected
%%%%%
close all
figure(1)
clf
subplot(2,2,1)
plot(datIM(:,7),sqrt(datIM(:,1).^2+datIM(:,2).^2))
%title('psi_s(t)')
xlabel('(a) t [s]');
ylabel('psi_s [Wb]');
grid
subplot(2,2,3)
plot(datIM(:,7),datIM(:,5))
%title('Torque(t)')
xlabel('(b) t [s]');
ylabel('T_e [Nm]');
grid
subplot(2,2,2)
plot(datIM(:,7),datIM(:,6))
%title('speed(t)')
xlabel('(c) t [s]');
```

```

ylabel('w_m [rad/sec]');
grid
subplot(2,2,4)
plot(datIM(:,7),sqrt(datIM(:,3).^2+datIM(:,4).^2))
%title('psi_f(If)')
xlabel('d      t [s]');
ylabel('i_s [A]'); grid

```

9.7.5 Tutorial 5

This tutorial is concerned with a Caspoc implementation of the generic model given in figure 9.6(b). The parameters and excitation conditions are according to those given in the previous Simulink based version of this tutorial. Figure 9.23 shows the Caspoc implementation of the induction machine connected to a mechanical load. The user is able to vary the load torque during simulation using the ‘UPDOWN’ module. The scope modules shown in figure 9.23 display, as

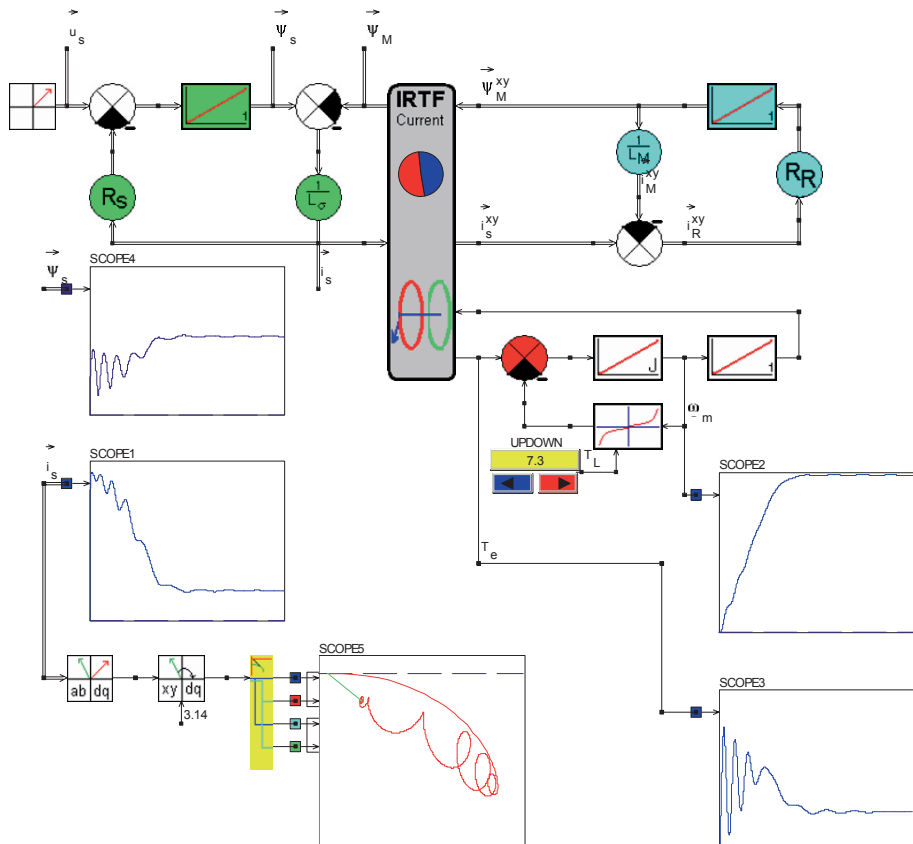


Figure 9.23. Caspoc simulation: asynchronous machine, full model

function of time, the variables $|\vec{i}|_s$ (scope1), $|\vec{\psi}|_s$ (scope4), T_e (scope3) and ω_m (scope2). These results concur with those obtained with the Simulink tutorial (see figure 9.22) of the same problem. The modules $ab-dq$, $xy-dq$ are used to show the current vector \vec{i}_s in a reference frame tied to the stator voltage vector \vec{u}_s . This implies that the locus of the stator current vector (shown in scope5) coincides (under steady-state conditions) with a Heyland diagram when the load is varied.

9.7.6 Tutorial 6

This tutorial is concerned with verifying the results obtained from simulations 4 and 5. A convenient solution to this type of problem is to consider the steady-state results obtained with the dynamic model. In this example we will base our calculations on the steady-state shaft speed as obtained from the simulation results (see figure 9.22). From the sub-plot $\omega_m(t)$ given in this figure the steady-state shaft speed was found to be $\omega_m = 295.7$ rad/s.

Write an m-file which, on the basis of the given steady-state shaft speed ω_m , will calculate the stator current phasor magnitude $|i_s|$, stator flux phasor magnitude $|\psi_s|$ and shaft torque T_e (steady-state). Compare the results obtained from your m-file with those obtained via the simulation given in figure 9.22.

A comparison of the results obtained from this m-file and those obtained via the dynamic simulation is given in table 9.5. An example of an m-file which

Table 9.5. Comparison of Simulation and MATLAB results, general IM model

Parameters		MATLAB	Simulink
Stator current phasor amplitude	$ i_s $	7.63 A	7.64 A
Stator flux phasor amplitude	$ \psi_s $	1.06 Wb	1.06 Wb
Shaft torque	T_e	7.15 Nm	7.16 Nm

shows the required calculations for this tutorial is given below:

m-file Tutorial 6, chapter 9

```
%Tutorial 6, chapter 9
% steady-state analysis general IM model
% machine parameters
Rs=6.9; %stator resistance
RR=2.7; %rotor resistance
Lsig=11.93e-3; %leakage inductance
LM=335e-3; %magnetizing inductance
p=1; %pole pair number
%%%5
wm=295.7; %shaft speed rad/s from simulation
Us=220; %RMS supply voltage
ws=100*pi; %supply frequency rad/s
```

```
%%%%%%%%5
% calculate variables
slip=(ws-wm)/ws;                                %slip
us_ph=Us*sqrt(3);                               %supply phasor, assumed real
% from equivalent circuit calculate is_ph
Z1=j*ws*LM*RR/slip/(RR/slip+j*ws*LM);      %%RR/s parallel to LM
Zsig=Rs+j*ws*Lsig;                            %lsig series with Rs
Zs=Zsig+Z1;                                    %total stator impedance
is_ph=us_ph/Zs;                                %stator current phasor
is_hat=abs(is_ph);                            %amplitude stator current phasor
psis_ph=(us_ph-is_ph*Rs)/(j*ws);              %stator flux phasor
psis_hat=abs(psis_ph);                         %amplitude stator flux phasor
Te=imag(conj(psis_ph)*is_ph);      %Torque conj psi phasor time current phasor
```

Chapter 11

ANALYSIS OF A SIMPLE DRIVE SYSTEM

11.1 Introduction

In this chapter we will look at some basic drive implementations with a DC machine as discussed in section 10.5 starting at page 272. Our aim is to arrive at generic models of all major drive components, (excluding the DC machine which has already been discussed) which we can then transpose to a Simulink and/or Caspoc type environment in the tutorials at the end of this chapter.

In the sequel of the chapter a so-called ‘predictive dead-beat’ current control algorithm will be presented [Svensson, 1988] which will allow precise torque control of the DC machine used. The techniques described here are fundamental not only to the DC machine but to all the machines discussed in this book.

11.2 Basic single phase uni-polar drive circuit

An elementary drive model as shown in figure 11.1 has almost the same structure as the general drive model given in figure 1.2 on page 4. In this exam-

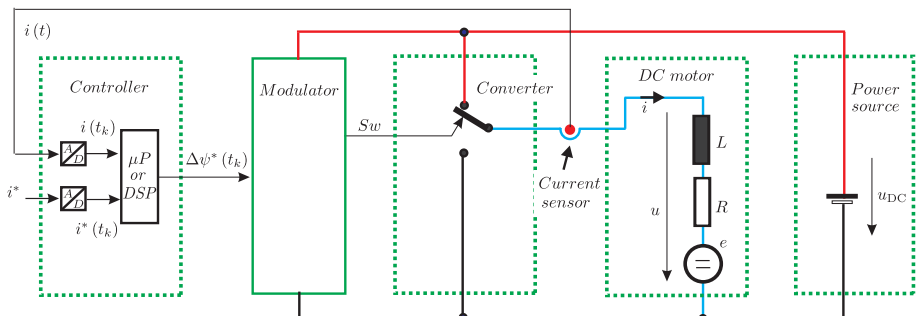


Figure 11.1. Basic electrical drive

ple the mechanical ‘load’ module has been removed. Furthermore, the power source is now shown in a two-wire configuration (+, −) which is helpful here because a symbolic implementation of the ‘converter’ module is shown. The DC motor is represented as an $R-L-e$ network as was discussed in section 10.5.2 on page 276. The purpose of the modulator is to control the converter switch shown in figure 11.1 on the basis of a set-point given by the controller. A simple controller structure is also given in figure 11.1 which shows a micro-processor (μ P or DSP), which is a digital computational element that implements the control algorithm of the drive. The input to the control module is the load current $i(t)$ which is obtained via a current sensor which measures the load current, i.e. the armature current of the DC machine in this case. A user input value i^* is also shown which represents the reference current level.

The aim of this drive circuit is to control the current in the motor in such a way that the reference current value matches the actual load current under all circumstances, i.e. transient as well as in steady-state. A typical situation to be discussed is to apply a step change to the reference current and our aim is to ensure that the load current will match this step change, within the limits of the system. To achieve this aim we will need to initially discuss in some detail the functioning of the modules shown in figure 11.1. Afterwards we will develop a control structure which can be implemented in the micro-processor (μ P or DSP) as to realize our task.

11.2.1 Power source

A DC voltage source is assumed here which has a value of u_{DC} . The bottom side is set to 0V which means that the upper wire (red) shown in figure 11.1 has a potential of u_{DC} . The voltage source is ‘uni-polar’ which means that there is only one voltage level other than zero. At a later stage in this chapter we will replace the power source by a bipolar power source which gives us a positive and a negative supply voltage level with respect to 0V. The term ‘uni-polar drive’ reflects the ability to operate with a variable but single positive supply value.

11.2.2 Converter module

The converter module shown in figure 11.1 consists of a single two-way switch. In reality such a switch is formed by two switches as shown in figure 11.2 which also gives the power source module. The switches are controlled by two logic signals Sw_t , Sw_b where logic 1 corresponds to a ‘closed’ switch state and logic 0 to an ‘open’ switch state. In this case there are four possible switch combinations of switch states: $Sw_t = 1$, $Sw_b = 1$ (both switches closed; ‘shoot-through’ mode, this state should always be avoided) and $Sw_t = 0$, $Sw_b = 0$ (both switches open; ‘idle’ mode, normally used to disable the inverter

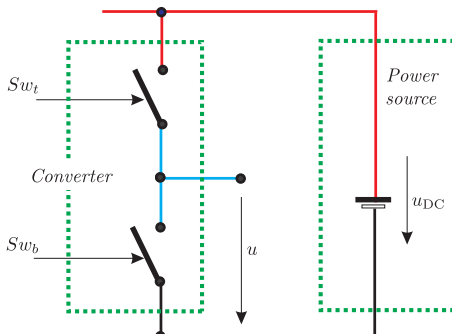


Figure 11.2. Two switch converter with power source

output), both are not considered in the following part. The remaining two states are: $Sw_t = 1, Sw_b = 0$ (top switch closed/bottom switch open), $Sw_t = 0, Sw_b = 1$ (top switch open/bottom switch closed). In the first case ($Sw_t = 1, Sw_b = 0$), the converter output is connected to the positive supply line, i.e. $u = u_{DC}$, while in the second case $Sw_t = 0, Sw_b = 1$, the output line is connected to the lower supply line, i.e. $u = 0$. The two switches can therefore in symbolic form be replaced by a single two-way switch as shown in figure 11.1, where the logic signal Sw is used to control its state. The state $Sw = 1$ corresponds to the switch in the ‘up’ state, i.e. the output voltage is given as $u = u_{DC}$. As expected, the switch state $Sw = 0$ corresponds to the switch in the ‘down’ state, i.e. the output voltage is given as $u = 0$.

11.2.3 Controller module

Today, the controller is in most cases digital. This means that the analog input variables, here in the form of the measured current $i(t)$ and user defined reference current $i^*(t)$, need to be converted to a digital form. We have therefore introduced in figure 11.1 a new building block in the form of an ‘analog-digital’ (A/D) converter.

The function of the unit is readily shown with the aid of figure 11.3: an input function $x(t)$ to the A/D converter. The diagram shows an example waveform together with a set of discrete time points t_{k-1}, t_k, t_{k+1} where k can be any integer value. The difference in time between any two time points is constant and equal to the ‘sampling interval period’ T_s . For drive systems the sampling time is in the order of $100\mu\text{s}$, 1ms . The output of the converter module is such that at these time points the input is ‘sampled’ i.e. the output is then set to equal the input value. Hence, at these ‘sampling points’ the output changes to match the instantaneous value found at the input of the converter. The output is therefore held constant during the sampling time. For example, the output $x(t_k)$ represents the value of the input variable as sampled at the time mark t_k .

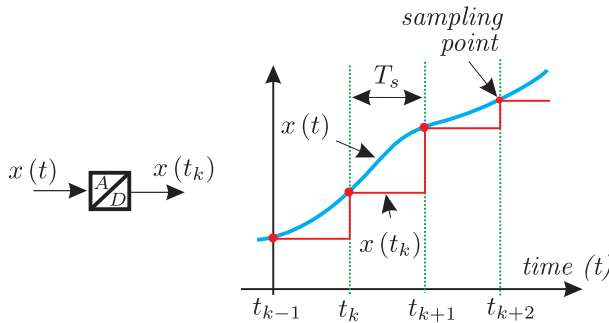


Figure 11.3. A/D converter unit with example input/output waveforms

The A/D units are used to sample the measured current and reference current values. These inputs, at for example t_k , are then used by the micro-processor or DSP to calculate an output variable known as the ‘reference incremental flux’ $\Delta\Psi^*(t_k)$, which acts as an input to the modulator. We will define the variable $\Delta\Psi^*(t_k)$ in the next section.

11.2.4 Modulator module

The basic task of the modulator module is to control the switch or switches of the converter module in such a way that the condition according to equation (11.1) is met (within the constraint of this unit) for each sampling interval.

$$\Delta\Psi^*(t_k) = \Delta\Psi(t_k) \quad (11.1)$$

where $\Delta\Psi(t_k)$ is known as the incremental flux level which is defined as

$$\Delta\Psi(t_k) = \int_{t_k}^{t_{k+1}} u(\tau) d\tau \quad (11.2)$$

The term $u(t)$ shown in equation (11.2) represents the instantaneous voltage across the load (output from the converter) within a sample period, in this case between sample points t_k, t_{k+1} . We have in the past (see equation (2.7)) commented on the fact that it is the incremental flux which controls the current in an inductance. The inductance forms a key element for our machine models and it is therefore appropriate to work with the ‘incremental flux’ as a control variable [Svensson, 1988]. Condition (11.1) in fact states that the modulator should set the converter switches during each sampling interval in such a way as to ensure that the reference incremental flux value at, for example, time t_k (as provided by the controller) matches the converter incremental flux value (as defined by equation (11.2)).

We will now consider two basic ‘single edged’ modulation strategies by examining the converter incremental flux as a function of the switch on/off

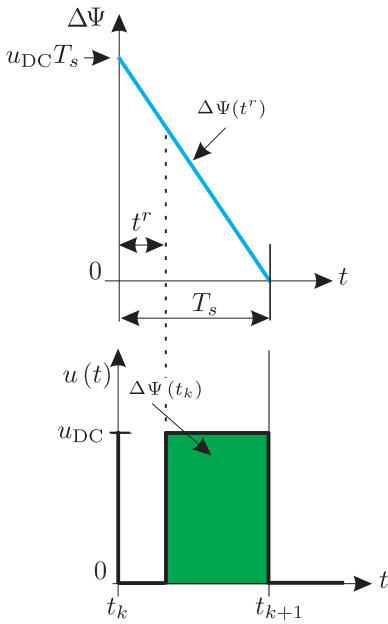


Figure 11.4. Incremental flux and output wave forms: rising edge modulation

time within a sample interval $t_k \dots t_{k+1}$. We will in the first instance make use of the converter configuration as shown in figure 11.1.

The so-called ‘rising edge’ type modulation strategy calls for the switch S_w to be placed in the ‘up’ (switch logical control level 1) position after a time t^r measured from the start of the sampling interval. The switch is placed in the ‘down’ (switch logical control level 0) position at the end of each sampling interval. An example of the output voltage waveform which appears as a result of this modulation strategy is given in figure 11.4 for the sampling interval $t_k \dots t_{k+1}$. Also shown in figure 11.4 is the incremental flux value as a function of the rise time t^r . This variable can change between zero and T_s . For a particular value t^r we can evaluate the incremental flux by making use of equation 11.2 which in this case gives the function $\Delta\Psi(t^r) = u_{DC}(T_s - t^r)$, which is illustrated in figure 11.4. It is noted that this function repeats each sample interval and this gives us the possibility to find the required t^r value for a given incremental flux reference value.

The basic algorithm for finding the rise time t^r is based on the use of equation (11.1). Basically, we compare for each sample interval the required reference value with the incremental flux function $\Delta\Psi(t^r)$ and move the converter switch to the ‘up’ position when the condition $\Delta\Psi^* \geq \Delta\Psi(t^r)$ is met. An example as given in figure 11.5, shows two consecutive sampling intervals where the reference incremental flux levels (as provided by the controller) are taken to be $\Delta\Psi^*(t_{k-1})$ and $\Delta\Psi^*(t_k)$ respectively. The switching point for

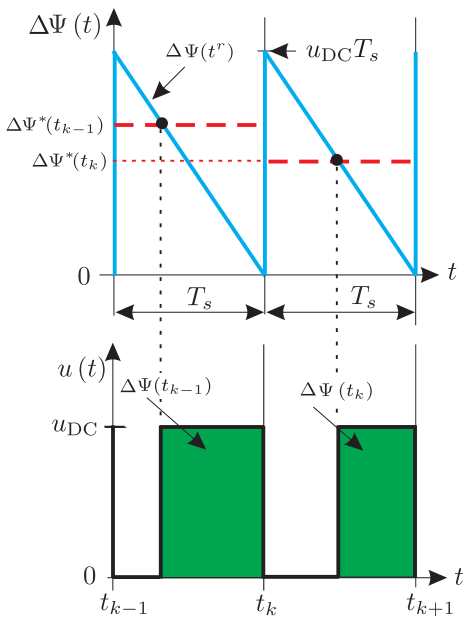


Figure 11.5. Switch algorithm for rising edge modulation

the converter (which corresponds to the required t^r value) is identified by comparison with the $\Delta\Psi(t^r)$ function for each sample interval. We note that the converter will provide the correct incremental flux value which means that the modulator will achieve its aim.

A further two observations of figure 11.5 are of interest. Firstly, this modulator-converter combination will provide an incremental flux value between zero and $u_{DC}T_s$, which is why this converter topology is ‘uni-polar’. Secondly, the required incremental flux value produced by the converter is realized by adjusting the *width* of the output voltage pulse for each sample interval. This is why this modulation strategy is known as ‘pulse width modulation’ (PWM). So far, we have discussed a ‘single rising edge’ PWM scheme which operates with a uni-polar converter.

The so-called ‘falling edge’ type PWM modulation strategy calls for the switch Sw to be placed in the ‘up’ (switch logical control level 1) position at the start of each sampling interval and moved to its ‘down’ (switch logical control level 0) position after a time t^f (measured from the start of the sampling interval). An example of the output voltage waveform which appears as a result of this modulation strategy is given in figure 11.6 for the sampling interval $t_k \dots t_{k+1}$. Also shown in figure 11.6 is the incremental flux value as a function of the fall time t^f . This variable can change between zero and T_s . For a particular value t^f we can evaluate the incremental flux by making use of equation (11.2), which in this case gives the function $\Delta\Psi(t^r) = u_{DC}t^f$ which is also illustrated in figure 11.6.

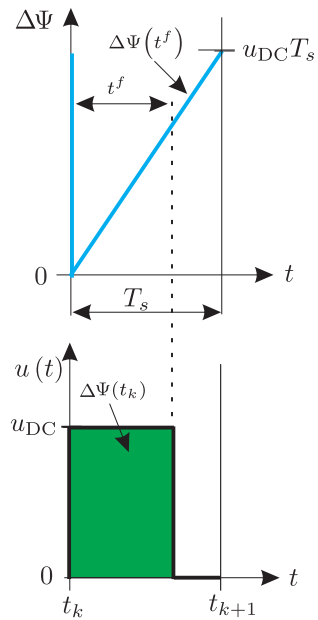


Figure 11.6. Incremental flux and output wave forms: falling edge modulation

The algorithm for finding the time t^f is again based on the use of equation (11.1). Basically, we compare for each sample interval the required reference value with the incremental flux function $\Delta\Psi(t^f)$ and move the converter switch to the ‘down’ position when the condition $\Delta\Psi^*(t_k) < \Delta\Psi(t^f)$ is met. How this is achieved is illustrated in figure 11.7 on page 302, which shows two consecutive sampling intervals where the reference incremental flux levels (as provided by the controller) are taken to be $\Delta\Psi^*(t_{k-1})$ and $\Delta\Psi^*(t_k)$ respectively. The switching point for the converter (which corresponds to the required t^f value) is identified by comparison with the $\Delta\Psi(t^f)$ function for each sample interval. We note that the converter will provide the correct incremental flux value which means that the modulator will achieve its aim. Note that in this case we have discussed a ‘single falling edge’ PWM scheme which operates with a uni-polar converter.

A generic implementation of a ‘falling edge’ PWM strategy is given in figure 11.8 on page 302. Shown in figure 11.8 are two A/D modules which take the incremental reference flux value (from the controller) and the measured u_{DC} value from the converter module. We in fact use this value as to allow us to adjust the converter switch or switches as to accommodate voltage changes as will be discussed shortly. The sampled DC voltage is multiplied by a gain T_s which gives us the maximum sampled incremental flux value $u_{DC}T_s$ and this value is multiplied by a ‘saw tooth’ function which is in fact the $\Delta\Psi(t^f)$ function with a maximum value set to 1. We could have implemented this function directly

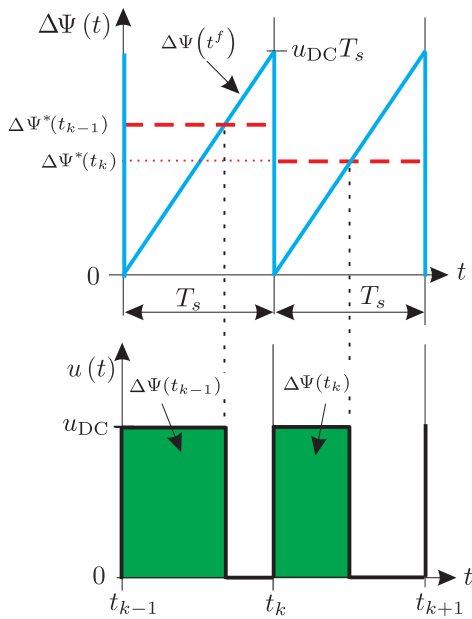


Figure 11.7. Switch algorithm for falling edge modulation

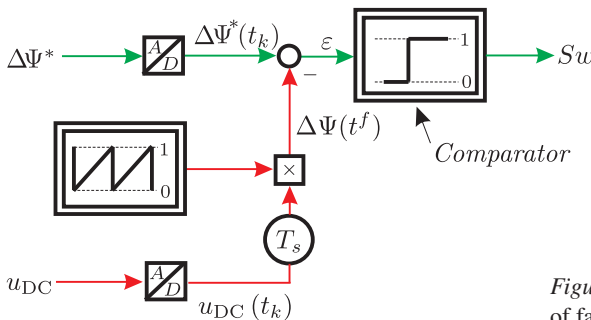


Figure 11.8. Generic model of falling edge PWM

in the ‘function generator’ module shown. However, the chosen implementation allows us to take into consideration changes to the supply voltage u_{DC} . A summation module compares the two incremental flux values and its output ε is used by a so-called comparator module. This is a new addition to our building block library and its function is given by equation (11.3).

$$\text{if } \varepsilon > 0 \quad \text{comparator output} = 1 \quad (11.3a)$$

$$\text{if } \varepsilon \leq 0 \quad \text{comparator output} = 0 \quad (11.3b)$$

In our case the output of the comparator is known as Sw and drives the converter switch. A logical level $Sw = 1$ moves the converter switch to the ‘up’ position and $Sw = 0$ sets it to the ‘down’ position. It is left to the reader to consider

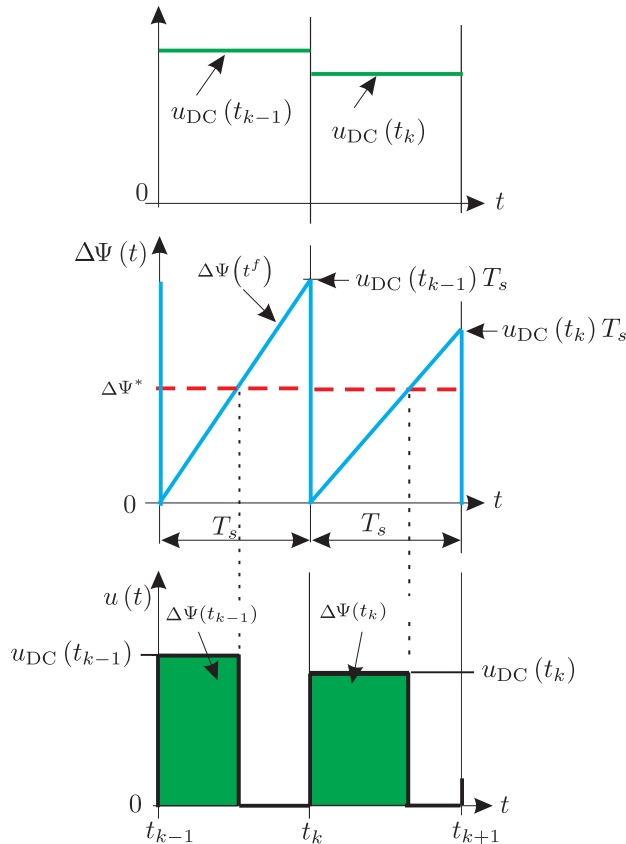


Figure 11.9. Falling edge PWM, with change of supply voltage

how figure 11.8 should be changed when a rising edge PWM strategy is to be implemented.

The modulator generic structure as given by figure 11.8 was specifically chosen to allow changes to the supply voltage which (within limits) will *not* affect the ability of the modulator/converter combination to meet condition (11.1). With the aid of figure 11.9, we will show how the modulator/converter combination is able to cope with a change in supply voltage. In this example, the incremental flux reference $\Delta\Psi^*$ is held constant. The supply voltage has been changed with time and this is reflected by the sampled DC bus voltage, which in the second sample is arbitrarily taken to be lower than in the first sample. The immediate effect is that the incremental flux function $\Delta\Psi(t^f)$ in the second sample will have a *lower* gradient than in the first. The consequence of this is that the fall time for the second sample is *increased*. Furthermore, the output waveform voltage in the second sample has reduced (because the converter sup-

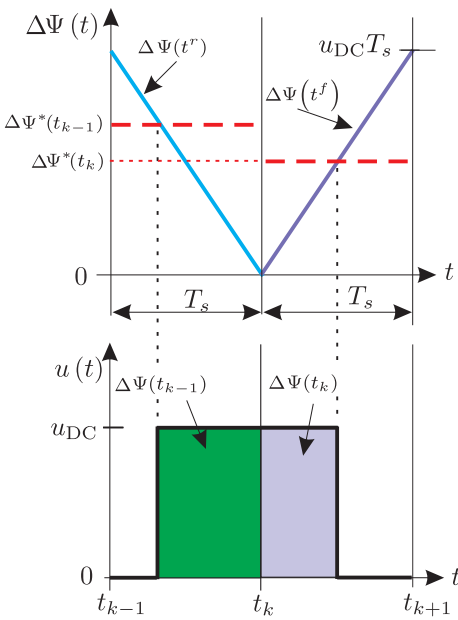


Figure 11.10. Double edged PWM strategy

ply was lowered). What in fact has occurred is that the modulator has increased the fall time in the second sample to offset the reduced output voltage level of the converter. This means that the incremental flux value delivered to the load remains *unaffected* by the supply voltage change as long as the supply voltage is of sufficient magnitude.

At the conclusion of the discussion on single edged PWM we will look at an important modulation strategy known as ‘double edged’ PWM. This modulation strategy combines the rising and falling edged PWM strategies into one. Basically this new modulation strategy alternates between the two single edged PWM options every sample. For example, in the first sample we use rising edge PWM and in the next we use falling edge PWM. How this operates in practice is shown in figure 11.10. Two sample intervals are shown and in the first sample interval a rising edged PWM strategy (as given in figure 11.5) is shown. In the second sample a falling edge strategy is shown (as given earlier in figure 11.7). The incremental flux reference for the second sample was arbitrarily set to a lower value than in the first sample. The generic module according to figure 11.8 is readily modified given that the ‘saw tooth’ generator is now replaced by a triangular function (of unity amplitude). Several important observations are to be made with respect to this modulation strategy.

Firstly, the fundamental frequency f_{mod} of the new modulator is now changed from $1/T_s$ to $1/(2T_s)$, i.e. it is halved. Secondly, each so-called modulator period or carrier-wave period $1/f_{mod}$ consists of two samples. This type of

PWM strategy is in this text referred to as double edged PWM. However, a variety of other names are found in the literature such as for example ‘center-aligned PWM with double update’, ‘symmetric PWM’ (referring to the symmetrical carrier wave) and also ‘asymmetrically sampled PWM’ (referring to the sampling) or ‘sine-triangle modulation’. It has been shown [Holmes, 1997] that this type of modulation is superior to single edged PWM strategies, due to its double update frequency and the fact that the pulse’s center of gravity does not depend on its width (for a DC set-point).

11.3 Basic single phase bipolar drive circuit

The converter module shown in figure 11.1 on page 295 consists of a single two-way switch, which in reality is formed by two switches as was shown in figure 11.2, which also gives the power source module.

The problem with the uni-polar circuit is that we cannot change the sign of the incremental flux quantity delivered (each sample) to the load. We can improve the situation by splitting the supply source u_{DC} and rearranging the two new supply sources as shown in figure 11.11. The load is in this case connected between the converter midpoint, i.e. to both switches and the 0 V (neutral) point shown in figure 11.11. The switches are controlled by two logic signals Sw_t , Sw_b where logic 1 corresponds to a closed switch state, similar to the half bridge in figure 11.2. The only difference with the explanation in section 11.2.2 is a shift in output voltage by $u_{DC}/2$. For the half bridge converter in figure 11.11, the state $Sw = 1$ corresponds to the switch in the ‘up’ state, i.e. the output voltage is given as $u = u_{DC}/2$. As expected the switch state $Sw = 0$ corresponds to the switch in the ‘down’ state, i.e. the output voltage is given as $u = -u_{DC}/2$.

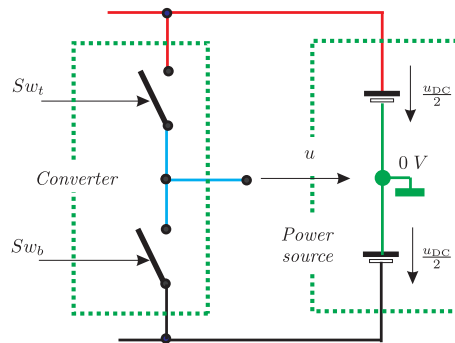


Figure 11.11. Two switch ‘half bridge’ bipolar converter with power source

11.3.1 Modulation strategy for the half bridge converter

Similar to the uni-polar modulator we can make a choice as to whether we use a single or doubled edged PWM strategy. The double edged strategy is preferable and will therefore be applied to this case. Note that the output waveforms will now change during each sample as shown in figure 11.12. Furthermore, the incremental flux versus rise and fall time must in this case be recalculated using equation (11.2). Figure 11.12 shows two samples, which correspond to one modulator period of operation. The first sample shows rising edge modulation and this means that the converter sets the load voltage to $u = -u_{DC}/2$ at the beginning of the sampling interval and after a time interval t^r the output voltage is changed to $u = u_{DC}/2$. Use of equation (11.2) allows us to find the incremental flux versus rise time function, which is in this case of the form $\Delta\Psi(t^r) = -u_{DC}t^r/2 + u_{DC}(T_s - t^r)/2$. In the second sample a falling edge PWM strategy is used, which means that the converter switches the load voltage to $u = u_{DC}/2$ at the beginning of the sample interval and after a time interval t^f is switched to $u = -u_{DC}/2$. Use of equation (11.2) allows us to find the incremental flux versus fall time function which is in this case of the form $\Delta\Psi(t^f) = u_{DC}t^f/2 - u_{DC}(T_s - t^f)/2$. The combination of both rising and falling single edged PWM strategies gives us the doubled edged PWM strategy. A comparison between the reference incremental flux value and the flux versus rise or fall time gives us the correct value for t^r , t^f , as to meet

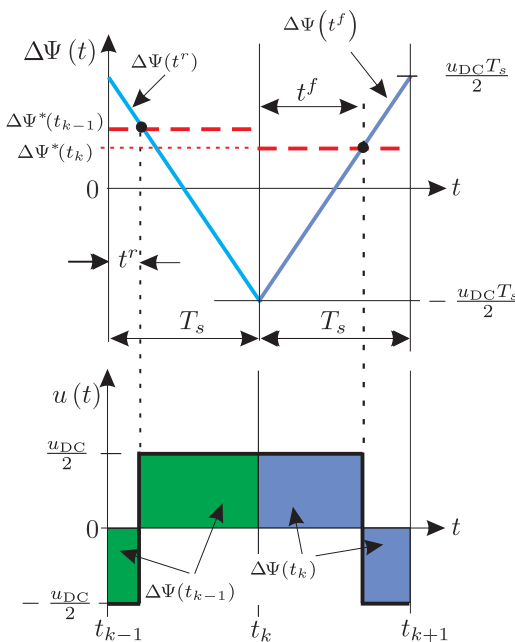


Figure 11.12. Double edged PWM strategy, with half bridge converter

the condition as specified by equation (11.1) for each sample. Bipolar output-voltage capability enables negative output voltages, but reduces the maximum positive output voltage in comparison with the uni-polar case (assuming the same total DC supply voltage). One main reason not to use bipolar half bridge converters for low-frequency applications such as DC motors, is the fact that energy is not only moved from the supply to the load, but also from the upper supply to the lower supply (so-called supply pumping). The always present supply capacitors can handle the effect of an AC output voltage and current, but low frequency or DC output cannot be maintained by a half bridge converter with a practical supply. For this reason most converters intended to drive DC loads are of the full bridge (H-bridge) type. Supply pumping does not occur in H-bridge converters.

11.4 Control algorithm

For regularly sampled control systems, as considered here, we are able to derive a simple controller structure which can be used to control the current in the DC machine (in this case represented as an R, L, e circuit). Central to our proposed controller is the use of a modulator/converter combination which is designed to deliver in (a given sampling interval T_s) an incremental inverter flux quantity $\Delta\Psi(t_k)$, which corresponds to the set-point (reference) $\Delta\Psi^*(t_k)$ value provided by the control module. The task of the control module is thus reduced to determining this set-point (reference) incremental inverter flux value on the basis of the measured discretized load current $i(t_k)$ and the set-point current value i^* .

This means that the controller must calculate the required set-point incremental inverter flux quantity at the beginning of each sampling interval t_k to ensure that the actual current at the end of that interval corresponds to the set-point current value at the start of the interval hence

$$i(t_{k+1}) = i^*(t_k) \quad (11.4)$$

Condition (11.4) is known as the ‘predictive dead-beat’ control condition. Its purpose is to ‘predict’ an incremental inverter flux quantity that will be required for the coming interval as to eliminate the error between the measured and reference current value at the end of each interval. How this is achieved is shown in figure 11.13, where the reference and actual current are shown for a sequence of sampling intervals from $t = t_0$ to $t = t_4$ with $i(t_0) = 0$. The modulator/converter module will insure that the following condition is satisfied

$$\Delta\Psi^*(t_k) = \int_{t_k}^{t_{k+1}} u(\tau) d\tau \quad (11.5)$$

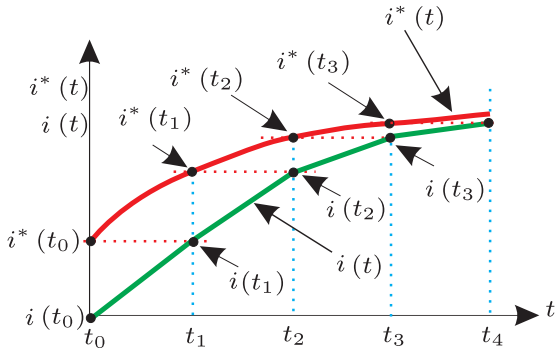


Figure 11.13. Predictive dead-beat control

where u represents the voltage across the load (see figure 11.1). An observation of figure 11.1 learns that the load voltage may be expressed as

$$u = Ri + L \frac{di}{dt} + e \quad (11.6)$$

which is precisely the differential equation used to represent the rotor (armature) circuit of the alternative DC model (see equation (10.12)). For simplicity the armature ‘a’ subscripts have been removed). Use of equation (11.6) with equation (11.5) allows the latter to be written as

$$\Delta\Psi^*(t_k) = R \int_{t_k}^{t_{k+1}} i(\tau) d\tau + L \int_{i(t_k)}^{i(t_{k+1})} di + \int_{t_k}^{t_{k+1}} e(\tau) d\tau \quad (11.7)$$

Equation (11.7) forms the basis for determining a generic control structure that is able to calculate the required incremental inverter flux quantity capable of satisfying condition (11.4). It is noted that this set-point value can only be determined on the basis of a detailed knowledge of the load parameters R, L .

For a discrete (use of sampled data for processing via a micro-processor) type controller considered here, discretization of equation (11.7) is required. A first order approximation technique based on ‘Simpson’s law’ is used in which case the resistive term of (11.7) is reduced to

$$R \int_{t_k}^{t_{k+1}} i(\tau) d\tau \cong \frac{RT_s}{2} (i(t_{k+1}) + i(t_k)) \quad (11.8)$$

The inductive term present in equation (11.7) can be directly evaluated which gives

$$L \int_{i(t_k)}^{i(t_{k+1})} di = L (i(t_{k+1}) - i(t_k)) \quad (11.9)$$

The third term which contains the induced voltage is reduced to the form

$$\int_{t_k}^{t_{k+1}} e(\tau) d\tau \cong e(t_k) T_s \quad (11.10)$$

where use is made of the fact that the voltage variations of $e(t)$ are relatively small within one sampling period. The reason being that such variations are linked to the mechanical time constant of the machine.

The resultant incremental reference flux is found by adding together the three terms given in equations (11.8), (11.9) and (11.10) which upon use of (11.4) gives

$$\Delta\Psi^*(t_k) \cong \frac{RT_s}{2} (i^*(t_k) + i(t_k)) + L(i^*(t_k) - i(t_k)) + e(t_k)T_s \quad (11.11)$$

A further simplification is possible by rewriting the resistive term in equation (11.11) as

$$\frac{RT_s}{2} (i^*(t_k) + i(t_k)) = \frac{RT_s}{2} (i^*(t_k) - i(t_k)) + RT_s i(t_k) \quad (11.12)$$

in which case the set-point incremental flux value is given as

$$\Delta\Psi^*(t_k) \cong RT_s i(t_k) + \left(L + \frac{RT_s}{2} \right) (i^*(t_k) - i(t_k)) + e(t_k)T_s \quad (11.13)$$

A control structure based on equation (11.13) is basically a so-called proportional type controller. In practice, a so-called proportional-integral type structure is preferable and this may be achieved by rewriting the term $RT_s i(t_k)$ as

$$RT_s i(t_k) \cong RT_s \sum_{j=0}^{j=k-1} (i^*(t_j) - i(t_j)) \quad (11.14)$$

which means that the current $i(t_k)$ is composed of a series of difference terms as can be observed from figure 11.13. Use of equation (11.14) with (11.13) leads to

$$\begin{aligned} \Delta\Psi^*(t_k) &\cong RT_s \sum_{j=0}^{j=k-1} (i^*(t_j) - i(t_j)) + \\ &\quad \left(L + \frac{RT_s}{2} \right) (i^*(t_k) - i(t_k)) + e(t_k)T_s \end{aligned} \quad (11.15)$$

The generic structure which corresponds to equation (11.15) as shown in figure 11.14 contains a so-called *PI* (proportional-integral) controller and ‘feed-forward’ term $e(t_k) T_s$. The proportional *P* and integral *I* gain settings for this ‘discrete’ controller are set to $\left(L + \frac{RT_s}{2} \right)$ and RT_s respectively.

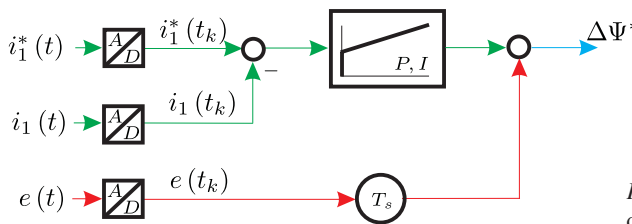


Figure 11.14. Predictive dead-beat controller

11.5 Tutorials for Chapter 11

11.5.1 Tutorial 1

This tutorial considers a simple example which consists of a modulator, unipolar converter and a load in the form of an ideal inductance. A single ‘rising’ edge type modulator will be considered. The incremental flux value is taken to be the input to the modulator. A sampled (discrete) system is assumed with a sampling time $T_s = 1\text{ms}$. The supply voltage u_{DC} is taken to be 300V. Furthermore, the load inductance is set to 100mH. The aims are to build this system in Simulink in order to analyze the converter output and verify that the converter is able to supply an incremental flux value which is equal to the reference flux value. We then reduce for the single edge PWM version the supply voltage to 200V and determine if the converter is still able to meet the reference incremental flux value $\Delta\Psi^*$. The incremental flux reference is taken to be of the form $\Delta\Psi^* = (100 T_s) \sin \omega t$ where $\omega = 100\pi \text{ rad/s}$.

Figure 11.15 shows a Simulink implementation of a model which addresses the requirements of this tutorial. The ‘sinus’ module produces the incremental flux reference value $\Delta\Psi^*$, which is then fed to an A/D converter. In Simulink this module is found in the discrete library and called ‘zero-order hold’. In

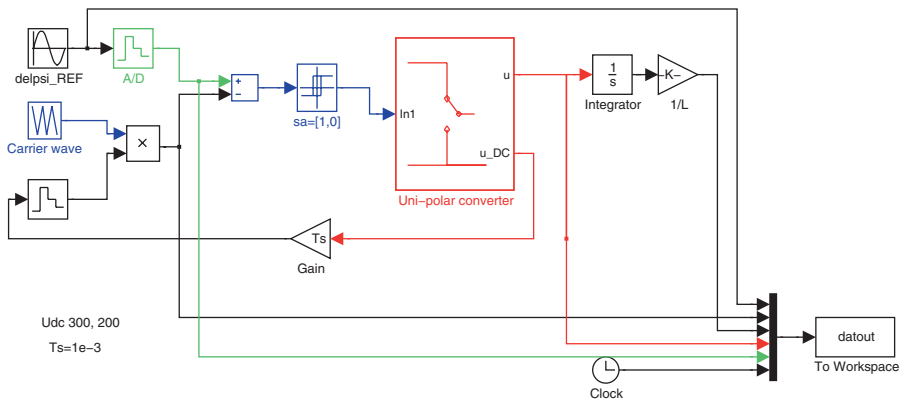


Figure 11.15. Simulink model of converter with single edged PWM

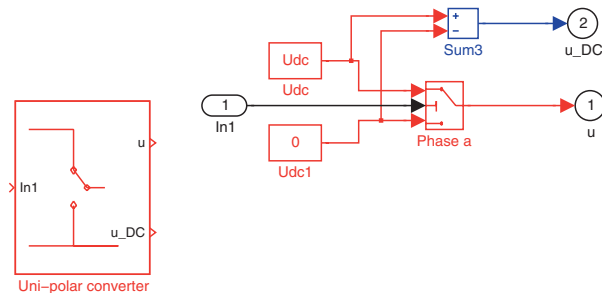


Figure 11.16. Simulink model of uni-polar converter

this module, set the sampling time to T_s . Define $T_s = 10^{-3}$ s in the MATLAB Workspace prior to running your simulation. Simulink then ‘knows’ this value of T_s for any block in the system. The ‘carrier’ module is found under ‘sources’ and called ‘repeating sequence’. Within this module, set in the entry ‘time values’ the vector [0 Ts/1000 Ts] and ‘output values’ the entry [0 1 0]. This in effect sets up the modulator saw-tooth function as shown in figure 11.8 for ‘rising’ edge PWM. The output of this module is multiplied by $u_{DC} T_s$. An A/D unit is used to sample the u_{DC} value from the converter in order to obtain $u_{DC}(t_k)$ and this value is multiplied by a gain module with value T_s .

A summation unit takes the reference and modulator incremental flux values and produces an input ϵ for the comparator. In Simulink a ‘relay’ (found in the non-linear library) is used. Open the dialog box for this unit and enter the following settings: ‘switch on point:’ eps, ‘switch off point:’ eps, ‘output when on:’ 1, ‘output when off:’ 0. The output of the comparator module is led to the ‘converter’ sub-module which can, for example, be of the form given in figure 11.16.‘ The ‘converter’ module has a ‘switch’ (found in the non-linear library) and within this module, set the ‘Threshold:’ to 0.5. Two constant blocks are used to make the DC voltage source. In this case set the upper constant block value to u_{DC} and lower to 0. Then in the MATLAB Workspace (or m-file) set $u_{DC} = 300$. A second sub-module output is made which represents the difference between the two constant blocks which is in fact the supply voltage u_{DC} value as required by the modulator.

Set the ‘simulation parameters’ to an initial run time of 0.005s (five samples) and in the solver choose ‘variable step’ ode45. Set the ‘max step size’ to 10^{-5} s.

Test your Simulink file step by step. Consider first the incremental flux reference value before and after the A/D unit by adding a ‘mux’ and ‘scope’ and plot the result. An example as to the waveform you should see is given in figure 11.17(a). The ‘blue’ line represents the reference flux $\Delta\Psi^*$, the ‘red’ line is the sampled version of this function.

Next observe the modulator flux (carrier) and sampled reference flux, an example of which is given in figure 11.17(b). The ‘green’ plot is the modulator flux and the ‘red’ waveform is the sampled reference flux. Check (by calculating the voltage time area within the sample interval) for one sample if the incremental flux produced by the converter is equal to the reference value.

Add the $L = 100\text{mH}$ inductance to the converter output and run your simulation. Observe the converter voltage (divide by 100, to view the result with the other outputs) and current waveforms together by adding a ‘mux’ and scope. Alternatively, process the results via MATLAB. An example of the converter voltage and current waveforms is given in figure 11.17(c). The current change will occur as a result of a converter output pulse, the area of which (being the incremental flux value) will determine the amplitude of the variation as shown in figure 2.3. The m-file at the end of this section contains all the code required to generate the results given in figure 11.17. We now look at the effect of changing the DC supply voltage level by changing U_{DC} from 300 V to 200 V. Make this change in the MATLAB Workspace and rerun the simulation. Observe and plot the inductance current together with the converter voltage $u/100$. An example of the new waveforms is given in figure 11.17(c). A comparison between figures 11.17(c) and 11.18(c) learns that the current waveform (shown in ‘red’) is unaffected (in terms of the current step which takes place each sample) by the change, which is precisely what should happen as shown in figure 11.9 for the

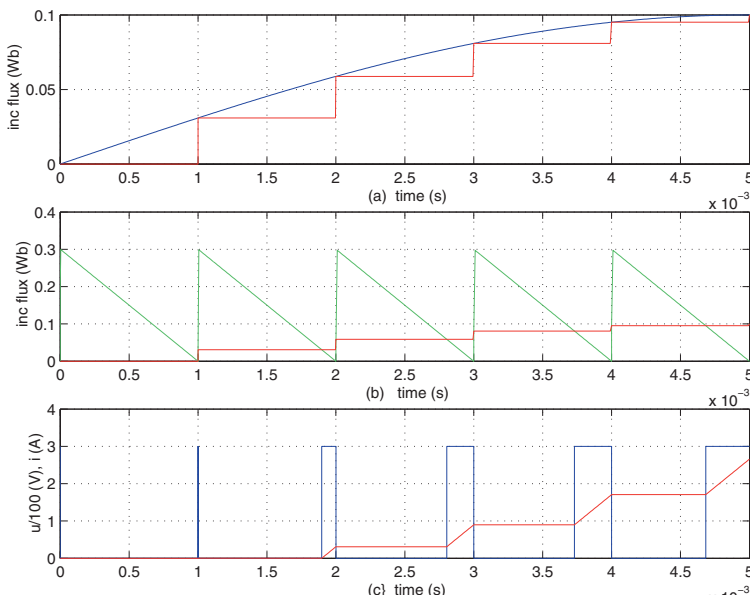


Figure 11.17. Simulink results: uni-polar converter, $u_{DC} = 300\text{V}$

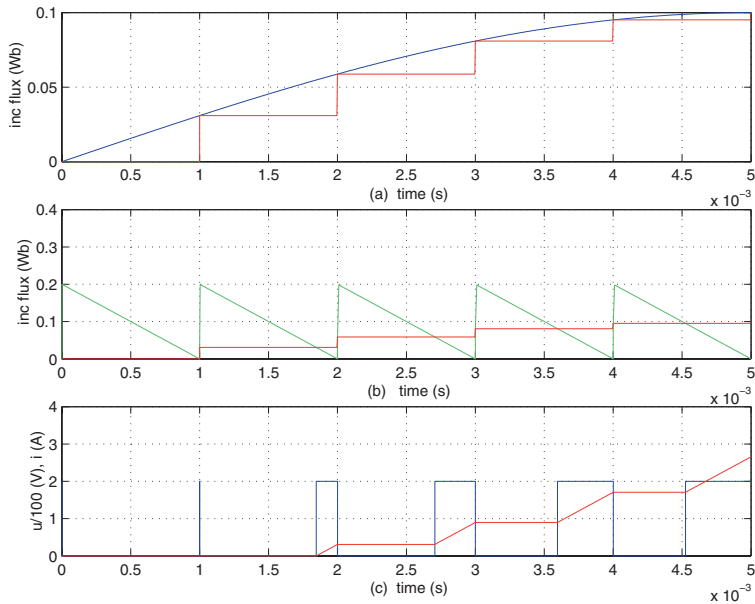


Figure 11.18. Simulink results: uni-polar converter, $u_{DC} = 200V$

case of ‘falling edge’ PWM. The converter output voltage amplitude is reduced, but the modulator flux waveform amplitude is also reduced, as can be observed by comparing figures 11.17(b) and 11.18(b). This in turn implies that the width of the output pulses will be increased given the same sampled incremental flux reference.

m-file Tutorial 1, chapter 11

```
%Tutorial 1, chapter 11
%inductive load 100 mH
close all
Ts=1e-3; % sample time
subplot(3,1,1)
plot(datout(:,6), datout(:,1)); % reference incremental flux
hold on
plot(datout(:,6), datout(:,5),'r'); % reference sampled incremental flux
grid
ylabel(' inc flux (Wb)')
xlabel(' (a) time (s)')
subplot(3,1,2)
plot(datout(:,6), datout(:,2),'g'); % carrier incremental flux
grid
hold on
plot(datout(:,6), datout(:,5),'r');
axis([0 5e-3 0 0.4])
ylabel(' inc flux (Wb)')
xlabel(' (b) time (s)')
```

```

subplot(3,1,3)
plot(datout(:,6), datout(:,4)/100, 'b'); % output voltage/100
hold on
grid
plot(datout(:,6), datout(:,3), 'r');      % load current
xlabel(' (c) time (s)')
ylabel('u/100 (V), i (A)');
axis([0 5e-3 0 4])

```

11.5.2 Tutorial 2

This tutorial considers a Caspoc based model of a ‘falling edge’ type modulator as described by the generic diagram given in figure 11.8. The tutorial is similar in terms of the activities to be undertaken, converter configuration and variables used. An example of a Caspoc based model for this tutorial is given in figure 11.19. An observation of this figure learns that the converter is implemented by way of actual ideal switching devices, in this case Mosfet’s, which in turn are connected to the comparator via two AND gates. The latter are used in combination with an ‘enable’ signal provided by a signal generator. The ‘enable’ signal disables the converter during the first 1ms sample of the run cycle. The reason for this is to allow the sample-and-hold units to first acquire appropriate data prior to activating the converter. The load and power supply are also shown in this diagram and their values are as given in the previous tutorial. A sinusoidal incremental flux reference source is added to the simulation together with a set of ‘scope’ modules to observe the results produced by this simulation over a period of 5ms (five samples). The following results are shown on the scope units:

SCOPE1 Voltage across the ideal coil and the the current through this component.

SCOPE2 Incremental reference flux signal and this signal after it has been sampled.

SCOPE3 The incremental flux function $\Delta\Psi(t^f)$ and sampled incremental flux reference signal.

The first sample of the simulation, as given on the scope units, shows no activity of the converter, given that the unit has been disabled during this time, for reasons discussed above. The results obtained should reinforce the concepts outlined in section 11.2.4 and figure 11.7 in particular.

11.5.3 Tutorial 3

In this tutorial we will look at building/analyzing a double edged ‘pulse width modulator’ (PWM) with so-called asymmetrical sampling. The modulator will be connected to a bipolar half bridge converter which in turn is connected to an inductive load.

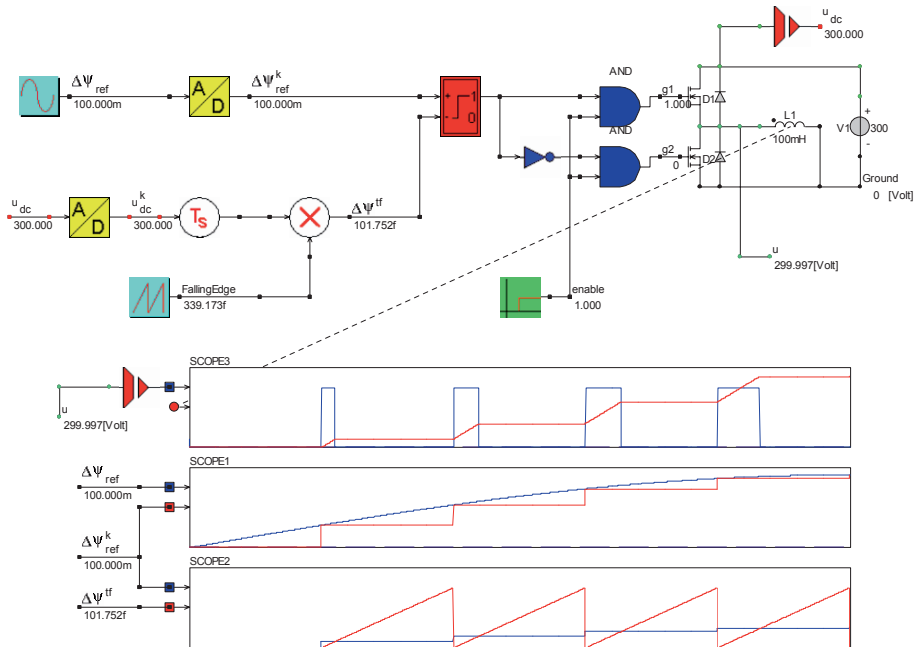


Figure 11.19. Caspoc model of uni-polar converter

The basic Simulink structure according to figure 11.15 must be modified in terms of the modulator and converter module. The revised simulation model as shown in figure 11.20 contains a new ‘modulator’ module. The modulator module as is given in figure 11.21, contains the modulation components discussed in the previous tutorial. In this case the carrier module needs to be changed so that the ‘time values’ entry becomes $[0 \text{ } Ts \text{ } 2*Ts]$ and the ‘output values’

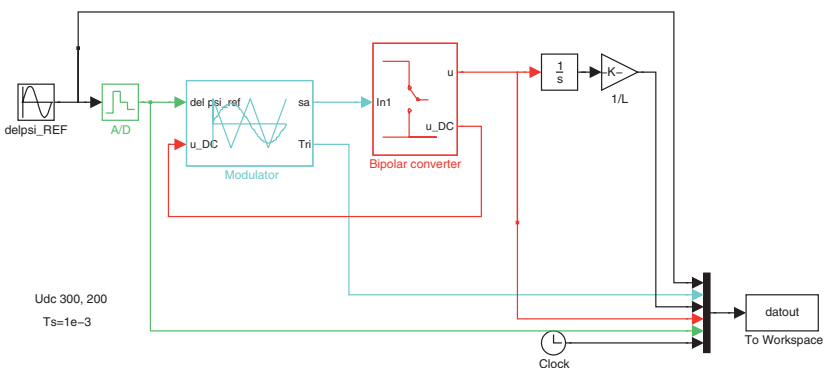


Figure 11.20. Simulink model of bipolar converter

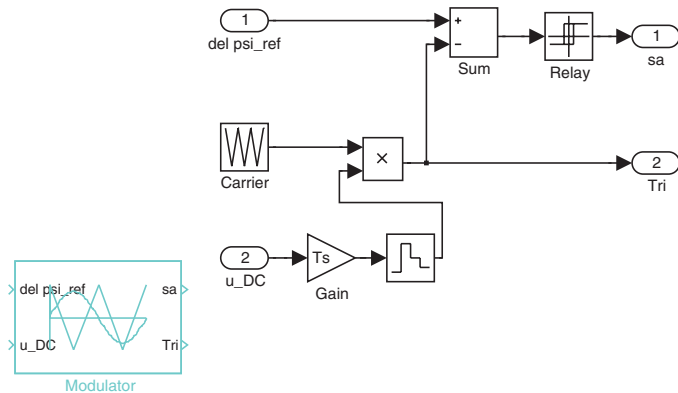


Figure 11.21. Simulink model: PWM modulator

entry reads [1/2 -1/2 1/2]. The inputs to the modulator are the incremental flux reference and supply voltage level as obtained from the converter. Note that an output ‘Tri’ is present which represents the incremental flux waveform. This modulator must be connected to the bipolar converter unit shown in figure 11.22. With regard to the converter sub-module the two constants must be changed. The upper supply constant, changes from u_{DC} to $u_{DC}/2$. The bottom supply constant, changes from 0 to $-u_{DC}/2$.

Make sure that u_{DC} in the MATLAB Workspace (or in the sub-module) is set to 300V. The inductance value is changed to $L = 200\text{mH}$. An example of implementation of the bipolar converter is given in figure 11.22. Use the same simulation parameters as discussed in the previous tutorial but change the run time to 10ms. The m-file which corresponds with this simulation is given at the end of this tutorial. Typical results which should appear after running the simulation and m-file should be according to figure 11.23.

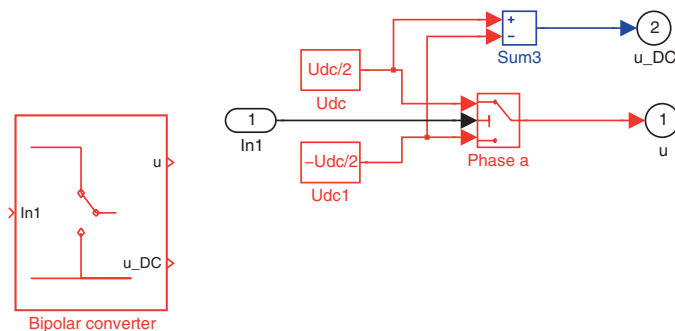


Figure 11.22. Simulink model: bipolar converter

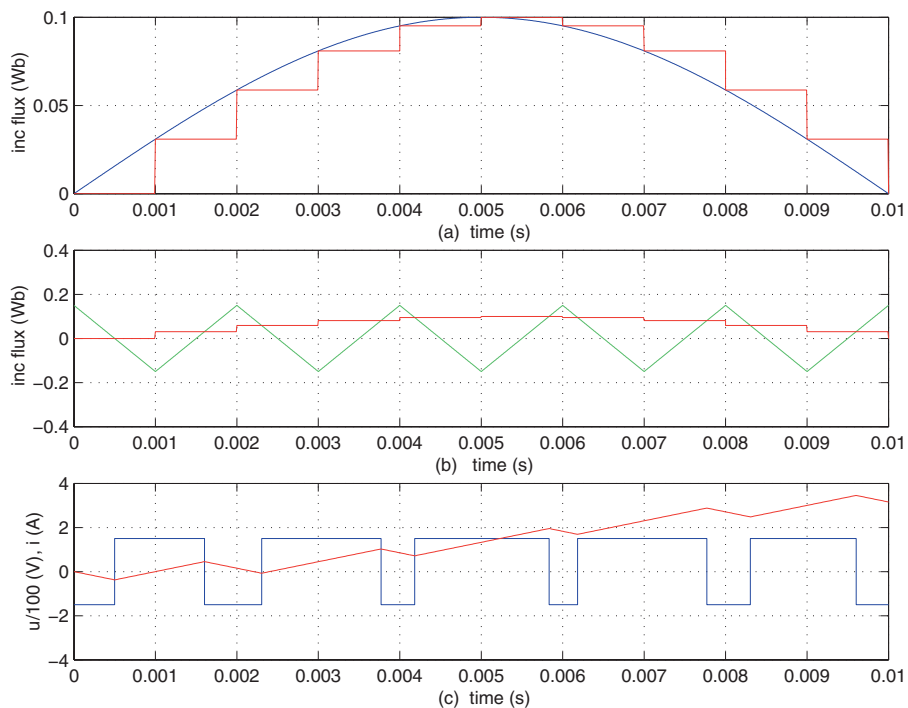


Figure 11.23. Simulink results: bipolar converter, $u_{DC} = 300V$

m-file Tutorial 3, chapter 11

```

%%Tutorial 3, chapter 11
%inductive load 200 mH
close all
Ts=1e-3;                                     % sample time
subplot(3,1,1)
plot(datout(:,6), datout(:,1));               % reference incremental flux
hold on
plot(datout(:,6), datout(:,5), 'r');          % reference sampled incremental flux
grid
ylabel(' inc flux (Wb)');
xlabel(' (a) time (s)')
subplot(3,1,2)
plot(datout(:,6), datout(:,2), 'g');          % carrier incremental flux
grid
hold on
plot(datout(:,6), datout(:,5), 'r');
axis([0 10e-3 -0.4 0.4])
ylabel(' inc flux (Wb)');
xlabel(' (b) time (s)')
subplot(3,1,3)
plot(datout(:,6), datout(:,4)/100, 'b');      % output voltage/100
hold on
grid

```

```

plot(datout(:,6), datout(:,3), 'r'); % load current
xlabel(' (c) time (s)')
ylabel('u/100 (V), i (A)');
axis([0 10e-3 -4 4])

```

11.5.4 Tutorial 4

The aim is to analyze a ‘predictive dead-beat’ type current controller with the bipolar converter and modulator as discussed in the previous tutorial. A ‘discrete’ controller is to be used which will deliver the required incremental flux value to the modulator needed to control the current in the load.

The load is taken to be a resistance $R = 10\Omega$ and inductance $L = 200mH$ (series connected). A sampling time of $T_s = 1ms$ is again assumed for this example. The supply voltage for the converter is set to $u_{DC} = 300V$.

An example of the Simulink model for this tutorial, as given in figure 11.24, shows the converter as well as the modulator in sub-module form. Both these modules have been discussed in the previous tutorial.

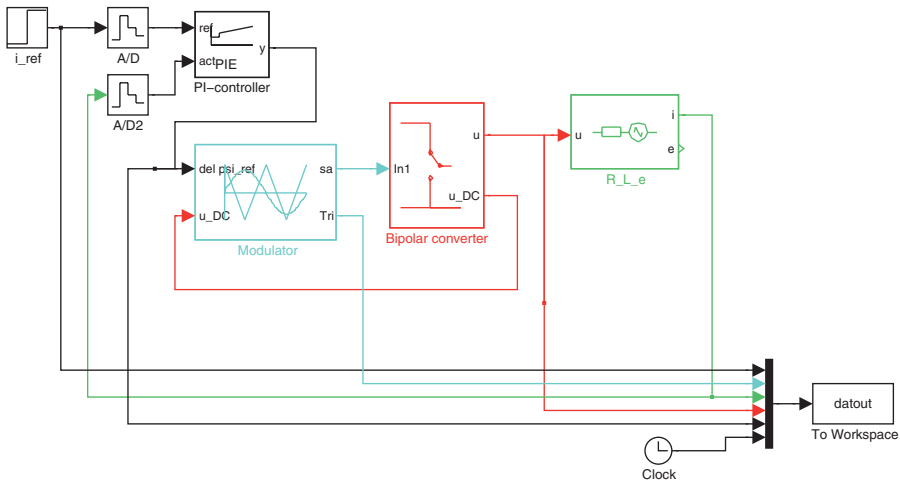


Figure 11.24. Simulink model: modulator/converter with R/L load

The $R-L-e$ sub-module shown in figure 11.24 represents a series connected resistance, inductance, voltage source load module as used in section 5.5.3 on page 140. The voltage source value in this module is set to zero in this example. We will examine the performance of this system by making use of a step module which generates the reference current i^* function. The current reference is held to zero until $t = 2ms$ when a step change to $1A$ is to be made.

The variables T_s , L and R should be specified in the MATLAB Workspace prior to running the Simulink file. The run time of your simulation should be

10ms and the solver is ode45 (Dormand-Prince). Note that in the ‘dialog’ box you need to set the ‘Max step size’ to 10^{-5} s.

The Simulink model of the current controller is a direct implementation of the generic model shown in figure 11.14. An example of the PI controller in Simulink form is given in figure 11.25.

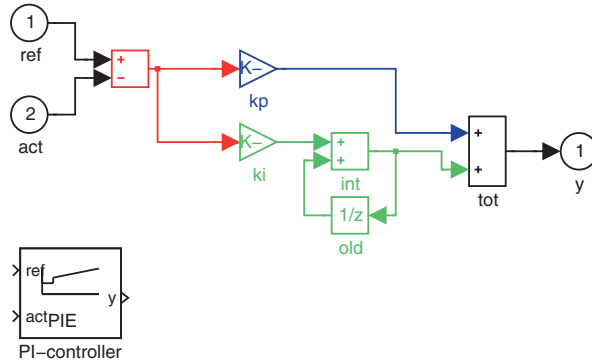


Figure 11.25. Simulink model: PI control unit

The PI controller has as inputs the sampled reference current $i^*(t_k)$ and sampled measured current $i(t_k)$. No induced voltage term e is used as yet, hence this input is not included in the model at present. The proportional term is formed in figure 11.25 by the gain module ‘kp’, which in turn has as input the signal $(i^*(t_k) - i(t_k))$ formed by a summation module. This module has as inputs ‘ref’ (for the sampled reference current) and ‘act’ (for the sampled measured current). This difference signal from the summation unit is also connected to a ‘ki’ gain module, which forms the first part of the implementation of the integral term of the algorithm. The summation term is of the form $\sum_{j=0}^{k-1} \varepsilon(t_j)$, where $\varepsilon(t_j) = (i^*(t_j) - i(t_j))$. The summation term may also be written as $\varepsilon(t_0) + \varepsilon(t_1) + \varepsilon(t_2) + \text{etc}$. This means that we can build this module by adding the last sampled ε value to the present sampled value. The ‘ $1/z$ ’ module output represents the previous sampled ε value, which is then added to the present value. This module is found in the ‘discrete’ library and called ‘unit delay’, in which we must enter the sampling time as ‘Ts’ (note that we have already defined Ts in the MATLAB Workspace). Finally, we add the proportional and integral terms together by using the summation unit ‘tot’ (see figure 11.25) in order to find the required control output which is the reference incremental reference flux value.

When building this module define the gains ‘kp’ and ‘ki’ by way of the parameters L , R and T_s as shown in equation (11.15). The m-file given at the end of this tutorial is used to generate the results given in figure 11.26.

Sub-plot(a) of figure 11.26 shows the reference and actual load current for the simulation sequence in use. Note that the controller works correctly, given that the sampled current corresponds to the reference current at the sample interval points 1, 2, 4ms, etc. The exception being at sampling point $t = 3\text{ms}$ where the reference incremental flux value exceeds the maximum value of $\frac{u_{DC}T_s}{2}$ (as can be observed from sub-plot (b) figure 11.26), which can be provided by the converter during one sample interval.

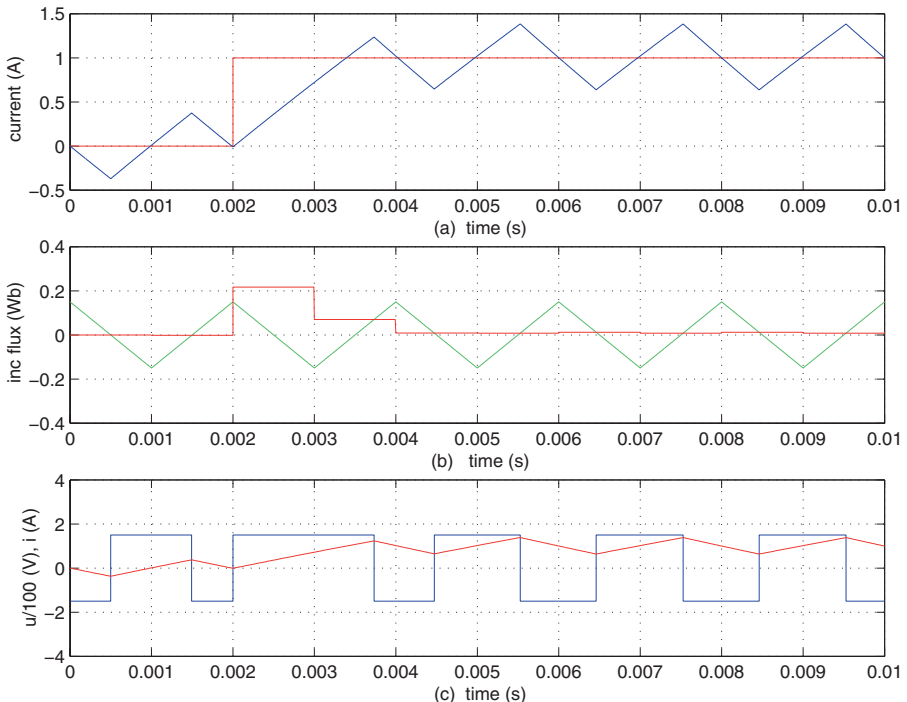


Figure 11.26. Simulink results: Modulator/converter with R/L load

m-file Tutorial 4, chapter 11

```
%Tutorial 4, chapter 11
close all
Ts=1e-3; % sample time
R=10; % load resistance
L=200e-3; % load inductance
subplot(3,1,1)
plot(datout(:,6), datout(:,1), 'r'); % reference current
hold on
plot(datout(:,6), datout(:,3), 'b'); % load current
grid
ylabel(' current (A)');
xlabel(' (a) time (s)')
```

```

subplot(3,1,2)
plot(datout(:,6), datout(:,2), 'g'); %carrier incremental flux
grid
hold on
plot(datout(:,6), datout(:,5), 'r'); % incremental flux reference
axis([0 10e-3 -0.4 0.4])
ylabel(' inc flux (Wb)')
xlabel(' (b) time (s)')
subplot(3,1,3)
plot(datout(:,6), datout(:,4)/100, 'b'); % output voltage/100
hold on
grid
plot(datout(:,6), datout(:,3), 'r'); % load current
xlabel(' (c) time (s)')
ylabel('u/100 (V), i (A)');
axis([0 10e-3 -4 4])

```

11.5.5 Tutorial 5

In this tutorial the R/L load module as used in the previous tutorial is to be replaced with the DC motor model as discussed in tutorial 10.7.5 on page 286. The DC model with load module must be connected as shown in figure 11.27. The controller module shown in figure 11.27 can be extended to accommodate the feed-forward term $e_a = \hat{\psi}_f \omega_m$ in accordance with the generic diagram given in figure 11.14. Use of a feed-forward term is preferable because it improves the transient response, but access to this variable e_a is not straight forward in a practical drive, given the need to have a knowledge of the variable $\hat{\psi}_f$. The reader is encouraged to consider the impact of adding the feed-forward term. The induced voltage input for the feed-forward control input is derived

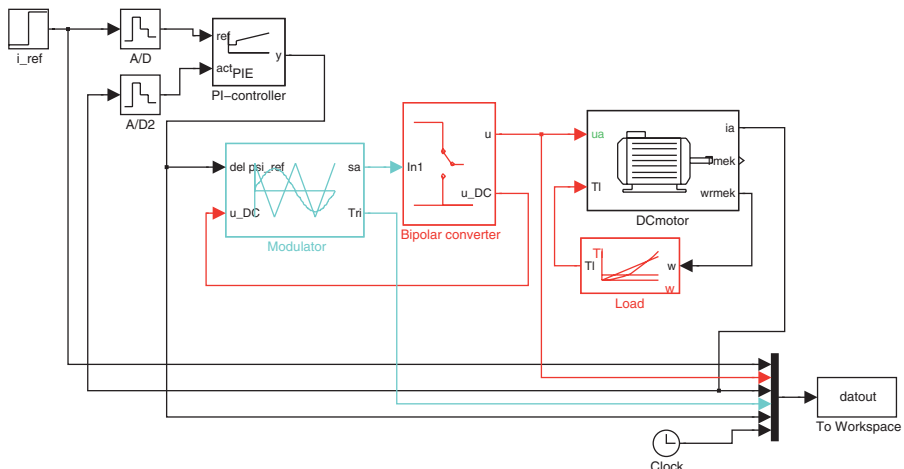


Figure 11.27. Simulink model: Modulator/converter with DC machine as load

by making use of the measured shaft speed and a given field flux value (for the DC machine in use) taken to be $\hat{\psi}_f = 1.0 \text{ Wb}$.

A current reference step of $0 \rightarrow 8\text{A}$ is required at $t = 0\text{s}$. The simulation run time must be set to 60ms. Choose a quadratic load speed curve characteristic with a nominal torque level of 8Nm and speed of 300rpm . The simulation parameters remain unchanged with respect to the previous tutorial. In the MATLAB Workspace set the values $L_a = 0.05$ and $R_a = 10$, which represent the armature inductance and armature resistance of the DC machine used in this tutorial. These values are used together with the earlier defined value of T_s for computation of the gain values in the discrete PI controller.

A typical set of results obtained after running the simulation should look like those given in figure 11.28. These results were, as mentioned above, obtained without using a feed-forward term in the current controller. Modify the controller to include this term and rerun the simulation in order to view the effects of adding the feed-forward term. The m-file used to generate the results shown in figure 11.28 is provided at the end of this tutorial. An observation of

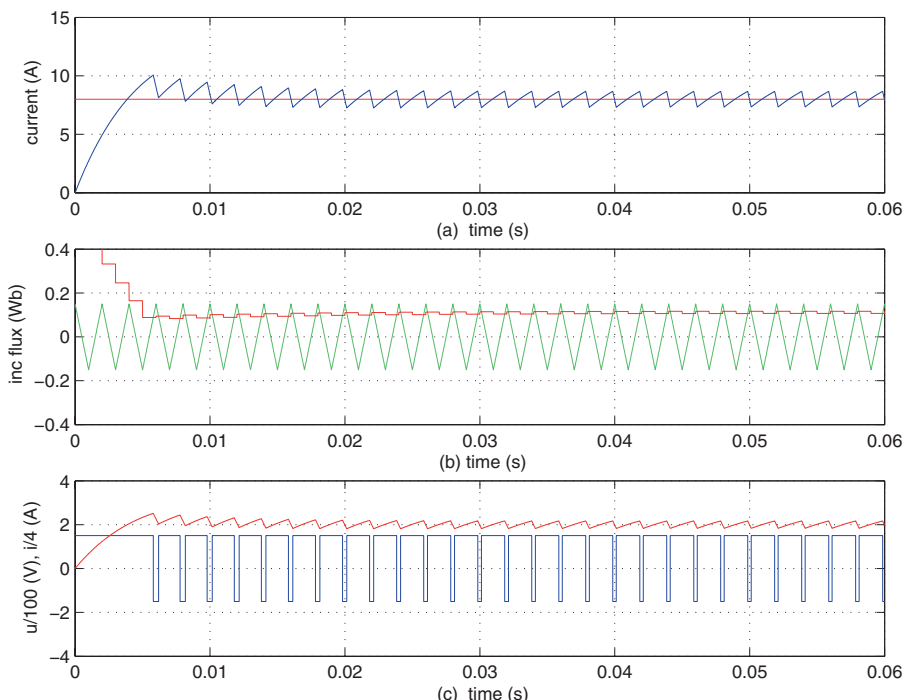


Figure 11.28. Simulink results: Modulator/converter with DC machine (without feed-forward term) as load

the results shows that the controller, modulator/converter is able to provide the correct excitation as to control the armature current to the desired value.

m-file Tutorial 5, chapter 11

```
%Tutorial 5, chapter 11
close all
Ts=1e-3; % sample time
Ra=10; % load resistance
La=0.05; % load inductance
psiF=1; % peak flux value
subplot(3,1,1)
plot(datout(:,6), datout(:,1),'r'); % reference current
hold on
plot(datout(:,6), datout(:,3),'b'); % load current
grid
ylabel(' current (A)');
xlabel(' (a) time (s)')
subplot(3,1,2)
plot(datout(:,6), datout(:,4),'g'); % carrier incremental flux
grid
hold on
plot(datout(:,6), datout(:,5),'r'); % incremental flux reference
axis([0 60e-3 -0.4 0.4])
ylabel(' inc flux (Wb)');
xlabel(' (b) time (s)')
subplot(3,1,3)
plot(datout(:,6), datout(:,2)/100,'b'); %output voltage/100
hold on
grid
plot(datout(:,6), datout(:,3)/4,'r'); % load current
xlabel(' (c) time (s)')
ylabel('u/100 (V), i/4 (A)');
axis([0 60e-3 -4 4])
```

11.5.6 Tutorial 6

This tutorial deals with a Caspoc based simulation of a DC machine connected to a half bridge converter. A predictive dead-beat current control method is envisaged for this electrical drive system. This tutorial is similar to the previous Simulink example, in terms of excitation conditions, drive configuration and choice of parameters. However, the Caspoc based tutorial allows the integration of circuit and block diagram components as will shortly become apparent.

An example of a Caspoc simulation implementation of this problem is shown in figure 11.29. The circuit component of this simulation is represented by the half bridge configuration as given in figure 11.11. However, in this simulation the two switches are replaced by two ideal semiconductor MOSFET switches. These switches are connected to a comparator which is part of the modulator circuit, as was discussed in tutorial 11.5.2. The half bridge converter is connected to a DC machine which is in this case represented in a block diagram format, i.e. a generic diagram type structure. The machine and mechanical load

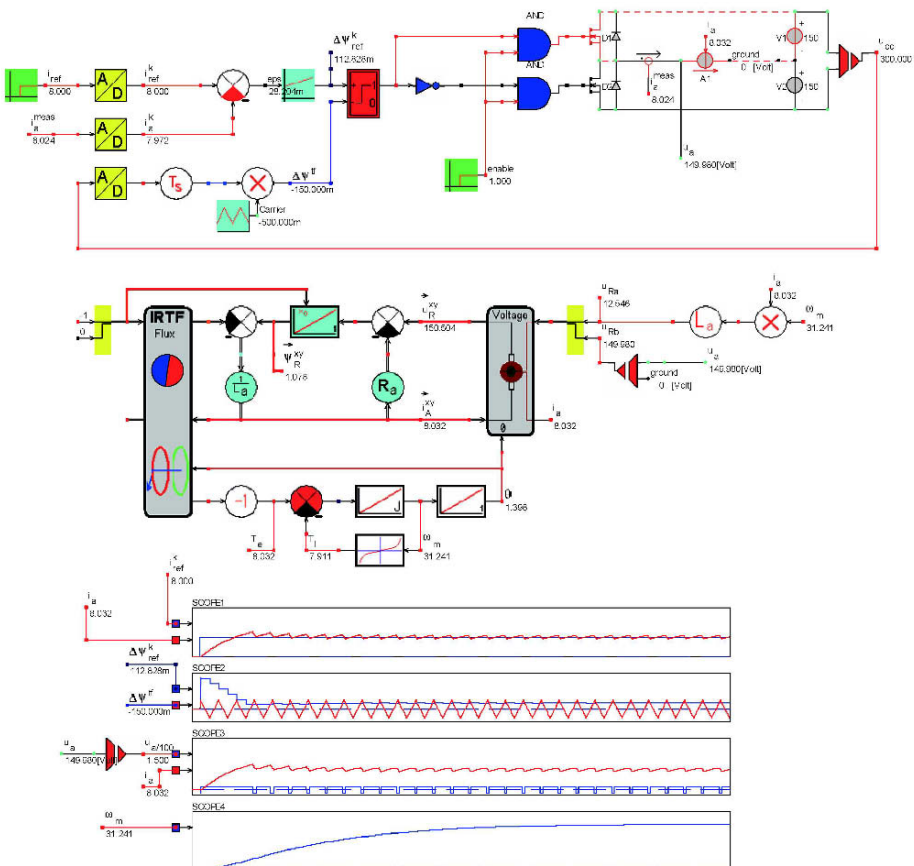


Figure 11.29. Caspoc model: Modulator/converter with DC machine as load

structure used in this tutorial have been discussed in section 10.5. The circuit model, of the half bridge converter provides the voltage excitation of the motor which in turn generates the armature current variable i_a . This variable is returned to the circuit model via a current source circuit component ‘A1’ shown in figure figure 11.29. The predictive dead-beat current controller as shown in figure 11.14 is also present in the Caspoc simulation (without the feed-forward term). The PI controller unit given in this diagram generates the incremental flux reference for the modulator. A reference current module is introduced together with a current sensor in the circuit model which represents the measured armature current input value for the current controller. A double edged PWM modulation strategy is deployed in this example (see figure 11.10). The PWM carrier module and A/D converter units which are part of this modulator are clearly shown in figure 11.29.

The excitation conditions are identical to those discussed in the previous tutorial, hence the results are almost identical to those shown in figure 11.28. A minor difference exists between the two simulations during the start up sequence. The reason for this is that in the Caspoc simulation the converter switches are disabled for the first time sample. The simulation model as presented in this tutorial represents a complete drive system which can be readily analyzed and extended to cover a range of electrical machines.

Appendix A

Concept of sinusoidal distributed windings

Electrical machines are designed in such a manner that the flux density distribution in the airgap due to a single phase winding is approximately sinusoidal. This appendix aims to make plausible the reason for this and the way in which this is realized. In this context the so-called sinusoidally distributed winding concept will be discussed.

Figure A.1 represents an ITF based transformer or IRTF based electrical machine with a finite airgap g . A two-phase representation is shown with two n_1 turn stator phase windings. The windings which carry the currents $i_{1\alpha}$, $i_{1\beta}$ respectively, are shown symbolically. This implies that the winding symbol shown on the airgap circumference represents the locations of the majority windings in each case, not the actual distribution, as will be discussed shortly. If we consider the α winding initially, i.e. we only excite this winding with a current $i_{1\alpha}$, then the aim is to arrange the winding distribution of this phase in such a manner that the flux density in the airgap can be represented as $B_{1\alpha} = \hat{B}_\alpha \cos \xi$. Similarly, if we only excite the β winding with a current $i_{1\beta}$, a sinusoidal variation of the flux density should appear which is of the form $B_{1\beta} = \hat{B}_\beta \sin \xi$. The relationship between phase currents and peak flux density values is of the form $B_{1\alpha} = Ci_{1\alpha}$, $B_{1\beta} = Ci_{1\beta}$ where C is a constant to be defined shortly. In space vector terms the following relationships hold

$$\vec{i}_1 = i_{1\alpha} + j i_{1\beta} \quad (\text{A.1a})$$

$$\vec{B}_1 = \hat{B}_{1\alpha} + j \hat{B}_{1\beta} \quad (\text{A.1b})$$

Given that the current and flux density components are linked by a constant C , it is important to ensure that the following relationship holds, namely

$$\vec{B}_1 = C \vec{i}_1 \quad (\text{A.2})$$

If for example the current is of the form $\vec{i}_1 = \hat{i}_1 e^{j\rho}$ then the flux density should be of the form $\vec{B}_1 = C \hat{i}_1 e^{j\rho}$ for any value of ρ and values of \hat{i}_1 which fall within the linear operating range of the machine. The space vector components are in this case of the form $i_{1\alpha} = \hat{i}_1 \cos \rho$, $i_{1\beta} = \hat{i}_1 \sin \rho$. If we assume that the flux density distributions are indeed sinusoidal then the resultant flux density B_{res} in the airgap will be the sum of the contributions of both phases namely

$$B_{res}(\xi) = \underbrace{C \hat{i}_1 \cos \rho \cos \xi}_{\hat{B}_{1\alpha}} + \underbrace{C \hat{i}_1 \sin \rho \sin \xi}_{\hat{B}_{1\beta}} \quad (\text{A.3})$$

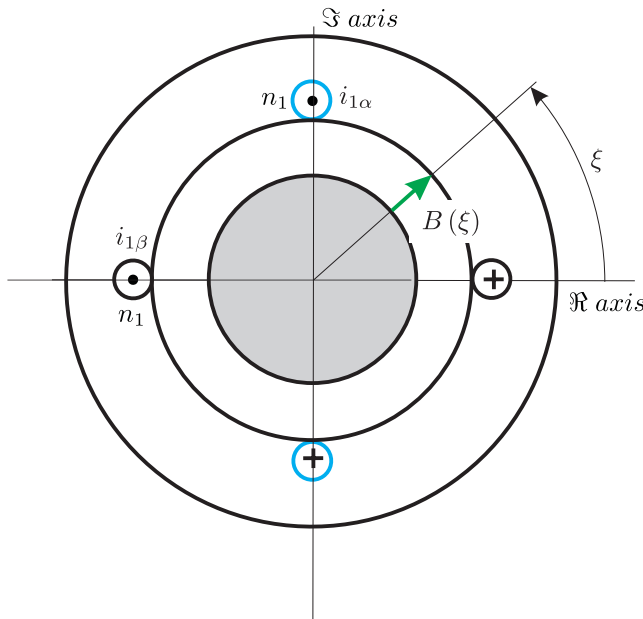


Figure A.1. Simplified ITF model, with finite airgap, no secondary winding shown

Expression (A.3) can also be written as $B_{res} = C \hat{i}_1 \cos(\xi - \rho)$ which means that the resultant airgap flux density is again a sinusoidal waveform with its peak amplitude (for this example) at $\xi = \rho$, which is precisely the value which should appear in the event that expression (A.2) is used directly. It is instructive to consider the case where $\rho = \omega_s t$, which implies that the currents i_α , i_β are sinusoidal waveforms with a frequency of ω_s . Under these circumstances the location within the airgap where the resultant flux density is at its maximum is equal to $\xi = \omega_s t$. A traveling wave exists in the airgap in this case, which has a rotational speed of ω_s rad/s.

Having established the importance of realizing a sinusoidal flux distribution in the airgap for each phase we will now examine how the distribution of the windings affects this goal.

For this purpose it is instructive to consider the relationship between the flux density in the airgap at locations ξ , $\xi + \Delta\xi$ with the aid of figure A.2. If we consider a loop formed by the two ‘contour’ sections and the flux density values at locations ξ , $\xi + \Delta\xi$, then it is instructive to examine the sum of the magnetic potentials along the loop and the corresponding MMF enclosed by this loop. The MMF enclosed by the loop is taken to be of the form $N_\xi i$, where N_ξ represents all or part of the α phase winding and i the phase current. The magnetic potentials in the ‘red’ contour part of the loop are zero because the magnetic material is assumed to be magnetically ideal (zero magnetic potential). The remaining magnetic potential contributions when we traverse the loop in the anti-clockwise direction must be equal to the enclosed MMF which leads to

$$\frac{g}{\mu_o} B(\xi) - \frac{g}{\mu_o} B(\xi + \Delta\xi) = N_\xi i \quad (\text{A.4})$$

Expression (A.4) can also be rewritten in a more convenient form by introducing the variable $n(\xi) = \frac{N_\xi}{\Delta\xi}$ which represents the phase winding distribution per radian. Use of this variable

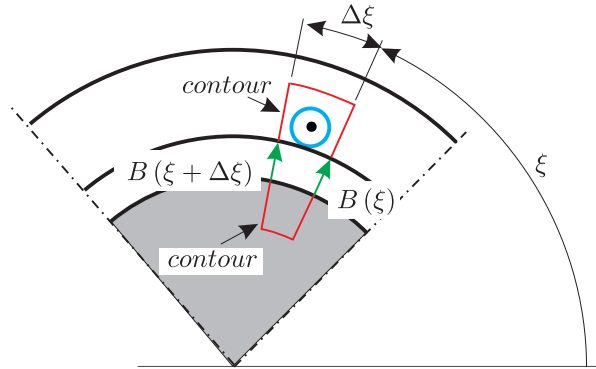


Figure A.2. Sectional view of phase winding and enlarged airgap

with equation (A.4) gives

$$\frac{B(\xi + \Delta\xi) - B(\xi)}{\Delta\xi} = -\frac{g}{\mu_o} n(\xi)i \quad (\text{A.5})$$

which can be further developed by imposing the condition $\Delta\xi \rightarrow 0$ which allows equation (A.5) to be written as

$$\frac{dB(\xi)}{d\xi} = -\frac{g}{\mu_o} n(\xi)i \quad (\text{A.6})$$

The left hand side of equation (A.6) represents the gradient of the flux density with respect to ξ . An important observation of equation (A.6) is that a change in flux density in the airgap is linked to the presence of a non-zero $n(\xi)i$ term, hence we are able to construct the flux density in the airgap if we know (or choose) the winding distribution $n(\xi)$ and phase current. Vice versa we can determine the required winding distribution needed to arrive at for example a sinusoidal flux density distribution.

A second condition must also be considered when constructing the flux density plot around the entire airgap namely

$$\int_{-\pi}^{\pi} B(\xi) d\xi = 0 \quad (\text{A.7})$$

Equation (A.7) basically states that the flux density versus angle ξ distribution along the entire airgap of the machine cannot contain an non-zero average component. Two examples are considered below which demonstrate the use of equations (A.6) and (A.7). The first example as shown in figure A.3 shows the winding distribution $n(\xi)$ which corresponds to a so-called ‘concentrated’ winding. This means that the entire number of N turns of the phase winding are concentrated in a single slot (per winding half) with width $\Delta\xi$, hence $N_\xi = N$. The corresponding flux density distribution is in this case trapezoidal and not sinusoidal as required.

The second example given by figure A.4 shows a distributed phase winding as often used in practical three-phase machines. In this case the phase winding is split into three parts (and three slots (per winding half), spaced λ rad apart) hence, $N_\xi = \frac{N}{3}$. The total number of windings of the phase is again equal to N . The flux density plot which corresponds with the distributed

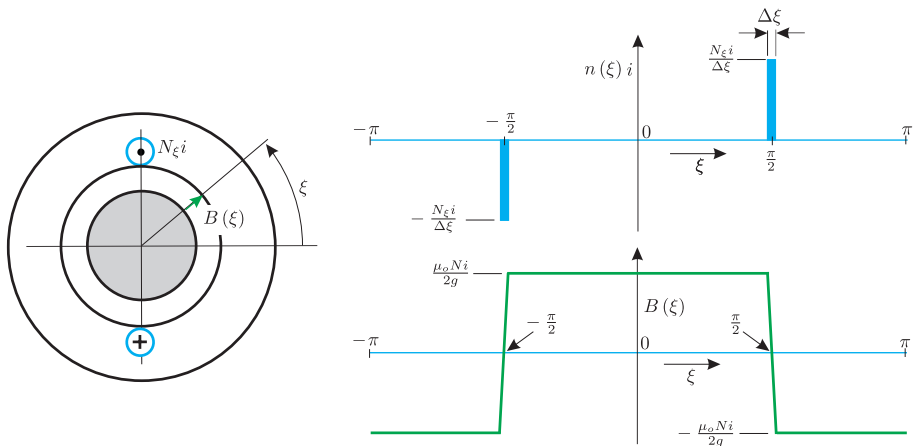


Figure A.3. Example: concentrated winding, $N_\xi = N$

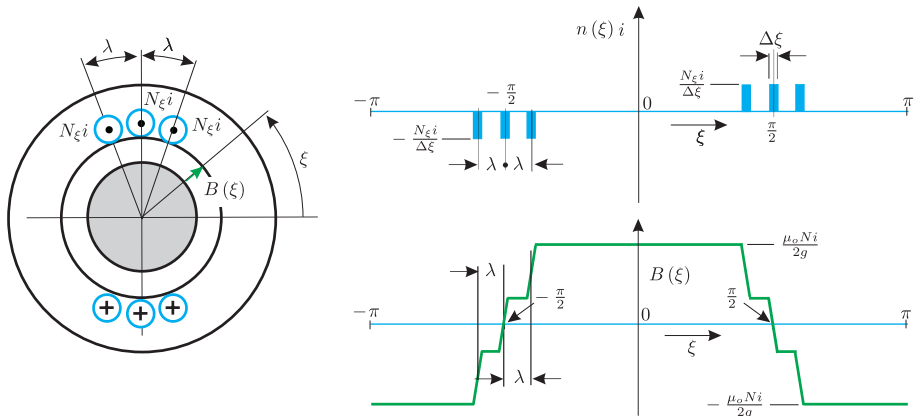


Figure A.4. Example: distributed winding, $N_\xi = \frac{N}{3}$

winding is a step forward in terms of representing a sinusoidal function. The ideal case would according to equation (A.6) require a $n(\xi)i$ representation of the form

$$n(\xi)i = \frac{g}{\mu_o} \hat{B} \sin(\xi) \quad (\text{A.8})$$

in which \hat{B} represents the peak value of the desired flux density function $B(\xi) = \hat{B} \cos(\xi)$. Equation (A.8) shows that the winding distribution needs to be sinusoidal. The practical implementation of equation (A.8) would require a large number of slots with varying number of turns placed in each slot. This is not realistic given the need to typically house three phase windings, hence in practice the three slot distribution shown in figure A.4 is normally used and provides a flux density versus angle distribution which is sufficiently sinusoidal.

In conclusion it is important to consider the relationship between phase flux-linkage and circuit flux values. The phase circuit flux (for the α phase) is of the form

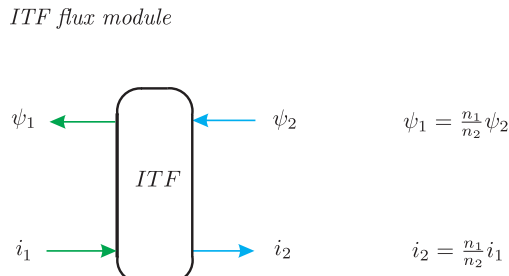
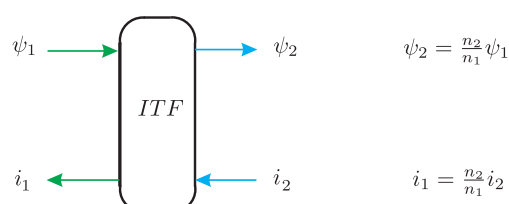
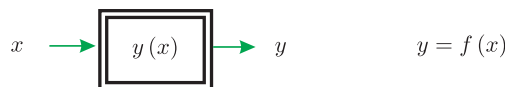
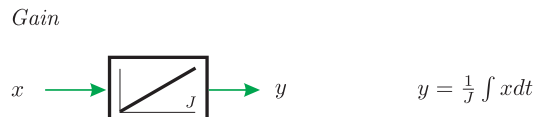
$$\phi_{m\alpha} = \int_{-\frac{\pi}{2}}^{\frac{\pi}{2}} B(\xi) d\xi \quad (\text{A.9})$$

which for a concentrated winding corresponds to a flux-linkage value $\psi_{1\alpha} = N\phi_{m\alpha}$. If a distributed winding is used then not all the circuit flux is linked with all the distributed winding components in which case the flux-linkage is given as $\psi_{1\alpha} = N_{eff}\phi_{m\alpha}$, where N_{eff} represents the ‘effective’ number of turns.

Appendix B

Generic module library

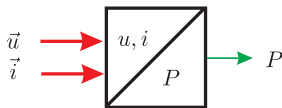
The generic modules used in this book are presented in this section. In addition to the generic representation an example of a corresponding transfer function (for the module in question) is provided. Transfer functions given, are in space vector and/or scalar format. Some modules, such as for example the ITF module, can be used in scalar or space vector format. However, some functions, such as for example the IRTF module, can only be used with space vectors.





$$y = \frac{dx}{dt}$$

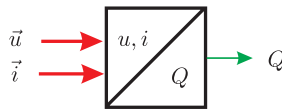
Differentiator



$$P = \Re \left\{ \vec{u} \left(\vec{i} \right)^* \right\}$$

$$P = u_\alpha i_\alpha + u_\beta i_\beta$$

Real power module



$$Q = \Im \left\{ \vec{u} \left(\vec{i} \right)^* \right\}$$

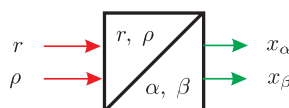
$$Q = u_\beta i_\alpha - u_\alpha i_\beta$$

Reactive power module



$$x = \frac{1}{\sqrt{3}} \sqrt{(x_\alpha)^2 + (x_\beta)^2}$$

Vector to RMS converter (power invariant)



$$x_\alpha = r \cos \rho$$

$$x_\beta = r \sin \rho$$

Polar to Cartesian converter

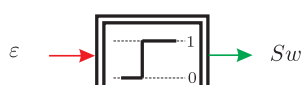


$$x(t_{k-1}, t_k, t_{k+1}, \text{etc})$$

Analog to Digital converter



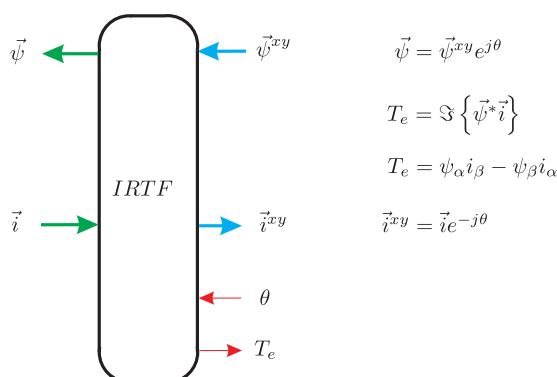
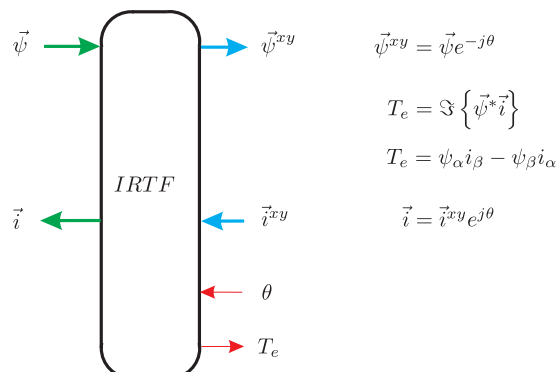
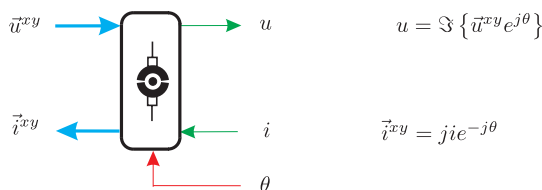
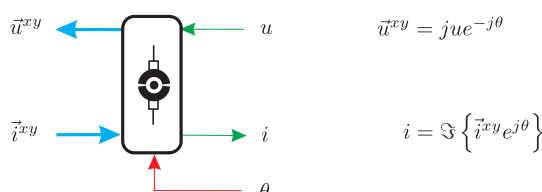
Ramp generator (falling edge PWM)

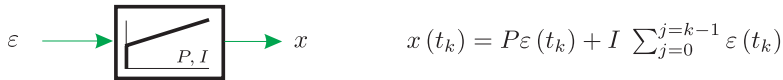


$$S_w = 1 ; \text{ if } \varepsilon > 0$$

$$S_w = 0 ; \text{ if } \varepsilon \leq 0$$

Comparator

*IRTF current module**Brush/commutator-current unit (ideal)**Brush/commutator-voltage unit (ideal)*



Proportional-Integral controller (discrete)

$$\begin{array}{ccc} i_R & \xrightarrow{\text{3φ}} & i_{S1} \\ i_S & \xrightarrow{\text{3φ}} & i_{S2} \\ i_T & \xrightarrow{\text{3φ}} & i_{S3} \end{array} \quad \begin{bmatrix} i_{S1} \\ i_{S2} \\ i_{S3} \end{bmatrix} = \begin{bmatrix} 1 & 0 & 0 \\ 0 & 1 & 0 \\ 0 & 0 & 1 \end{bmatrix} \begin{bmatrix} i_R \\ i_S \\ i_T \end{bmatrix}$$

Current conversion (star): supply → phase

$$\begin{array}{ccc} i_{S1} & \xrightarrow{\text{3φ}} & i_R \\ i_{S2} & \xrightarrow{\text{3φ}} & i_S \\ i_{S3} & \xrightarrow{\text{3φ}} & i_T \end{array} \quad \begin{bmatrix} i_R \\ i_S \\ i_T \end{bmatrix} = \begin{bmatrix} 1 & 0 & 0 \\ 0 & 1 & 0 \\ 0 & 0 & 1 \end{bmatrix} \begin{bmatrix} i_{S1} \\ i_{S2} \\ i_{S3} \end{bmatrix}$$

Current conversion (star): phase → supply

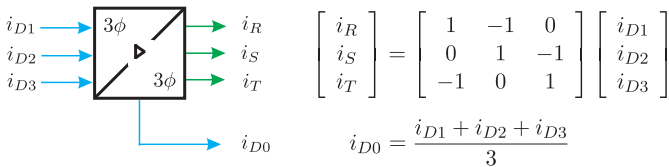
$$\begin{array}{ccc} u_R & \xrightarrow{\text{3φ}} & u_{S1} \\ u_S & \xrightarrow{\text{3φ}} & u_{S2} \\ u_T & \xrightarrow{\text{3φ}} & u_{S3} \end{array} \quad \begin{bmatrix} u_{S1} \\ u_{S2} \\ u_{S3} \end{bmatrix} = \begin{bmatrix} 1 & 0 & 0 \\ 0 & 1 & 0 \\ 0 & 0 & 1 \end{bmatrix} \begin{bmatrix} u_R \\ u_S \\ u_T \end{bmatrix} - \begin{bmatrix} 1 \\ 1 \\ 1 \end{bmatrix} u_{S0}$$

$$u_{S0} = \frac{u_R + u_S + u_T}{3}$$

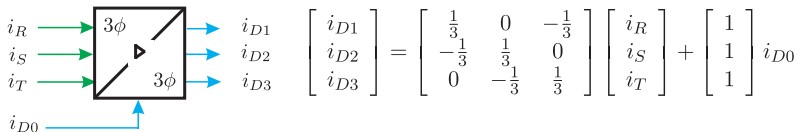
Voltage conversion (star): supply → phase

$$\begin{array}{ccc} u_{S1} & \xrightarrow{\text{3φ}} & u_R \\ u_{S2} & \xrightarrow{\text{3φ}} & u_S \\ u_{S3} & \xrightarrow{\text{3φ}} & u_T \end{array} \quad \begin{bmatrix} u_R \\ u_S \\ u_T \end{bmatrix} = \begin{bmatrix} 1 & 0 & 0 \\ 0 & 1 & 0 \\ 0 & 0 & 1 \end{bmatrix} \begin{bmatrix} u_{S1} \\ u_{S2} \\ u_{S3} \end{bmatrix} + \begin{bmatrix} 1 \\ 1 \\ 1 \end{bmatrix} u_{S0}$$

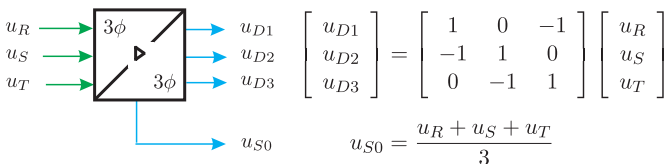
Voltage conversion (star): phase → supply



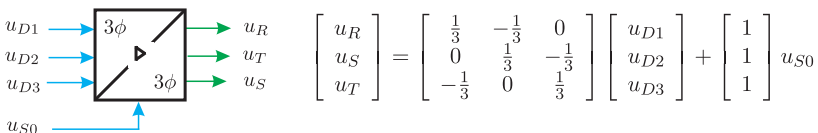
Current conversion (delta) : phase → supply



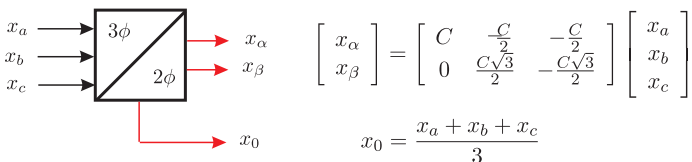
Current conversion (delta) : supply → phase



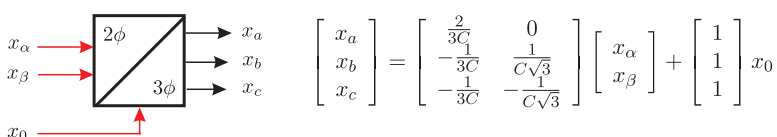
Voltage conversion (delta) : supply → phase



Voltage conversion (delta) : phase → supply



Scalar to Space vector, $C = \sqrt{\frac{2}{3}}$: power invariant, $C = \frac{2}{3}$: amplitude invariant



Vector to Scalar

$$\begin{bmatrix} u_{D\alpha} \\ u_{D\beta} \end{bmatrix} = \sqrt{3} \begin{bmatrix} \cos \frac{\gamma}{4} & \sin \frac{\gamma}{4} \\ -\sin \frac{\gamma}{4} & \cos \frac{\gamma}{4} \end{bmatrix} \begin{bmatrix} u_\alpha \\ u_\beta \end{bmatrix}$$

$$\vec{u}_{D123} \rightarrow \vec{u}_{RST}$$

$$\begin{bmatrix} u_\alpha \\ u_\beta \end{bmatrix} = \frac{1}{\sqrt{3}} \begin{bmatrix} \cos \frac{\gamma}{4} & -\sin \frac{\gamma}{4} \\ \sin \frac{\gamma}{4} & \cos \frac{\gamma}{4} \end{bmatrix} \begin{bmatrix} u_{D\alpha} \\ u_{D\beta} \end{bmatrix}$$

$$\vec{u}_{RST} \rightarrow \vec{u}_{D123}$$

$$\begin{bmatrix} i_\alpha \\ i_\beta \end{bmatrix} = \sqrt{3} \begin{bmatrix} \cos \frac{\gamma}{4} & -\sin \frac{\gamma}{4} \\ \sin \frac{\gamma}{4} & \cos \frac{\gamma}{4} \end{bmatrix} \begin{bmatrix} i_{D\alpha} \\ i_{D\beta} \end{bmatrix}$$

$$\text{Current conversion (delta)} : \vec{i}_{D123} \rightarrow \vec{i}_{RST}$$

$$\begin{bmatrix} i_\alpha \\ i_\beta \end{bmatrix} = \frac{1}{\sqrt{3}} \begin{bmatrix} \cos \frac{\gamma}{4} & \sin \frac{\gamma}{4} \\ -\sin \frac{\gamma}{4} & \cos \frac{\gamma}{4} \end{bmatrix} \begin{bmatrix} i_{D\alpha} \\ i_{D\beta} \end{bmatrix}$$

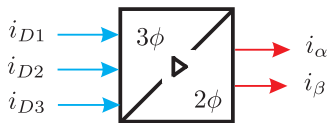
$$\text{Current conversion (delta)} : \vec{i}_{RST} \rightarrow \vec{i}_{D123}$$

$$\begin{bmatrix} u_\alpha \\ u_\beta \end{bmatrix} = \begin{bmatrix} \frac{C}{2} & -\frac{C}{2} & 0 \\ \frac{C}{2\sqrt{3}} & \frac{C}{2\sqrt{3}} & -\frac{C}{\sqrt{3}} \end{bmatrix} \begin{bmatrix} u_{D1} \\ u_{D2} \\ u_{D3} \end{bmatrix}$$

$$\text{Voltage conversion (delta)} : \text{Scalar} \rightarrow \vec{u}_{RST}$$

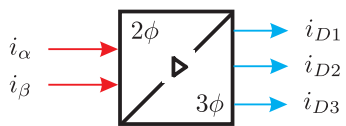
$$\begin{bmatrix} u_{D1} \\ u_{D2} \\ u_{D3} \end{bmatrix} = \begin{bmatrix} \frac{1}{C} & \frac{1}{C\sqrt{3}} \\ -\frac{1}{C} & \frac{C\sqrt{3}}{3C} \\ 0 & -\frac{2\sqrt{3}}{3C} \end{bmatrix} \begin{bmatrix} u_\alpha \\ u_\beta \end{bmatrix}$$

$$\text{Voltage conversion (delta)} : \vec{u}_{RST} \rightarrow \text{Scalar}$$



$$\begin{bmatrix} i_\alpha \\ i_\beta \end{bmatrix} = \begin{bmatrix} \frac{3C}{2} & -\frac{3C}{2} \\ \frac{\sqrt{3}C}{2} & \frac{\sqrt{3}C}{2} \end{bmatrix} \begin{bmatrix} i_{D1} \\ i_{D2} \\ i_{D3} \end{bmatrix}$$

Current conversion (delta) : Scalar $\rightarrow i_{RST}$



$$\begin{bmatrix} i_{D1} \\ i_{D2} \\ i_{D3} \end{bmatrix} = \begin{bmatrix} \frac{1}{3C} & \frac{1}{C3\sqrt{3}} \\ -\frac{1}{3C} & \frac{1}{C3\sqrt{3}} \\ 0 & -\frac{2\sqrt{3}}{9C} \end{bmatrix} \begin{bmatrix} i_\alpha \\ i_\beta \end{bmatrix}$$

Current conversion (delta) : $\vec{i}_{RST} \rightarrow$ Scalar

References

- Bödefeld, Th. and Sequenz, H. (1962). *Elektrische Maschinen*. Springer-Verlag, 6th edition.
- Holmes, D.G. (1997). *A generalised approach to modulation and control of hard switched converters*. PhD thesis, Department of Electrical and Computer engineering, Monash University, Australia.
- Hughes, A. (1994). *Electric Motors and Drives*. Newnes.
- Leonhard, W. (1990). *Control of Electrical Drives*. Springer-Verlag, Berlin Heidelberg New York Tokyo, 2 edition.
- Mathworks, The (2000). Matlab, simulink. WWW.MATHWORKS.COM.
- Miller, T. J. E. (1989). *Brushless Permanent-Magnet and Reluctance Motor Drives*. Number 21 in Monographs in Electrical and Electronic Engineering. Oxford Science Publications.
- Mohan, N. (2001). *Advanced Electrical Drives, Analysis, Control and Modeling using Simulink*. MNPERE, Minneapolis, USA.
- Svensson, T. (1988). On modulation and control of electronic power converters. Technical Report 186, Chalmers University of Technology, School of Electrical and Computer engineering.
- van Duijzen, P.J. (2005). Simulation research, caspoc 2005. WWW.CASPOC.COM.
- Veltman, A. (1994). *The Fish Method: interaction between AC-machines and Switching Power Converters*. PhD thesis, Department of Electrical Engineering, Delft University of Technology, the Netherlands.

Index

- actuators, 2, 33
- airgap, 18, 19, 22, 25, 50, 170, 175, 183, 239
- algebraic loop, 57, 254
- alternative differentiator module, 155
- Ampère, A. H., 265
- amplitude invariant, 87, 88
- armature, 269, 273
- armature reaction, 271
- asymmetrically sampled, 305
- asynchronous, 169, 233, 237, 246, 266
- bar magnet, 13, 14
- bipolar, 296, 305, 314, 316, 318
- Blondel diagram, 201, 205, 207
- braking, 3
- brushes, 194, 267
- brushless machines, 195
- building block, 9, 10, 169, 297, 302
- Carter, 25
- cartesian, 153
- Caspoc, 7
- classical, 5, 169, 179
- commutator, 265, 267–270, 279
- commutator segments, 271, 272, 284
- comparator, 302, 311
- compensation winding, 269
- complex plane, 34, 36
- control algorithm, 6, 7
- convention, 8, 172, 201
- conversion module, 186
- converter, 6, 7, 75, 76, 104, 169, 193, 195, 296–302, 304–306, 310, 314–316, 318, 323
- converter switch, 299, 301, 302
- Cumming, J. S., 265
- current control, 295, 318
- current density, 22, 23
- current sensor, 296
- damper winding, 197
- Davenport, T., 265
- DC machine, 272
- delta connected, 80, 84, 93, 95–97, 102, 103, 145, 146
- discrete, 297, 308–310
- double edged, 306
- drives, 2–4, 6, 12, 30, 193, 243, 266
- DSP, 6, 7, 296
- efficiency, 2, 6
- electro-magnetic interaction, 29
- energy, 3, 5, 75, 122, 124, 125, 172, 173
- falling edge, 300
- Faraday, M., 265
- feed-forward, 309, 321
- field current, 195, 203, 218
- finite-element, 7
- flux density, 13–16, 18, 20, 23
- flux lines, 13–16, 25
- flux-linkage, 19–22, 32, 47, 50, 61, 152, 153, 156, 171
- four parameter model, 185
- four-quadrant, 2
- fringing, 14, 17, 18, 25
- generator, 5, 169, 203, 204, 209, 222, 244
- generic model, 9, 295, 319
- grid, 6, 75
- half bridge converter, 306, 314
- Heyland diagram, 242, 244–247
- Holmes, G., 305
- Hopkinson, 16, 20, 50
- Hughes, A., 12, 193, 194
- idle mode, 296
- imaginary power, 124

incremental flux, 30, 298, 300, 304, 316

inductance, 20, 21, 31, 32, 273

induction machine, 231

inertia, 174, 211

iron losses, 67

IRTF, 169, 173, 197, 271

ITF, 45, 48, 49, 149

Kirchhoff, 76, 81

leakage inductance, 55, 56, 58

Leonhard, W., 10

linear-motors, 23

load, 3, 5, 211, 234, 276, 286, 287, 296

load angle, 195, 201

load torque, 211

logic signal, 297

Lorentz, 12, 173

m-file, 36, 41, 65

machine sizing, 22, 23

magnetic circuit, 14, 16, 20, 45, 46, 50

magnetic field, 12, 13, 17, 22, 182, 195, 231, 265

magnetic poles, 181

magnetizing inductance, 50, 51, 58, 183

MATLAB, 7

maximum output power point, 208

micro-processor, 6, 296, 298

Miller, T. J. E., 23

modulator, 6, 7, 296, 298, 301, 303, 304, 306, 307, 310, 311, 313, 314, 316, 318

motoring, 204, 208, 233, 240

multi-pole, 182, 183

mutual inductance, 60, 61

neutral, 76

no-load, 2, 67, 233, 276

non-linear, 21, 29, 33, 39, 42

non-salient, 197, 201

Oersted, H. C., 265

permanent magnet, 195, 222, 267

permeability, 16, 17, 29, 45, 46, 50

phasor, 33–35

polar, 153

pole-pair, 181

power factor, 124, 203, 204, 208, 244

power invariant, 87–89

power supply, 4, 6, 14, 194

predictive dead-beat, 307, 321

primary, 45–50

primary referred, 51, 52, 61

proportional, 309, 319

proportional-integral, 309

pull-out slip, 241, 243

PWM, 300, 301

quasi-stationary, 268

quasi-steady-state, 179

reactive power, 124, 125, 127, 132–134, 137, 218

real power, 124, 131, 132

reference incremental flux, 298, 306, 320

regenerative, 3

reluctance, 16, 17, 20, 50, 51, 175

rising edge, 299, 306

robots, 1

rotating flux vector, 178, 195

rotating reference frame, 180

rotor, 170, 171, 195, 231

rotor angle, 173

rotor speed, 178, 195, 233

sampling interval, 298–300, 306, 307

saturation, 19, 21, 23, 32, 33, 38

saw tooth, 301, 311

Schweigger, J. C. S., 265

secondary, 45–48, 152

self inductance, 19, 29, 61

sensors, 5–7

separately excited DC, 277

series wound DC, 278

set-point, 307

shear-stress, 23

shoot-through mode, 296

shunt DC machine, 277

simplified model, 196, 235, 240, 268

Simpson, 308

Simulink, 36

sinusoidal, 33, 34, 53, 178, 200

sinusoidal distributed, 185, 327

slip, 233, 238–241

slipring machine, 232

slipring/brush, 194, 195, 267

space vector, 84

speed condition, 179

squirrel cage, 231

stable operation, 208

star connected, 76, 91, 102, 103, 109

star point, 76

stationary reference frame, 180

stator, 170, 171, 175, 193, 266

steady-state, 276

Sturgeon, S., 265

supply voltage, 84, 100, 296, 302–304, 310, 316

switching point, 299, 301

symbolic model, 32

synchronous, 169, 193–197, 201, 231, 267

synchronous speed, 211, 239

Tesla, N., 231

three inductance model, 57

- three-phase, 75, 76, 84, 103, 121, 136, 149, 193,
195
- toroidal, 29, 45
- torque, 172, 173, 175
- traction drives, 277
- transformer, 45, 46, 49, 50, 149, 157, 169
- triangular function, 304
- two inductance model, 57, 59, 60, 157, 183
- two-phase, 84, 183

- uni-polar, 295, 296, 300, 301, 307
- universal DC machine, 278

- universal machine, 267
- V/f drive, 243
- Vector to RMS module, 136
- Veltman, A., 169

- Westinghouse, 231
- winding ratio, 47, 63, 174
- Wye connected, 76

- zero sequence, 81, 89, 91, 93, 96, 97, 99, 104
- zero-order hold, 310